Mechanisms Underlying the Essential Role of Mitochondria in Chronological Aging of the Yeast *Saccharomyces cerevisiae*

Adam Beach

A Thesis
in
The Department
of
Biology

Presented in Partial Fulfillment of the Requirements
For the Degree of
Doctor of Philosophy (Biology) at
Concordia University
Montreal, Quebec, Canada

February 2015

© Adam Beach, 2015

CONCORDIA UNIVERSITY

School of Graduate Studies

This is to certify that the thesis prepared

By: Adam Beach

Entitled: Mechanisms Underlying the Essential Role of Mitochondria in Chronological Aging of the Yeast *Saccharomyces cerevisiae*

and submitted in partial fulfillment of the requirements for the degree of

Doctor of Philosophy (Biology)

complies with the regulations of the University and meets the accepted standards with respect to originality and quality.

Signed by the final Examining Committee:

_____ Chair
Dr. Peter Darlington

_____ External Examiner
Dr. Luis Rokeach

_____ External to Program
Dr. Ann English

_____ Examiner
Dr. Catherine Bachewich

_____ Examiner
Dr. Patrick Gulick

_____ Thesis Supervisor
Dr. Vladimir Titorenko

Approved by _____
Dr. Selvadurai Dayanandan, Graduate Program Director

April 2015 _____
Dean of Faculty

ABSTRACT

Mechanisms Underlying the Essential Role of Mitochondria in Chronological Aging of the Yeast *Saccharomyces cerevisiae*

Adam Beach, PhD
Concordia University, 2015

This thesis describes studies that have resulted in uncovering molecular and cellular mechanisms underlying the essential role of mitochondria in chronological aging of the baker's yeast, *Saccharomyces cerevisiae*. The Titorenko laboratory has recently identified lithocholic acid (LCA), a bile acid and a natural compound that operates synergistically with caloric restriction (CR) to cause a substantial increase in yeast chronological lifespan under longevity-extending CR conditions. As a first step towards establishing a mechanism by which LCA extends longevity of chronologically aging yeast limited in calorie supply, I investigated the distribution of LCA within yeast cells. I found that exogenously added LCA enters yeast cells, is sorted only to mitochondria, resides mainly in the inner mitochondrial membrane and also associates with the outer membrane of mitochondria. I demonstrated that LCA-elicited changes in the membrane lipidome of mitochondria trigger age-related alterations in mitochondrial respiration, membrane potential, reactive oxygen species (ROS) quantity, oxidative macromolecular damage, respiratory complexes composition and ATP concentration. My findings provided evidence that the longevity-extending potential of LCA is due in part to its ability to alter the age-related dynamics of mitochondrially produced ROS in both chronologically ″young″ and ″old″ cells, thus reducing the damaging effect of these ROS in ″young″ cells and amplifying their ″hormetic″ effect in ″old″ cells. I demonstrated that LCA

alters the age-related dynamics of changes in the levels of many mitochondrial proteins, as well as numerous proteins in cellular locations outside of mitochondria. My findings imply that LCA-driven changes in the mitochondrial lipidome alter the mitochondrial proteome and functionality, thereby enabling mitochondria to operate as signaling organelles that orchestrate the establishment of an anti-aging transcriptional program for many longevity-defining nuclear genes. Based on these findings, I proposed a model for how such LCA-driven changes early and late in the life of chronologically aging yeast cause a stepwise development of an anti-aging cellular pattern and its maintenance throughout lifespan. Moreover, I provided evidence that mitophagy, a selective autophagic degradation of aged and dysfunctional mitochondria, is a longevity assurance process that in chronologically aging yeast underlies the synergistic beneficial effects of CR and LCA on lifespan.

Acknowledgements

First and foremost, I would like to thank my supervisor, Dr. Vladimir Titorenko, for his continued mentorship, guidance, support and sense of humour over the course of my research career, beginning with a BIOL 490 Honours Project and culminating with this PhD. I have had the opportunity to pursue various research interests here at Concordia University and thanks to Dr. Titorenko's support, I have been fortunate to travel for international conferences, meetings, and a short-term research project in Japan.

On that note, I would like to thank Dr. Tomotake Kanki for hosting me in his lab at Niigata University. Your kindness and hospitality were greatly appreciated; I will never forget my research and cultural experiences in Japan.

I would also like to thank my Thesis Committee members, Dr. Catherine Bachewich and Dr. Partick Gulick, for their input, questions and support with my graduate studies.

I would like to acknowledge the help and guidance of both Alain Tessier and Jean-Pierre Falgueyret from the Centre for Biological Applications of Mass Spectrometry (CBAMS), for their assistance with training and instrumentation in my mass spectrometry-based projects.

My doctoral studies were funded by the Canadian Institutes of Health Research (CIHR). I also received a Michael Smith Foreign Study Supplement (MSFSS) from CIHR to pursue a research project in Japan. This research project was also supplemented by a Graduate Student Mobility Award from Concordia University. I also received a Hydro-Québec Graduate Award, Campaign for a New Millenium Graduate Scholarship and a Concordia Accelerator Award.

My time in the lab has been a wonderful experience; thank you to my labmates and friends Vincent Richard, Rachel Feldman, Anthony Arlia-Ciommo, Anna Leonov, Berly Cortes, Alejandra Gomez-Perez, Olivia Koupaki, Michelle Burstein, Alex Goldberg, Pavlo Kyryakov, Simon Bourque, Anastasia Glebov, Tatiana Boukh-Viner and Daniel Aguirre. I would also like to acknowledge the seemingly endless number of volunteers, undergraduate students, summer

research students, international exchange students as well as graduate and diploma students who have made the lab a truly interesting workplace. To the members of the Titorenko Lab - past, present and future - best of luck in your endeavours!

To my father, Percy, my mother, Debra, my sister, Tamara and my Grama, Rose, thank you all for your love and support, not just through this degree but over the course of my entire life. To my friends (you all know who you are), while you may not have always understood what I have been working on these past years, thank you for your support through it all. To my cats, you each took a turn sitting on my keyboard as I typed essays and papers over the years. Sadly, I complete this thesis without any such appreciated distraction. Your contributions are not forgotten.

Finally, to my wife and the love of my life, Vanessa, who has been with me since I first decided to pursue the sciences back in high school, thank you for always supporting, understanding and loving me through all of our adventures. I am excited to be moving on to the next chapter of our lives together and cannot wait to see what the future holds!

My sincerest thanks to everyone who has helped and supported me in pursuit of this great accomplishment; I am truly blessed and grateful for everything. Thank you!

Yours truly,
Adam Percy Bellarmino Beach

Basic research is what I'm doing when I don't know what I'm doing.

Wernher von Braun

Table of Contents

List of Figures and Tables

List of Abbreviations

ABC	ammonium bicarbonate
acetyl-COA	acetyl-Coenzyme A
ACO	aconitase
ACN	acetonitrile
ADP	adenosine diphosphate
AMP	adenosine monophosphate
ATG	autophagy-related gene
ATP	adenosine triphosphate
AU	arbitrary units
cAMP	cyclic adenosine monophosphate
CCCP	carbonyl cyanide m-chlorophenylhydrazone
CCO	cytochrome c oxidase
CFU	colony-forming units
CL	cardiolipin
CLS	chronological life span
CW	calcofluor white M2R
D	diauxic
DAMP	damage-associated molecular pattern
DHR	dihydrorhodamine 123
DMSO	dimethylsulfoxide
DTT	dithiothreitol
EE	ergosteryl esters
ER	endoplasmic reticulum
ERC	extrachromosomal rDNA circle
ETC	eletron transport chain
FFA	free fatty acid
IAA	iodoacetamide
IDE	insulin degrading enzyme
IMM	inner mitochondrial membrane
IMS	intermembrane space
ISC	iron-sulfur cluster
L	logarithmic
LA/LCA	lithocholic acid
m-AAA	ATPase associated with various cellular activities
MALDI-TOF	matrix-assisted laser desorption/ionization time-of-flight
MAM	mitochondria-associated membrane
MLCL	monolysocardiolipin
MOMP	mitochondrial outer membrane permeabilization
MPT	mitochondrial permeability transition
MTC	mitochondrial translation control
mtDNA	mitochondrial DNA

NAD+/NADH	nicotinamide adenine dinucleotide
NADP+/NADPH	nicotinamide adenine dinucleotide phosphate
NL	neutral lipid
OMM	outer mitochondrial membrane
OS	oxidative stress
OXPHOS	oxidative phosphorylation
PA	phosphatidic acid
PC	phosphatidylcholine
PCD	programmed cell death
PD	post-diauxic
PE	phosphatidylethanolamine
PexAD	peroxisome-associated protein degradation
PG	phosphatidylglycerol
PI	phosphatidylinositol
PINK1	PTEN (Phosphatase and tensin homolog)-induced putative kinase 1
PKA	protein kinase A
PM	plasma membrane
PMD	partial mitochondrial dysfunction
PS	phosphatidylserine
PTS1/2	peroxisomal targeting signal
R123	rhodamine 123
RADAR	receptor accumulation and degradation in the absence of recycling
RNS	reactive nitrogen species
ROS	reactive oxygen species
RTG	retrograde
SCFA ACS	short-chain fatty acids acetyl-CoA synthetase
SDH	succinate dehydrogenase
SMP	submitochondrial particles
ST	stationary phase
TAG	triacylglycerol
TCA	tricarboxylic acid
TOR	target of rapamycin
UC	uncoupled
UPRmt	mitochondrial unfolded protein response
YNB	yeast nitrogen base
YP	yeast extract, peptone
YEPD	yeast extract, peptone, dextrose

1 Introduction

The functional state of mitochondria is crucial for organismal physiology in all eukaryotes [1-5]. This is in part because mitochondria produce the bulk of cellular ATP and synthesize (or generate biosynthetic intermediates for) amino acids, lipids and nucleotides [3-7]. This is also because mitochondria can operate as intracellular signaling compartments and organizing platforms whose different functional states and dynamic communications with other organelles orchestrate a range of cellular responses to changes in various physiological conditions [1, 3, 5, 7-28]. Several mechanistically diverse strategies have been implicated in enabling mitochondria to function as such signaling compartments and organizing platforms within eukaryotic cells; these strategies are depicted in Figure 1.1 and outlined below.

First strategy: mitochondria can respond to variations in cellular energy status by altering NAD^+/NADH, AMP/ATP and acetyl-CoA/CoA ratios inside and outside of these organelles [3, 23, 29] (Figure 1.1). Such alterations in the relative levels of the key mitochondria-derived metabolites modulate activities of several protein sensors (including sirtuins Sirt1, Sirt3 and Sirt5 as well as the AMP-activated protein kinase and histone acetyltransferase GCN5), which then amend the extent of acetylation and phosphorylation (and thereby activities) of many downstream protein targets; this elicits a remodeling of a network of anabolic and catabolic pathways defining cellular energy status [3, 19, 23, 29-38].

Second strategy: mitochondria can generate reactive oxygen species (ROS) – mainly as by-products of mitochondrial respiration in all eukaryotes, but also via oxidation of cytochrome *c* by the inter-membrane space protein $p66^{shc}$ in mice [39-41] (Figure 1.1). If the concentration of ROS released from mitochondria exceeds a toxic threshold, ROS impair many vital cellular processes by eliciting health-demoting oxidative damage to proteins, lipids and nucleic acids in various cellular locations [39-43]. However, if the concentration of ROS released from mitochondria is sustained at a sub-lethal (hormetic) level, ROS operate as potent signaling molecules that modulate activities of some protein sensors [18, 19, 39, 42-47]. Among these ROS-modulated sensors are several protein kinases, transcription factors and antioxidant enzymes; they respond to ROS by altering activities of a network of downstream protein targets to stimulate a number of vital health-promoting cellular processes [18, 19, 39, 42-53].

Third strategy: mitochondria can synthesize and assemble iron-sulfur clusters (ISC); ISCs are cofactors of many proteins that reside in mitochondria as well as in the cytosol, nucleus and

endoplasmic reticulum (ER) [54-59] (Figure 1.1). Mitochondrial ISC proteins are essential components of the tricarboxylic acid (TCA) cycle and electron transport chain (ETC); they are also involved in the synthesis of some amino acids, heme, molybdenum cofactor, lipoic acid and biotin within mitochondria [54-59]. Cytosolic ISC proteins have been implicated in nucleotide metabolism, amino acid synthesis, iron homeostasis regulation, xenobiotic metabolism, translation initiation, tRNA modification and receptor tyrosine kinase signaling [54-59]. Nuclear ISC proteins function in DNA replication and repair, telomere maintenance, gene expression regulation, rRNA processing, and ribosome assembly [54-63].

Fourth strategy: mitochondria can respond to various stress conditions inside and outside of these organelles by releasing signaling peptides, proteins, mitochondrial DNA (mtDNA) and mtDNA fragments that act intracellularly and extracellularly to elicit cellular and organismal responses to such conditions (Figure 1.1). These mitochondria-derived stress signaling macromolecules include the following: (1) peptides formed due to the proteolytic degradation of unfolded and misfolded proteins excessively accumulated within the mitochondrial matrix; after being released from mitochondria, these peptides trigger several unfolded protein response (UPR^{mt}) pathways of mitochondria-to-nucleus communications that stimulate transcription of nuclear genes involved in mitochondrial quality control and metabolism [18, 19, 53, 64-73]; (2) humanin, an *N*-formylated peptide; after being synthesized and released by dysfunctional mitochondria in the "host" cells, humanin acts in a cell-autonomous manner to suppress apoptosis of these cells as well as in a cell-non-autonomous fashion to promote survival, reduce inflammation and maintain metabolic homeostasis of the distal cells in other tissues [72, 74-81]; (3) signaling macromolecules that belong to the "mitochondrial damage-associated molecular pattern" (mitochondrial DAMP or MTD) family and include some *N*-formylated peptides, several proteins, mtDNA and mtDNA fragments; these MTDs function cell-autonomously and cell-non-autonomously to stimulate inflammation and elicit the innate immune response by activating transcription of nuclear genes coding for pro-inflammatory cytokines [10, 12, 72, 82-89]; (4) cytochrome *c* and other pro-apoptotic proteins; after being released from mitochondria in excessively stressed cells, these mitochondria-derived proteins either trigger caspase-dependent and caspase-independent pathways of programmed apoptotic cell death or control such non-apoptotic processes as cell metabolism, cell cycle progression, inflammation, innate immune response, autophagy and programmed necrotic cell death [3, 9, 10, 12, 13, 16, 17, 23, 24]; (5) the pyruvate

dehydrogenase complex, which in cultured human cells exposed to serum, epidermal growth factor or mitochondrial stress can move from the mitochondria to the nucleus to synthesize acetyl-CoA used for histone acetylation, S phase entry and cell-cycle progression [90]; and (6) mitokines in the nematode *Caenorhabditis elegans*; after these diffusible factors of unknown chemical nature exit mildly stressed mitochondria in neuronal cells, they act in an endocrine-like fashion to activate the longevity-extending UPR^{mt} pathway of mitochondria-to-nucleus communication in intestinal cells [72, 91, 92].

Fifth strategy: the surface of mitochondria can provide an organizing platform for assembly and disassembly of several multi-protein complexes (Figure 1.1). A regulated remodeling of these protein complexes on the outer face of mitochondria has been implicated in many vital processes, including (1) cell metabolism, signaling, immune response, hypoxic response, differentiation and death; and (2) mitochondrial fusion, fission, motility, inheritance, autophagic degradation and DNA maintenance [1, 3, 9, 14, 16, 21-24, 26, 93-99].

Sixth strategy: the outer mitochondrial membrane can form zones of close apposition to the mitochondria-associated membrane (MAM) domains of other organellar and cellular membranes, including the ER, peroxisomes, vacuoles, autophagosomes, melanosomes and plasma membrane [3, 27, 28, 100-108] (Figure 1.1). The MAM domains are known to play essential roles in ATP and ROS production, mitochondrial biogenesis and morphology, mitochondrial fission and motility, ER stress regulation, cellular Ca^{2+} homeostasis, membrane phospholipids metabolism and transfer, autophagosome biogenesis, innate immune and inflammatory responses, and programmed apoptotic cell death [3, 16, 18, 21, 24-28, 100-115].

Seventh strategy: mitochondria can form small vesicles that transport distinct subsets of mitochondrial proteins and lipids to peroxisomes and lysosomes (Figure 1.1). Such vesicular transport of mitochondria-derived protein and lipid cargos has been implicated in mitochondrial quality control; it may also play a role in peroxisome biogenesis and function [116-121].

Because mitochondrial functionality is vital to organismal physiology and health, mitochondrial dysfunction is a cause of numerous human mitochondrial disorders; these inborn disorders are due to mutations in nuclear genes and/or mtDNA, affect various tissues and organs, and exhibit a wide spectrum of clinical features [3, 4, 122-125]. Furthermore, mitochondrial dysfunction has been implicated in a variety of common human disorders, such as metabolic syndrome, obesity, type 2 diabetes, cardiomyopathies, neurodegenerative disorders and cancer [3,

[5, 10, 15, 34, 126-131]. Most of these common human disorders are aging-associated pathologies; moreover, a gradual deterioration of mitochondrial function is a distinctive and, likely, a causative feature of aging in eukaryotic organisms across phyla [2, 10, 18, 19, 132, 133]. Therefore, an age-related progressive decline in mitochondrial function is considered as one of the hallmarks of cellular and organismal aging in evolutionarily distant eukaryotes [133]. Studies of the budding yeast *Saccharomyces cerevisiae*, a unicellular eukaryote, have provided insights into mechanisms linking mitochondrial functionality and cellular aging [2, 18-20, 134-140].

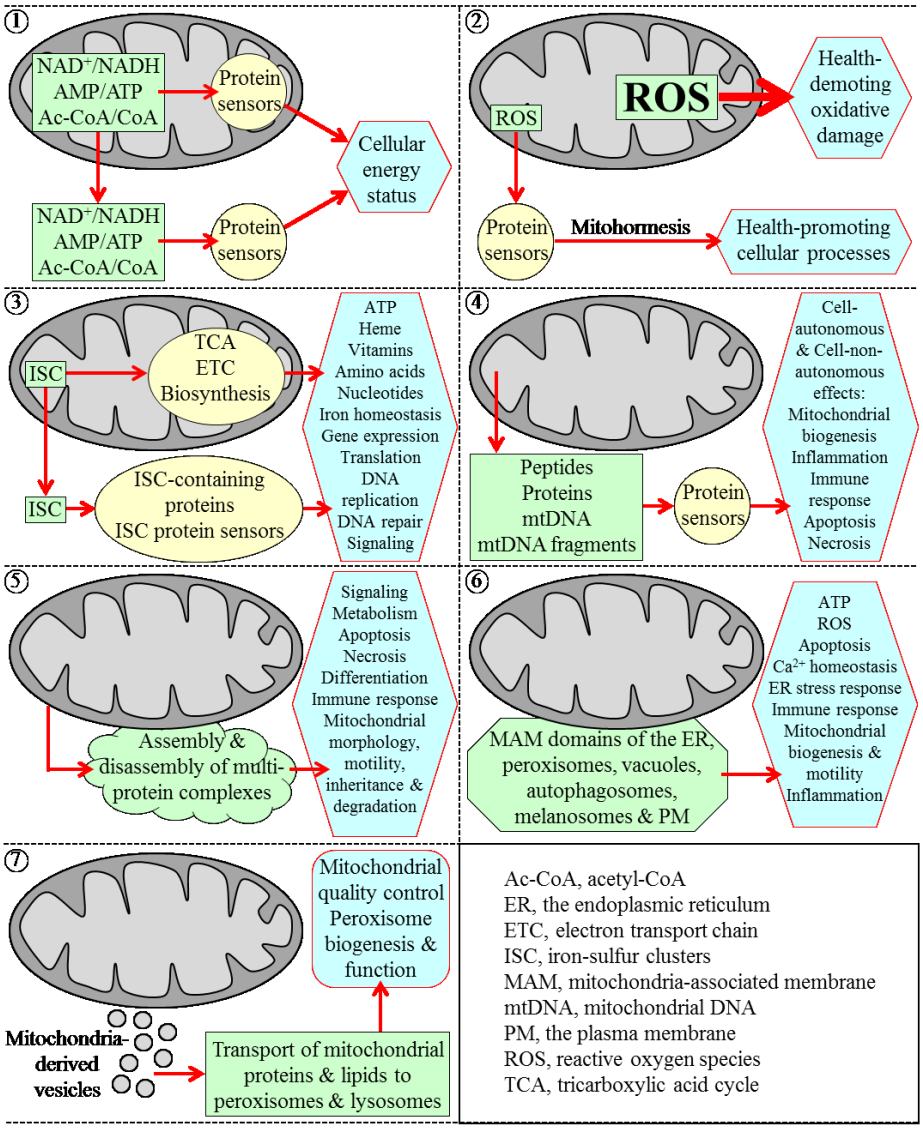

Figure 1.1. Seven strategies allow mitochondria to operate as intracellular signaling compartments and organizing platforms that orchestrate cellular responses to changes in physiological conditions.

Strategy 1: mitochondria can change NAD+/NADH, AMP/ATP and acetyl-CoA/CoA ratios inside and outside of mitochondria, thus enabling these key metabolites to modulate activities of several protein sensors. These sensors then alter cellular energy status by amending activities of proteins involved in various metabolic pathways. Strategy 2: mitochondria can generate and release reactive oxygen species (ROS). If the concentration of ROS released from mitochondria surpasses a toxic threshold, ROS cause health-demoting oxidative damage to cellular macromolecules. In contrast, if it is maintained at a sub-lethal (hormetic) level, ROS modulate activities of several protein sensors, which then alter activities of many protein targets to accelerate health-promoting cellular processes. Strategy 3: mitochondria can synthesize and assemble iron-sulfur clusters (ISC). ISCs are essential cofactors of numerous proteins located inside and outside of mitochondria; these proteins are involved in many cellular processes. Strategy 4: mitochondria can release peptides, proteins, mitochondrial DNA (mtDNA) and mtDNA fragments. These mitochondria-derived signaling macromolecules act in a cell-autonomous and cell-non-autonomous manner to elicit changes in vital processes that take place within the "host" cells and within the distal cells in other tissues. Strategy 5: mitochondrial surface can serve as an organizing platform for assembly and disassembly of multi-protein complexes implicated in a number of essential processes. Strategy 6: mitochondria can form zones of close apposition to the mitochondria-associated membrane (MAM) domains of other organellar and cellular membranes. These MAM domains are known for their essential roles in many cellular processes. Strategy 7: mitochondria can form small vesicles. These vesicles deliver certain proteins and lipids to lysosomes and peroxisomes, thereby enabling mitochondrial quality control and playing a role in peroxisome biogenesis and function. See the text for additional details.

1.1.1 The yeast *S. cerevisiae* is a beneficial model organism for elucidating mechanisms of cellular aging in multicellular eukaryotes

Aging of budding yeast is studied using robust assays. These assays are carried out under controllable laboratory conditions and measure two different aspects of the aging process in *S. cerevisiae*. Some of these assays monitor the replicative lifespan of yeast by measuring how many asymmetric mitotic divisions a mother cell could undergo before cell cycle arrest; replicative aging of yeast is believed to model aging of mitotic (i.e. capable of dividing) human cell types, such as fibroblasts, granulocytes, monocytes, lymphocytes and stem cells from amniotic fluid [137, 141-144]. Other assays monitor the chronological lifespan of yeast by measuring how long a cell remains viable after cell cycle arrest; chronological aging of yeast is likely to mimic aging of post-mitotic (i.e. incapable of dividing) human cell types, such as mature neurons, adipocytes and mature muscle cells [137, 143, 145-147]. *S. cerevisiae* has relatively short replicative and chronological lifespans; moreover, it is amenable to comprehensive biochemical, molecular biological and cell biological analyses [137, 142, 146, 148-151]. Because of these beneficial

features of *S. cerevisiae* as a model for unveiling mechanisms of aging in multicellular eukaryotes, the baker's yeast has is an invaluable tool employed to discover genes, signaling pathways and chemical compounds that govern longevity-defining cellular processes in eukaryotic organisms across phyla [18-20, 137, 143, 144, 146, 147, 150, 152-162].

1.1.2 Mitochondria are signaling organelles that establish the rate of cellular aging in yeast by orchestrating many processes outside of mitochondria

A body of recent evidence implies that alterations in certain traits of mitochondrial functionality early in life of replicatively or chronologically aging yeast impact many cellular processes outside of mitochondria, thereby orchestrating a stepwise development of a longevity-defining cellular pattern and its maintenance throughout lifespan. The molecular mechanisms underlying the essential role of mitochondria as signaling organelles in yeast aging have begun to emerge; they involve unidirectional and bidirectional communications between mitochondria and other cellular compartments. These mechanisms are discussed below.

1.1.3 Mechanisms underlying the essential role of mitochondria in yeast replicative aging

A mitotically competent mother yeast cell progresses through three consecutive stages of replicative aging before becoming unable to produce daughter cells; these stages are called "early age", "intermediate age" and "late age" [20, 144]. Characteristic features of the intermediate-age stage of replicative aging include a decline in mitochondrial respiration and the resulting reduction of mitochondrial membrane potential [20, 144, 163] (Figure 1.2A). A replicatively aging mother yeast cell responds to such reduction of mitochondrial membrane potential by activating the Rtg2 protein in the cytosol; a mechanism underlying such activation remains to be established [136, 138, 164]. Rtg2 is essential for reducing the rate of yeast replicative aging because this protein (1) triggers the mitochondrial retrograde signaling pathway by stimulating nuclear import of the Rtg1-Rtg3 heterodimeric transcription factor; this factor then orchestrates an anti-aging transcriptional program by activating expression of many nuclear genes involved in carbohydrate and nitrogen metabolism, peroxisomal fatty acid oxidation and anaplerotic reactions, peroxisome proliferation, stabilization of nuclear and mitochondrial genomes, and stress response [136, 138, 164]; and (2) is imported into the nucleus, where it increases genome stability and also slows down the synthesis of extrachromosomal rDNA circles known to be one

of the "aging factors" limiting the replicative lifespan of the mother cell [136, 138, 164] (Figure 1.2A). The reduction of mitochondrial membrane potential during the intermediate-age stage of replicative aging slows down the aging process not only by activating the two Rtg2-driven mechanisms but also by inhibiting the target of rapamycin (TOR) complex 1 protein kinase activity [136, 138, 164] (Figure 1.2A); a mechanism of such inhibition of this key component of the pro-aging TOR signaling pathway is unknown. Moreover, the decline in mitochondrial membrane potential during the intermediate-age stage of replicative aging also decelerates mitochondrial synthesis of ISCs and/or slows down their efflux from mitochondria [60] (Figure 1.2A). Because ISCs are essential cofactors of nuclear proteins that in yeast are involved in DNA replication, DNA repair and telomere maintenance, their reduced quantity in replicatively aging yeast compromises genome integrity [18, 20, 60, 62]. Moreover, because ISCs mitigate activity and/or decelerate nuclear import of the transcription activator Aft1, their reduced quantity in replicatively aging yeast allows Aft1 to stimulate expression of nuclear genes needed for iron entry into and distribution within the cell; the ensuing rise in free intracellular iron accelerates replicative aging by promoting iron-driven oxidative damage of many cellular proteins [18, 56, 60].

During the intermediate-age stage of replicative aging, mitochondria in the mother cell not only exhibit reduced membrane potential but also generate elevated quantities of ROS and undergo fragmentation; during the subsequent late-age stage of replicative aging, the functionality of mitochondria is further declined as these organelles accumulate excessive levels of ROS, aggregate and fail to keep mtDNA [18, 20, 144, 163, 165-168] (Figure 1.2B). The dysfunctional mitochondria exhibiting these age-related traits of deteriorated functionality are known to be one of the aging factors limiting the replicative lifespan of the mother cell [20, 137, 141, 144, 161, 163]. A mechanism exists for retaining these dysfunctional mitochondria within the mother cell, thus preventing their transmission into the daughter cell. In this mechanism, the dysfunctional mitochondria move from the mother cell to the daughter cell slower than their fully functional counterparts; such movement of mitochondria on actin cables is driven by the sirtuin Sir2 and type V myosin motor Myo2 [20, 165, 169-171] (Figure 1.2B).

The rate of yeast replicative aging is also modulated by the quantity of the Afo1 protein component of the large subunit of the mitochondrial ribosome; such modulation is not due to an effect of variations in Afo1 quantities on the efficiency of protein synthesis in mitochondria [2, 18, 172, 173]. The absence of Afo1 in mitochondria of replicatively aging yeast elicits the following

alterations in two signaling pathways of longevity regulation: (1) the anti-aging "back signaling" pathway is activated, thus enabling the Sfp1 protein to stimulate transcription of nuclear genes coding for protein components of cytoplasmic ribosomes [2, 18, 172]; and (2) the pro-aging TOR signaling pathway is inhibited, thus allowing to slow down the pro-aging process of protein synthesis in the cytosol and also to accelerate the anti-aging processes of autophagy, protein synthesis in mitochondria and transcription of many nuclear genes involved in cellular stress response [2, 18, 172] (Figure 1.2C).

Another group of mitochondrial processes that contribute to yeast replicative aging include the processing, stabilization and translational activation of mRNAs encoded by mtDNA; these processes are orchestrated by mitochondrial proteins constituting the so-called mitochondrial translation control (MTC) module [18, 173-177] (Figure 1.2D). In the absence of any of these MTC proteins, the replicative aging of yeast is decelerated via the following two mechanisms: (1) the Pnc1- and Sir2-driven inhibition of the synthesis of extrachromosomal rDNA circles, one of the aging factors known to limit the replicative lifespan of the mother cell [18, 176]; and (2) a decrease in the cellular concentration of cAMP and the ensuing attenuation of the cAMP-dependent protein kinase A (PKA) activity known to decelerate the anti-aging processes of autophagy and transcription of many stress-response genes in the nucleus as well as to accelerate the pro-aging process of protein synthesis in the cytosol [18, 137, 173, 176] (Figure 1.2D).

The maintenance of protein homeostasis (proteostasis) in mitochondria also contributes to the essential role of these organelles as signaling compartments in yeast replicative aging [2, 18, 20, 178-180]. One of the mitochondrial protein components implicated in maintaining mitochondrial proteostasis is the m-AAA protease Afg3. It is actively involved in several proteostatic processes within the inner mitochondrial membrane – including degradation of misfolded proteins, assembly of several ETC protein complexes and processing of a protein component of the large subunit of the mitochondrial ribosome [178, 179] (Figure 1.2E). These Afg3-driven proteostatic processes in mitochondria increase the rate of yeast replicative aging, likely because of their demonstrated ability to promote such pro-aging processes outside of mitochondria as protein synthesis in the cytosol and the accumulation of unfolded proteins in the ER [180].

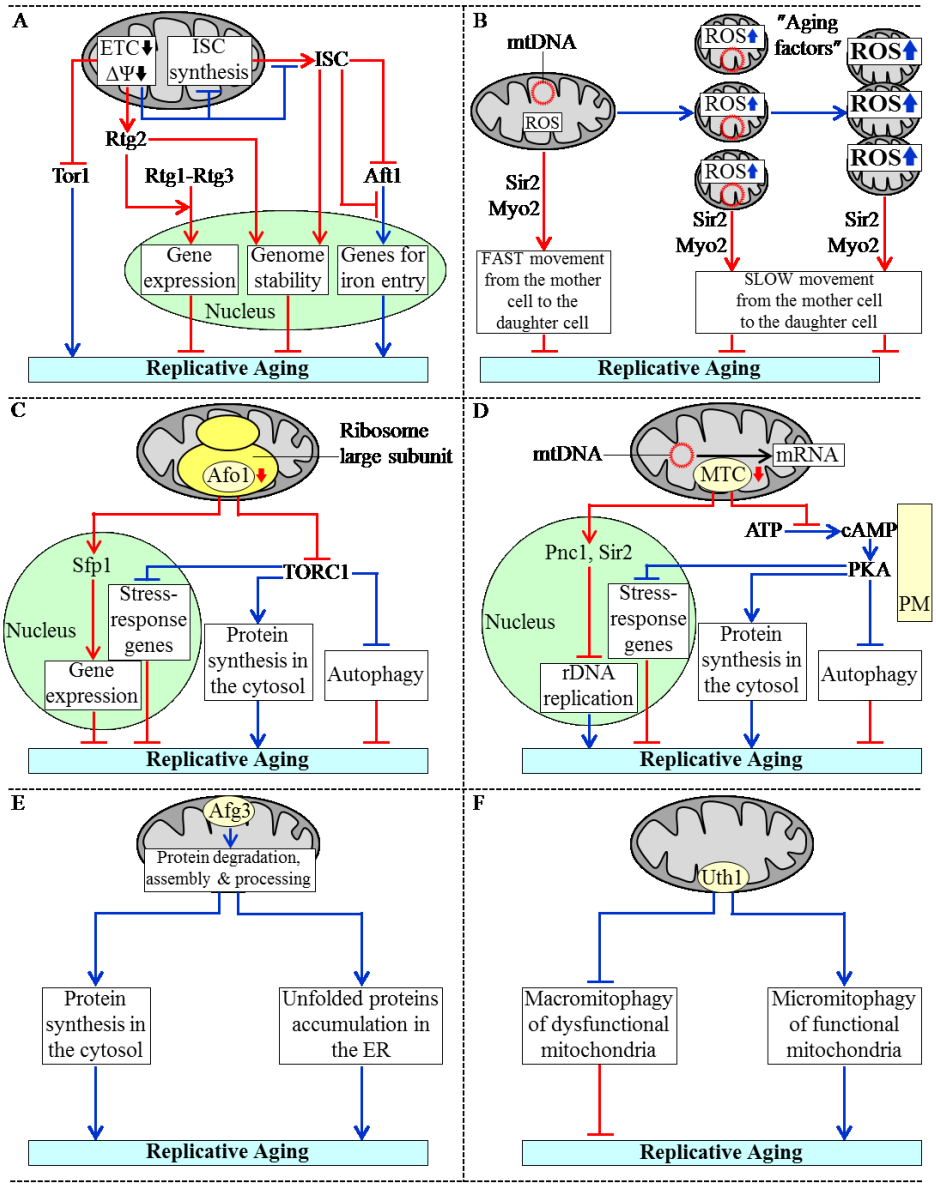

Figure 1.2. Mechanisms underlying the essential role of mitochondria in yeast replicative aging.

(A) A decline in the mitochondrial electron transport chain (ETC) and the resulting reduction of mitochondrial membrane potential (ΔΨ) delay replicative aging in yeast by: (1) stimulating Rtg2-dependent nuclear import of the Rtg1-Rtg3 heterodimeric transcription factor, thereby activating the mitochondrial retrograde signaling pathway; (2) promoting the import of Rtg2 into the nucleus, where it increases genome stability; and (3) reducing a protein kinase activity of the target of rapamycin protein 1 (Tor1). The reduction of ΔΨ also attenuates mitochondrial synthesis and/or export of iron-sulfur clusters (ISC), which are needed for maintaining genome stability and inhibiting the Aft1-diven transcription of nuclear genes involved in iron entry into the cell. (B) A transition from the early-age stage to the intermediate-age stage of replicative aging coincides with a rise of mitochondrial reactive oxygen species (ROS) and fragmentation of mitochondria in the mother cell; these fragmented mitochondria produce more ROS, aggregate and lose mitochondrial DNA (mtDNA) during the subsequent late-age stage of replicative aging.

The dysfunctional mitochondria formed during the intermediate-age and late-age stages of replicative aging are so-called ″aging factors″. They limit the replicative lifespan of the mother cell; their Sir2- and Myo2-driven movement to the daughter cell occurs slower than that of fully functional mitochondria. (C) A reduction in the quantity of the Afo1 protein component of the large subunit of the mitochondrial ribosome delays replicative aging in yeast by: (1) stimulating Sfp1-driven transcription of nuclear genes encoding protein components of cytoplasmic ribosomes; and (2) attenuating the TOR signaling pathway, which accelerates the pro-aging process of protein synthesis in the cytosol and also slows down the anti-aging processes of autophagy and transcription of stress-response genes in the nucleus. (D) Mitochondrial translation control (MTC) proteins assist in processing, stabilization and translation of mRNAs encoded by mtDNA. A reduction in the quantity of MTC proteins slows down replicative aging in yeast by: (1) triggering the Pnc1- and Sir2-dependent inhibition of the synthesis of extrachromosomal rDNA circles; and (2) reducing the cellular concentration of cAMP and thus attenuating the cAMP-dependent protein kinase A (PKA) activity, which decelerates the anti-aging processes of autophagy and transcription of stress-response genes in the nucleus and also accelerates the pro-aging process of protein synthesis in the cytosol. (E) Afg3 is a mitochondrial protease involved in maintaining protein homeostasis (proteostasis) in mitochondria. The Afg3-driven processes in mitochondria include degradation of misfolded proteins, assembly of ETC protein complexes and processing of a protein component of the large subunit of the mitochondrial ribosome; these proteostatic processes within mitochondria stimulate such pro-aging processes outside of these organelles as protein synthesis in the cytosol and the accumulation of unfolded proteins in the endoplasmic reticulum (ER). (F) The Uth1 protein in the outer mitochondrial membrane is a pro-aging factor that accelerates replicative aging in yeast by concurrently weakening macromitophagic degradation of dysfunctional mitochondria and enhancing micromitophagic degradation of functional mitochondria. Activation arrows and inhibition bars denote pro-aging processes (displayed in blue color) or anti-aging processes (displayed in red color). See the text for additional details.

Finally, it seems that the quantity of the Uth1 protein in the outer mitochondrial membrane is inversely proportional to the efficiency with which only dysfunctional mitochondria exhibiting the age-related traits of deteriorated functionality are degraded within vacuoles of replicatively aging yeast. Indeed, it has been shown that lack of Uth1 (1) impairs micromitophagy, an autophagic mode of non-selective vacuolar degradation of both functional and dysfunctional mitochondria; and (2) does not affect macromitophagy, an autophagic mode of selective vacuolar degradation of only dysfunctional mitochondria [181-183]. Importantly, lack of Uth1 also extends longevity of replicatively aging yeast [181-183]. Thus, Uth1 may function as a pro-aging protein factor on the surface of mitochondria; any intervention that reduces its abundance is therefore expected to delay replicative aging in yeast by concomitantly enhancing macromitophagic degradation of dysfunctional mitochondria and weakening micromitophagic degradation of functional mitochondria [18, 182] (Figure 1.2F).

1.1.4 Mechanisms by which mitochondrial functionality impacts chronological aging of yeast

A culture of chronologically aging yeast in a liquid medium progresses through a series of critical lifespan periods that define its longevity; we have recently proposed to use the term "lifespan checkpoint" (or simply "checkpoint") for describing each of these consecutive periods of yeast chronological lifespan [18-20, 145, 184]. The early-life checkpoints exist in logarithmic (L), diauxic (D) and post-diauxic (PD) growth phases; the late-life checkpoints take place in stationary (ST) phase of culturing [19, 20, 184]. A recently proposed concept of a "biomolecular network" posits that the rate and efficiency of progression through each of these lifespan checkpoints are monitored and/or modulated by a distinct set of checkpoint-specific "master regulator" proteins and protein complexes; a synergistic action of such master regulators defines longevity of chronologically aging yeast by orchestrating a stepwise development of a pro- or anti-aging cellular pattern [19, 20, 184]. A body of recent evidence supports the notion that different, age-related functional states of mitochondria define longevity of chronologically aging yeast by playing essential roles at several of the early-life and late-life checkpoints; this evidence is discussed below.

It seems that the earliest lifespan checkpoint defined by certain traits of mitochondrial functionality exists in L growth phase [19, 20, 145, 155, 184-188]; we call it "checkpoint 1". At checkpoint 1, the rapamycin-sensitive protein kinase TOR1 (a key component of the pro-aging TOR pathway) attenuates mitochondrial synthesis of oxidative phosphorylation (OXPHOS) enzymes that are encoded by mtDNA [185-188]. The extent of such attenuation (1) is modulated by variations in cellular energy status; and (2) establishes a certain rate of coupled mitochondrial respiration and a certain value of mitochondrial membrane potential; both these key traits of mitochondrial functionality define longevity of chronologically aging yeast cells - in part by influencing stress resistance of such cells [19, 20, 145, 155, 185-188]. The rate of coupled mitochondrial respiration and the value of mitochondrial membrane potential at checkpoint 1 are also modulated by caloric restriction, a longevity-extending dietary regimen whose impact on these characteristic traits of mitochondrial functionality at checkpoint 1 is mediated in part by its inhibitory effect on Tor1 [19, 20, 137, 155, 185-188].

Mitochondria, along with the pentose phosphate pathway, generate NADPH [189-191]. In mitochondria of chronologically "young" yeast cells, this primary source of cellular reducing

equivalents is produced in two reactions of the TCA cycle as well as in reactions catalyzed by an acetaldehyde dehydrogenase and an NADH kinase [189-191]. NADPH drives reductive reactions of the biosynthetic pathways for amino acids, fatty acids and sterols [189-191]; moreover, NADPH is also an electron donor for thioredoxin and glutathione reductase systems that maintain cellular redox homeostasis [189, 191]. At lifespan checkpoint 2, which exists in D and PD growth phases, these two enzymatic systems play essential roles in delaying yeast chronological aging because they both reduce the extent of oxidative damage to many thiol-containing proteins in the mitochondria, nucleus and cytosol [19, 20, 191].

The rate of coupled mitochondrial respiration in yeast cells progressing through D and PD growth phases defines their chronological lifespan in part by modulating cellular concentration of trehalose [19, 20, 145, 188, 192]. A lifespan checkpoint at which coupled mitochondrial respiration is linked to the maintenance of cellular trehalose homeostasis is called checkpoint 3 [19, 20]. Trehalose is a non-reducing disaccharide that controls cellular proteostasis (i.e. a dynamic balance between protein folding, misfolding, unfolding, refolding, oxidative damage, solubility and aggregation) throughout lifespan of chronologically aging yeast [19, 192].

A distinct lifespan checkpoint, which we call checkpoint 4, is defined by the concentration of ROS produced by and released from mitochondria in chronologically "young" yeast cells; this checkpoint exists in D and PD growth phases [19, 20, 139, 140, 145, 193-195]. If the concentration of mitochondria-derived ROS in such cells is maintained at a hormetic level, these ROS act as signaling molecules that extend yeast longevity by: (1) stimulating the transcription factors Gis1, Msn2 and Msn4, which respond by activating expression of many nuclear genes known for their essential longevity-extending roles in nutrient sensing, carbohydrate metabolism, stress resistance and survival [140, 194-197]; and (2) triggering the anti-aging Tel1-Rad53-Rph1 signaling pathway, which in response reduces the extent of damage to telomeric DNA by attenuating transcription of subtelomeric chromatin regions in the nucleus [140, 194, 195].

The abilities of mitochondria to convert some of the intermediates of the TCA cycle into amino acids and to release these amino acids [189, 190, 198] define lifespan checkpoint 5, which exists in D and PD growth phases [18, 19]. Following their release from mitochondria, some of these amino acids stimulate protein kinase Tor1; the ensuing activation of the pro-aging TOR signaling pathway accelerates chronological aging by promoting protein synthesis in the cytosol, attenuating protein synthesis in mitochondria, slowing down transcription of many nuclear genes

involved in stress response, and hindering autophagic degradation of dysfunctional organelles and macromolecules [18, 19, 185, 186, 198-203]. Transcription of stress-response genes in the nucleus and autophagy in the cytoplasm are also attenuated by the pro-aging cAMP/PKA (cAMP/protein kinase A) signaling pathway, which overlaps with the TOR pathway [18, 19, 137, 154, 201, 203].

The fragmentation of a tubular mitochondrial network into individual mitochondria and the efflux of some proteins (including cytochrome c as well as the "moonlighting" endonucleases Aif1 and Nuc1) from the fragmented mitochondria take place in chronologically "old" yeast cells that enter ST growth phase; these characteristic changes in mitochondrial morphology limit yeast chronological lifespan by eliciting the caspase-dependent and caspase-independent pathways of apoptotic programmed cell death (PCD) [19, 145, 155, 204-209]. A lifespan checkpoint at which such age-related changes in mitochondrial morphology are linked to age-related forms of mitochondria-controlled apoptotic PCD exists in ST growth phase; we call it checkpoint 6 [19, 20, 145].

A lifespan checkpoint at which several distinct traits of mitochondrial functionality and homeostasis are linked to an age-related "liponecrotic" form of PCD is called checkpoint 7; it exists in ST growth phase [19, 20, 210, 211]. These traits include (1) the efficiency with which mitochondria generate energy needed for the detoxification of non-esterified fatty acids through their incorporation into neutral lipids; an age-related decline in such efficiency accelerates age-related liponecrotic PCD by causing the excessive accumulation of monounsaturated fatty acids in cellular membranes; (2) the efficiencies with which mitochondria produce and release ROS; an age-related rise in such efficiencies above a threshold accelerates age-related liponecrotic PCD by causing oxidative damage to cellular macromolecules and organelles; and (3) the efficiency with which aged and dysfunctional mitochondria undergo an Atg32- and Aup1-driven selective autophagic degradation; an age-related decline in such efficiency accelerates age-related liponecrotic PCD by impairing the maintenance of a healthy population of fully functional mitochondria [18-20, 158, 159, 182, 210-215].

Some traits of mitochondrial functionality have not been linked to a particular lifespan checkpoint yet and may be associated with more than one of such checkpoints in chronologically aging yeast. One of these traits is the maintenance of mitochondrial genome integrity and copy number; the essential role of this trait in defining the rate of chronological aging depends on the mitochondrial base-excision repair enzyme Ntg1 [195]. It seems conceivable that an aging-

associated mitigation of the Ntg1-governed pathway for maintaining mitochondrial genome integrity and copy number may underlie such longevity-shortening process observed in chronologically aging yeast as an age-related rise in the rates of mtDNA fragments migration to the nucleus and in their insertion into nuclear DNA [216, 217]. The ensuing reduction of nuclear genome stability is an important contributing factor to chronological aging in yeast [18, 19, 195, 216, 217]. Of note, the Ntg1-governed pathway: (1) overlaps with a branch of the pro-aging TOR signaling pathway which at checkpoint 1 operates in attenuating mitochondrial synthesis of mtDNA-encoded OXPHOS enzymes; (2) modulates the anti-aging Tel1-Rad53-Rph1 signaling pathway which at checkpoint 4 responses to hormetic concentrations of mitochondria-generated ROS by decreasing the extent of damage to telomeric DNA [140, 194, 195]. These observations further support the notion that the Ntg1-dependent maintenance of mitochondrial genome integrity and copy number is a trait of mitochondrial functionality that may be associated with more than one of the lifespan checkpoints in chronologically aging yeast.

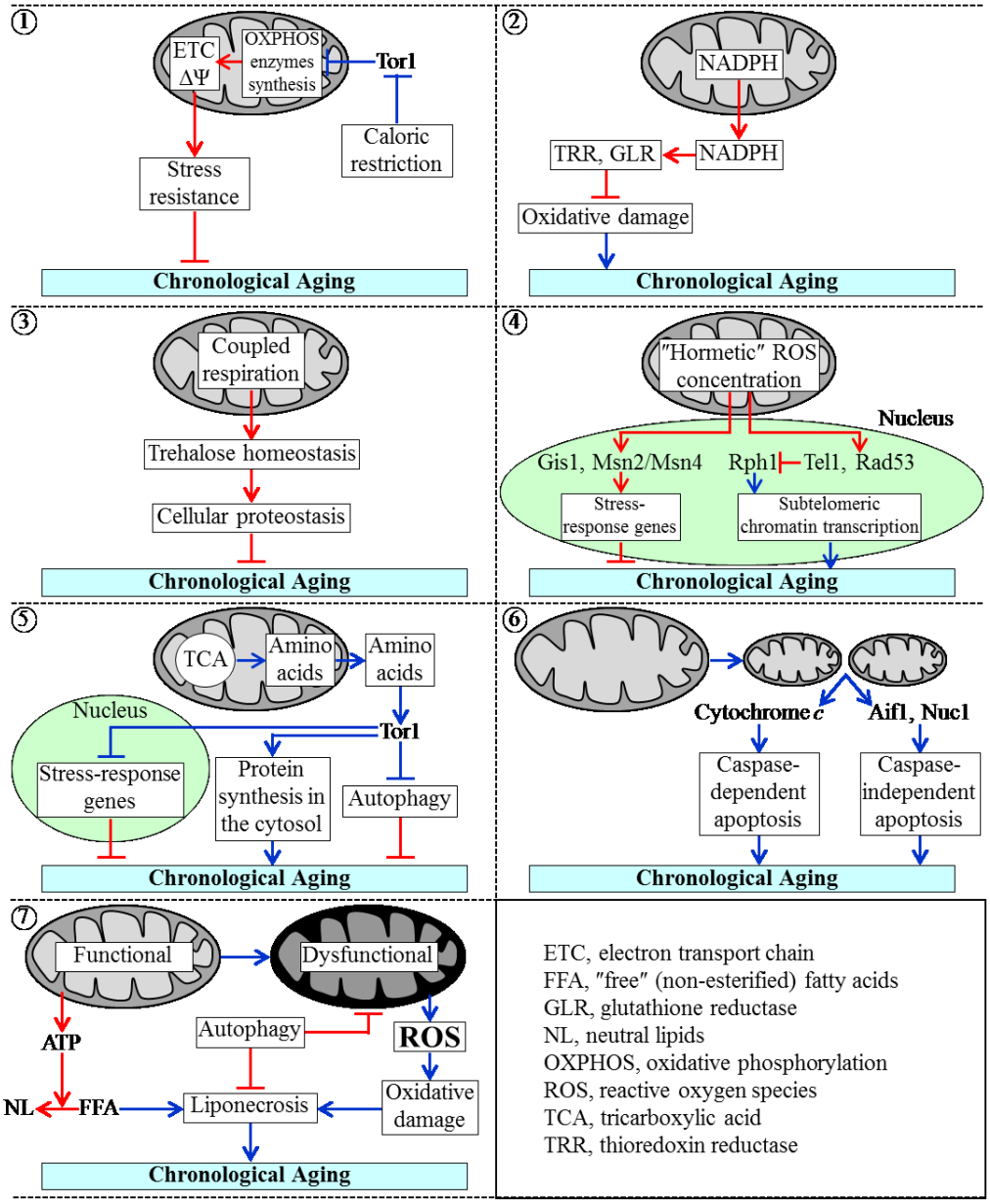

Figure 1.3. A chronologically aging culture of yeast cells progresses through at least seven consecutive "checkpoints", each of which defines yeast longevity.

Checkpoint 1: The protein kinase Tor1 mitigates the synthesis of mitochondrial DNA-encoded enzymes of the oxidative phosphorylation (OXPHOS) system in mitochondria, thereby allowing to set up a certain rate of electron flow through the mitochondrial electron transport chain (ETC) and a certain value of mitochondrial membrane potential (ΔΨ). These two traits of mitochondrial functionality establish a magnitude of cell resistance to stresses and, thus, define the chronological lifespan of yeast. Caloric restriction extends yeast chronological lifespan by suppressing Tor1. Checkpoint 2: Mitochondria-generated NADPH is an electron donor for thioredoxin and glutathione reductase (TRR and GLR, respectively) systems outside of mitochondria. Both these systems delay yeast chronological aging by reducing the degree of oxidative damage to many proteins in various cellular locations.

Checkpoint 3: The efficiency of coupled mitochondrial respiration defines the cellular concentration of trehalose, which in chronologically ″young″ yeast cells acts as a longevity-extending metabolite by enhancing cellular proteostasis. Checkpoint 4: If mitochondria-generated reactive oxygen species (ROS) in chronologically "young" yeast cells are maintained at a "hormetic" level, ROS extend chronological lifespan by: (1) activating the transcription factors Gis1, Msn2 and Msn4, which promote expression of many longevity-extending nuclear genes; and (2) stimulating the longevity-extending Tel1-Rad53-Rph1 signaling pathway, which reduces the extent of damage to telomeric DNA in the nucleus. Checkpoint 5: Amino acids that are synthesized in and released from mitochondria activate the TOR signaling pathway, which accelerates chronological aging by simulating protein synthesis in the cytosol, attenuating transcription of many stress-response genes in the nucleus, and suppressing autophagy of dysfunctional organelles and macromolecules. Checkpoint 6: A release of cytochrome c, Aif1 and Nuc1 from fragmented mitochondria in chronologically "old" yeast cells stimulates caspase-dependent and caspase-independent modes of apoptotic cell death, thus limiting yeast chronological lifespan. Checkpoint 7: Yeast chronological lifespan is shortened by "liponecrosis", a mode of cell death that in chronologically "old" yeast cells is triggered due to (1) a reduced ability of mitochondria to generate ATP for the incorporation of non-esterified (″free″) fatty acids (FFA) into neutral lipids (NL); (2) a decline in the efficiency of an autophagic degradation of aged and dysfunctional mitochondria; and (3) a rise in the efficiencies with which mitochondria generate and release ROS. Activation arrows and inhibition bars denote pro-aging processes (displayed in blue color) or anti-aging processes (displayed in red color). See the text for additional details.

Another trait of mitochondrial functionality that may define more than one of the lifespan checkpoints in chronologically aging yeast is the lipid compositions of both mitochondrial membranes. Indeed, lithocholic bile acid (LCA) extends yeast chronological lifespan by eliciting an age-related remodeling of the mitochondrial membrane lipidome [139, 193, 218]. Such remodeling is likely to be responsible for the age-related changes in mitochondrial size, number and morphology observed in chronologically aging yeast cells exposed to LCA, as well as for LCA-driven alterations in the age-related dynamics of mitochondrial respiration, membrane potential, ATP synthesis and ROS homeostasis seen in these cells [139, 193, 218]. Recent data suggest that these characteristic changes in the mitochondrial membrane lipidome and functionality elicited by LCA in chronologically aging yeast cells enable mitochondria to operate as signaling organelles that modulate activities of several transcription factors linked to some of the above lifespan checkpoints; these factors respond by altering transcription of many longevity-defining nuclear genes, thus establishing an anti-aging transcriptional program [219].

1.2 Thesis outline and contributions of colleagues

Chapter 2 describes how I used a combination of subcellular fractionation by differential centrifugation, organelle separation by equilibrium density gradient centrifugation, fractionation of purified mitochondria into various subcompartments and quantitative mass spectrometric analysis to make an initial step towards establishing a mechanism by which lithocholic bile acid (LCA) extends longevity of chronologically aging yeast limited in calorie supply. I carried out all of the experiments described in this chapter of my thesis and wrote the first draft of it. Findings described in Chapter 2 provide evidence that exogenously added LCA enters yeast cells, is sorted only to mitochondria, resides mainly in the inner mitochondrial membrane and also associates with the outer membrane of mitochondria. All findings described in Chapter 2 have been published in *Aging*: Beach, A., Richard, V.R., Leonov, A., Burstein, M.T., Bourque, S.D., Koupaki, O., Juneau, M., Feldman, R., Iouk, T., Titorenko, V.I. Mitochondrial membrane lipidome defines yeast longevity. *Aging* **5,** 551–574 (2013), along with data that were attained by other co-authors on the manuscript and that are not presented in Chapter 2 of this thesis. Dr. Titorenko provided intellectual leadership of this project; he also edited the first draft of Chapter 2 and the entire manuscript of the above article.

Findings presented in Chapter 3 support the validity of my hypothesis that the LCA-elicited changes in the membrane lipidome of mitochondria alter the age-related dynamics of several longevity-defining mitochondrial processes. These processes include mitochondrial respiration, maintenance of mitochondrial membrane potential and ROS homeostasis, prevention of excessive oxidative damage to mitochondrial macromolecules, preservation of certain respiratory supercomplexes in the inner mitochondrial membrane, and ATP synthesis. All findings described in Chapter 3, along with data attained by others and therefore not presented here, are included into a manuscript that is currently in preparation and will be submitted for publication in May or June of 2015. Dr. Titorenko provided intellectual leadership of this project; he also edited the first draft of Chapter 3.

Findings described in Chapter 4 provide conclusive evidence in strong support of my hypothesis in which the longevity-extending potential of LCA is due in part to its ability to alter the age-related dynamics of mitochondrially produced ROS in both chronologically ″young″ and ″old″ cells, thus reducing the damaging effect of these ROS in ″young″ cells and amplifying their ″hormetic″ effect in ″old″ cells. All findings described in Chapter 4, along with data attained by

others and therefore not presented here, are included into a manuscript that is currently in preparation and will be submitted for publication in May or June of 2015. Dr. Titorenko provided intellectual leadership of this project; he also edited the first draft of Chapter 4.

Chapter 5 describes how, using quantitative mass spectrometry, I demonstrated that LCA alters the age-related dynamics of changes in levels of many mitochondrial proteins, as well as numerous proteins in cellular locations outside of mitochondria. Findings presented in this Chapter suggest that LCA-driven changes in mitochondrial lipidome alter mitochondrial proteome and functionality, thereby enabling mitochondria to operate as signaling organelles that orchestrate an establishment of an anti-aging transcriptional program for many longevity-defining nuclear genes. Based on these findings, in Chapter 5 of my thesis I proposed a model for how such LCA-driven changes early and late in life of chronologically aging yeast cause a stepwise development of an anti-aging cellular pattern and its maintenance throughout lifespan. All findings described in Chapter 5, along with data attained by others and therefore not presented here, are included into a manuscript that has been recently submitted to *Cell Cycle*. Dr. Titorenko provided intellectual leadership of this project; he also edited the first draft of Chapter 5.

Findings presented in Chapter 6 imply that mitophagy, a selective autophagic degradation of aged and dysfunctional mitochondria, is a longevity assurance process that in chronologically aging yeast underlies the synergistic beneficial effects of anti-aging dietary and pharmacological interventions (such as caloric restriction and LCA) on lifespan. All findings described in this Chapter of my thesis have been published in *Aging:* Richard, V.R., Leonov, A., Beach, A., Burstein M.T., Koupaki, O., Gomez-Perez, A., Levy, S., Pluska, L., Mattie, S., Rafesh, R., Iouk, T., Sheibani, S., Greenwood, M., Vali, H., Titorenko, V.I. Macromitophagy is a longevity assurance process that in chronologically aging yeast limited in calorie supply sustains functional mitochondria and maintains cellular lipid homeostasis. *Aging (Albany NY)* **5,** 234–269 (2013), along with data that were attained by other co-authors on the manuscript and that are not presented in Chapter 6 of this thesis. Dr. Titorenko provided intellectual leadership of this project; he also edited the first draft of Chapter 6 and the entire manuscript of the above article.

In Chapter 7 of my thesis I summarized the evidence that peroxisomes are dynamically integrated into an endomembrane system that governs cellular aging, discussed various strategies through which peroxisomes are integrated into such endomembrane system, critically evaluated

mechanisms underlying each of these strategies, and analyzed the age-related dynamics of communications between peroxisomes and other cellular compartments composing the longevity-defining endomembrane system. In this Chapter, I also outlined recent progress in understanding how communications between peroxisomes and other cellular compartments within this endomembrane system influence the development of a pro- or anti-aging cellular pattern. Based on the available evidence, I proposed a model for the integration of peroxisomes into the endomembrane system governing cellular aging. Chapter 7 has been published as a review article in *Frontiers in Physiology*: Beach, A., Burstein, M.T., Richard, V.R., Leonov, A., Levy, S., Titorenko, V.I. Integration of peroxisomes into an endomembrane system that governs cellular aging. *Front Physiol* **3,** 283 (2012). Dr. Titorenko provided intellectual leadership of this project; he also edited the first draft of Chapter 7 and the entire manuscript of the above review article.

All of the abbreviations, citations, and the numbering of figures and tables that have been taken from either published papers or manuscripts in preparation have been edited to match the formatting and style of this thesis.

2 Exogenously added lithocholic acid (LCA) enters yeast cells, is sorted to mitochondria, resides mainly in the inner mitochondrial membrane and also associates with the outer mitochondrial membrane

2.1 Introduction

The Titorenko laboratory has recently identified lithocholic acid (LCA), a bile acid, as a natural compound that acts synergistically with caloric restriction (CR) to cause a substantial increase in yeast chronological lifespan under longevity-extending CR conditions [155]. This chapter summarizes my studies that led to the establishment of the mechanism through which LCA extends longevity by altering lipid compositions of mitochondrial membranes and amending mitochondrial functionality in chronologically aging yeast.

2.2 Materials and methods

2.2.1 Strains and media

The wild-type strain *Saccharomyces cerevisiae* BY4742 (*MATα his3Δ1 leu2Δ0 lys2Δ0 ura3Δ0*) was used in this study. Media components were as follows: (1) YEPD (0.2% glucose), 1% yeast extract, 2% peptone, 0.2% glucose; and (2) YEPD (2% glucose), 1% yeast extract, 2% peptone, 2% glucose.

2.2.2 A plating assay for the analysis of chronological lifespan

Cells were grown in YEPD (0.2% glucose) medium at 30^{o}C with rotational shaking at 200 rpm in Erlenmeyer flasks at a flask volume/medium volume ratio of 5:1. A sample of cells was removed from each culture at various time points. A fraction of the cell sample was diluted in order to determine the total number of cells per ml of culture using a hemacytometer. 10 μl of serial dilutions (1:10 to 1:10^3) of cells were applied to the hemacytometer, where each large square is calibrated to hold 0.1 μl. The number of cells in 4 large squares was then counted and an average was taken in order to ensure greater accuracy. The concentration of cells was calculated as follows: number of cells per large square x dilution factor x 10 x 1,000 = total number of cells per ml of culture. A second fraction of the cell sample was diluted and serial dilutions (1:10^2 to 1:10^5) of cells were plated onto YEPD (2% glucose) plates in triplicate in order to count the number of viable cells per ml of each culture. 100 μl of diluted culture was

plated onto each plate. After a 48-h incubation at 30^{o}C, the number of colonies per plate was counted. The number of colony forming units (CFU) equals to the number of viable cells in a sample. Therefore, the number of viable cells was calculated as follows: number of colonies x dilution factor x 10 = number of viable cells per ml. For each culture assayed, % viability of the cells was calculated as follows: number of viable cells per ml / total number of cells per ml x 100%. The % viability of cells in mid-logarithmic phase was set at 100% viability for that particular culture. The life span curves for wild-type and some of the mutant strains were also validated using a LIVE/DEAD yeast viability kit (Invitrogen) following the manufacturer's instructions for stationary-phase cultures.

2.2.3 Pharmacological manipulation of chronological lifespan

Chronological lifespan analysis was performed as described above in this section. The lithocholic (LCA) bile acid was from Sigma. The stock solution of LCA in DMSO was made on the day of adding this compound to cell cultures. LCA was added to growth medium at the final concentration of 50 μM immediately following cell inoculation into the medium. The final concentration of DMSO in yeast cultures supplemented with LCA (and in the corresponding control cultures supplemented with drug vehicle) was 1% (v/v).

2.2.4 Quantitative analysis of LCA associated with cells or remaining in the cultural medium

Yeast cells cultured in the presence of LCA were pelleted by centrifugation for 5 min at 3,000 × g at room temperature. The recovered supernatant of the cultural medium was stored at room temperature. The recovered pellet of cells was washed twice with distilled water; the supernatant recovered after each centrifugation was combined with the cultural medium. Established procedures [151, 220] were used for lipid extraction from the washed cells and from the cultural medium combined with the two washes. Mass spectrometric identification and quantitation of LCA in the extracts of lipids were performed as previously described [151, 220].

2.2.5 Quantitative analysis of LCA recovered in subcellular fractions separated by differential centrifugation

Subcellular fractionation of yeast cell homogenates through sequential centrifugation steps of increasing force and duration [222], lipid extraction from the recovered subcellular fractions [220], and mass spectrometric identification and quantitation of LCA in the extracts of lipids [151, 221] were performed according to established procedures.

2.2.6 Quantitative analysis of LCA recovered in organelles pelleted by centrifugation at 12,000 × g and then separated by equilibrium density gradient centrifugation

A mix of mitochondria, endoplasmic reticulum, Golgi, vacuoles, plasma membrane and nuclei was recovered in a 12,000 × g pellet by sequential centrifugation of yeast cell homogenates at 1,000 × g and 12,000 × g as previously described [222]. An established procedure [223] was used for separating the recovered mix of organelles by centrifugation to equilibrium in a sucrose density gradient. Lipid extraction from equal volumes of gradient fractions [220], and mass spectrometric identification and quantitation of LCA in the extracts of lipids [151, 221] were performed according to established procedures.

2.2.7 Subfractionation of purified mitochondria using a swell-shrink procedure and equilibrium density gradient centrifugation

Mitochondria purified as previously described [223] were subjected to subfractionation using a modified swell-shrink procedure and subsequent equilibrium density gradient centrifugation [224]. Briefly, the purified mitochondria were resuspended in hypotonic buffer KH (10 mM KCl, 2 mM HEPES, pH 7.2) at 2 mg/ml with gentle agitation for 20 min on ice. This caused the mitochondria to swell, ruptured the outer mitochondrial membrane (OMM) and resulted in the formation of mitoplasts consisting of mitochondrial matrix surrounded by the intact inner mitochondrial membrane (IMM). One-third volume of hypertonic buffer SAMH (1.8 M sucrose, 2 mM ATP, 2 mM $MgSO_4$, 2 mM HEPES, pH 7.2) was then added and the mitoplasts attached to ruptured OMM vesicles were subjected to gentle homogenization for an additional 10 min. This caused the mitoplasts to shrink, disrupted the OMM/IMM contact sites and resulted in the release of ruptured OMM vesicles. The swollen/shrunk mitochondrial suspension was then subjected to centrifugation on a discontinuous sucrose (26, 34.2, 45.2 and

61.6%; wt/v in KH buffer) gradient at 75,000 × g for 3 h at 4°C in a SW28 rotor (Beckman Coulter). 19 fractions of 2 ml each were collected. Equal volumes of gradient fractions were subjected to SDS-PAGE and immunoblotting with antibodies to Por1p (a protein marker of the OMM fraction), Ccp1p (a protein marker of the intermembrane space [IMS] fraction), Cox2p (a protein marker of the IMM fraction) and Mge1p (a protein marker of the matrix fraction). Lipid extraction from equal volumes of gradient fractions [220], and mass spectrometric identification and quantitation of LCA in the extracts of lipids [151, 221] were performed according to established procedures.

2.2.8 Subfractionation of purified mitochondria using sonication and differential centrifugation

Mitochondria purified as previously described [223] were subjected to subfractionation using a modified procedure of sonication and subsequent differential centrifugation [224]. The procedure results in a reconstruction of so-called submitochondrial particles (SMP) depleted of protein and other components of the mitochondrial matrix and IMS; these vesicular particles are surrounded by the IMM and OMM that are resealed in the inside-out orientation [224]. To reconstruct SMP, the purified mitochondria were gently resuspended in buffer SEH (250 mM sucrose, 2 mM EGTA, 5 mM HEPES, pH 7.2) at 2 mg/ml on ice. The suspension of mitochondria was sonicated 3 × 1 min on ice with 1 min intervals. The sonicated suspension was then subjected to centrifugation for 10 min at 12,000 × g at 4oC to remove unbroken mitochondria. The recovered supernatant was spun for 45 min at 120,000 × g at 4oC to yield the pellet of SMP and the supernatant containing protein and other components of the mitochondrial matrix and IMS. The pellet of SMP was gently resuspended in ice-cold SEH buffer and spun for 45 min at 120,000 × g at 4^{o}C to wash and re-pellet SMP.

2.2.9 Analysis of lipids by mass spectrometry

Extraction of lipids from purified mitochondria, ER and PM and following mass spectrometric identification and quantitation of various lipid species were carried out as previously described [151, 220, 221]. Mass spectrometric analyses were performed with a Thermo OrbitrapVelos mass spectrometer equipped with a HESI-II ion source (#10145339; Thermo Scientific) operating at a flow rate of 5 µl/min. Numerous lipid species were separated by Fourier

transform tandem mass spectrometry. Mass spectra were converted to an open format (mzXML, mzML) using the ProteoWizard MSConvert software freely available from http://proteowizard.sourceforge.net/. The raw data were then imported into the open source software LipidXplorer (freely available from https://wiki.mpi-cbg.de/wiki/lipidx/index.php/Main_Page) for the automated detection and quantitation of lipid species.

2.2.10 Statistical analysis

Statistical analysis was performed using Microsoft Excel's (2010) Analysis ToolPack-VBA. All data are presented as mean ± SEM. The *p* values were calculated using an unpaired two-tailed *t* test.

2.3 Results and Discussion

2.3.1 LCA enters yeast cells

In the high-throughput screen that led to the identification of LCA as an anti-aging molecule, all of the tested chemical compounds derived from several commercial libraries were dissolved in dimethyl sulfoxide (DMSO) and the final concentration of this solvent in yeast cultures was 1% (v/v) [155]. Due to the well-known ability of DMSO to create pores in the hydrophobic core of a membrane bilayer and to increase its fluidity, this amphiphilic enhancer of cell membrane permeability for drugs and DNA is traditionally used as a vehicle for delivering various chemical compounds into a cell [225]. If LCA was first dissolved in DMSO and then added to growth medium at a final concentration of 50 μM immediately following cell inoculation into the medium, this bile acid significantly extended the chronological lifespan (CLS) of yeast cells that were cultured under caloric restriction (CR) conditions on 0.2% glucose (Figure 2.1A) [155].

Noteworthy, LCA at a final concentration of 50 μM displayed a similar strong beneficial effect on the CLS of yeast cells cultured under CR at 0.2% glucose if it was added to growth medium in water, i.e., under conditions that are unlikely to enhance cell membrane permeability for exogenous chemical compounds (Figure 2.1B) [221]. This observation suggested that, akin to the established mechanism underlying an anti-tumor effect of LCA in cultured human cells [226], a mechanism by which this bile acid extends longevity of chronologically aging yeast under CR conditions does not involve its delivery into cells. As a first step towards addressing this

important spatial aspect of the longevity-extending effect of exogenously added LCA, I used a quantitative mass spectrometric analysis to compare the relative level of cell-associated LCA to that of LCA in the cultural medium. My analysis of the age-related dynamics of changes in the levels of LCA associated with cells or remaining in the cultural medium revealed that in yeast cultures incubated with exogenously added 50 μM LCA in the presence of DMSO, only a minor portion of this bile acid (from 6.1% to 14.6% at different periods of chronological lifespan) was present in a cell-associated form (Figure 2.1C). In contrast, in yeast cultures incubated with exogenously added 50 μM LCA in the absence of DMSO, the major portion of this bile acid (from 76.7% to 94.8%, depending on a period of chronological lifespan) was associated with cells (Figure 2.1D).

I then used subcellular fractionation by differential centrifugation (Figure 2.1G) followed by mass spectrometric quantitation of LCA to assess its relative levels in various subcellular fractions. I found that in yeast cultured with exogenously added LCA in the presence of DMSO 1) LCA was present mostly (from 71.3% to 90.2%, depending on a period of chronological lifespan) in the cytosolic (100KgS) fraction; 2) from 5.2% to 21.6% of LCA was recovered in the 12KgP fraction containing mitochondria, endoplasmic reticulum (ER), Golgi, vacuoles, plasma membrane (PM) and nuclei; and 3) from 4.2% to 7.1% of LCA was associated with cell surface, as it was recovered in the 1KgP fraction known to consist of unspheroplasted cells and cell debris (Figure 2.1E). In contrast, in yeast cultured with exogenously added LCA in the absence of DMSO 1) LCA was mostly (from 73.3% to 92.2%) associated with cell surface (1KgP fraction); 2) from 4.1% to 23.6% of LCA was recovered in the 12KgP fraction consisting of mitochondria, ER, Golgi, vacuoles, PM and nuclei; and 3) only a minor portion (from 2.9% to 4.4%) of LCA was present in the cytosolic (100KgS) fraction (Figure 2.1F).

In sum, my quantitative analysis of LCA recovered in various subcellular fractions separated by differential centrifugation implies that in yeast cultured with exogenously added LCA in the presence of DMSO, this bile acid is evenly distributed between the cultural medium and the cytosol – perhaps because of its high solubility in DMSO present in the cultural medium and the cytosol and probably due to its passive diffusion through pores in the PM created by DMSO. Importantly, in yeast cultured with LCA in the presence of DMSO, up to 21.6% of the intracellular pool of this bile acid is confined to the 12KgP fraction containing mitochondria, ER, Golgi, vacuoles, PM and nuclei. Furthermore, in yeast cultured with exogenously added LCA in

the absence of DMSO, this most hydrophobic molecular form of bile acids [155] associates mainly with cell surface – possibly because of its low solubility in water leading to its adhesion to the cell wall and perhaps due to lack of pores in the PM. Yet, even in yeast cultured with LCA in the absence of DMSO, up to 28% of this bile acid enters yeast cells and associates mainly with the 12KgP fraction consisting of mitochondria, ER, Golgi, vacuoles, PM and nuclei.

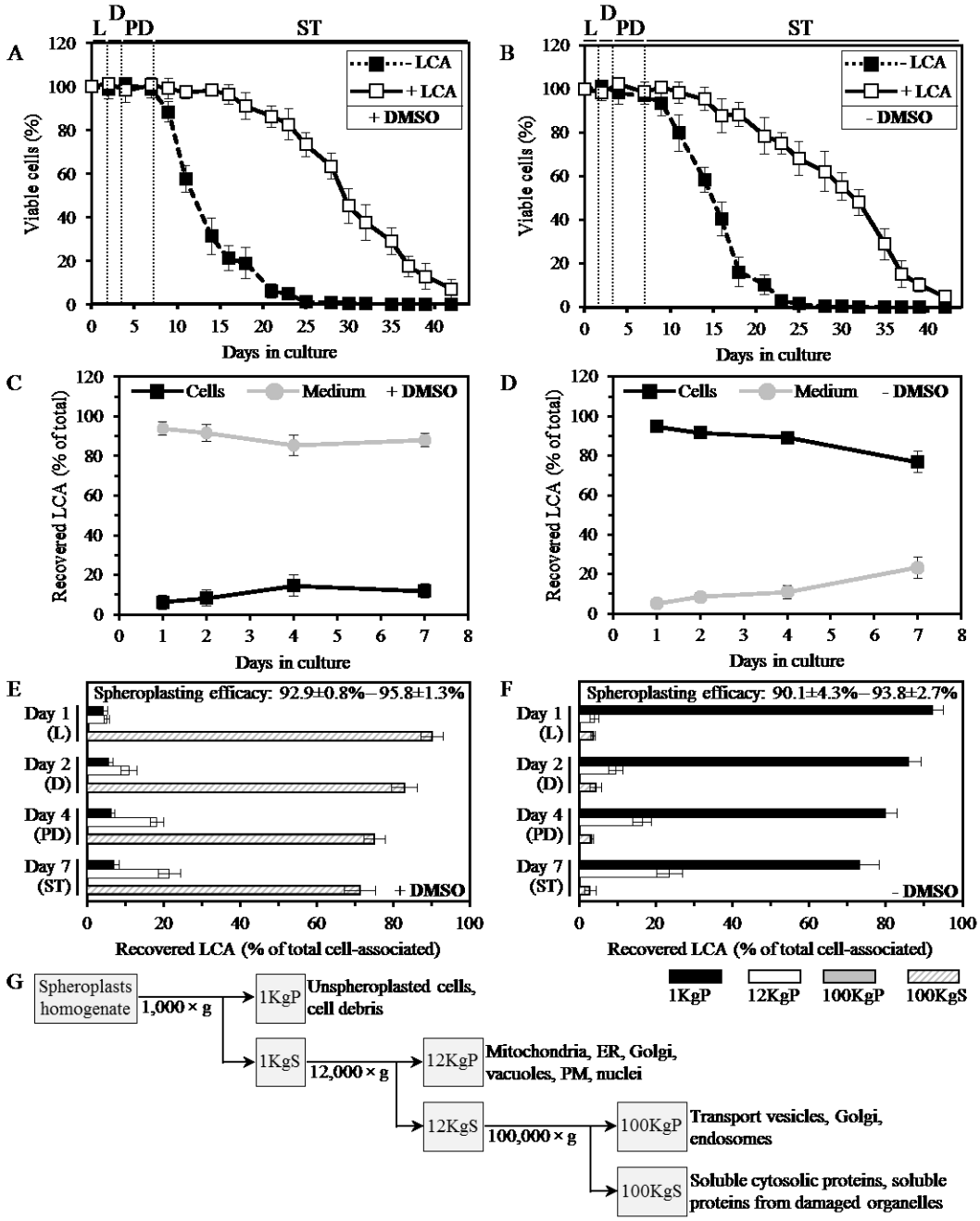

Figure 2.1. In yeast cultured with exogenously added LCA in the presence or absence of DMSO, this bile acid enters cells and accumulates in a subcellular fraction consisting of mitochondria, ER, Golgi, vacuoles, PM and nuclei.

(**A** and **B**) Cells were cultured in the nutrient-rich YP medium initially containing 0.2% glucose with 50 μM LCA or without it, in the presence of 1% DMSO (**A**) or in its absence (**B**). Survival curves of chronologically aging yeast are shown; data are presented as means ± SEM (n = 11-14). (**C** and **D**) The age-related dynamics of changes in the levels of LCA associated with cells or remaining in the cultural medium in yeast cultures that were incubated with exogenously added 50 μM LCA in the presence of 1% DMSO (**C**) or in its absence (**D**); data are presented as means ± SEM (n = 5-6). (**E** and **F**) The age-related dynamics of changes in the levels of LCA recovered in various subcellular fractions that were separated by differential centrifugation of yeast cell homogenates; data for subcellular fractions recovered from yeast cultures that were incubated with exogenously added 50 μM LCA in the presence of DMSO (**E**) or in its absence (**F**) are presented as means ± SEM (n = 4). The efficacy of spheroplast formation is also shown as means ± SEM (n = 4). (**G**) Outline of a procedure for subcellular fractionation of yeast cell homogenates through sequential centrifugation steps of increasing force and duration. Abbreviations: Diauxic (D), logarithmic (L), post-diauxic (PD) or stationary (ST) growth phase.

2.3.2 Intracellular LCA accumulates in mitochondria

To elucidate in which organelle or organelles present in the 12KgP subcellular fraction LCA resides, I subjected the mix of mitochondria, ER, Golgi, vacuoles, PM and nuclei recovered in this organellar fraction to separation by centrifugation to equilibrium in a sucrose density gradient. The shape of this gradient has been previously optimized for the purification of mitochondria devoid of contamination by other organelles present in the 12KgP fraction (Figure 2.) [223]. My mass spectrometric identification and quantitation of LCA in gradient fractions revealed that the 12KgP-associated pool of LCA is almost exclusively confined to mitochondria of yeast cultured with this bile acid in the presence of DMSO (Figures 2.2A and 2.2B) or in its absence (Figures 2.2C and 2.2D). I therefore concluded that, regardless of the presence of DMSO in yeast cultures containing exogenously added LCA, the only kind of cellular organelle this longevity-extending bile acid accumulates in is the mitochondrion.

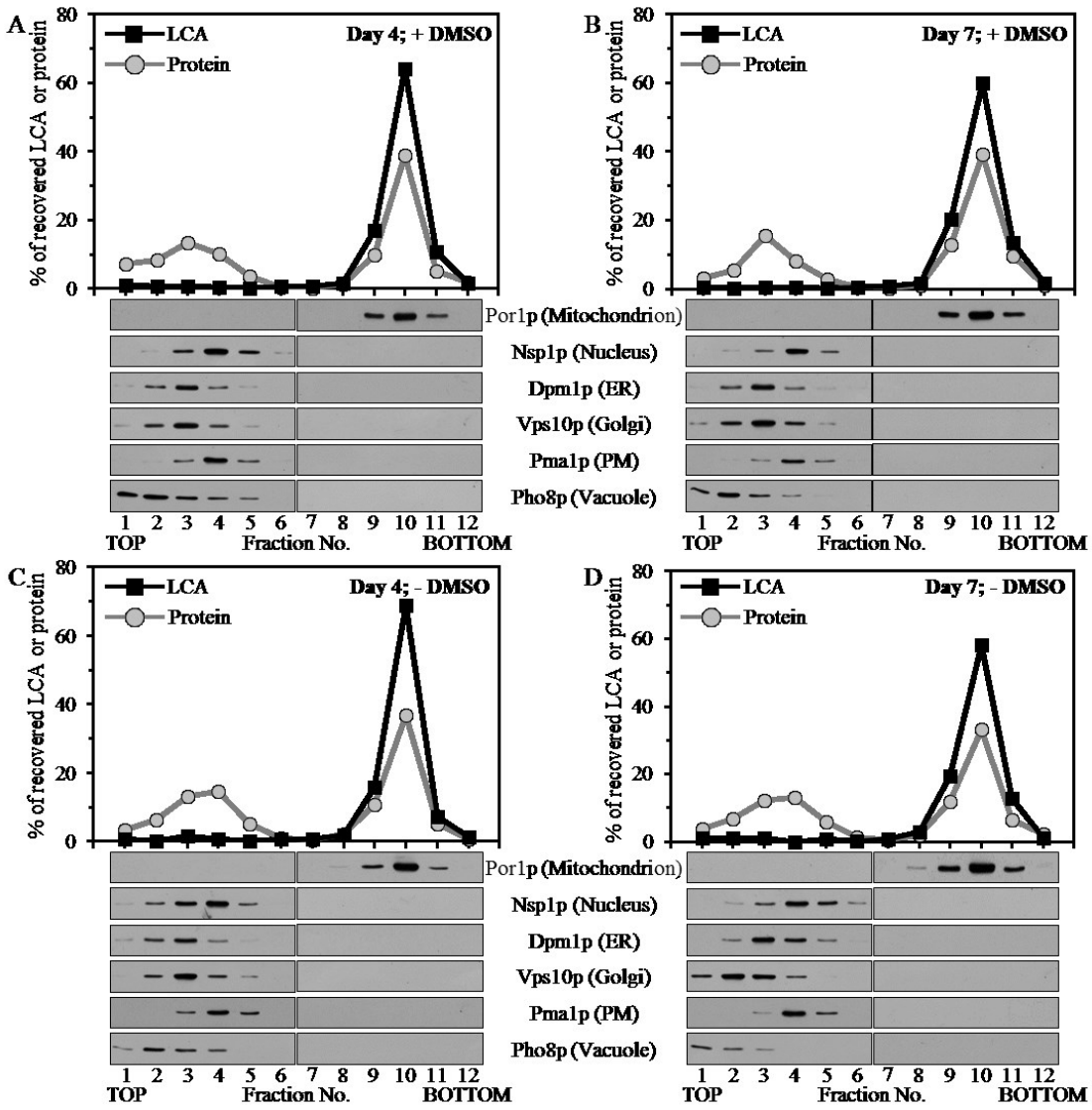

Figure 2.2. Intracellular LCA accumulates in mitochondria.

Cells were cultured in the nutrient-rich YP medium initially containing 0.2% glucose with exogenously added 50 μM LCA in the presence of 1% DMSO (**A** and **B**) or in its absence (**C** and **D**). Homogenates of cells that were taken at day 4 (**A** and **C**) or 7 (**B** and **D**) of cell culturing were subjected to subcellular fractionation to recover a mix of mitochondria, endoplasmic reticulum (ER), Golgi, vacuoles, plasma membrane (PM) and nuclei in a 12,000 × g pellet. The recovered mix of organelles was fractionated using centrifugation to equilibrium in a sucrose density gradient. The percent recoveries of loaded protein and LCA in sucrose gradient fractions are presented. Equal volumes of gradient fractions were subjected to lipid extraction followed by mass spectrometric identification and quantitation of LCA in the extracts of lipids. Equal volumes of gradient fractions were also analyzed by immunoblotting with antibodies to Por1p (a protein marker of mitochondria), Nsp1p (a protein marker of the nucleus), Dpm1p (a protein marker of the ER), Vps10p (a protein marker of the Golgi), Pma1p (a protein marker of the PM) and Pho8p (a protein marker of the vacuole).

2.3.3 Mitochondria-associated LCA resides mainly in the inner mitochondrial membrane (IMM)

To examine in which mitochondrial sub-compartment LCA resides, I first subjected purified mitochondria to fractionation using a swell-shrink procedure and subsequent equilibrium density gradient centrifugation. This fractionation approach enables to separate mitochondria into the intact outer mitochondrial membrane (OMM) fraction, the intact intermembrane space (IMS) fraction and the mitoplast fraction consisting of mitochondrial matrix surrounded by the intact IMM [224]. I found that, regardless of the presence of DMSO in yeast cultures containing exogenously added LCA, the bulk quantities of this bile acid (from 69.5% to 74.6% of the total pool of mitochondria-associated LCA) were confined to mitoplasts (Figures 2.3A and 2.3B). A smaller portion of LCA (from 20.7% to 26.6% of the total pool of mitochondrial LCA) was recovered in the OMM, and only minute quantities of it (from 1.4% to 8.3% of the total pool of mitochondria-associated LCA) were found in the IMS (Figures 2.3A and 2.3B).

I then quantitatively assessed the relative abundance of LCA in the membrane (i.e., the OMM and IMM) and soluble (i.e., the IMS and matrix) mitochondrial sub-compartments by subjecting purified mitochondria to fractionation using sonication and subsequent differential centrifugation. This fractionation approach results in a reconstruction of so-called submitochondrial particles (SMP). These vesicular particles (1) are depleted of protein and other components of the mitochondrial matrix and IMS; and (2) are surrounded by the IMM and OMM resealed in the inside-out orientation [224]. High-speed centrifugation of sonicated mitochondria yields the pellet of SMP, whereas protein and other components of the mitochondrial matrix and IMS remain in the supernatant. I found that, in yeast cultured with LCA in the presence of DMSO or in its absence, this bile acid was confined mostly (from 92.8% to 98.5% of the total pool of mitochondrial LCA) to the pellet of SMP (Figures 2.3C and 2.3D). Minor quantities of LCA (from 1.5% to 7.2% of the total pool of mitochondria-associated LCA) were recovered in the supernatant consisting of mitochondrial matrix and the IMS (Figures 2.3C and 2.3D).

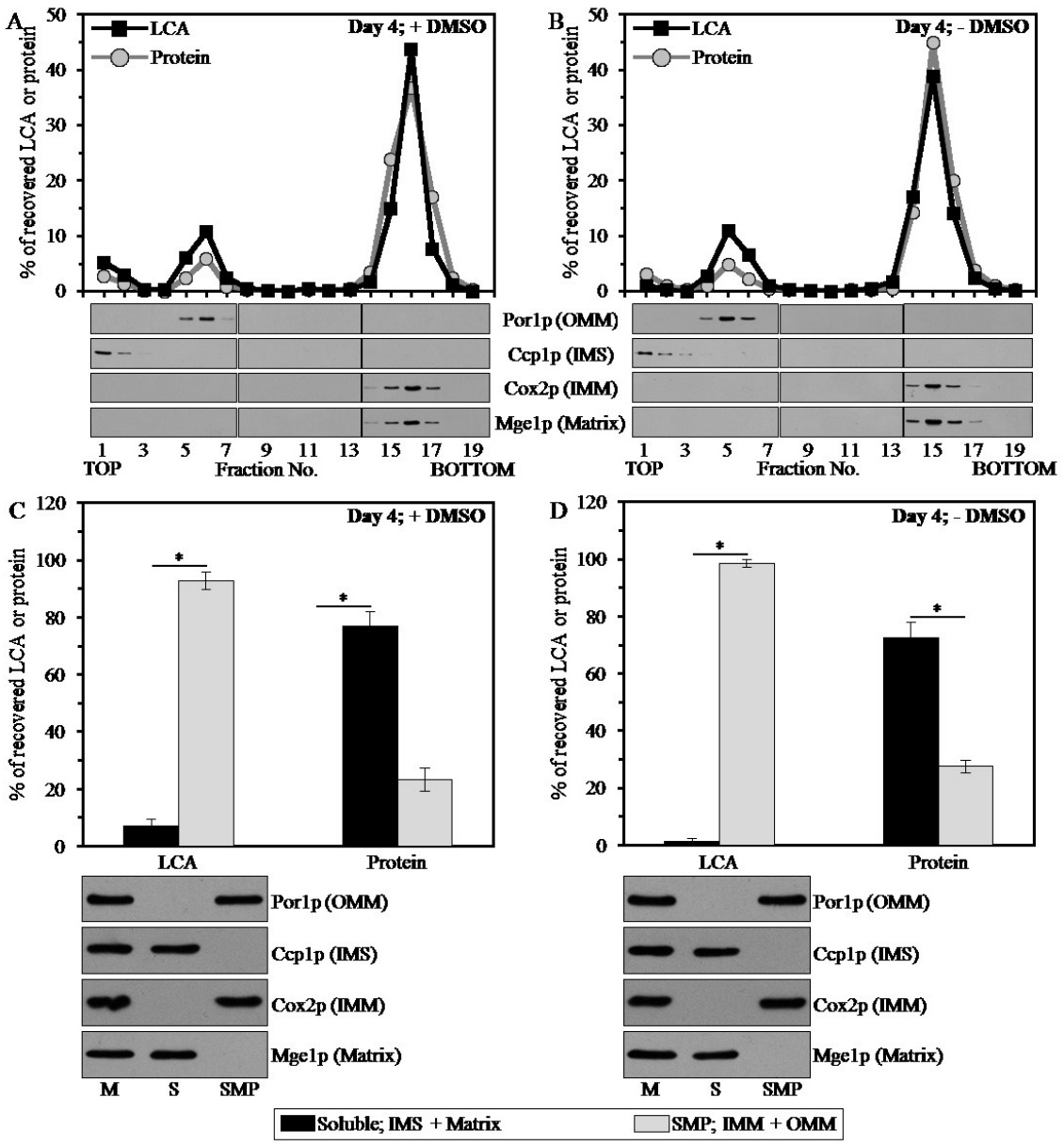

Figure 2.3. Mitochondria-associated LCA is confined mainly to the IMM, and also resides in the OMM.

Cells were cultured in the nutrient-rich YP medium initially containing 0.2% glucose with exogenously added 50 μM LCA in the presence of 1% DMSO (A and C) or in its absence (B and D). Purified mitochondria of cells that were taken at day 4 of cell culturing were subjected to fractionation using a swell-shrink procedure and subsequent equilibrium density gradient centrifugation (A and B) or to fractionation using sonication and subsequent differential centrifugation (C and D). (A and B) The percent recoveries of loaded protein and LCA in sucrose gradient fractions are presented. Equal volumes of gradient fractions were subjected to lipid extraction followed by mass spectrometric identification and quantitation of LCA in the extracts of lipids. Equal volumes of gradient fractions were also analyzed by immunoblotting with antibodies to Por1p (a protein marker of the OMM), Ccp1p (a protein marker of the IMS), Cox2p (a protein marker of the IMM) and Mge1p (a protein marker of the mitochondrial matrix). (C and

D) The percent recoveries of protein and LCA in the pellet of SMP (consisting of vesicular particles surrounded by the IMM and OMM resealed in the inside-out orientation) and the supernatant (containing protein and other components of the mitochondrial matrix and IMS); the pellet and supernatant fractions were recovered after high-speed centrifugation of sonicated mitochondria. Data are presented as means ± SEM (n = 3; *p < 0.01).

Altogether, my quantitative analysis of LCA recovered in various mitochondrial sub-compartments implies that, regardless of the presence of DMSO in yeast cultures containing exogenously added LCA, the mitochondria-associated pool of LCA resides mainly in the IMM. A smaller portion of this bile acid (from 20.7% to 26.6% of the total pool of mitochondrial LCA) associates with the OMM.

2.3.4 Conclusion

In sum, I used a combination of subcellular fractionation by differential centrifugation, organelle separation by equilibrium density gradient centrifugation, fractionation of purified mitochondria into various subcompartments and quantitative mass spectrometric analysis to make an initial step towards establishing a mechanism by which LCA extends longevity of chronologically aging yeast limited in calorie supply. My findings imply that exogenously added LCA enters yeast cells, is sorted only to mitochondria, resides mainly in the IMM, and also associates with the OMM.

3 A permanent exposure of yeast cells to LCA changes the age-related chronology of several longevity-defining processes taking place within mitochondria

3.1 Introduction

Dr. Vincent Richard, a former graduate student in the Titorenko laboratory, has used mass spectrometry to compare the membrane lipidomes of mitochondria purified from yeast cultured under caloric restriction (CR) conditions with or without LCA. He found that exogenously added LCA exhibits differential effects on the concentrations of different molecular forms of mitochondrial membrane phospholipids; moreover, these effects of LCA appeared to be age-dependent [193]. Specifically, he demonstrated that: (1) LCA causes a rise in the levels of mitochondrial phosphatidic acid (PA), phosphatidylglycerol (PG), phosphatidylserine (PS), phosphatidylcholine (PC) and phosphatidylinositol (PI); (2) the extent of such effect of LCA on PA, PG, PS, PC and PI levels increases with the chronological age of yeast cells; and (3) for the PG and PI classes of mitochondrial membrane glycerophospholipids, this effect of LCA can be seen only in cells recovered at post-diauxic (PD) or stationary (ST) growth phase on day 4 or 7 (respectively) of cell culturing [193]. Furthermore, mass spectrometric identification and quantitation of mitochondrial membrane phospholipids also revealed that (1) LCA elicits a decline in the levels of mitochondrial cardiolipin (CL), monolysocardiolipin (MLCL) and phosphatidylethanolamine (PE); (2) the extent of such effect of LCA on CL, MLCL and PE levels decreases with the chronological age of yeast cells; and (3) for the MLCL species of mitochondrial membrane glycerophospholipids, this effect of LCA can be seen only in cells recovered at PD or ST growth phase on day 4 or 7 (respectively) of cell culturing [193]. Taken together, these findings imply that the accumulation of LCA in the IMM and OMM causes significant changes in the phospholipid compositions of both mitochondrial membranes.

Two of the phospholipids whose levels were substantially reduced by LCA, namely PE and CL [193], have been shown to modulate protein complexes and supercomplexes that reside in the IMM and drive such longevity-defining processes as mitochondrial respiration, the maintenance of electrochemical membrane potential and preservation of ROS homeostasis [227 - 229]. I therefore hypothesized that the LCA-elicited changes in the membrane lipidome of mitochondria may impact these longevity-defining mitochondrial processes. Chapter 3 describes experiments that I conducted to test the validity of my hypothesis.

3.2 Materials and methods

3.2.1 Strains and media

The wild-type strain *Saccharomyces cerevisiae* BY4742 (*MATα his3Δ1 leu2Δ0 lys2Δ0 ura3Δ0*) was used in this study. The composition of YEPD (0.2% glucose) medium was as follows: 1% yeast extract, 2% peptone, 0.2% glucose. Cells were cultured at 30^{o}C with rotational shaking at 200 rpm in Erlenmeyer flasks at a ″flask volume/medium volume″ ratio of 5:1.

3.2.2 Pharmacological manipulation of chronological lifespan

Chronological lifespan analysis was performed as described above in this section. The lithocholic (LCA) [#L6250] bile acid was from Sigma. The stock solution of LCA in DMSO was made on the day of adding this compound to cell cultures. LCA was added to growth medium at the final concentration of 50 μM immediately following cell inoculation into the medium. The final concentration of DMSO in yeast cultures supplemented with LCA (and in the corresponding control cultures supplemented with drug vehicle) was 1% (v/v).

3.2.3 Monitoring the formation of ROS

Wild-type and mutant cells grown in YEPD (0.2% glucose) were tested microscopically for the production of ROS by incubation with dihydrorhodamine 123 (DHR). In the cell, this nonfluorescent compound can be oxidized to the fluorescent chromophore rhodamine 123 by ROS. Cells were also probed with a fluorescent counterstain Calcofluor White M2R (CW), which stains the yeast cell walls fluorescent blue. CW was added to each sample in order to label all cells for their proper visualization. DHR was stored in the dark at –20^{o}C as 50 μl aliquots of a 1 mg/ml solution in ethanol. CW was stored in the dark at –20^{o}C as the 5 mM stock solution in anhydrous DMSO (dimethylsulfoxide).

The concurrent staining of cells with DHR and CW was carried out as follows. The required amounts of the 50 μl DHR aliquots (1 mg/ml) and of the 5 mM stock solution of CW were taken out of the freezer and warmed to room temperature. The solutions of DHR and CW were then centrifuged at 21,000 x g for 5 min in order to clear them of any aggregates of fluorophores. For cell cultures with a titre of ~ 10^7 cells/ml, 100 μl was taken out of the culture to be treated. If the cell titre was lower, proportionally larger volumes were used. 6 μl of the 1 mg/ml DHR and 1 μl of the 5 mM CW solutions were added to each 100 μl aliquot of culture.

After a 2-h incubation in the dark at room temperature, the samples were centrifuged at 21,000 x g for 5 min. Pellets were resuspended in 10 μl of PBS buffer (20 mM KH_2PO_4/KOH, pH 7.5, and 150 mM NaCl). Each sample was then supplemented with 5 μl of mounting medium, added to a microscope slide, covered with a coverslip, and sealed using nail polish. Once the slides were prepared, they were visualized under the Zeiss Axioplan fluorescence microscope mounted with a SPOT Insight 2 megapixel color mosaic digital camera. Several pictures of the cells on each slide were taken, with two pictures taken of each frame. One of the two pictures was of the cells seen through a rhodamine filter in order to detect cells dyed with DHR. The second picture was of the cells seen through a DAPI filter in order to visualize CW, and therefore all the cells present in the frame.

For evaluating the percentage of DHR-positive cells, the UTHSCSA Image Tool (Version 3.0) software was used to calculate both the total number of cells and the number of stained cells. Fluorescence of individual DHR-positive cells in arbitrary units was determined by using the UTHSCSA Image Tool software (Version 3.0). In each of 3-5 independent experiments, the value of median fluorescence was calculated by analyzing at least 800-1000 cells that were collected at each time point. The median fluorescence values were plotted as a function of the number of days cells were cultured.

3.2.4 Monitoring the mitochondrial membrane potential (ΔΨ)

Rhodamine 123 (R123) (Invitrogen) staining for monitoring the mitochondrial membrane potential (ΔΨ) was performed according to established procedure (Invitrogen manual for the Yeast Mitochondrial Stain Sampler Kit). Images were collected with a Zeiss Axioplan fluorescence microscope (Zeiss) mounted with a SPOT Insight 2 megapixel color mosaic digital camera (Spot Diagnostic Instruments). For evaluating the percentage of R123-positive cells, the UTHSCSA Image Tool (Version 3.0) software was used to calculate both the total number of cells and the number of stained cells. Fluorescence of individual R123-positive cells in arbitrary units was determined by using the UTHSCSA Image Tool software (Version 3.0). In each of 3-6 independent experiments, the value of median fluorescence was calculated by analyzing at least 800-1000 cells that were collected at each time point. The median fluorescence values were plotted as a function of the number of days cells were cultured.

3.2.5 Immunofluorescence microscopy

Cell cultures were fixed in 3.7% formaldehyde for 45 min at room temperature. The cells were washed in solution B (100 mM KH_2PO_4/KOH pH 7.5, 1.2 M sorbitol), treated with Zymolyase 100T (MP Biomedicals, 1 µg Zymolyase 100T/1 mg cells) for 30 min at 30°C and then processed as previously described (Pringle *et al*., 1991). Monoclonal antibody raised against porin (Invitrogen, 0.25 µg/µl in TBSB buffer [20 mM Tris/HCl pH 7.5, 150 mM NaCl, 1 mg/ml BSA] was used as a primary antibody. Alexa Fluor 568 goat anti-mouse IgG (Invitrogen, 2 µg/µl in TBSB buffer) was used as a secondary antibody. The labeled samples were mounted in mounting solution (16.7 mM Tris/HCl pH 9.0, 1.7 mg/ml p-phenylenediamine, 83% glycerol). Images were collected with a Zeiss Axioplan fluorescence microscope (Zeiss) mounted with a SPOT Insight 2 megapixel color mosaic digital camera (Spot Diagnostic Instruments).

3.2.6 Oxygen consumption assay

The rate of oxygen consumption by yeast cells recovered at various time points was measured continuously in a 2-ml stirred chamber using a custom-designed biological oxygen monitor (Science Technical Center of Concordia University) equipped with a Clark-type oxygen electrode. 1 ml of YEPD medium supplemented with 0.2% glucose was added to the electrode for approximately 5 minutes to obtain a baseline. Cultured cells of a known titre were spun down at 3,000 x g for 5 minutes. The resulting pellet was resuspended in YEPD medium supplemented with 0.2% glucose and then added to the electrode with the medium that was used to obtain a baseline. The resulting slope was used to calculate the rate of oxygen consumption in $O_2\% \times min^{-1}$ x 10^9 cells.

3.2.7 Measurement of the frequency of mitochondrial mutations affecting mitochondrial components

The frequency of spontaneous single-gene (*mit*$^-$ and *syn*$^-$) and deletion (*rho*$^-$ and *rho*^{o}) mutations in mtDNA affecting essential mitochondrial components was evaluated by measuring the fraction of respiratory-competent (*rho*$^+$) yeast cells remaining in their aging population. *rho*$^+$ cells maintained intact their mtDNA and their nuclear genes encoding essential mitochondrial components. Therefore, *rho*$^+$ cells were able to grow on glycerol, a non-fermentable carbon source. In contrast, mutant cells deficient in mitochondrial respiration were unable to grow on

glycerol. These mutant cells carried mutations in mtDNA (including single-gene *mit*$^-$ and *syn*$^-$ mutations or large deletions *rho*$^-$) or completely lacked this DNA (*rho*^{o} mutants). Serial dilutions of cell samples removed from different phases of growth were plated in triplicate onto YP plates containing either 2% glucose or 3% glycerol (#BP229-4; Fisher Scientific) as carbon source. Plates were incubated at 30^{o}C. The number of CFU on YP plates containing 2% glucose was counted after 2 d of incubation, whereas the number of CFU on YP plates containing 3% glycerol was counted after 6 d of incubation. For each culture, the percentage of respiratory-deficient (*mit*$^-$, *syn*$^-$, *rho*$^-$, *rho*^{o} and *pet*$^-$) cells was calculated as follows: 100 – [(number of CFU per ml on YP plates containing 3% glycerol/number of CFU per ml on YP plates containing 2% glucose) × 100].

The frequency of spontaneous point mutations in the *rib2* and *rib3* loci of mtDNA was evaluated by measuring the frequency of mtDNA mutations that caused resistance to the antibiotic erythromycin. These mutations impair only mtDNA. A sample of cells was removed from each culture at various time-points. Cells were plated in triplicate onto YP plates containing 3% glycerol and erythromycin (1 mg/ml) [#227330050; Acros Organics]. In addition, serial dilutions of each sample were plated in triplicate onto YP plates containing 3% glycerol as carbon source for measuring the number of respiratory-competent (*rho*$^+$) cells. The number of CFU was counted after 6 d of incubation at 30^{o}C. For each culture, the frequency of mutations that caused resistance to erythromycin was calculated as follows: number of CFU per ml on YP plates containing 3% glycerol and erythromycin/number of CFU per ml on YP plates containing 3% glycerol.

3.2.8 Immunodetection of carbonyl groups in oxidatively damaged cellular proteins

Total cell lysates were made by vortexing the cells in ice-cold TCL buffer (25 mM MOPS/KOH, pH 7.2, 150 mM NaCl, 50 mM DTT, and 1% CHAPS) with glass beads three times for 1 min. Lysates were then centrifuged for 5 min at 21,000 × g at 4^{o}C, and the supernatants of total cell lysates were collected. The carbonyl groups of proteins recovered in total cell lysates were derivatized to 2,4-dinitrophenylhydrazones using the OxyBlot^{TM} Protein Oxidation Detection Kit (Chemicon), according to the manufacturer's instructions. Briefly, total cellular proteins were denatured by adding 12% SDS to an equal volume of the total cell lysate containing 10 μg of protein. Denatured proteins were incubated with 2,4-dinitrophenylhydrazine

for 15 min at room temperature. Proteins were separated by 12.5% SDS-PAGE. Immunoblotting using a Trans-Blot SD semi-dry electrophoretic transfer system (Bio-Rad) was performed as described [230]. The derivatized carbonyl groups were detected with a 2,4-dinitrophenyl-specific antibody (Chemicon) and the Amersham ECL Western Blotting System (GE Healthcare).

3.2.9 Isolation of crude mitochondrial fraction from yeast cells

3.2.9.1 Reagents

1. Dithiothreitol (DTT) buffer [100 mM Tris-H2SO4, 10 mM dithiothreitol]
2. Zymolyase 100T from *Arthrobacter luteus* (MP Biomedicals)
3. Zymolyase buffer [1.2 M sorbitol, 20 mM potassium phosphate]
4. Homogenization buffer [0.6 M sorbitol, 10 mM Tris-HCl (pH 7.4), 1 mM EDTA, 0.2% (w/v) BSA]
5. SEM buffer [250 mM sucrose, 1 mM EDTA, 10 mM Mops (pH 7.2)]

3.2.9.2 Procedure

Cell cultures were combined in pre-weighed centrifuge bottles and cells were pelleted at 3,000 × g for 5 min at room temperature using a Beckman JA-10 rotor. The cells were washed twice with distilled water, followed by the determination of their wet weight. The cell pellets were resuspended in 2 ml/g DTT buffer and incubated on a shaker at 80 rpm for 20 min at 30ºC. The cells were pelleted as per initial centrifugation, washed in 7 ml/g Zymolyase buffer without Zymolyase and pelleted once more. The cells were incubated on a shaker at 80 rpm for 45 min at 30ºC with 1 mg/g (wet weight) of Zymolyase-100T in 7 ml/g Zymolyase buffer. Zymolyase was used because of its well-known strong lytic activity required to digest yeast cell wall. The spheroplasts obtained were then spun down at 2,200 × g for 8 min at 4ºC. All subsequent steps were carried out on ice or at 4°C with the use of cut pipette tips to avoid breaking organelles. The spheroplasts were resuspended in 6.5 ml/g ice-cold homogenization buffer and washed by centrifugation at 2,200 × g for 8 min at 4ºC. The spheroplasts were then mechanically homogenized with 15 strokes in 6.5 ml/g ice-cold homogenization buffer to disrupt yeast plasma membrane for releasing organelles and cytoplasm. Following the homogenization, the cell debris was pelleted by centrifuging at 1,500 × g for 5 min at 4ºC using a Beckman JA-17 rotor. The resulting lysate supernatant was subjected to centrifugation twice at 3000 × g for 5 min at 4ºC to

pellet the nuclei and 12,000 × g for 15 min at 4ºC. The newly obtained pellet contains mostly mitochondria, but also the endoplasmic reticulum (ER), Golgi, peroxisomes, lysosomes and vacuoles, whereas the supernatant contains the cytosol, microsomes from the ER and vacuoles. The pellet was resuspended in 6.5 ml/g in ice-cold homogenizing buffer, spun down for 5 min at 3,000 × g at 4ºC to obtain a supernatant containing mitochondria, which was then subjected to a spin at 12, 000 × g for 15 min at 4ºC. The resulting pellet was resuspended in 3 ml of SEM to be overlaid onto a sucrose gradient.

3.2.10 Purification of S. cerevisiae mitochondria devoid of microsomal and cytosolic contaminations

3.2.10.1 Reagents

1. SEM buffer [250 mM sucrose, 1 mM EDTA, 10 mM Mops (pH 7.2)]
2. EM buffer [10 mM Mops (pH 7.2), 1 mM EDTA]

3.2.10.2 Procedure

In order to purify yeast mitochondria from the crude mitochondrial fraction, an equilibrium density-gradient centrifugation was performed. Yeast mitochondria have a density of 1.18 g/cm^3 whereas 10% and 50% sucrose respectively have a density of 1.10 g/cm^3 and 1.30 g/cm^3. To prepare a sucrose density gradient for the purification of mitochondria, 1.5 ml of 60% sucrose in EM buffer was overlaid with 4 ml of 32%, 1.5 ml of 23% and 1.5 ml of 15% sucrose in EM buffer, followed by 3 ml of the crude mitochondrial suspension. The sucrose density gradient containing the mitochondrial suspension was subjected to centrifugation in a Beckman SW41 Ti swinging-bucket rotor at 134,000 × g for 60 min at 4ºC. The mitochondrial band, which was easily distinguishable, appeared at the interface between 60% and 32% sucrose. Fractions of 1 ml were recovered using a cut pipette tip and placed in 1.5 ml Eppendorf tubes and frozen at -80ºC until use. In order to quickly freeze the mitochondrial fractions, the fractions were immersed, with the aid of long tweezers, in a beaker of isopropyl alcohol kept in the -80ºC freezer.

3.2.11 Blue-native gel electrophoresis (BN-PAGE)

3.2.11.1 Equipment

1. Hoefer SE 400 vertical slab gel electrophoresis unit
2. Bio Rad Power Pac 3000 Power supply

3.2.11.2 Reagents

1. 4% acrylamide running gel [1.5 ml AB (acrylamide/bis-acrylamide)-3 mix, 6 ml gel buffer 3×, 10.4 ml distilled water, 100 µl APS, 10 µl TEMED]
2. 13% acrylamide running gel
3. 3.5% acrylamide sample gel
4. Solubilization buffer A [50 mM sodium chloride, 50 mM imidazole/HCl, 2 mM 6-aminohexanoic acid, 1 mM EDTA, pH 7.0]
5. Coomassie blue G-250 dye stock [5% wt/vol in 500 mM 6-aminohexanoic acid]
6. Cathode buffer B [50 mM Tricine, 7.5 mM imidazole, 0.02% Coomassie blue G-250, pH 7.0]
7. Cathode buffer B/10 [50 mM Tricine, 7.5 mM imidazole, 0.002% Coomassie blue G-250, pH 7.0]
8. Anode buffer [25 mM imidazole, pH 7.0]

3.2.11.3 Procedure

Mitochondria protein aliquots of 400 µg were pelleted by centrifugation at 50,000 × g for 30 min using a Beckman MLS-50 rotor. The mitochondria pellet was resuspended in 40 µl of solubilization buffer A and the mitochondria membranes were homogenized by twirling a tiny spatula. The detergent digitonin at 20% (3.0 g/g; *i.e.*, 6 µl) was added to the homogenate, which was incubated for 10 min at room temperature. The sample was subsequently centrifuged at 20,000 × g for 20 min at room temperature. To the resulting supernatant, 5 µl of 5% Coomassie blue G-250 dye in 50% glycerol was added at an 8 g/g detergent/dye ratio (*i.e.*, 3 µl). The sample containing solubilized mitochondrial membrane was loaded to a 0.16 × 0.5 cm well of a gradient separation gel with dimensions 1.5 × 14 × 15 cm composed of 4% and 13% acrylamide mixture with a sample gel of 3.5% acrylamide. Urease at 1mg/ml was also loaded on an adjacent well and used as a molecular marker (10 µl urease, 10 µl buffer A, 2.4 µl 50 % glycerol, 1.6 µl 5%

Coomassie blue G-250). BN-PAGE was performed at 4°C under the following conditions: 300 ml of Cathode buffer B in the upper chamber and 300 ml of Anode buffer in the lower chamber were used and the power supply set at constant 100 V, 15 mA, 400 W until the sample entered the gradient gel. Electrophoresis was then continued at 500 V and 15 mA until the blue running front moved about a third of the total running distance. At this point, Cathode Buffer B was replaced with 300 ml of Cathode buffer B/10 for better detection of faint protein bands and electrophoresis was continued for a total of 4 h or until the blue running front was 1 cm from the bottom of the gel. Once electrophoresis was completed the blue native gel stained with Coomassie blue G-250 was photographed, documented and stored at 4°C.

3.2.12 Tricine-SDS-PAGE

3.2.12.1 Equipment

1. Hoefer SE 400 vertical slab gel electrophoresis unit
2. Bio Rad Power Pac 3000 Power supply

3.2.12.2 Reagents

1. 10%T, 3%C Tricine-SDS running gel
2. 10% acrylamide native stacking gel
3. Anode buffer 10× [1.0 M Tris, 0.225 M HCl, pH 8.9]
4. Cathode buffer 10× [1.0 M Tris, 1.0 M Tricine, 1% SDS, pH 8.25]
5. Precision Plus Protein™ Unstained standards 10 - 250 kD (Bio-Rad)

3.2.12.3 Procedure

A 0.5-cm gel strip was cut from the 1st dimension (1D) BN-PAGE gel and placed on a glass plate with the top of the strip to the left and the bottom of the strip to the right. The strip was soaked with 5 ml of a solution containing 1% SDS and 1% mercaptoethanol for 2 h at room temperature. Following the incubation, the strip was thoroughly rinsed with water and squeezed in between 1.5-mm spacers and 18 × 16 cm glass plates. A 30-ml separating gel mixture composed of 10%T, 3%C Tricine-SDS was poured in between the glass plates leaving a gap of 0.5 cm from the native gel strip. After polymerization, a 0.5-cm spacer was inserted between the plates, and placed to the right of the gel to create a well to load protein markers. In order to fill

the 0.5-cm gap between the running gel and the native strip, as well as the space between the native gel and the spacers, 5 ml of a 10% acrylamide native gel mixture was used, and Unstained protein molecular markers (Bio-Rad) were loaded to the far right of the gel for reference. Electrophoresis was performed at constant 200 V, 50 mA, 400 W for 3 h at room temperature.

3.2.13 Silver stain after 1D-BN-PAGE followed by 2D-Tricine-SDS-PAGE

Protein bands are then visualized by silver staining using the Silver Stain Plus Kit from Bio-Rad.

3.2.13.1 Reagents

1. Fixative solution [200 ml methanol, 40 ml acetic acid, 40 ml Fixative Enhancer solution, 120 ml distilled water]
2. Staining solution [35 ml distilled water, 5 ml Silver complex solution, 5 ml Reduction Moderator solution, 5 ml Image Development solution, 50 ml Development Accelerator solution]
3. Stop solution [5% acetic acid]

3.2.13.2 Procedure

Once electrophoresis was completed, the gel was incubated in 400 ml of 50% methanol on a shaker at 55 rpm for 2 h. The gel was then incubated in 200 ml of the Fixative solution for 20 min and washed twice with 200 ml of distilled water for 10 min. The gel was then immersed in 100 ml of the Staining Solution composed of Silver complex, Reduction Moderator, Image Development and Development Accelerator solutions. Once the desired staining intensity was reached, development was immediately stopped by incubating the silver stained gel in 400 ml of 5% acetic acid for 15 min, which was followed by a rinse with 400 ml of distilled water for 5 min. The gel was then photographed, documented and stored at 4°C in 400 ml of distilled water.

3.2.14 In-gel digestion of proteins separated by 2D-Tricine-SDS-PAGE

3.2.14.1 Reagents

1. 30 mM Potassium Ferricyanide
2. 100 mM Sodium Thiosulfate

3. 100mM Ammonium Bicarbonate (ABC)
4. 10 mM Dithiothreitol (DTT) [in 5ml of 100mM Ammonium Bicarbonate (ABC)]
5. 55 mM Iodoacetamide (IAA) [in 5ml of 100mM Ammonium Bicarbonate (ABC)]
6. Trypsin, Proteomics Grade (Sigma Aldrich)

3.2.14.2 Procedure

Once the individual mitochondrial proteins were separated, each band on the 1D BN-2D Tricine-SDS gel was cut out with a razor blade and the gel piece was placed in 0.5-ml siliconized Eppendorf tubes. The bands were washed with distilled water and destained with 50 µl of a 1:1 mixture of 20 mM potassium ferricyanide and 100 mM sodium thiosulfate for 20 min in the dark with occasional vortexing. The destaining solution was removed and the bands were washed twice with distilled water. The bands were then incubated in 50 µl of acetonitrile (ACN) for 5 min at 37°C, after which ACN was removed and the bands were dried at 37°C. Next, the destained bands were incubated in 50 µl of 10 mM dithiothreitol for 30 min at 37°C to reduce thiol groups in peptides. DTT was discarded and the bands were incubated in 50 µl of 55 mM iodoacetamide for 20 min at 37°C in the dark to remove the residual DTT. IAA was removed and the bands were incubated in 50 µl of a 1:1 mixture of 100 mM ABC and 50% acetonitrile for 10 min at 37°C. The mixture was discarded and the bands were incubated twice in 50 µl of ACN under the same conditions and dried at 37°C. The trypsin and trypsin buffer were prepared as follows: (1) 1.6 ml of a 1:1 mixture of 100 mM ABC and 10mM $CaCl_2$ were used to resuspend 20 µg of trypsin; and (2) for protein digest, 50 µl of trypsin solution (1 mg/ml) was added to the bands, which were then incubated overnight at 37°C.

3.2.15 Extracting peptides from yeast mitochondrial proteins digested with trypsin

The following day, the samples were spun down and the supernatants containing peptides were transferred to new 0.5-ml siliconized Eppendorf tubes. To extract more peptides, the gel pieces were subjected to several washes and treatments at room temperature; the supernatants were conserved and combined with the first set to extracted peptides. For the first extraction, the bands were initially incubated in 50 µl of 25 mM ABC for 10 min and then in 50 µl of ACN for 10 min. The samples were spun down and the supernatant were added to the first set of extracted peptides. For the second extraction, the bands were incubated in 50 µl of 5% formic acid for 10

min and then in 50 µl of ACN for 10 min. The samples were spun down and the supernatant were combined with the first set of extracted peptides. The gel pieces were no longer used and discarded. To prevent possible oxidation during storage, 12.5 µl of 100 mM DTT was added to each set of peptides. The peptides were completely dried in a Speed-Vac at medium temperature settings (37°C) for 2 h and stored at -20°C until MS analysis.

3.2.16 Sample preparation for MS analysis

Dried peptides were resuspended in 20 µl of 5% ACN. For each recovered protein band, an aliquot of 10 µl of dried peptides in 5% ACN was diluted 2-fold in Nano pure water for MS analysis. Samples can be stored at -20°C until being subjected to MS analysis.

3.2.17 MS analysis

Individual proteins composing each band were then identified by reverse phase high performance liquid chromatography coupled to mass spectrometry (RP-HPLC/MS) using an LTQ Orbitrap. 3-µl aliquots of peptides were separated in ACN gradient using a 100-µM capillary column packed with C18 mobile phase.

3.2.18 Analysis using the Thermo Proteome Discoverer application and SEQUEST

Once acquiring time was completed using the LTQ Orbitrap, the raw mass spectrometry data file obtained by Xcalibur were analyzed using the Thermo Scientific Xcalibur Proteome Discoverer application (version 1.3) hereafter referred to as the Proteome Discoverer. The Proteome Discoverer was used to identify individual protein components of the isolated mitochondrial respiratory complexes and supercomplexes by comparing the raw data of mass spectra of digested fragments to the mass spectra of peptides within the Uniprot FASTA database. The analysis by the Proteome Discoverer coupled to the FASTA database was enabled by using the peak-finding search engine SEQUEST. The SEQUEST engine processes MS data using a peak-finding algorithm to search the raw data for generating a peak probability list with relative protein abundances.

3.2.18.1 SEQUEST search wizard within the Proteome Discoverer application

3.2.18.1.1 Raw file and Scan Range Selection Parameters

The raw file was selected and the Base peak ion chromatogram appeared to reveal: (1) the "Intensity (counts)" corresponding to the intensity of the largest peak in the spectrum; and (2) the "Time (min)" showing the retention time (RT). The following algorithm and settings were used:

Lower RT Limit (min): The beginning of the RT of the scan range of interest: 10 min.

Upper RT Limit (min): The end of the retention time of the scan range of interest: 18 min.

Scan Extraction Parameters

First mass: The mass of the first precursor ion in the range of ion fragments to search for in the database: 350 Daltons (Da).

Last mass: The mass of the last precursor ion in the range of ion fragments to search for in the database: 5000 Daltons (Da).

Activation type: The fragmentation method to use for activating the scan: Collision Induced Dissociation (CID).

Unrecognized charge replacement: Specifies the charge number of the precursor ions: Automatic (Default), assigns a charge number of +2 and +3 to the spectrum.

Intensity threshold: Specifies the intensity threshold below which ions are filtered out. The default value of 0.0 was used.

Minimum ion count: The minimum ion count corresponds to the minimum number of ions that must be present in an MS/MS spectrum for it to be included in a search. The default value of 1 was used.

S/N threshold: The signal-to-noise threshold is the intensity of the signal to the intensity of the background noise. The use of this threshold filters out low-intensity ions that function as a noise. The value of 1.5 was used.

Database: Uniprot_sprot FASTA

Enzyme: Trypsin

Missed Cleavages: The maximum number of internal cleavage sites per peptide fragment that is acceptable for an enzyme to miss during proteolytic digest. The default value of 2 was used.

Precursor mass tolerance: The precursor mass tolerance value used for finding peptide candidates. The possible range of values is 0.01 to 5000 ppm. The default value of 10 ppm was used.

Fragment mass tolerance: The default mass tolerance value of 0.8 Da was used for matching fragment peaks. The possible range of values was 0.0001 to 2.0 Da.

Ions series calculated: Specifies the ion factors for a, b, c, x, y, and z ions for the experiment type. The possible range is 0 through 1.0 for all ion factors. The ion factors used are b ions: 1 and y ions :1.

Search against decoy database: Specifies if the application uses a decoy database in the search; the "yes" was used.

Target FDR (strict): Specifies a strict target false discovery rate (FDR) for peptide matches with high confidence. The possible value range of 0.0 to 1.0 was used. The default value of 0.01 (1% FDR) was used.

Target FDR (relaxed): Specifies a relaxed target false discovery rate (FDR) for peptide matches with moderate confidence. The possible value range from 0.0 to 1.0 was used. The default value of 0.05 (5% FDR) was used.

3.2.18.1.2 Identification of yeast mitochondria complexes and supercomplexes using the Thermo Proteome Search Results Report

Protein Results Parameters

The protein page displays all the proteins and their corresponding peptides found in the sample during the database search. For each protein, the report shows the following results:

Accession: The unique identifier was assigned to the protein by the Uniprot FASTA database.

Description: The name and description of the protein of the identifier appeared in the corresponding Accession column.

Score: The SEQUEST protein score is the sum of all peptide XCorr values above the specified score threshold. The score threshold was calculated as "0.8 + *peptide charge* * *peptide relevance factor*", where *peptide relevance factor* has a default value of 0.4. For each spectrum, only the highest-scoring match was used. For each spectrum and sequence, the Proteome Discoverer application uses only the highest scored peptide.

Coverage: Represents the percentage of the protein sequence covered by the identified peptides.

 # *Proteins:* Represents the number of identified proteins in the protein group of a master protein. When the Protein Grouping setting is disabled, the #Proteins is always equal to 1.

 # *Unique Peptides:* Represents the number of peptide sequences unique to a protein.

 # *Peptides:* Represents the number of different peptide sequences identified in the protein.

 # *PSMs:* The peptide spectrum matches (PSMs) value corresponds to the total number of identified peptide sequences for the protein, including those that have been identified redundantly.

 # *AAs:* Represents the number of amino acid in the sequence length of the protein.

MW ^{kDa}: Represents the calculated molecular weight of the protein.

Calc. pI: Represents the theoretically calculated isoelectric point, *i.e.* the pH value at which a particular molecule carries no net electrical charge.

Peptides Results Parameters: For each identified peptide, the report shows the following results:

Protein Descriptions: Identifies a protein associated with the peptides. This description is taken from the Uniprot FASTA file.

 # *Proteins:* Represents the total number of proteins in which this peptide can be found.

Probability: Represents the probability score for the peptide.

SpScore (search-dependent): Represents the raw value of the preliminary score of the SEQUEST algorithm.

XCorr (search-dependent): Scores the number of fragment ions that are common to two different peptides with the same precursor mass; calculates the cross-correlation score for all candidate peptides queried from the database.

Δ Score: A measure of the difference between the top two scores for the peptides identified by that spectrum; the Proteome Discoverer application calculates this score as follows: ΔScore = Score(Rank N Peptide) – Score(Rank 1 Peptide)/Score(Rank 1 Peptide).

ΔCn: Represents the normalized score difference between the currently selected PSM and the highest-scoring PSM for that spectrum.

 # *Missed Cleavages:* Represents the number of cleavage sites in a peptide sequence that trypsin did not cleave, excluding the cases where the presence of proline prevents trypsin from cleaving the peptide bond.

Peptides Matched: Represents the number of peptides included in the precursor mass tolerance window set for the search.

Charge: Represents the charge state of the peptide.

Intensity: Represents the intensity of the precursor ion.

MH+ ^{Da}: Represents the protonated monoisotopic mass of the peptide, in Daltons.

ΔM ^{ppm}: Represents the difference between the theoretical mass of the peptide and the experimental mass of the precursor ion.

RT ^{min}: Represents the retention time when the peptide was observed, in minutes.

Xcalibur is a registered trademark of Thermo Fisher Scientific Inc. in the United States. SEQUEST is a registered trademark of the University of Washington in the United States.

3.2.19 Miscellaneous procedures

Total cell lysates were made by vortexing the cells in TCL buffer (25 mM Tris/HCl pH 8.5, 150 mM NaCl, 1 mM EDTA, 0.1 mM DTT, 4% CHAPS, 1 mM PMSF, protease inhibitor cocktail [Sigma]) with glass beads three times for 1 min. Lysates were then centrifuged and supernatants collected. Protein concentration was determined with an RC DC protein assay kit (Bio-Rad) following the manufacturer's instructions. Enzymatic activities of cytochrome *c* oxidase [231] and aconitase [232] were determined by established methods. Preparation of cellular extracts and microanalytic biochemical assays for measuring ATP were performed as previously described [233].

3.2.20 Statistical analysis

Statistical analysis was performed using Microsoft Excel's (2010) Analysis ToolPack-VBA. All data are presented as mean ± SEM. The *p* values were calculated using an unpaired two-tailed *t* test.

3.3 Results and Discussion

3.3.1 Treatment of yeast cells with LCA alters the age-related dynamics of changes in the rate of mitochondrial respiration, value of mitochondrial membrane potential and concentration of mitochondrial reactive oxygen species (ROS)

I first examined how LCA influences the age-related chronology of changes in mitochondrial respiration. I found that in yeast cells grown under CR on 0.2% glucose in the

absence of LCA and recovered at different periods of chronological lifespan, the efficiency of mitochondrial respiration was (1) greatly amplified when yeast entered D growth phase on day 2 of cell culturing; and (2) sharply declined through the subsequent PD and ST growth phases (Figure 3.1). In yeast cells cultured under CR on 0.2% glucose in the presence of exogenous LCA, the efficiency of mitochondrial respiration (1) increased to a much lesser extent during D phase than it increased in yeast cultured in the absence of LCA; and (2) reached a plateau in PD phase and declined slowly during the subsequent ST phase (Figure 3.1). It needs to be emphasized that, following entry of yeast cells into a quiescent state (i.e., during ST phase), the efficiency of mitochondrial respiration in yeast cultured in the presence of exogenous LCA significantly exceeded that in yeast cultured in its absence (Figure 3.1).

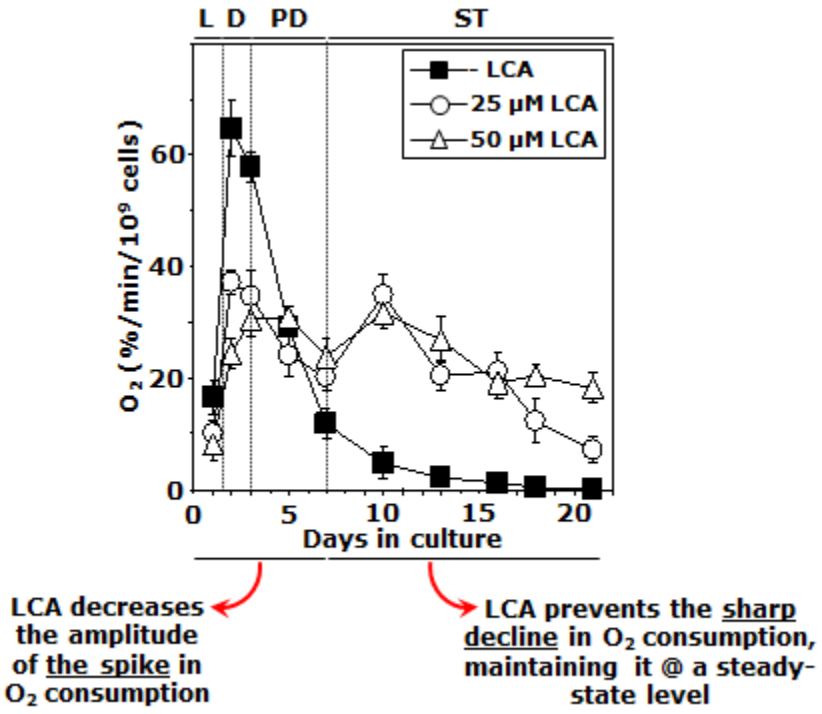

Figure 3.1. LCA alters the age-related chronology of changes in mitochondrial respiration.

Cells of the wild-type strain BY4742 were cultured in the nutrient-rich YP medium initially containing 0.2% glucose with LCA (added at the final concentration of 25 μM or 50 μM) or without it. The dynamics of age-related changes in the rate of oxygen consumption by cells was monitored as described in ″Materials and Methods″. Data are presented as means ± SEM (n = 3-7).

I then assessed how LCA affects the age-related dynamics of changes in (1) electrochemical potential across the IMM (ΔΨ); and (2) intracellular levels of hydrogen peroxide and superoxide radicals, the two major species of ROS known to be generated mainly as by-products of mitochondrial respiration [39]. I found that in yeast cells grown under CR on 0.2% glucose in the absence of LCA and recovered at different periods of chronological lifespan, the value of ΔΨ and the levels of both ROS species were (1) significantly magnified when yeast entered D growth phase on day 2 of cell culturing; and (2) abruptly reduced through the subsequent PD and ST growth phases (Figure 3.2). In yeast cells cultured under CR on 0.2% glucose in the presence of exogenous LCA, the value of ΔΨ and the levels of both ROS species were (1) elevated to a much lesser degree during D phase than they were elevated in yeast cultured in the absence of LCA; and (2) attained a plateau in PD phase and declined slowly (in case of ΔΨ), remained mainly unchanged (in case of hydrogen peroxide) or increased slightly and slowly (in case of superoxide radicals) during the subsequent ST phase (Figure 3.2). Importantly, in yeast cells that have entered a quiescent state (i.e., reach ST phase), the value of ΔΨ and the levels of both ROS species in yeast cultured in the presence of exogenous LCA substantially surpassed those in yeast cultured in its absence (Figure 3.2).

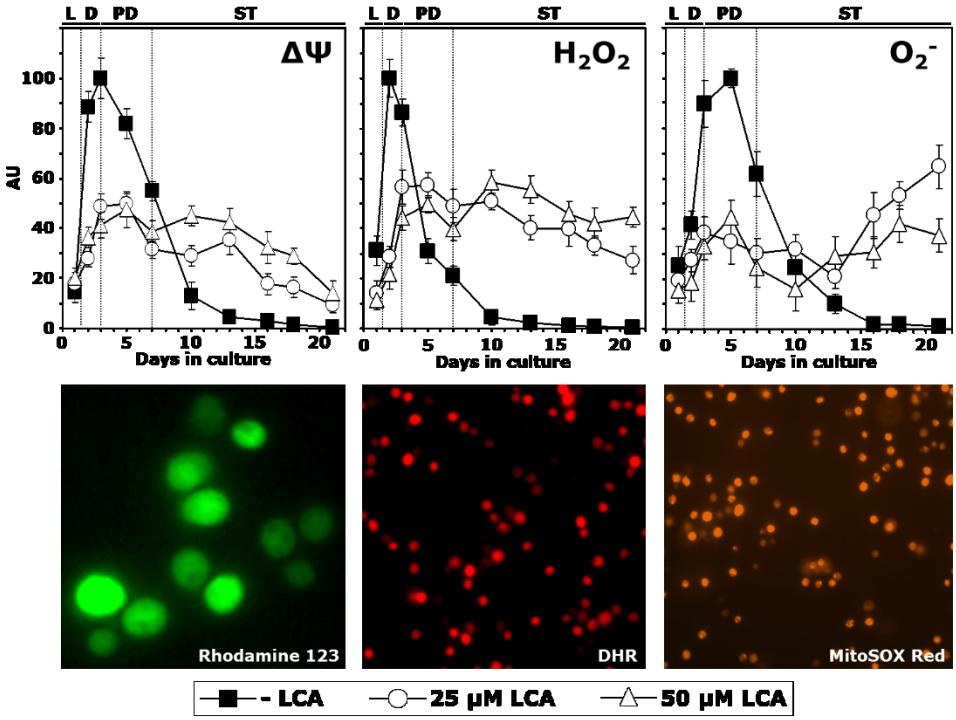

Figure 3.2. LCA alters the age-related dynamics of mitochondrial membrane potential (ΔΨ) and ROS generation.

Cells of the wild-type strain BY4742 were cultured in the nutrient-rich YP medium initially containing 0.2% glucose with LCA (added at the final concentration of 25 μM or 50 μM) or without it. The dynamics of age-related changes in the value of ΔΨ and the levels of both ROS species (i.e., hydrogen peroxide ^{H2O2} measured using DHR and superoxide radicals $^{O2-}$ measured using MitoSOX Red) were monitored as described in ″Materials and Methods″. Data are presented as means ± SEM (n = 4-6).

Taken together, these findings validate my hypothesis that LCA can significantly alter the age-related chronology of the efficiency of mitochondrial respiration, the value of ΔΨ and the levels of both major ROS species (i.e., H_2O_2 and O_2^-) produced in mitochondria. It is conceivable that such effect of LCA is due to the LCA-elicited specific changes in the membrane lipidome of mitochondria; indeed, the lipid composition of the IMM is known to modulate protein complexes and supercomplexes that reside within this mitochondrial membrane and are involved in mitochondrial respiration, the maintenance of electrochemical membrane potential and preservation of ROS homeostasis [193, 227 - 229].

3.3.2 LCA-driven decline of mitochondrially generated ROS in chronologically ″young″ yeast reduces the extent of oxidative damage to mitochondrial macromolecules, alters the abundance and composition of respiratory supercomplexes in the IMM, and elevates the levels of ATP produced in mitochondria

Based on findings described in the previous section, I hypothesized that the LCA-driven decline of mitochondrially generated ROS seen in chronologically ″young″ yeast cells may reduce the extent of oxidative damage to mitochondrial macromolecules. In support of this hypothesis, I found that a permanent exposure of yeast cells to exogenous LCA (1) reduces the degree of oxidative damage to mitochondrial proteins and lipids through the entire lifespan (Figure 3.3); (2) decreases the frequencies of deletion (i.e., *rho*$^-$ and *rho*^{0}) and point (i.e., *rib2* and *rib3*) mutations in mitochondrial DNA (mtDNA) following entry of yeast into a quiescent state, likely by protecting mtDNA from age-related oxidative damage (Figure 3.3); (3) enables to maintain enzymatic activities of cytochrome *c* oxidase and succinate dehydrogenase, two protein components of the mitochondrial electron transport chain (ETC) and the tricarboxylic acid (TCA) cycle (respectively), at the levels that through the entire ST phase considerably exceed those seen in mitochondria of yeast cultured in the absence of LCA (Figure 3.4); and (4) allows to sustain enzymatic activity of aconitase, a protein component of the mitochondrial TCA cycle,

at the level that through the entire ST phase is substantially higher than that observed in yeast grown without LCA - regardless whether or not the oxidation-dependent loss of one iron from the [4Fe-4S] cluster of aconitase was restored by incubation with Fe^{3+} and S^{2-} (Figure 3.5).

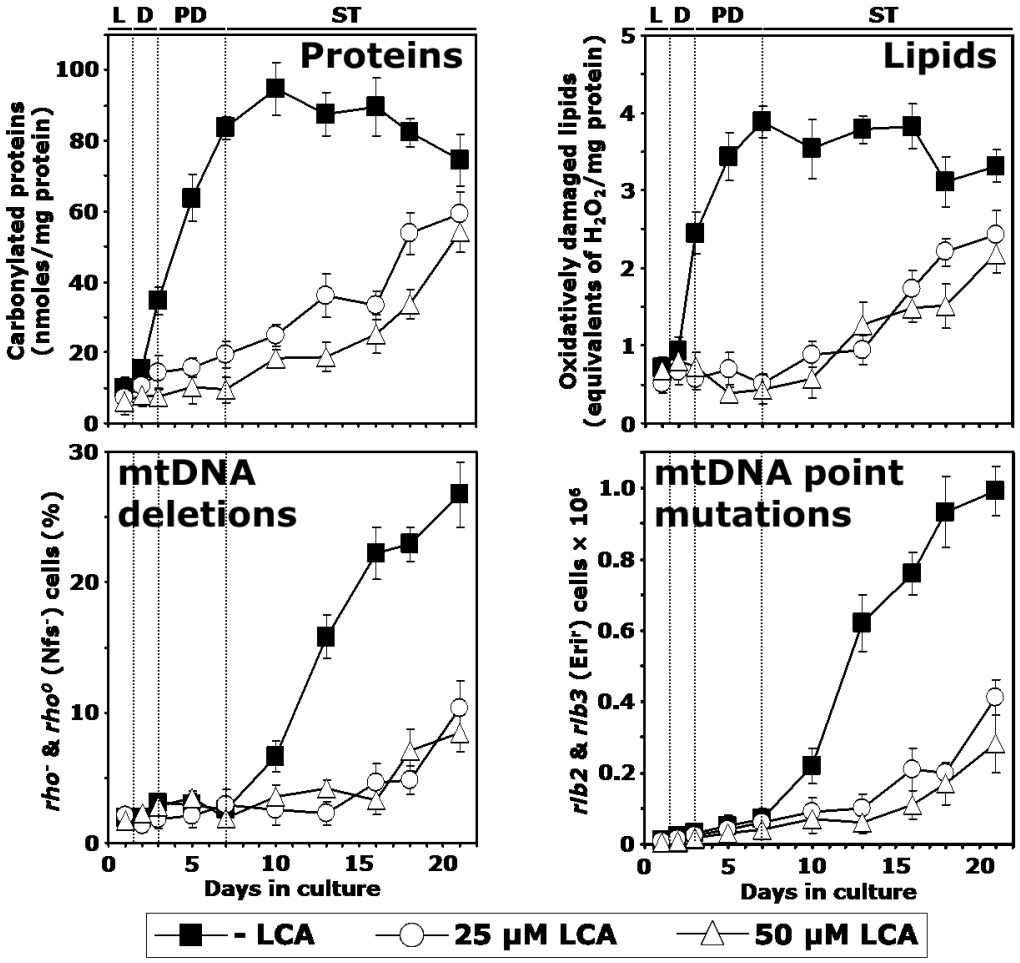

Figure 3.3. Permanent exposure of yeast cells to exogenous LCA protects mitochondrial proteins and lipids from oxidative damage as well as reduces the frequencies of mutations in mitochondrial DNA (mtDNA), likely by protecting it from age-related oxidative damage.

Cells of the wild-type strain BY4742 were cultured in the nutrient-rich YP medium initially containing 0.2% glucose with LCA (added at the final concentration of 25 μM or 50 μM) or without it. Mitochondria from cells recovered at different days of culturing were purified as described in ″Materials and Methods″. The quantities of carbonylated (i.e., oxidatively damaged) proteins and oxidatively damaged membrane lipids in purified mitochondria were measured as described in ″Materials and Methods″. The frequencies of deletion (i.e., rho- and rho0) and point (i.e., rib2 and rib3) mutations in mtDNA were monitored according to the procedures described in ″Materials and Methods″. Data are presented as means ± SEM (n = 3-9).

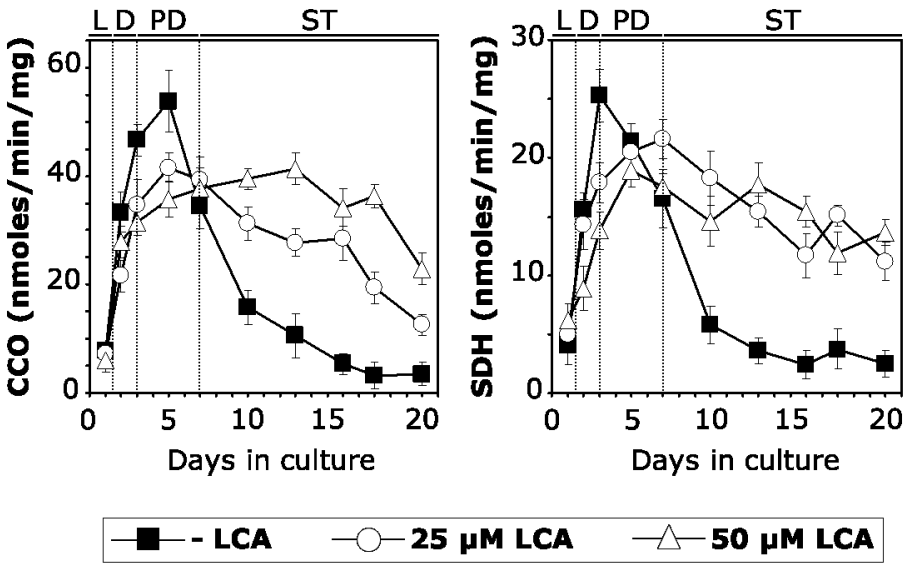

Figure 3.4. Permanent exposure of yeast cells to exogenous LCA enables to maintain enzymatic activities of cytochrome *c* oxidase and succinate dehydrogenase, two protein components of the mitochondrial electron transport chain and the tricarboxylic acid cycle (respectively), at the levels that through the entire ST phase considerably exceed those seen in mitochondria of yeast cultured in the absence of LCA.

Cells of the wild-type strain BY4742 were cultured in the nutrient-rich YP medium initially containing 0.2% glucose with LCA (added at the final concentration of 25 µM or 50 µM) or without it. Mitochondria from cells recovered at different days of culturing were purified as described in ″Materials and Methods″. Enzymatic activities of cytochrome *c* oxidase (CCO) and succinate dehydrogenase (SDH) in purified mitochondria were measured as described in ″Materials and Methods″. Data are presented as means ± SEM (n = 2-3).

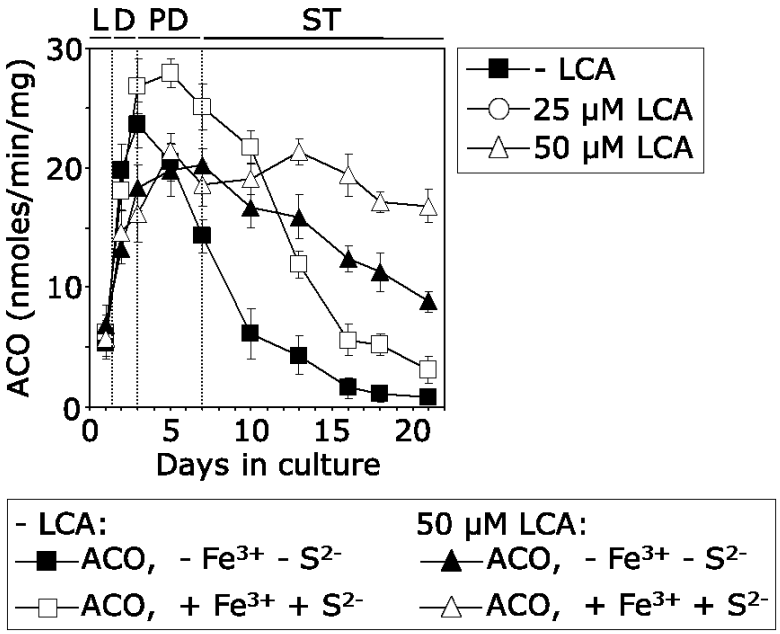

Figure 3.5. Permanent exposure of yeast cells to exogenous LCA sustains enzymatic activity of aconitase, a protein component of the mitochondrial TCA cycle, at the level that through the entire ST phase is substantially higher than that observed in yeast grown without LCA.

Cells of the wild-type strain BY4742 were cultured in the nutrient-rich YP medium initially containing 0.2% glucose with LCA (added at the final concentration of 25 μM or 50 μM) or without it. Enzymatic activities of aconitase (ACO) in total cell lysates were measured with or without the reactivation agents Fe^{3+} and Na_2S, as described in ″Materials and Methods″. Data are presented as means ± SEM (n = 4-6).

I then hypothesized that the LCA-driven reduction of the extent of oxidative damage to mitochondrial macromolecules can alter the abundance and/or composition of respiratory protein supercomplexes in the IMM and, thus, can cause some changes to the level of intracellular ATP known to be produced mainly as a product of coupling between ADP phosphorylation and electron transport in mitochondria [10, 132, 234]. A body of recent evidence supports the view that, instead of existing as separate units freely moving within the IMM, individual protein complexes of the mitochondrial ETC are assembled into supramolecular structures known as respiratory supercomplexes or respirasomes [235, 236]; some changes in such supramolecular organization of respiratory protein complexes are known to cause detrimental alterations of the mitochondrial respiratory chain, thereby eliciting certain age-related pathologies [237]. To validate this hypothesis, I purified mitochondria from wild-type cells cultured under CR on 0.2% glucose and

recovered on day 4 of culturing, used digitonin to solubilize protein complexes from the inner membrane of these mitochondria, and separated the solubilized protein complexes on a linear 4-13% acrylamide gradient gel for first-dimension blue native PAGE (1-D BN-PAGE). This gradient gel is known to resolve protein complexes within the mass range of 100 kDa - 3 MDa [238]. Such 1-D BN-PAGE analysis revealed that exposure of wild-type cells to LCA significantly increases the level of a respiratory supercomplex with the highest molecular weight (likely in a range of several MDa), which is marked by a red arrow in Figure 3.6. My mass spectrometry-based analysis demonstrated that this respiratory supercomplex in the IMM of LCA-treated wild-type cells consists of the complexes III and V of mitochondrial ETC as well as the ADP-ATP carrier protein AAC2 (Figure 3.7; respiratory supercomplex 1). My BN-PAGE analysis also revealed that exposure of wild-type cells to LCA increases the level of a respiratory supercomplex of a very high molecular weight (likely in an MDa range), which is marked by a yellow arrow in Figure 3.6. My mass spectrometry-based analysis showed that this respiratory supercomplex in the IMM of LCA-treated wild-type cells consists of (1) the ALD4 isoform of acetaldehyde dehydrogenase, an enzyme involved in the conversion of acetaldehyde to acetyl-CoA in yeast mitochondria; (2) the IDH1 and IDH2 isoforms of isocitrate dehydrogenase, an enzyme involved in the TCA cycle; and (3) HSP60, a tetradecameric mitochondrial chaperonin that not only drives the ATP-dependent folding of precursor polypeptides and complex assembly, but also prevents aggregation and mediates protein refolding after heat shock (Figure 3.7; respiratory supercomplex 6).

To define the composition of each of the protein supercomplexes recovered by 1-D BN-PAGE (Figure 3.6), I resolved their individual protein components by second-dimension tricine-SDS-PAGE (2-D SDS-PAGE), visualized these components by silver staining and identified them by mass spectrometry. I found that, in addition to one or more kinds of individual respiratory complexes, many protein supercomplexes in the IMM of wild-type cells exposed to exogenous LCA contain one or more proteins that have not been traditionally viewed as components associated (even transiently) with the mitochondrial respiratory chain. These novel protein components of respiratory protein supercomplexes in the IMM of wild-type cells treated with LCA include: (1) the ADP-ATP carrier protein Aac2p, a component of the supercomplexes 1, 2 and 5; (2) the tetradecameric mitochondrial chaperonin HSP60, a component of the respiratory supercomplex 6; (3) the ALD4 isoform of acetaldehyde dehydrogenase, a component

of the supercomplexes 6, 8 and 9; (4) the IDH1 and IDH2 isoforms of isocitrate dehydrogenase, two components of the supercomplexes 6 and 8; (5) the HSP70 family ATPase SSC1, a component of the supercomplexes 9 and 10; (6) the KGD1 subunit of the mitochondrial alpha-ketoglutarate dehydrogenase complex involved in the TCA cycle, a component of the supercomplexes 9 and 10; (7) aconitase ACO1 involved in the TCA cycle, a component of the supercomplexes 9 and 10; and (8) the valyl-tRNA synthetase VAS1, a component of the supercomplex 10 (Figure 3.7).

These findings revealed several ways of rearranging respiratory supercomplexes in the IMM of yeast cells exhibiting an altered mitochondrial membrane lipidome in response to LCA treatment. First, LCA-driven changes in the mitochondrial membrane lipidome increase the abundance of the major respiratory supercomplexes (respirasomes) 1 and 6 (Figure 3.6). Second, LCA-driven changes in the mitochondrial membrane lipidome cause a recruitment of several new mitochondrial protein components, not previously known for being permanently associated with the ETC, into the remodeled respirasomes (Figures 3.7 and 3.8). It should be emphasized that all these protein components newly recruited into the remodeled respirasomes are known for their essential roles in mitochondria-confined processes that define longevity. Specifically, the observed recruitment of AAC2 to the remodeled respiratory supercomplexes suggests a mechanism in which the ability of AAC2 to sense the rates/efficacies with which electrons are transferred through the ETC (by the respiratory complex III) and ATP is synthesized (by the respiratory complex V) in mitochondria enables this transport protein to modulate accordingly the rate of ATP-ADP exchange between mitochondria and cytosol (Figure 3.8). The resulting increase of the efficiency of ATP synthesis in mitochondria of chronologically aging yeast is likely to extend their longevity. Furthermore, the observed recruitment of IDH1, IDH2, KGD1, ACO1, ALD4, HSP60 and SSC1 to the remodeled respiratory supercomplexes is expected to provide an efficient way of coordinating the rates of NADH synthesis (by IDH1, IDH2, KGD1 and ACO1) and acetyl-CoA formation (by ALD4) with functional states of numerous proteins governed by the chaperone and protein import activities of HSP60 and SSC1 in mitochondria (Figure 3.8), thereby extending yeast longevity. Moreover, the observed recruitment of VAS1 (a valyl-tRNA synthetase for mitochondrial protein synthesis) to the remodeled respiratory supercomplexes is expected to provide an efficient way of coordinating the rate of mitochondrial NADH synthesis (by KGD1 and ACO1) with mitochondrial protein synthesis (by VAS1) and

mitochondrial protein import (by SSC1) (Figure 3.8); such remodeling of respiratory supercomplexes is likely to extend longevity of chronologically aging yeast.

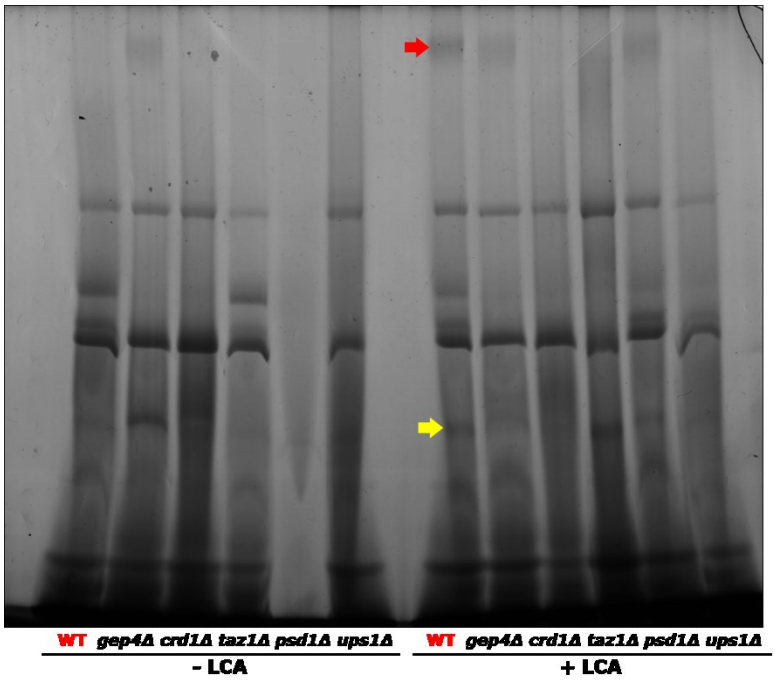

Figure 3.6. LCA (and genetic manipulations changing the makeup of mitochondrial membrane lipids) alter the abundance of respiratory supercomplexes in the inner mitochondrial membrane.

Cells of the wild-type strain BY4742 were cultured in the nutrient-rich YP medium initially containing 0.2% glucose with LCA (added at the final concentration of 50 μM) or without it. Mitochondria were purified from cells recovered on day 7 of culturing as described in ″Materials and Methods″. Digitonin-solubilized protein complexes from the inner membrane of these mitochondria were separated on a linear 4-13% acrylamide gradient gel for first-dimension blue native PAGE (1-D BN-PAGE) as described in ″Materials and Methods″. Arrows mark the positions of protein supercomplexes whose levels were elevated in mitochondria of cells exposed to LCA. Although protein supercomplexes that were recovered in mitochondria purified from the mutant strains *ups1Δ* (*MATα his3Δ1 leu2Δ0 lys2Δ0 ura3Δ0 ups1Δ::kanMX4*), *taz1Δ* (*MATα his3Δ1 leu2Δ0 lys2Δ0 ura3Δ0 taz1Δ::kanMX4*), *gep4Δ* (*MATα his3Δ1 leu2Δ0 lys2Δ0 ura3Δ0 gep4Δ::kanMX4*), *psd1Δ* (*MATα his3Δ1 leu2Δ0 lys2Δ0 ura3Δ0 psd1Δ::kanMX4*) and *crd1Δ* (*MATα his3Δ1 leu2Δ0 lys2Δ0 ura3Δ0 crd1Δ::kanMX4*) are shown here, these unpublished data are not discussed in my thesis.

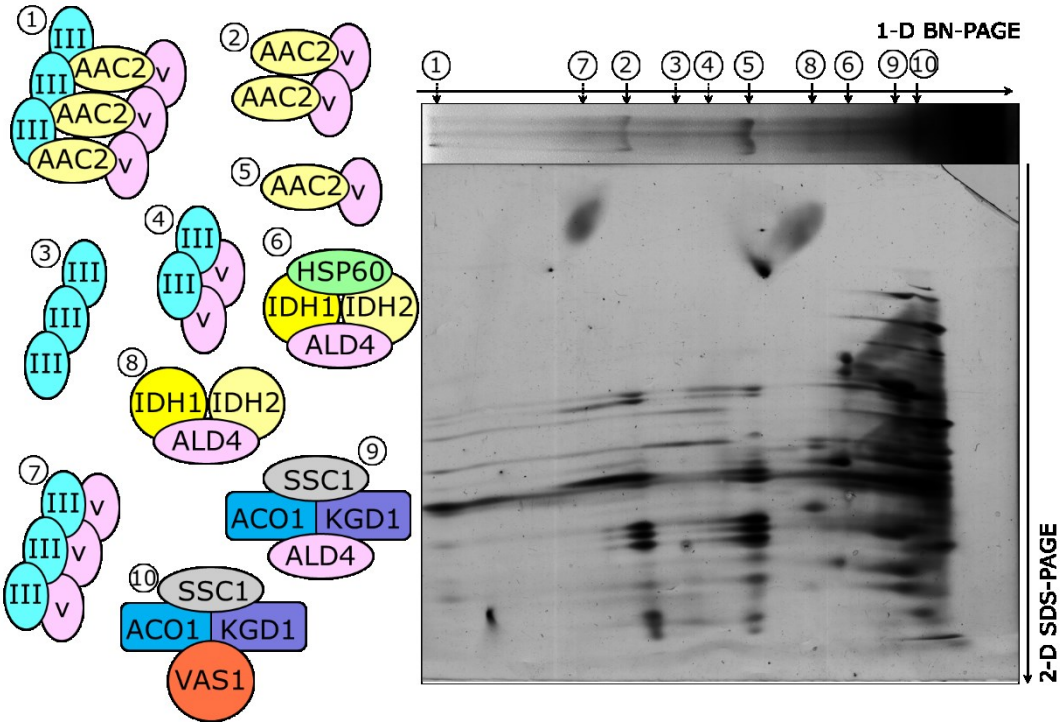

Figure 3.7. LCA alters the compositions of some of the respiratory supercomplexes residing in the inner mitochondrial membrane.

Cells of the wild-type strain BY4742 were cultured in the nutrient-rich YP medium initially containing 0.2% glucose with LCA (added at the final concentration of 50 μM) or without it. Mitochondria were purified from cells recovered on day 7 of culturing as described in ″Materials and Methods″. Digitonin-solubilized protein complexes from the inner membrane of these mitochondria were first separated on a linear 4-13% acrylamide gradient gel for first-dimension blue native PAGE (1-D BN-PAGE) and then resolved by second-dimension tricine-SDS-PAGE (2-D SDS-PAGE) as described in ″Materials and Methods″. Following silver staining, the separated by 2-D SDS-PAGE proteins were identified by mass spectrometry as described in ″Materials and Methods″.

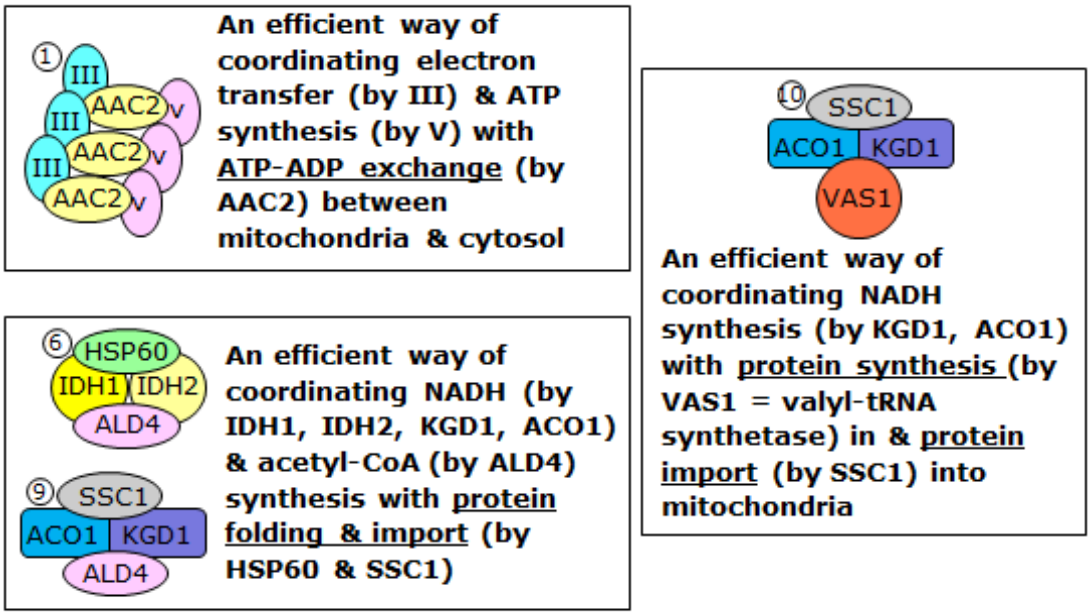

Figure 3.8. LCA causes a recruitment of certain mitochondrial protein components, not previously known for being permanently associated with the ETC, into the remodeled respirasomes within the inner mitochondrial membrane.

All these protein components newly recruited into the remodeled respirasomes are known for their essential roles in mitochondria-confined processes that define longevity. There are several ways through which such recruitment may improve mitochondrial functionality and, thus, may extend yeast longevity.

Because a coupling between ADP phosphorylation and electron transport in mitochondria is known to produce the bulk of ATP in yeast [10, 132, 234] and LCA alters the abundance and composition of respiratory protein supercomplexes in the IMM (as described above), I then assessed how a permanent exposure of yeast cells to exogenous LCA influences the level of intracellular ATP. I found that in yeast grown under CR on 0.2% glucose and recovered at different periods of chronological lifespan, LCA alters the age-related dynamics of changes in the cellular level of ATP (Figure 3.9). Specifically, during ST growth phase the level of ATP in yeast cells cultured under CR conditions in the presence of exogenous LCA considerably exceeded that detected in yeast cultured in its absence (Figure 3.9).

Taken together, these findings validate my hypothesis that the LCA-driven reduction of the extent of oxidative damage to mitochondrial macromolecules alters the abundance and

composition of respiratory protein supercomplexes in the IMM. This, in turn, increases the level of ATP in chronologically active yeast cells that have entered a quiescent state.

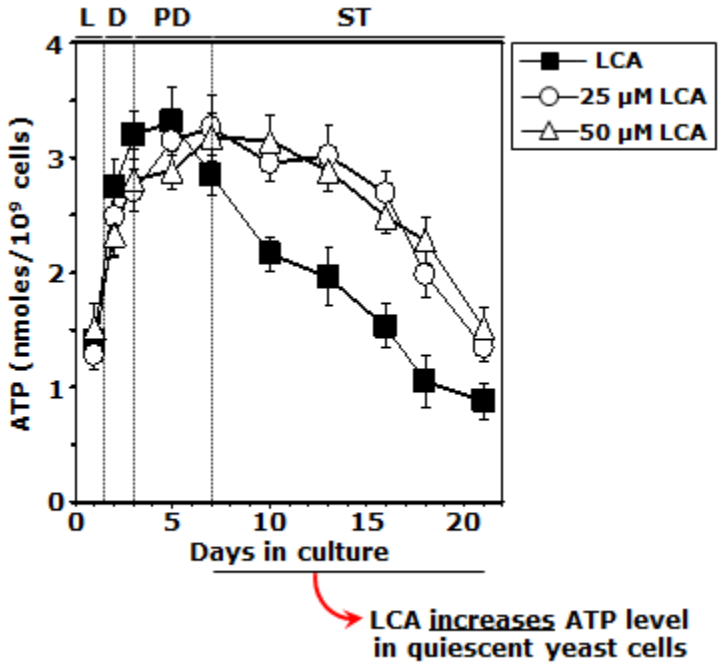

Figure 3.9. LCA alters the age-related dynamics of changes in the cellular level of ATP.

Cells of the wild-type strain BY4742 were cultured in the nutrient-rich YP medium initially containing 0.2% glucose with LCA (added at the final concentration of 25 μM or 50 μM) or without it. Intracellular levels of ATP were measured as described in ″Materials and Methods″. Data are presented as means ± SEM (n = 3-5).

3.4 Conclusions

In sum, findings presented in Chapter 3 support the validity of my hypothesis that the LCA-elicited changes in the membrane lipidome of mitochondria alter the age-related dynamics of several longevity-defining mitochondrial processes. These processes include mitochondrial respiration, maintenance of mitochondrial membrane potential and ROS homeostasis, prevention of excessive oxidative damage to mitochondrial macromolecules, preservation of certain respiratory supercomplexes in the IMM, and ATP synthesis.

4 LCA extends yeast longevity by reducing the damaging effect of mitochondrially produced ROS on macromolecules outside mitochondria and by amplifying the "hormetic" effect of mitochondrially generated ROS on cell resistance to stresses

4.1 Introduction

I hypothesized that LCA may delay aging in yeast by influencing longevity-defining processes taking place not only in mitochondria but also in cellular locations outside these organelles. In particular, I thought that LCA may extend yeast longevity by (1) reducing the damaging effect of mitochondrially produced ROS on macromolecules (i.e. proteins, lipids and/or nucleic acids) outside mitochondria; and (2) amplifying the ″hormetic″ effect of mitochondrially generated ROS through an induction of the synthesis and/or post-translational activation of proteins that protect cells from oxidative and other forms of stress, protein aggregation and damage of nuclear DNA (Figure 4.1).

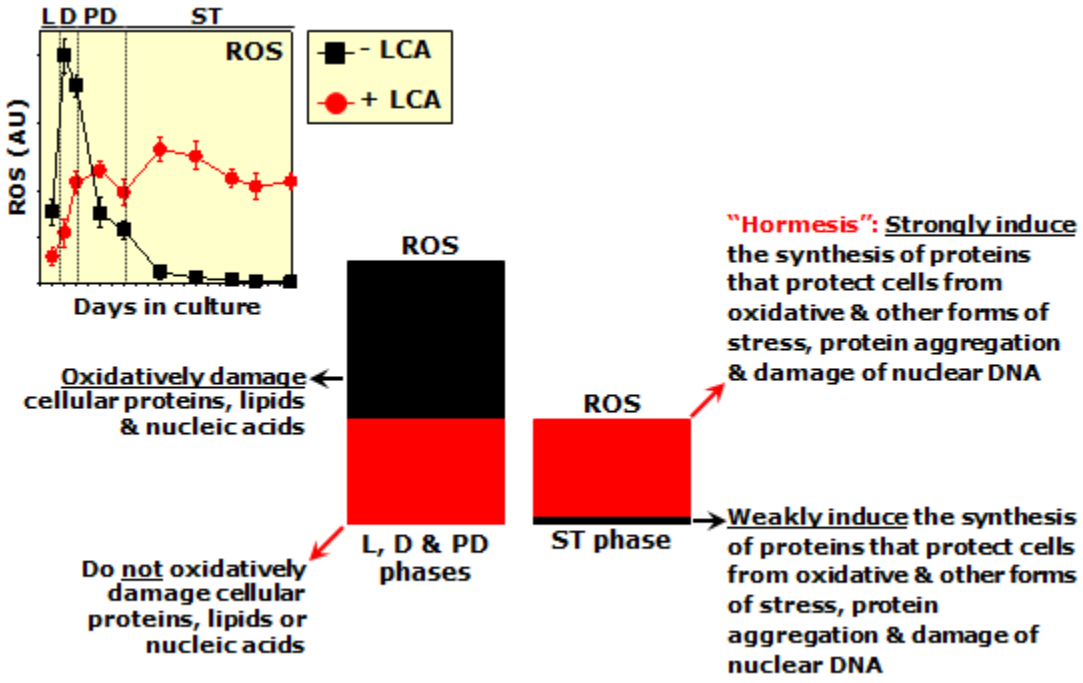

Figure 4.1. LCA may extend yeast longevity by reducing the damaging effect of mitochondrially produced ROS on cellular macromolecules outside mitochondria and by amplifying the ″hormetic″ effect of mitochondrially generated ROS.

See text for details.

4.2 Materials and methods

4.2.1 Strains and media

The wild-type strain *Saccharomyces cerevisiae* BY4742 (*MATα his3Δ1 leu2Δ0 lys2Δ0 ura3Δ0*) and mutant strains *ndi1Δ* (*MATα his3Δ1 leu2Δ0 lys2Δ0 ura3Δ0 ndi1Δ::kanMX4*), *gpx1Δ* (*MATα his3Δ1 leu2Δ0 lys2Δ0 ura3Δ0 gpx1Δ::kanMX4*), *sod1Δ* (*MATα his3Δ1 leu2Δ0 lys2Δ0 ura3Δ0 sod1Δ::kanMX4*), *sod2Δ* (*MATα his3Δ1 leu2Δ0 lys2Δ0 ura3Δ0 sod2Δ::kanMX4*), *ctt1Δ* (*MATα his3Δ1 leu2Δ0 lys2Δ0 ura3Δ0 ctt1Δ::kanMX4*), *cta1Δ* (*MATα his3Δ1 leu2Δ0 lys2Δ0 ura3Δ0 cta1Δ::kanMX4*), *ccp1Δ* (*MATα his3Δ1 leu2Δ0 lys2Δ0 ura3Δ0 ccp1Δ::kanMX4*), *trx1Δ* (*MATα his3Δ1 leu2Δ0 lys2Δ0 ura3Δ0 trx1Δ::kanMX4*), *trx2Δ* (*MATα his3Δ1 leu2Δ0 lys2Δ0 ura3Δ0 trx2Δ::kanMX4*), *trx3Δ* (*MATα his3Δ1 leu2Δ0 lys2Δ0 ura3Δ0 trx3Δ::kanMX4*), *tsa1Δ* (*MATα his3Δ1 leu2Δ0 lys2Δ0 ura3Δ0 tsa1Δ::kanMX4*), *tsa2Δ* (*MATα his3Δ1 leu2Δ0 lys2Δ0 ura3Δ0 tsa2Δ::kanMX4*), *gpx1Δ* (*MATα his3Δ1 leu2Δ0 lys2Δ0 ura3Δ0 gpx1Δ::kanMX4*), *hyr1Δ* (*MATα his3Δ1 leu2Δ0 lys2Δ0 ura3Δ0 hyr1Δ::kanMX4*) were used in this study. The composition of YEPD (0.2% glucose) medium was as follows: 1% yeast extract, 2% peptone, 0.2% glucose. Cells were cultured at 30^{o}C with rotational shaking at 200 rpm in Erlenmeyer flasks at a ″flask volume/medium volume″ ratio of 5:1.

4.2.2 A plating assay for the analysis of chronological lifespan

Cells were grown in YEPD (0.2% glucose) medium at 30^{o}C with rotational shaking at 200 rpm in Erlenmeyer flasks at a flask volume/medium volume ratio of 5:1. A sample of cells was removed from each culture at various time points. A fraction of the cell sample was diluted in order to determine the total number of cells per ml of culture using a hemacytometer. 10 μl of serial dilutions (1:10 to 1:10^{3}) of cells were applied to the hemacytometer, where each large square is calibrated to hold 0.1 μl. The number of cells in 4 large squares was then counted and an average was taken in order to ensure greater accuracy. The concentration of cells was calculated as follows: number of cells per large square x dilution factor x 10 x 1,000 = total number of cells per ml of culture. A second fraction of the cell sample was diluted and serial dilutions (1:10^{2} to 1:10^{5}) of cells were plated onto YEPD (2% glucose) plates in triplicate in order to count the number of viable cells per ml of each culture. 100 μl of diluted culture was plated onto each plate. After a 48-h incubation at 30^{o}C, the number of colonies per plate was

counted. The number of colony forming units (CFU) equals to the number of viable cells in a sample. Therefore, the number of viable cells was calculated as follows: number of colonies x dilution factor x 10 = number of viable cells per ml. For each culture assayed, % viability of the cells was calculated as follows: number of viable cells per ml / total number of cells per ml x 100%. The % viability of cells in mid-logarithmic phase was set at 100% viability for that particular culture. The life span curves for wild-type and some of the mutant strains were also validated using a LIVE/DEAD yeast viability kit (Invitrogen) following the manufacturer's instructions for stationary-phase cultures.

4.2.3 Pharmacological manipulation of chronological lifespan

Chronological lifespan analysis was performed as described above in this section. The lithocholic (LCA) [#L6250] bile acid was from Sigma. The stock solution of LCA in DMSO was made on the day of adding this compound to cell cultures. LCA was added to growth medium at the final concentration of 50 μM immediately following cell inoculation. The final concentration of DMSO in yeast cultures supplemented with LCA (and in the corresponding control cultures supplemented with drug vehicle) was 1% (v/v).

4.2.4 Plating assays for the analysis of resistance to various stresses

For the analysis of hydrogen peroxide resistance, serial dilutions ($1:10^0$ to $1:10^5$) of wild-type and mutant cells recovered from various phases of growth in YEPD (0.2% glucose) were spotted onto two sets of plates. One set of plates contained YEPD (2% glucose) medium alone, whereas the other set contained YEPD (2% glucose) medium supplemented with 5 mM hydrogen peroxide. Pictures were taken after a 3-day incubation at 30^oC.

For the analysis of heat-shock resistance, serial dilutions ($1:10^0$ to $1:10^5$) of wild-type and mutant cells recovered from various phases of growth in YEPD (0.2% glucose) were spotted onto two sets of YEPD (2% glucose) plates. One set of plates was incubated at 30^oC. The other set of plates was initially incubated at 55^oC for 30 min, and was then transferred to 30^oC. Pictures were taken after a 3-day incubation at 30^oC.

4.2.5 Monitoring the formation of ROS

Wild-type and mutant cells grown in YEPD (0.2% glucose) were tested microscopically for the production of ROS by incubation with dihydrorhodamine 123 (DHR). In the cell, this nonfluorescent compound can be oxidized to the fluorescent chromophore rhodamine 123 by ROS. Cells were also probed with a fluorescent counterstain Calcofluor White M2R (CW), which stains the yeast cell walls fluorescent blue. CW was added to each sample in order to label all cells for their proper visualization. DHR was stored in the dark at –20^{o}C as 50 µl aliquots of a 1 mg/ml solution in ethanol. CW was stored in the dark at –20^{o}C as the 5 mM stock solution in anhydrous DMSO (dimethylsulfoxide).

The concurrent staining of cells with DHR and CW was carried out as follows. The required amounts of the 50 µl DHR aliquots (1 mg/ml) and of the 5 mM stock solution of CW were taken out of the freezer and warmed to room temperature. The solutions of DHR and CW were then centrifuged at 21,000 x g for 5 min in order to clear them of any aggregates of fluorophores. For cell cultures with a titre of ~ 10^7 cells/ml, 100 µl was taken out of the culture to be treated. If the cell titre was lower, proportionally larger volumes were used. 6 µl of the 1 mg/ml DHR and 1 µl of the 5 mM CW solutions were added to each 100 µl aliquot of culture. After a 2-h incubation in the dark at room temperature, the samples were centrifuged at 21,000 x g for 5 min. Pellets were resuspended in 10 µl of PBS buffer (20 mM KH_2PO_4/KOH, pH 7.5, and 150 mM NaCl). Each sample was then supplemented with 5 µl of mounting medium, added to a microscope slide, covered with a coverslip, and sealed using nail polish. Once the slides were prepared, they were visualized under the Zeiss Axioplan fluorescence microscope mounted with a SPOT Insight 2 megapixel color mosaic digital camera. Several pictures of the cells on each slide were taken, with two pictures taken of each frame. One of the two pictures was of the cells seen through a rhodamine filter in order to detect cells dyed with DHR. The second picture was of the cells seen through a DAPI filter in order to visualize CW, and therefore all the cells present in the frame.

For evaluating the percentage of DHR-positive cells, the UTHSCSA Image Tool (Version 3.0) software was used to calculate both the total number of cells and the number of stained cells. Fluorescence of individual DHR-positive cells in arbitrary units was determined by using the UTHSCSA Image Tool software (Version 3.0). In each of 3-5 independent experiments, the value of median fluorescence was calculated by analyzing at least 800-1000 cells that were

collected at each time point. The median fluorescence values were plotted as a function of the number of days cells were cultured.

4.2.6 Immunofluorescence microscopy

Cell cultures were fixed in 3.7% formaldehyde for 45 min at room temperature. The cells were washed in solution B (100 mM KH_2PO_4/KOH pH 7.5, 1.2 M sorbitol), treated with Zymolyase 100T (MP Biomedicals, 1 µg Zymolyase 100T/1 mg cells) for 30 min at 30^{o}C and then processed as previously described (Pringle *et al*., 1991). Monoclonal antibody raised against porin (Invitrogen, 0.25 µg/µl in TBSB buffer [20 mM Tris/HCl pH 7.5, 150 mM NaCl, 1 mg/ml BSA]) was used as a primary antibody. Alexa Fluor 568 goat anti-mouse IgG (Invitrogen, 2 µg/µl in TBSB buffer) was used as a secondary antibody. The labeled samples were mounted in mounting solution (16.7 mM Tris/HCl pH 9.0, 1.7 mg/ml p-phenylenediamine, 83% glycerol). Images were collected with a Zeiss Axioplan fluorescence microscope (Zeiss) mounted with a SPOT Insight 2 megapixel color mosaic digital camera (Spot Diagnostic Instruments).

4.2.7 Measurement of the frequency of nuclear mutations

The frequency of spontaneous point mutations in the *CAN1* gene of nuclear DNA was evaluated by measuring the frequency of mutations that caused resistance to the antibiotic canavanine. A sample of cells was removed from each culture at various time-points. Cells were plated in triplicate onto YNB (0.67% Yeast Nitrogen Base without amino acids [#DF0919153; Fisher Scientific]) plates containing 2% glucose and supplemented with *L*-canavanine (50 mg/L), histidine, leucine, lysine and uracil (#C1625, #H8125, #L8912, #L5751 and #U0750, respectively; all from Sigma). In addition, serial dilutions of each sample were plated in triplicate onto YP plates containing 2% glucose for measuring the number of viable cells. The number of CFU was counted after 4 d of incubation at 30^{o}C. For each culture, the frequency of mutations that caused resistance to canavanine was calculated as follows: number of CFU per ml on YNB plates containing 2% glucose, L-canavanine (50 mg/L), histidine, leucine, lysine and uracil/number of CFU per ml on YP plates containing 2% glucose.

4.2.8 Immunodetection of carbonyl groups in oxidatively damaged cellular proteins

Total cell lysates were made by vortexing the cells in ice-cold TCL buffer (25 mM MOPS/KOH, pH 7.2, 150 mM NaCl, 50 mM DTT, and 1% CHAPS) with glass beads three times for 1 min. Lysates were then centrifuged for 5 min at 21,000 × g at 4^{o}C, and the supernatants of total cell lysates were collected. The carbonyl groups of proteins recovered in total cell lysates were derivatized to 2,4-dinitrophenylhydrazones using the OxyBlot^{TM} Protein Oxidation Detection Kit (Chemicon), according to the manufacturer's instructions. Briefly, total cellular proteins were denatured by adding 12% SDS to an equal volume of the total cell lysate containing 10 μg of protein. Denatured proteins were incubated with 2,4-dinitrophenylhydrazine for 15 min at room temperature. Proteins were separated by 12.5% SDS-PAGE. Immunoblotting using a Trans-Blot SD semi-dry electrophoretic transfer system (Bio-Rad) was performed as described (Titorenko et al., 1998). The derivatized carbonyl groups were detected with a 2,4-dinitrophenyl-specific antibody (Chemicon) and the Amersham ECL Western Blotting System (GE Healthcare).

4.2.9 Statistical analysis

Statistical analysis was performed using Microsoft Excel's (2010) Analysis ToolPack-VBA. All data are presented as mean ± SEM. The *p* values were calculated using an unpaired two-tailed *t* test.

4.3 Results and Discussion

4.3.1 Treatment of yeast cells with LCA reduces the extent of oxidative damage to macromolecules outside mitochondria and protects cells from oxidative and thermal stresses

In support of my hypothesis outlined in the ″Introduction″ section of this chapter, I found that a permanent exposure of yeast cells to exogenous LCA (1) considerably reduces the degree of oxidative damage to cellular proteins through the entire lifespan (Figures 4.2 and 4.3); (2) protects cellular lipids from oxidative damage through the entire lifespan (Figure 4.4); (3) decreases the frequencies of the *can1* point mutations in the nuclear DNA following entry of yeast into a quiescent state, likely by protecting this DNA from age-related oxidative damage

(Figure 4.5); and (4) increases the resistance of chronologically aging yeast to chronic oxidative and thermal stresses (Figures 4.6 and 4.7).

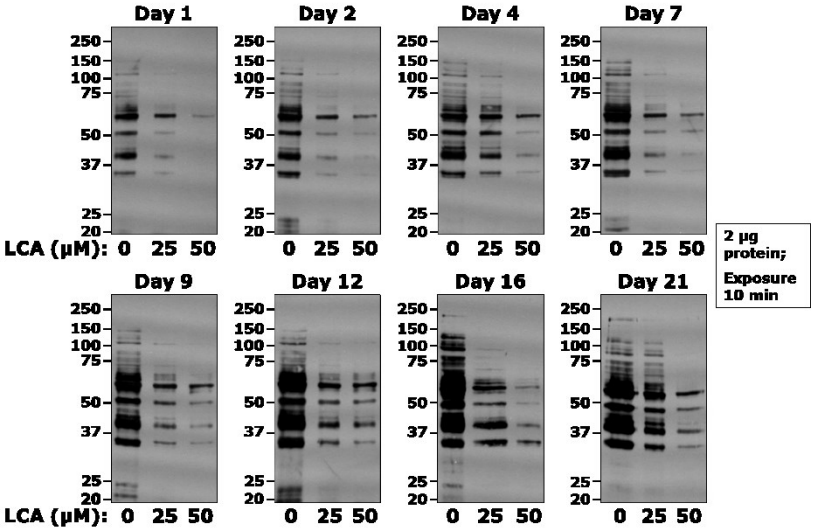

Figure 4.2. A permanent exposure of yeast cells to exogenous LCA considerably reduces the degree of oxidative damage to cellular proteins through the entire lifespan.

Cells of the wild-type strain BY4742 were cultured in the nutrient-rich YP medium initially containing 0.2% glucose with LCA (added at the final concentration of 25 μM or 50 μM) or without it. The extent of oxidative damage to cellular proteins was monitored using the OxyBlot Protein Oxidation Detection Kit as described in ″Materials and Methods″.

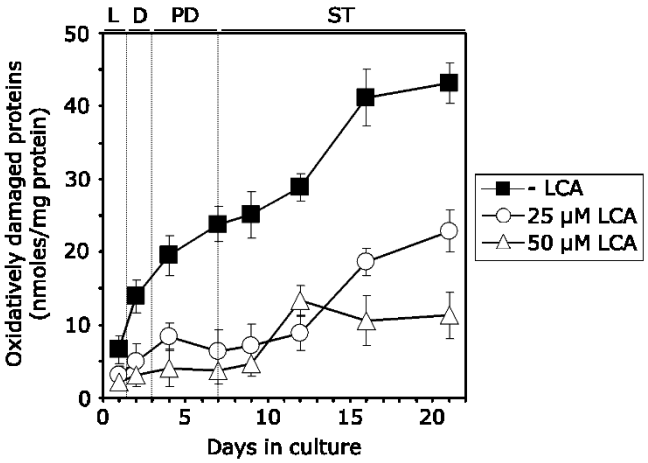

Figure 4.3. A permanent exposure of yeast cells to exogenous LCA considerably reduces the degree of oxidative damage to cellular proteins through the entire lifespan.

Cells of the wild-type strain BY4742 were cultured in the nutrient-rich YP medium initially containing 0.2% glucose with LCA (added at the final concentration of 25 μM or 50 μM) or without it. The extent of oxidative damage to cellular proteins was monitored using Protein Carbonyl Colorimetric Assay Kit as described in ″Materials and Methods″. Data are presented as means ± SEM (n = 4-5).

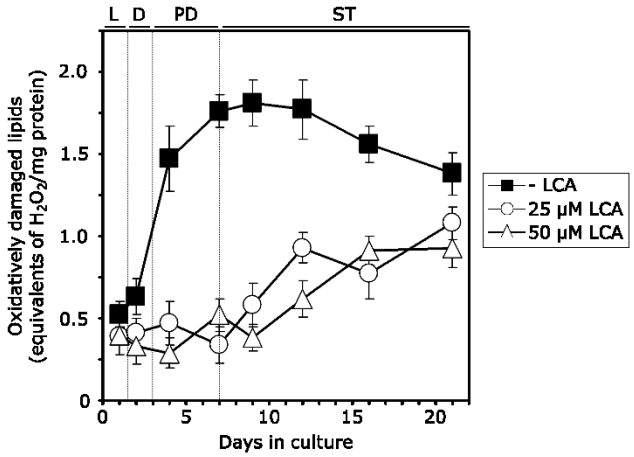

Figure 4.4. A permanent exposure of yeast cells to exogenous LCA protects cellular lipids from oxidative damage through the entire lifespan.

Cells of the wild-type strain BY4742 were cultured in the nutrient-rich YP medium initially containing 0.2% glucose with LCA (added at the final concentration of 25 μM or 50 μM) or without it. The extent of oxidative damage to cellular lipids was monitored using the PeroXOquant Quantitative Peroxide Assay Kit as described in ″Materials and Methods″. Data are presented as means ± SEM (n = 3-5).

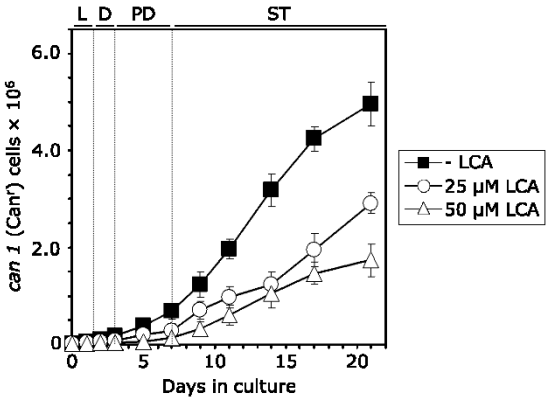

Figure 4.5. A permanent exposure of yeast cells to exogenous LCA decreases the frequencies of the *can1* point mutations in the nuclear DNA following entry of yeast into a quiescent state, likely by protecting this DNA from age-related oxidative damage.

Cells of the wild-type strain BY4742 were cultured in the nutrient-rich YP medium initially containing 0.2% glucose with LCA (added at the final concentration of 25 μM or 50 μM) or without it. The frequencies of the *can1* point mutations in the nuclear DNA were measured as described in ″Materials and Methods″. Data are presented as means ± SEM (n = 4-9).

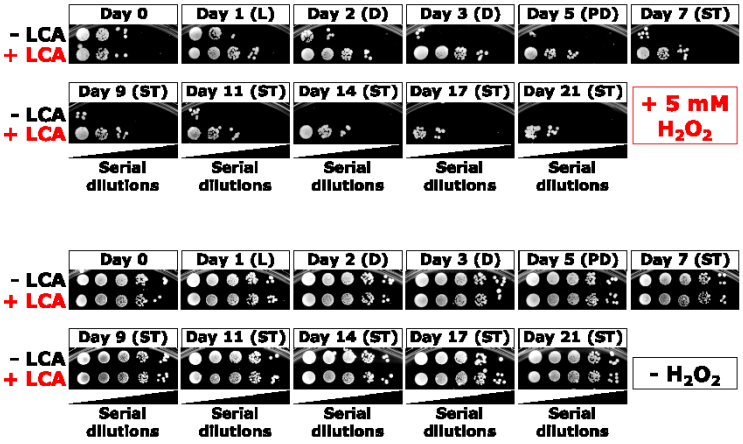

Figure 4.6. A permanent exposure of yeast cells to exogenous LCA increases the resistance of chronologically aging yeast to chronic oxidative stress.

Cells of the wild-type strain BY4742 were cultured in the nutrient-rich YP medium initially containing 0.2% glucose with LCA (added at the final concentration of 50 μM) or without it. Spot assays for monitoring oxidative stress resistance were performed as described in ″Materials and Methods″. Serial ten-fold dilutions of cells were spotted on plates with solid YP medium containing 2% glucose as carbon source and 5 mM hydrogen peroxide. All pictures were taken after a 3-day incubation at 30°C.

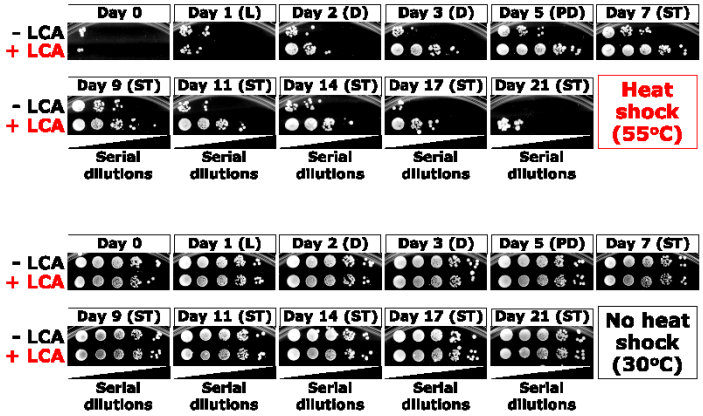

Figure 4.7. A permanent exposure of yeast cells to exogenous LCA increases the resistance of chronologically aging yeast to chronic thermal stress.

Cells of the wild-type strain BY4742 were cultured in the nutrient-rich YP medium initially containing 0.2% glucose with LCA (added at the final concentration of 50 μM) or without it. Spot assays for monitoring oxidative stress resistance were performed as described in ″Materials and Methods″. Serial ten-fold dilutions of cells were spotted on plates with solid YP medium containing 2% glucose as carbon source. Plates were initially incubated at 55°C for 30 min, and were then transferred to 30°C. All pictures were taken after a 3-day incubation at 30°C.

4.3.2 The ability of LCA to alter the age-related dynamics of mitochondrially produced ROS in chronologically ″young″ and ″old″ yeast cells underlies its longevity-extending effect

I then used a complementary functional genetics approach for validating my hypothesis in which the longevity-extending potential of LCA is due to its ability to alter the age-related dynamics of mitochondrially produced ROS in both chronologically ″young″ and ″old″ cells, thus reducing the damaging effect of these ROS in ″young″ cells and amplifying their ″hormetic″ effect in ″old″ cells. It needs to be emphasized that mitochondrially generated ROS account for about 90% of all ROS in the cell, with the remainder being produced at various sites (Figure 4.8), including the cytosol, endoplasmic reticulum (ER), plasma membrane (PM) and peroxisome [239 - 242]. Within the cell, the actual steady-state level of ROS is dependent upon the balance between ROS formation and decomposition in various cellular locations (Figure 4.9) [241, 242]. ROS decomposition is known to be accomplished through a network of antioxidant scavenger reactions; these reactions take place in mitochondria, the cytosol and peroxisomes (Figure 4.10). In the mitochondrion, superoxide radicals ($O_2^{\bullet-}$) are generated mainly from the incomplete metabolism of oxygen molecules in complex III of the ETC [241]. Through the action of cytosolic (Sod1p) and mitochondrial (Sod2p) superoxide dismutase enzymes, harmful superoxide radicals are converted to the more stable and less toxic ROS, hydrogen peroxide (H_2O_2) [241, 242]. Further detoxification of H_2O_2 is the result of other antioxidant scavenger enzymes (Figure 4.10), namely catalases, peroxiredoxins and glutathione peroxidases [241, 242]. ROS-induced oxidative damage within the mitochondrion primarily targets mitochondrial proteins, DNA (mtDNA), and lipids, as summarized in Figure 4.11 [239 - 242]. Of note, in contrast to the oxidative damage of various cellular components caused by high intracellular concentrations of ROS, lower levels of harmful ROS are actually beneficial to the cell, upregulating mechanisms that serve to protect cellular constituents from oxidative stress and damage [239, 242]. In their capacity as signaling molecules, ROS benefit cells on two fronts. First, ROS activate a group of proteins that function to prevent or delay apoptosis, thereby protecting the cells from ROS-induced programmed cell death (Figure 4.12) [241, 242]. In their second protective capacity, ROS have specific sensors in the cytosol and mitochondrion that interact with certain shuttling proteins (cytosol-to-nucleus and mitochondrion-to-nucleus), which are then shuttled to the nucleus (Figure 4.12) [240, 241]. Finally, these shuttling proteins activate transcriptional factors and cofactors in the nucleus, which serve

as activators of genes that encode both oxidative stress-response and anti-apoptotic proteins (Figure 4.12) [241, 242]. An ″optimal″, pro-longevity level of ROS can be defined as one that is unable to cause sufficient oxidative damage to cellular constituents that would promote aging, while concurrently activating signaling networks that function to upregulate oxidative stress response and other anti-aging proteins [241 – 243]. The latter role can be categorized as the ″hormetic″ effect of ROS, where hormesis is defined as a beneficial defence response of an organism that is subjected to a low-intensity biological stressor [244].

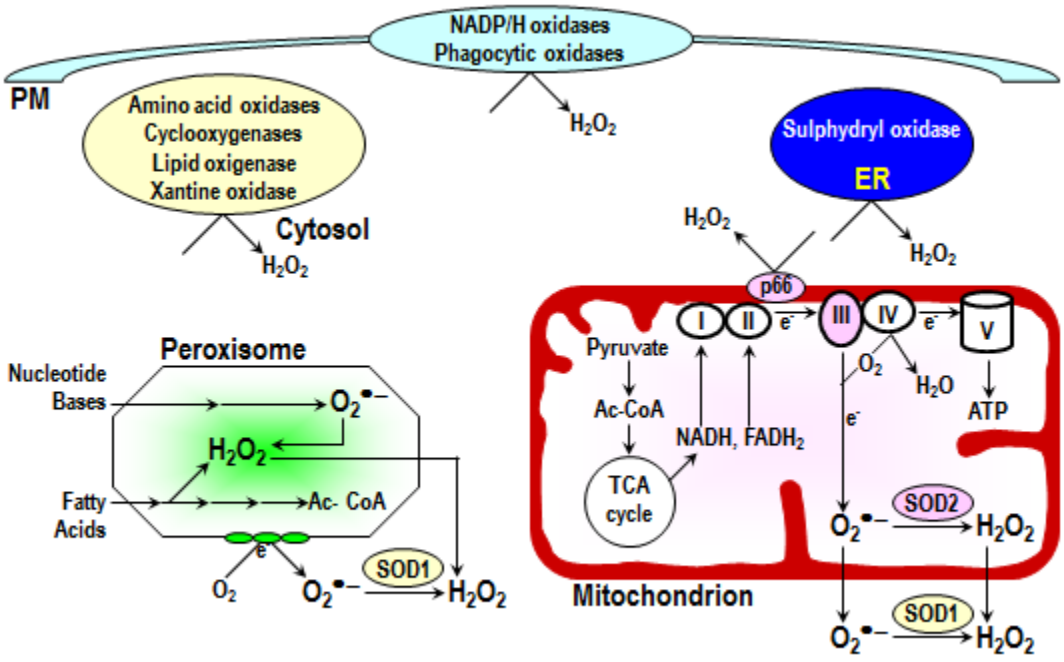

Figure 4.8. Sites of ROS production.

Superoxide radicals ($O_2^{\bullet-}$) are produced primarily in the mitochondrion, but also in the peroxisome. Hydrogen peroxide is formed from β-oxidation of fatty acids in the peroxisome as well as other cellular locations (the cytosol, plasma membrane [PM] and endoplasmic reticulum [ER]).

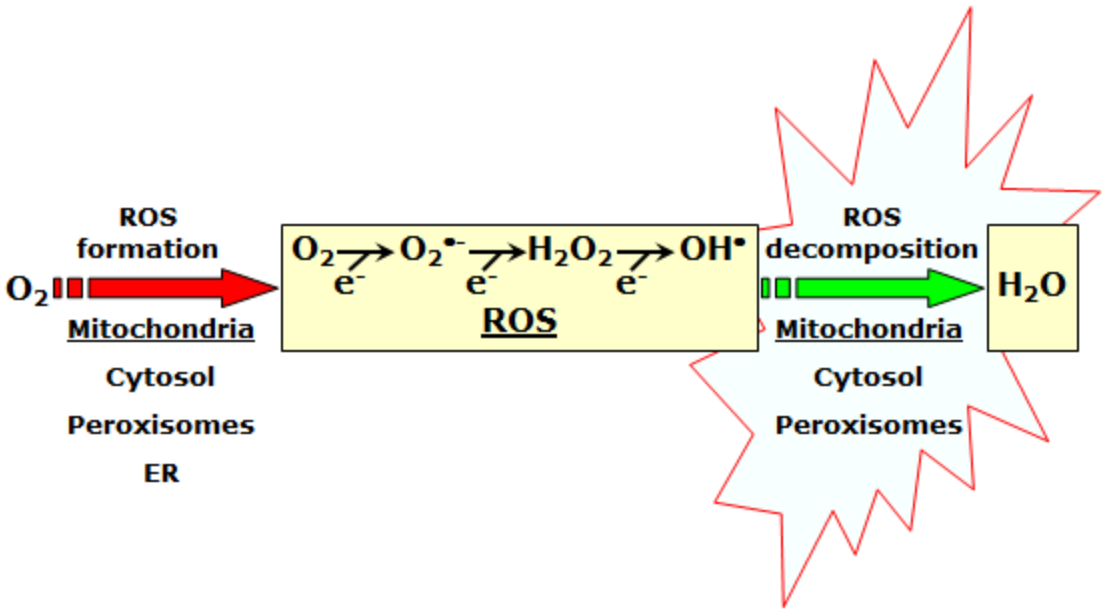

Figure 4.9. The steady-state level of ROS within a cell is dependent upon the balance between ROS formation and decomposition in various cellular locations, including the mitochondrion, cytosol, peroxisome and endoplasmic reticulum (ER).

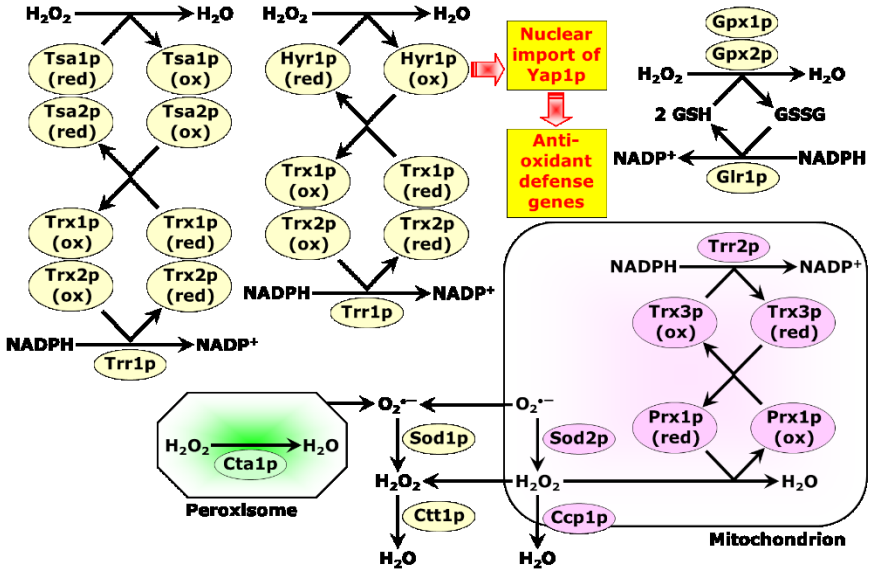

Figure 4.10. ROS decomposition is accomplished through a network of antioxidant scavenger reactions; these reactions take place in mitochondria, the cytosol and peroxisomes.

Color-coded localization of various detoxifying enzymes; pink – mitochondrion, green – peroxisome, beige – cytosol.

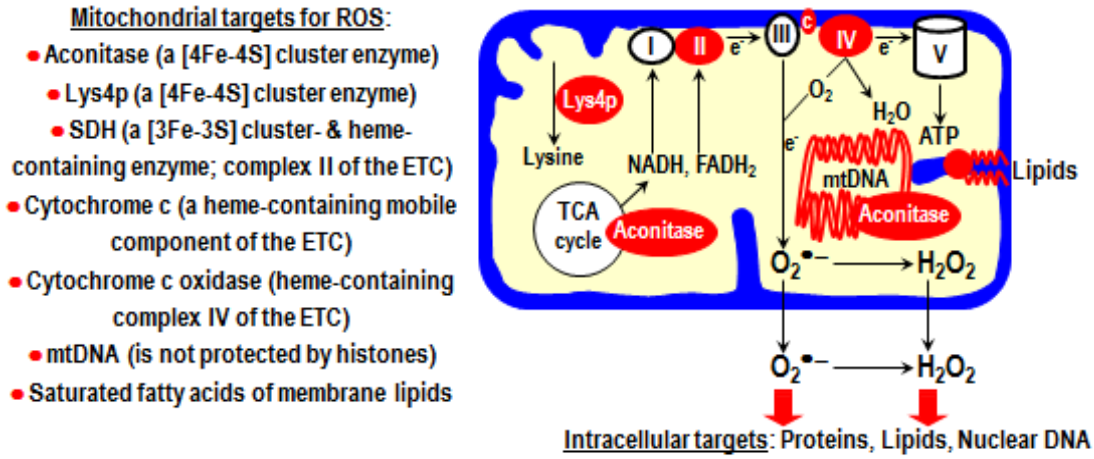

Figure 4.11. ROS-induced oxidative damage within the mitochondrion primarily targets mitochondrial proteins, DNA (mtDNA) and lipids.

ROS targets within the mitochondrion are highlighted in red.

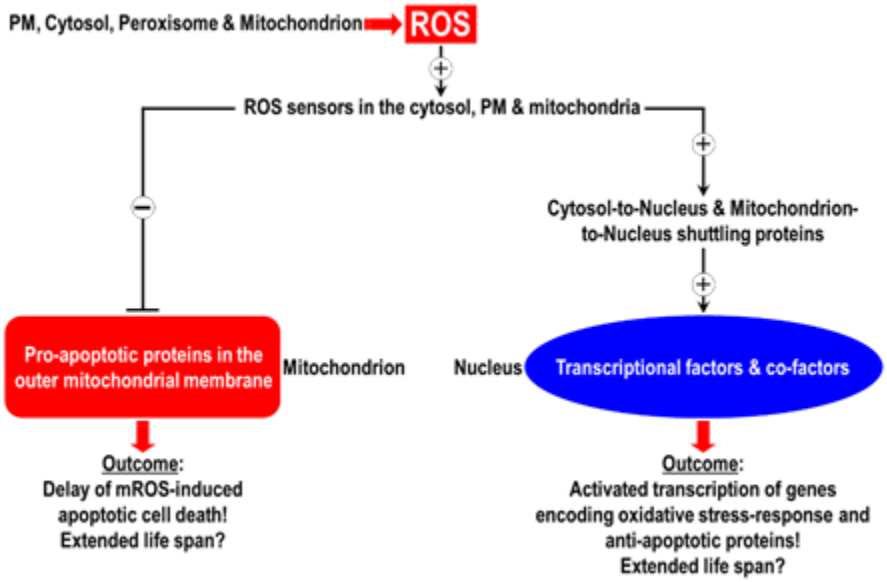

Figure 4.12. Low levels of harmful ROS can be beneficial to the cell, upregulating mechanisms that serve to protect cellular constituents from oxidative stress and damage.

In their capacity as signaling molecules, ROS: 1) activate a group of proteins that function to prevent or delay apoptosis, thereby protecting the cells from ROS-induced programmed cell death; and 2) have specific sensors in the cytosol and mitochondrion that interact with certain shuttling proteins (cytosol-to-nucleus and mitochondrion-to-nucleus), which are then shuttled to the nucleus. These shuttling proteins activate transcriptional factors and

cofactors in the nucleus, which serve as activators of genes that encode both oxidative stress-response and anti-apoptotic proteins.

To use a functional genetics approach for validating my hypothesis on the ability of LCA to extend yeast longevity by altering the age-related dynamics of mitochondrially produced ROS in both chronologically ″young″ and ″old″ cells, I sought to investigate how gene deletion mutations eliminating individual components of the mitochondrial ETC and cellular ROS scavenging network influence the ability of LCA to: (1) prolong yeast lifespan; and (2) alter the age-dependent dynamics of ROS production. Within such experimental framework, the functionalities of these components were placed into one of three categories: essential (activating) components, non-essential components or inhibitory components (Figure 4.13). These three categories were defined with respect to LCA's ability to extend yeast longevity. As such, a component of the mitochondrial ETC or a ROS scavenger deemed essential is required for LCA to exert its ability to extend longevity; i.e. there would be a reduction in the mean lifespan ^{MLS} of the deletion mutant with LCA as compared to that of the wild type with LCA (Figure 4.13). In the case of a non-essential component, the values of MLS for the deletion mutant with LCA should be very similar to that for the wild type with LCA (Figure 4.13). Finally, the inhibitory component is such a component of the mitochondrial ETC or such a ROS scavenger that its absence in the deletion mutant significantly enhances the longevity-extending ability of LCA as compared to that for the wild type; i.e. the presence of such a component hinders the ability of LCA to extend yeast lifespan (Figure 4.13).

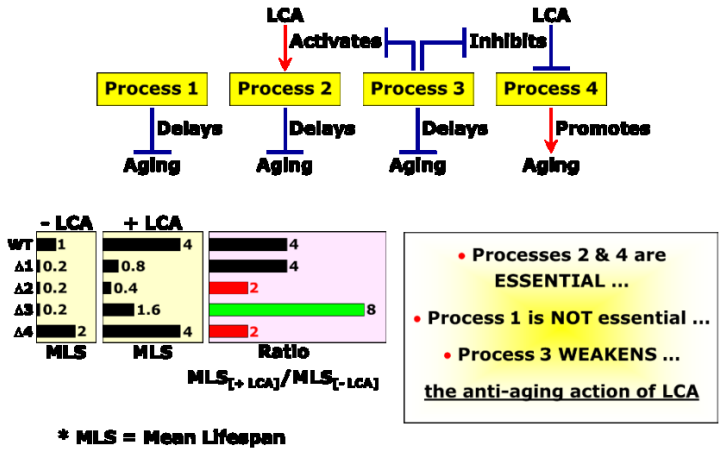

Figure 4.13. Three categories of mitochondrial ETC components or ROS scavengers with respect to LCA's ability to extend yeast longevity.

The functionalities of these components can be placed into one of three categories: essential (activating) components, non-essential components or inhibitory components. See text for details.

Within such experimental framework, if my hypothesis is valid, it is expected that: (1) any mutation that in the presence of LCA decreases the ″early″ spike in ROS in chronologically ″young″ cells may enhance the anti-aging effect of LCA; and (2) any mutation that in the presence of LCA increases the ″early″ spike in ROS in chronologically ″young″ cells may reduce or eliminate the anti-aging effect of LCA. In support of my hypothesis, I found that in yeast cells cultured in the presence of LCA, the *ndi1Δ* mutation (which eliminates complex I of the mitochondrial ETC) decreases the ″early″ spike in ROS in chronologically ″young″ cells and enhances the anti-aging effect of LCA (Figure 4.14).

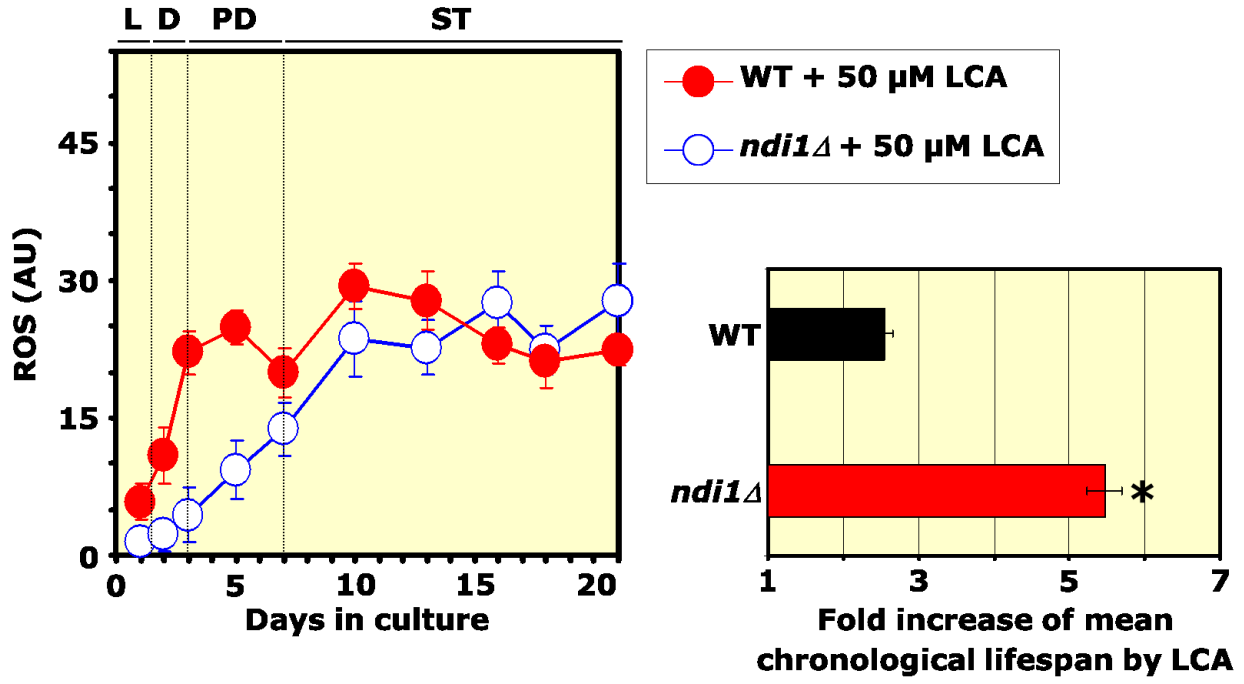

Figure 4.14. In yeast cells cultured in the presence of LCA, the *ndi1Δ* mutation (which eliminates complex I of the mitochondrial ETC) decreases the ″early″ spike in ROS in chronologically ″young″ cells and enhances the anti-aging effect of LCA.

Wild-type and *ndi1Δ* cells were cultured in the nutrient-rich YP medium initially containing 0.2% glucose and supplemented with 50 μM LCA. The levels of intracellular ROS and chronological lifespans were measured as described in ″Materials and Methods″. Data are presented as means ± SEM (n = 4-7; *p < 0.01).

Furthermore, if my hypothesis is valid, it is expected that: (1) any mutation that in the presence of LCA decreases the ″late″ spike in ROS in chronologically ″old″ cells may reduce or eliminate the anti-aging effect of LCA; and (2) any mutation that in the presence of LCA increases the ″late″ spike in ROS in chronologically ″old″ cells may enhance the anti-aging effect of LCA. In support of my hypothesis, I also found that in yeast cells cultured in the presence of LCA, the *gpx1Δ* mutation (which eliminates an isoform of the cytosolic phospholipid hydroperoxide glutathione peroxidase, one of the ROS scavengers; see Figure 4.10) increases the ″late″ spike in ROS in chronologically ″old″ cells and enhances the anti-aging effect of LCA (Figure 4.15).

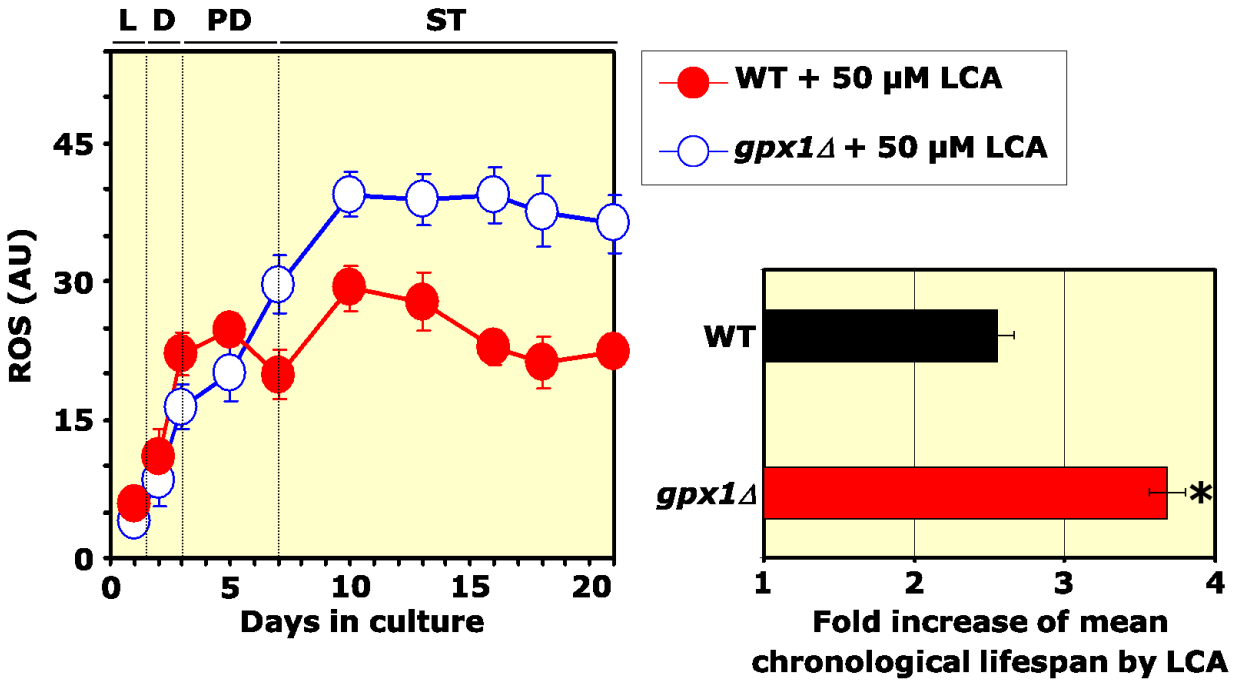

Figure 4.15 In yeast cells cultured in the presence of LCA, the *gpx1Δ* mutation (which eliminates an isoform of the cytosolic phospholipid hydroperoxide glutathione peroxidase, a ROS scavenger) increases the ″late″ spike in ROS in chronologically ″old″ cells and enhances the anti-aging effect of LCA.

Wild-type and *ndi1Δ* cells were cultured in the nutrient-rich YP medium initially containing 0.2% glucose and supplemented with 50 μM LCA. The levels of intracellular ROS and chronological lifespans were measured as described in ″Materials and Methods″. Data are presented as means ± SEM (n = 3-5; *p < 0.01).

As a next step towards validating my hypothesis, I assessed how gene deletion mutations eliminating various ROS scavengers and eliciting variations of intracellular ROS within a wide range of concentrations impact longevity-extending efficacy of LCA. Twelve single-gene-

deletions mutants were studied, each lacking one of the following ROS scavenging enzymes: cytosolic (Sod1p) and mitochondrial (Sod2p) superoxide dismutases; cytosolic (Ctt1p) and peroxisomal (Cta1p) catalases; mitochondrial cytochrome-c peroxidase (Ccp1p); cytosolic thioredoxin peroxidases isoforms 1 (Tsa1p) and 2 (Tsa2p); the cytosolic thioredoxin isoforms 1 (Trx1p) and 2 (Trx2p) as well as the mitochondrial thioredoxin (Trx2p); cytosolic glutathione peroxidases (Gpx1p); and cytosolic thiol peroxidases (Hyr1p) (see Figure 4.10). I found that: (1) LCA is unable to extend lifespan of the *sod1Δ* mutant strain and, thus, the cytosolic superoxide dismutase Sod1p is essential for the ability of LCA to extend yeast longevity (Figure 4.16); (2) LCA equally efficiently extends longevities of both the wild-type and mutant *ctt1Δ* strains and, thus, the cytosolic catalase Ctt1p is not essential for the ability of LCA to extend longevity (Figure 4.17); (3) LCA is unable to extend lifespan of the *sod2Δ* mutant strain and, thus, the mitochondrial superoxide dismutase Sod2p is essential for the ability of LCA to extend yeast longevity (Figure 4.18); (4) LCA equally efficiently extends longevities of both the wild-type and mutant *cta1Δ* strains and, thus, the peroxisomal catalase Cta1p is not essential for the ability of LCA to extend longevity (Figure 4.19). I concluded that both cytosolic and mitochondrial superoxide dismutases, but not cytosolic or peroxisomal catalase, are essential for lifespan extension by LCA (Figure 4.20).

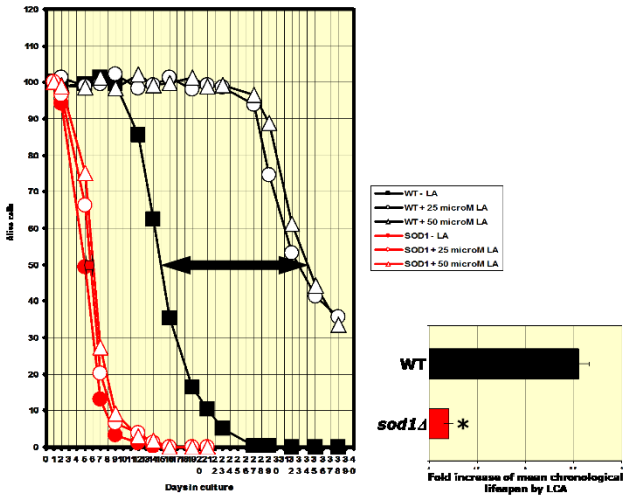

Figure 4.16. LCA is unable to extend lifespan of the *sod1Δ* mutant strain and, thus, the cytosolic superoxide dismutase Sod1p is essential for the ability of LCA to extend yeast longevity.

Wild-type and *sod1Δ* cells were cultured in the nutrient-rich YP medium initially containing 0.2% glucose and supplemented with LCA added at the final concentration of 25 μM or 50 μM. The chronological lifespans were measured as described in ″Materials and Methods″. Data are presented as means ± SEM (n = 3-4; *p < 0.01).

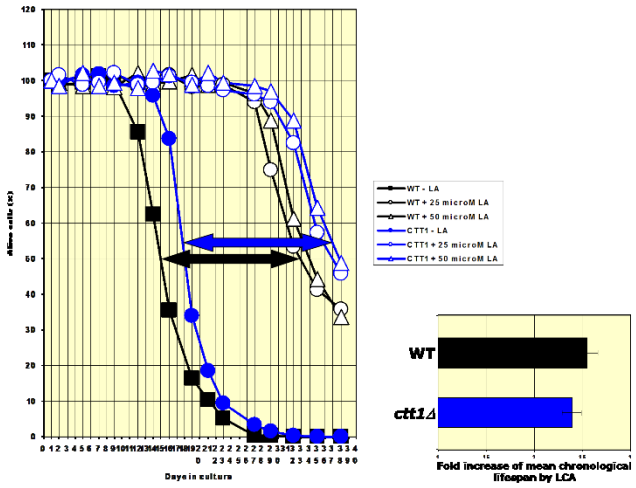

Figure 4.17. LCA equally efficiently extends longevities of both the wild-type and mutant *ctt1Δ* strains and, thus, the cytosolic catalase Ctt1p is not essential for the ability of LCA to extend longevity.

Wild-type and *ctt1Δ* cells were cultured in the nutrient-rich YP medium initially containing 0.2% glucose and supplemented with LCA added at the final concentration of 25 μM or 50 μM. The chronological lifespans were measured as described in ″Materials and Methods″. Data are presented as means ± SEM (n = 3-5).

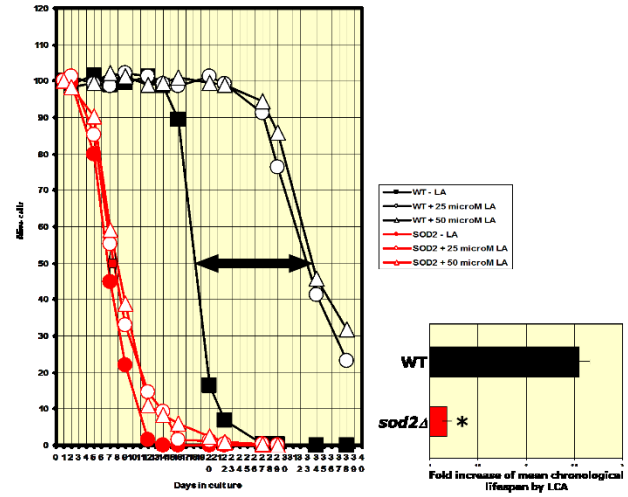

Figure 4.18. LCA is unable to extend lifespan of the *sod2Δ* mutant strain and, thus, the mitochondrial superoxide dismutase Sod2p is essential for the ability of LCA to extend yeast longevity.

Wild-type and *sod2Δ* cells were cultured in the nutrient-rich YP medium initially containing 0.2% glucose and supplemented with LCA added at the final concentration of 25 μM or 50 μM. The chronological lifespans were measured as described in ″Materials and Methods″. Data are presented as means ± SEM (n = 4; *p < 0.01).

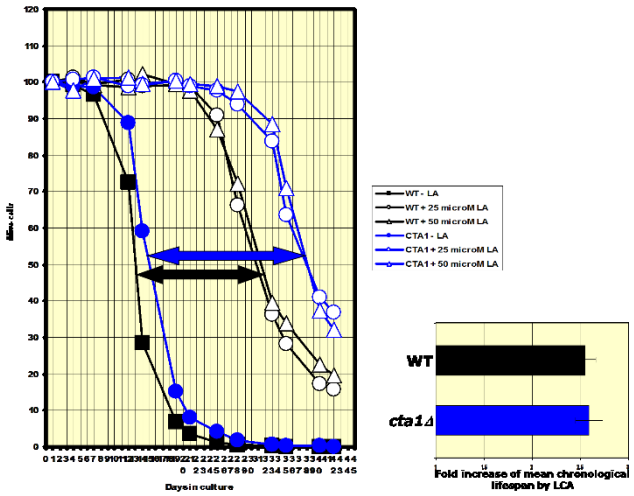

Figure 4.19. LCA equally efficiently extends longevities of both the wild-type and mutant *cta1Δ* strains and, thus, the peroxisomal catalase Cta1p is not essential for the ability of LCA to extend longevity.

Wild-type and *cta1Δ* cells were cultured in the nutrient-rich YP medium initially containing 0.2% glucose and supplemented with LCA added at the final concentration of 25 μM or 50 μM. The chronological lifespans were measured as described in ″Materials and Methods″. Data are presented as means ± SEM (n = 4).

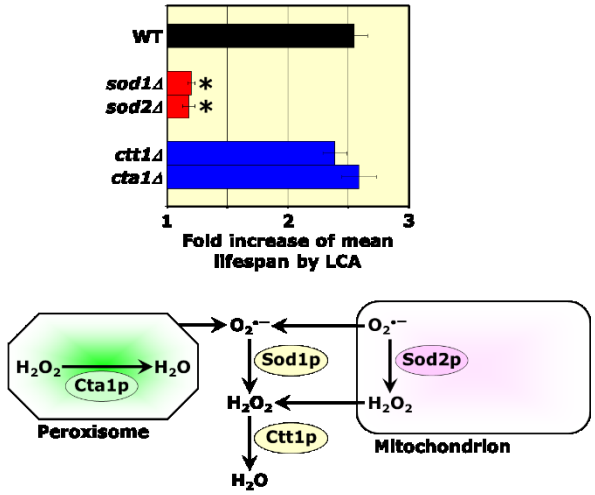

Figure 4.20. Both cytosolic and mitochondrial superoxide dismutases, but not cytosolic or peroxisomal catalase, are essential for lifespan extension by LCA.

Based on data presented in Figures 4.16 to 4.19.

Furthermore, I found that: (1) LCA is unable to extend lifespan of the *ccp1Δ* mutant strain lacking the mitochondrial cytochrome c peroxidase Ccp1p (Figure 4.21); and (2) LCA extends lifespan of the *trx3Δ* mutant strain (which lacks the mitochondrial thioredoxin Trx3p) to a significantly higher extent than that of the wild-type strain (Figure 4.22). I concluded that the

mitochondrial cytochrome *c* peroxidase Ccp1p is essential for the ability of LCA to extend yeast longevity, whereas the mitochondrial thioredoxin Trx3p weakens the longevity-extending effect of LCA in wild-type cells.

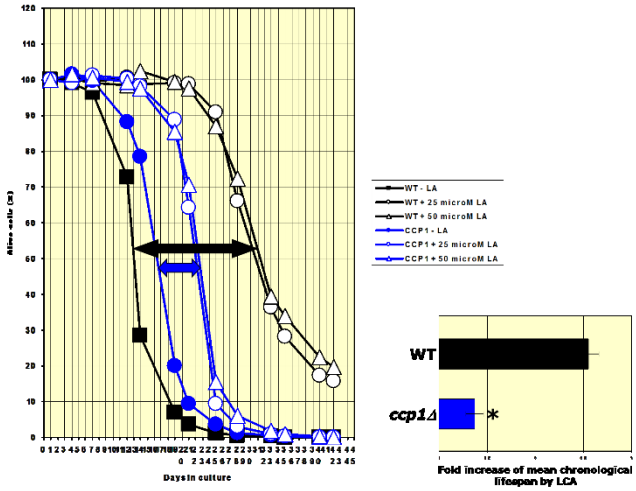

Figure 4.21. LCA is unable to extend lifespan of the *ccp1Δ* mutant strain and, thus, the mitochondrial cytochrome *c* peroxidase Ccp1p is essential for the ability of LCA to extend yeast longevity.

Wild-type and *ccp1Δ* cells were cultured in the nutrient-rich YP medium initially containing 0.2% glucose and supplemented with LCA added at the final concentration of 25 µM or 50 µM. The chronological lifespans were measured as described in ″Materials and Methods″. Data are presented as means ± SEM (n = 4; *p < 0.01).

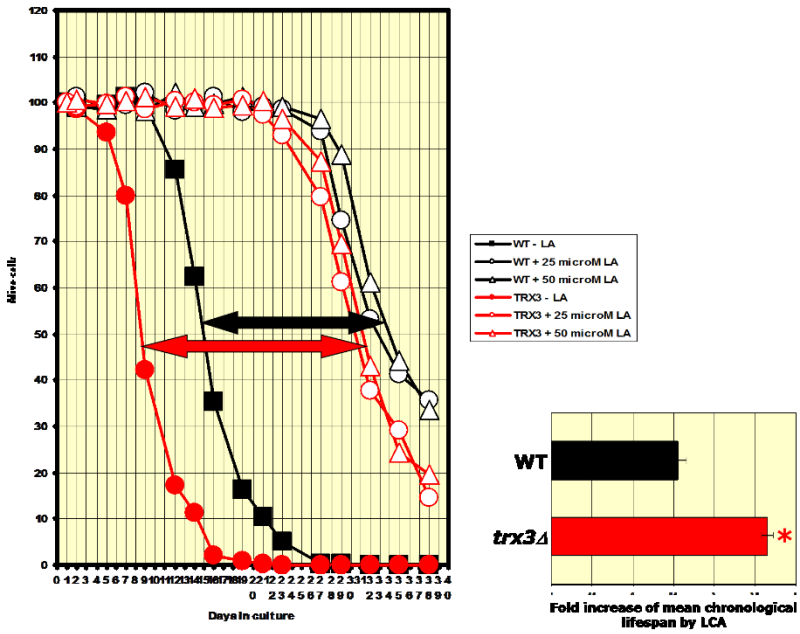

Figure 4.22. LCA extends lifespan of the *trx3Δ* mutant strain (which lacks the mitochondrial thioredoxin Trx3p) to a significantly higher extent than that of the wild-type strain and, thus, the mitochondrial thioredoxin Trx3p weakens the longevity-extending effect of LCA in wild-type cells.

Wild-type and *trx3Δ* cells were cultured in the nutrient-rich YP medium initially containing 0.2% glucose and supplemented with LCA added at the final concentration of 25 μM or 50 μM. The chronological lifespans were measured as described in "Materials and Methods". Data are presented as means ± SEM (n = 4; *p < 0.01).

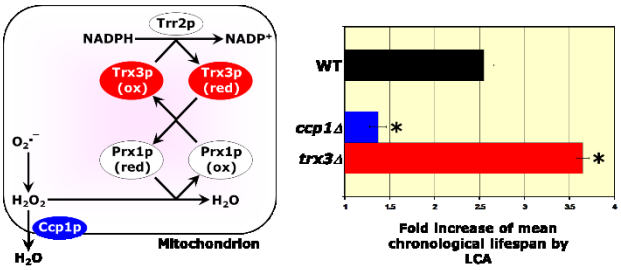

Figure 4.23. The mitochondrial cytochrome *c* peroxidase Ccp1p is essential for the ability of LCA to extend yeast longevity, whereas the mitochondrial thioredoxin Trx3p weakens the longevity-extending effect of LCA in wild-type cells.

Based on data presented in Figures 4.21 and 4.22.

Moreover, I revealed that: (1) LCA equally efficiently extends longevities of both the wild-type and mutant *trx1Δ* strains; this mutant stain lacks the Trx1p isoform of cytosolic thioredoxin (Figure 4.24); and (2) LCA extends lifespan of the *trx2Δ* mutant strain (which lacks the Trx2p isoform of cytosolic thioredoxin) to a significantly higher extent than that of the wild-type strain (Figure 4.25). These findings imply that the Trx1p isoform of cytosolic thioredoxin is not essential for the ability of LCA to extend longevity, whereas its Trx2p isoform weakens the anti-aging effect of LCA (Figure 4.26).

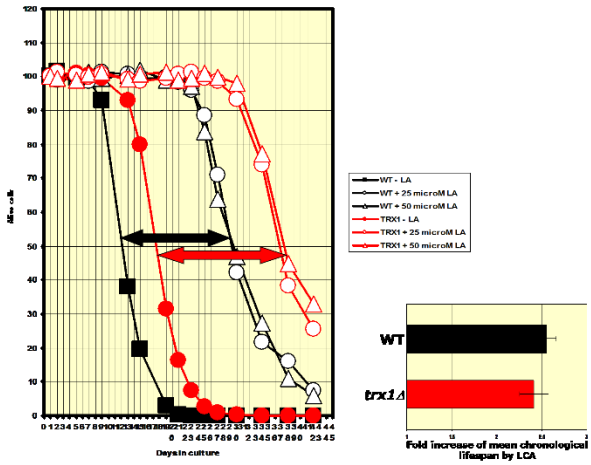

Figure 4.24. LCA equally efficiently extends longevities of both the wild-type and mutant *trx1Δ* strains and, thus, the Trx1p isoform of cytosolic thioredoxin is not essential for the ability of LCA to extend longevity.

Wild-type and *trx1Δ* cells were cultured in the nutrient-rich YP medium initially containing 0.2% glucose and supplemented with LCA added at the final concentration of 25 μM or 50 μM. The chronological lifespans were measured as described in ″Materials and Methods″. Data are presented as means ± SEM (n = 3-4).

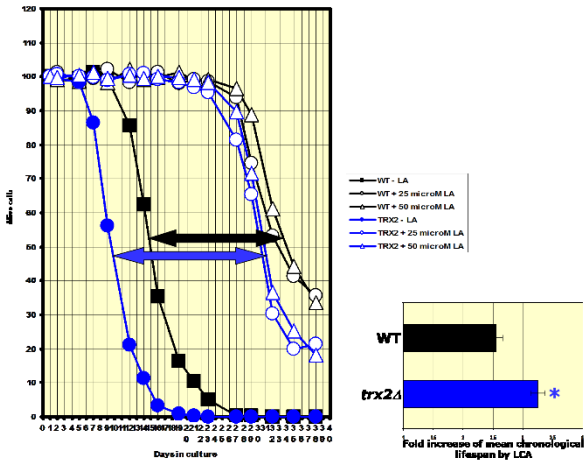

Figure 4.25. LCA extends lifespan of the *trx2Δ* mutant strain (which lacks the Trx2p isoform of cytosolic thioredoxin) to a significantly higher extent than that of the wild-type strain and, hence, the Trx2p isoform of cytosolic thioredoxin weakens the antiaging effect of LCA.

Wild-type and *trx2Δ* cells were cultured in the nutrient-rich YP medium initially containing 0.2% glucose and supplemented with LCA added at the final concentration of 25 μM or 50 μM. The chronological lifespans were measured as described in ″Materials and Methods″. Data are presented as means ± SEM (n = 4; *p < 0.01).

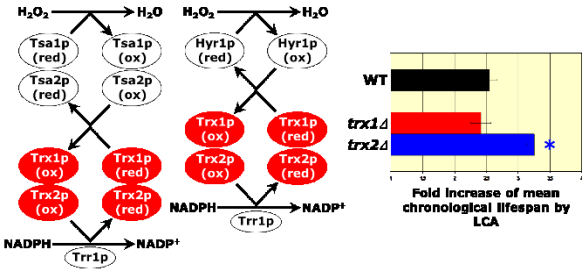

Figure 4.26. The Trx1p isoform of cytosolic thioredoxin is not essential for the ability of LCA to extend longevity, whereas its Trx2p isoform weakens the anti-aging effect of LCA.

Based on data presented in Figures 4.24 and 4.25.

In addition, I found that: (1) LCA is unable to extend lifespan of the *tsa1Δ* mutant strain lacking the Tsa1p isoform of cytosolic thioredoxin peroxidase (Figure 4.27); and (2) LCA extends lifespan of the *tsa2Δ* mutant strain (which lacks the Tsa2p isoform of cytosolic

thioredoxin peroxidase) to a significantly higher extent than that of the wild-type strain (Figure 4.28). Thus, the Tsa1p isoform of cytosolic thioredoxin peroxidase is essential for the ability of LCA to extend longevity, whereas its Tsa2p isoform weakens the anti-aging effect of LCA (Figure 4.29).

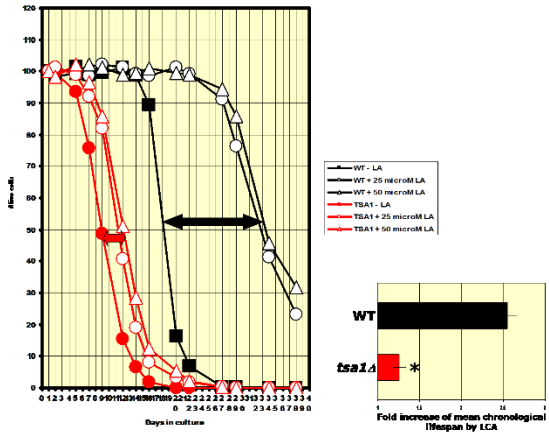

Figure 4.27. LCA is unable to extend lifespan of the *tsa1Δ* mutant strain and, thus, the Tsa1p isoform of cytosolic thioredoxin peroxidase is essential for the ability of LCA to extend longevity.

Wild-type and *tsa1Δ* cells were cultured in the nutrient-rich YP medium initially containing 0.2% glucose and supplemented with LCA added at the final concentration of 25 μM or 50 μM. The chronological lifespans were measured as described in ″Materials and Methods″. Data are presented as means ± SEM (n = 3-5; *p < 0.01).

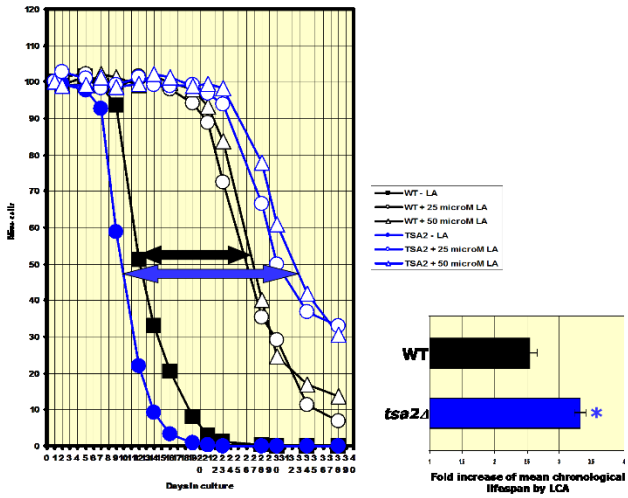

Figure 4.28. LCA extends lifespan of the *tsa2Δ* mutant strain to a significantly higher extent than that of the wild-type strain and, hence, the Tsa2p isoform of cytosolic thioredoxin peroxidase weakens the anti-aging effect of LCA.

Wild-type and *tsa2Δ* cells were cultured in the nutrient-rich YP medium initially containing 0.2% glucose and supplemented with LCA added at the final concentration of 25 μM or 50 μM. The chronological lifespans were measured as described in ″Materials and Methods″. Data are presented as means ± SEM (n = 4; *p < 0.01).

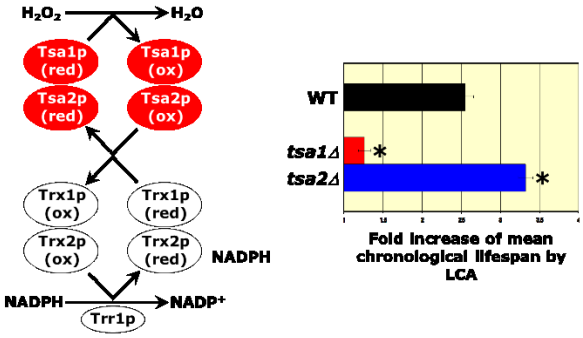

Figure 4.29. The Tsa1p isoform of cytosolic thioredoxin peroxidase is essential for the ability of LCA to extend longevity, whereas its Tsa2p isoform weakens the anti-aging effect of LCA.

Based on data presented in Figures 4.27 and 4.283.

I also found that: (1) LCA extends lifespan of the *gpx1Δ* mutant strain to a significantly higher extent than that of the wild-type strain and, hence, the Gpx1p isoform of cytosolic phospholipid hydroperoxide glutathione peroxidase weakens the anti-aging effect of LCA (Figure 4.30); and (2) LCA extends lifespan of the *hyr1Δ* mutant strain to a significantly higher extent than that of the wild-type strain and, hence, the cytosolic thiol peroxidase Hyr1p weakens the anti-aging effect of LCA (Figure 4.31).

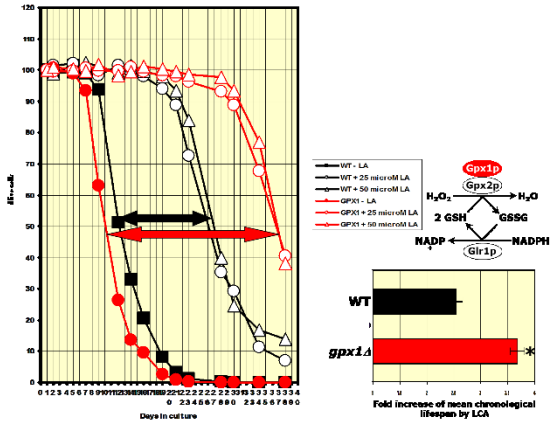

Figure 4.30. LCA extends lifespan of the *gpx1Δ* mutant strain to a significantly higher extent than that of the wild-type strain; thus, the Gpx1p isoform of cytosolic phospholipid hydroperoxide glutathione peroxidase weakens the anti-aging effect of LCA.

Wild-type and *gpx1Δ* cells were cultured in the nutrient-rich YP medium initially containing 0.2% glucose and supplemented with LCA added at the final concentration of 25 μM or 50 μM. The chronological lifespans were measured as described in ″Materials and Methods″. Data are presented as means ± SEM (n = 3; *p < 0.01).

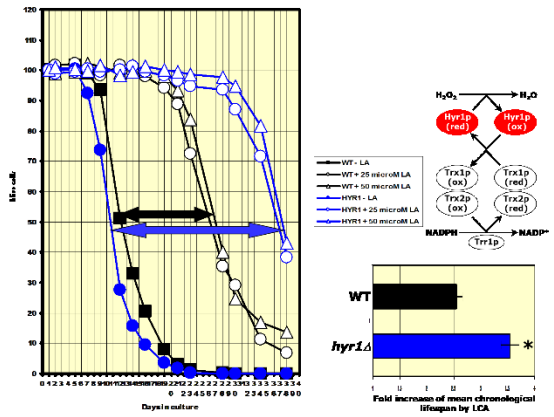

Figure 4.31. LCA extends lifespan of the *hyr1Δ* mutant strain to a significantly higher extent than that of the wild-type strain; hence, the cytosolic thiol peroxidase Hyr1p weakens the anti-aging effect of LCA.

Wild-type and *hyr1Δ* cells were cultured in the nutrient-rich YP medium initially containing 0.2% glucose and supplemented with LCA added at the final concentration of 25 μM or 50 μM. The chronological lifespans were measured as described in ″Materials and Methods″. Data are presented as means ± SEM (n = 4; *p < 0.01).

Altogether, the above findings revealed that out of twelve ROS scavenging enzymes: (1) four enzymes (i.e. Sod1p and Tsa1p in the cytosol as well as Sod2p and Ccp1p in mitochondria) are essential for the ability of LCA to delay aging; (2) five enzymes (i.e. Tsa2p, Trx2p, Gpx1p and Hyr1p in the cytosol as well as Trx3p in mitochondria) weaken the anti-aging effect of LCA; and (3) three enzymes (i.e. Trx1p and Ctt1p in the cytosol as well as Cta1p in the peroxisome) are not essential for the ability of LCA to delay aging (Figure 4.32).

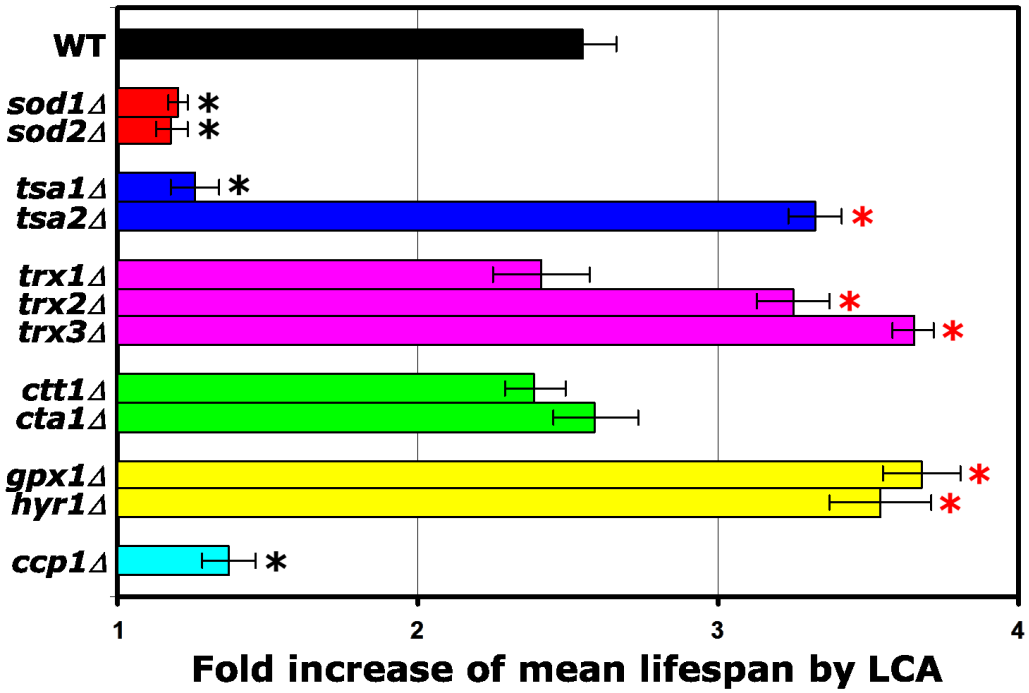

Figure 4.32. Some ROS scavenging enzymes are essential for the ability of LCA to delay aging, others weaken the anti-aging effect of LCA, whereas some of them are not essential for the ability of LCA to delay aging. Based on data presented in Figures 4.13-4.28. Data are presented as means ± SEM (n = 3-7; *p < 0.01).

To validate my hypothesis on the ability of LCA to extend yeast longevity by altering the age-related dynamics of mitochondrially produced ROS in both chronologically ″young″ and ″old″ cells, I then assessed how the *sod1Δ*, *sod2Δ*, *tsa1Δ* and *ccp1Δ* mutations (all of which impair the ability of LCA to extend yeast longevity) influence such dynamics. I found that the *sod1Δ*, *sod2Δ* and *tsa1Δ* mutations: (1) in the L, D and PD growth phases, increase the level of intracellular ROS above its critically high level of 40 AU (for the definition of a level of ROS that is critically high for these growth phases, see discussion below); and (2) in the ST growth phase, sharply decrease intracellular ROS concentration to the level seen in wild-type cells (Figures 4.33, 4.34 and 4.35). I also found that the *ccp1Δ* mutation: (1) in the L, D and PD growth phases, does not alter the level of intracellular ROS; and (2) in the ST growth phase, initially elevates the level of intracellular ROS above its critically high level of 50 AU (for the definition of a level of ROS that is critically high for this growth phase, see discussion below)

and then sharply decrease intracellular ROS concentration to the level seen in wild-type cells (Figure 4.36).

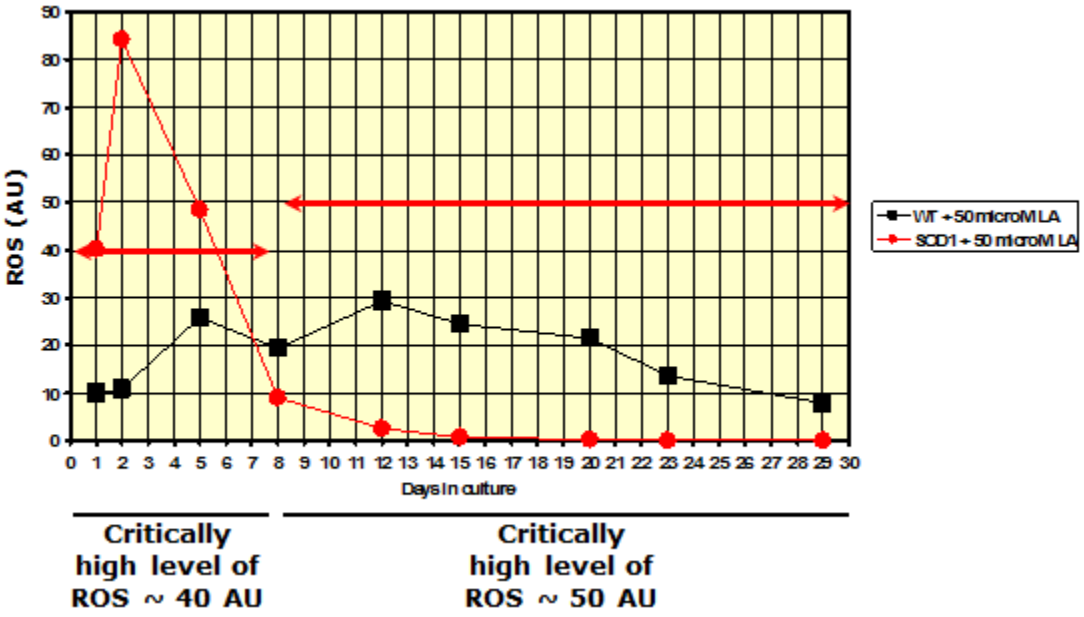

Figure 4.33. The *sod1Δ* mutation, which impairs the ability of LCA to extend longevity, alters the age-dependent dynamics of ROS production.

Wild-type and *sod1Δ* cells were cultured in the nutrient-rich YP medium initially containing 0.2% glucose and supplemented with LCA added at the final concentration of 50 μM. The levels of intracellular ROS were measured as described in ″Materials and Methods″. Red lines denote the levels of ROS that are critically high for the L, D and PD growth phases (days 1 to 7; 40 AU) or for the ST growth phase (Days 7 to 29; 50 AU).

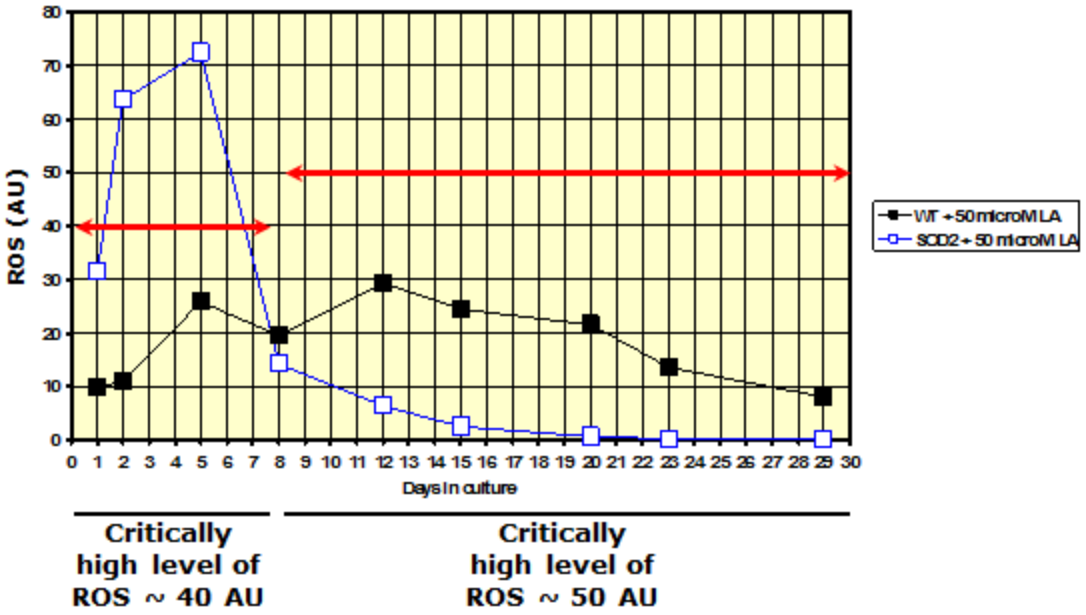

Figure 4.34. The *sod2Δ* mutation, which impairs the ability of LCA to extend longevity, alters the age-dependent dynamics of ROS production.

Wild-type and *sod2Δ* cells were cultured in the nutrient-rich YP medium initially containing 0.2% glucose and supplemented with LCA added at the final concentration of 50 μM. The levels of intracellular ROS were measured as described in ″Materials and Methods″. Red lines denote the levels of ROS that are critically high for the L, D and PD growth phases (days 1 to 7; 40 AU) or for the ST growth phase (Days 7 to 29; 50 AU).

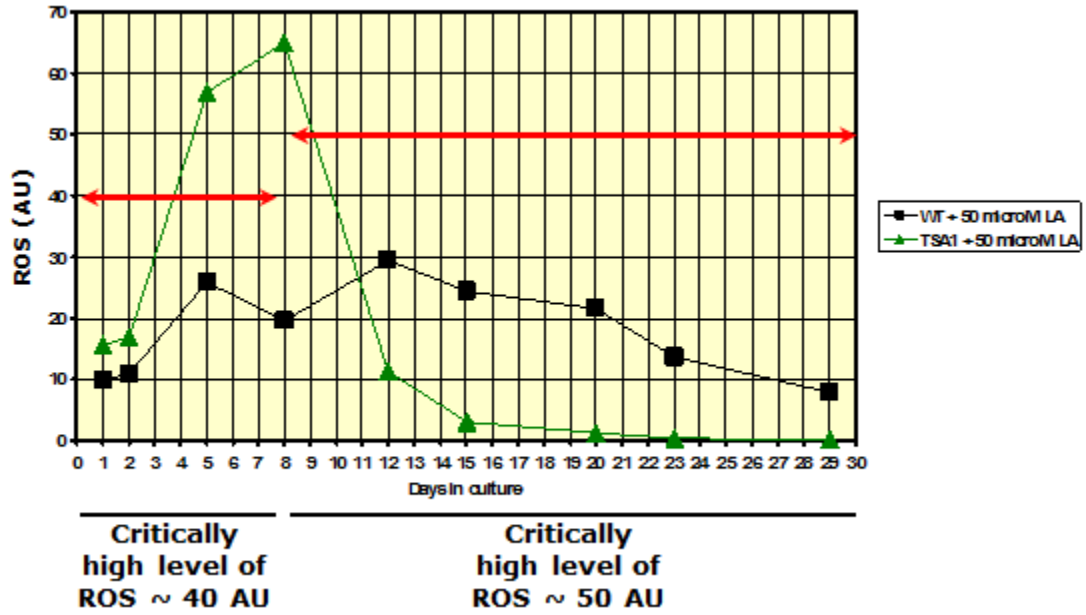

Figure 4.35. The *tsa1Δ* mutation, which impairs the ability of LCA to extend longevity, alters the age-dependent dynamics of ROS production.

Wild-type and *tsa1Δ* cells were cultured in the nutrient-rich YP medium initially containing 0.2% glucose and supplemented with LCA added at the final concentration of 50 μM. The levels of intracellular ROS were measured as described in ″Materials and Methods″. Red lines denote the levels of ROS that are critically high for the L, D and PD growth phases (days 1 to 7; 40 AU) or for the ST growth phase (Days 7 to 29; 50 AU).

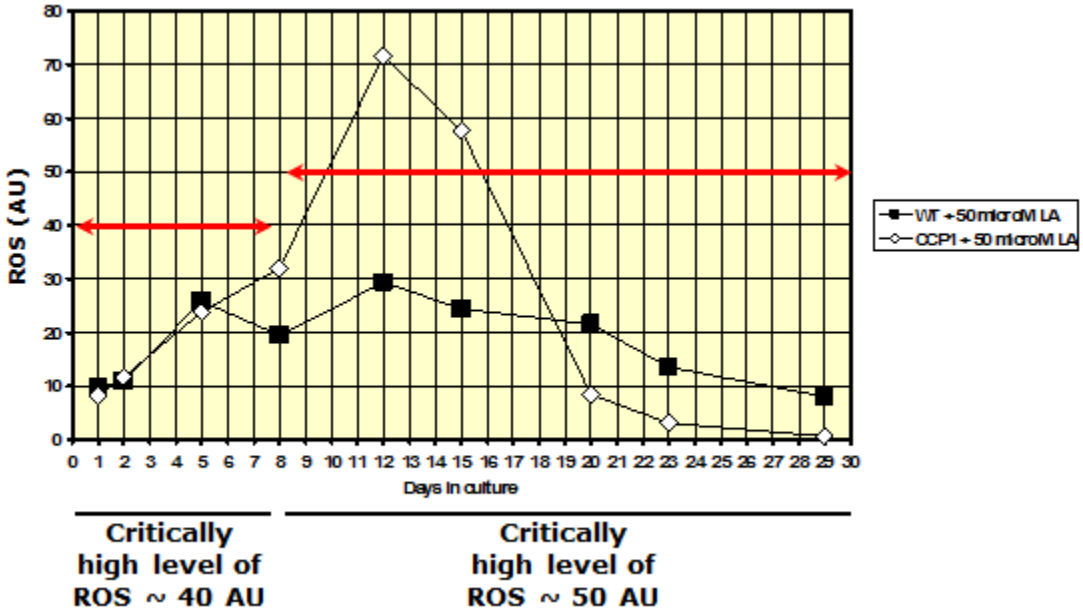

Figure 4.36. The *ccp1Δ* mutation, which impairs the ability of LCA to extend longevity, alters the age-dependent dynamics of ROS production.

Wild-type and *ccp1Δ* cells were cultured in the nutrient-rich YP medium initially containing 0.2% glucose and supplemented with LCA added at the final concentration of 50 μM. The levels of intracellular ROS were measured as described in ″Materials and Methods″. Red lines denote the levels of ROS that are critically high for the L, D and PD growth phases (days 1 to 7; 40 AU) or for the ST growth phase (Days 7 to 29; 50 AU).

As a further test of the validity of my hypothesis, I then examined how the *tsa2Δ*, *trx2Δ*, *trx3Δ*, *gpx1Δ* and *hyr1Δ* mutations (all of which enhance the ability of LCA to extend yeast longevity) influence the age-related dynamics of mitochondrially produced ROS in both chronologically ″young″ and ″old″ cells. I found that the *tsa2Δ* mutation: (1) in the L, D and PD growth phases, does not alter the level of intracellular ROS; and (2) in the ST growth phase, increases the level of intracellular ROS but allows to maintain it below a critically high level of

50 AU (for the definition of a level of ROS that is critically high for this growth phase, see discussion below) (Figure 4.37). Furthermore, I revealed that the *trx2Δ* and *trx3Δ* mutations: (1) in the L, D and PD growth phases, elevate the level of intracellular ROS but permit to uphold it below a critically high level of 40 AU (I define this level as the highest level of ROS seen during the L, D and PD growth phases in cells that carry a mutation enhancing the ability of LCA to extend yeast longevity); and (2) in the ST growth phase, increase the level of intracellular ROS but allow to maintain it below a critically high level of 50 AU (I define this level as the highest level of ROS seen during the ST growth phase in cells that carry a mutation enhancing the ability of LCA to extend yeast longevity) most of the time (Figures 4.38 and 4.39). Moreover, I found that the *gpx1Δ* and *hyr1Δ* mutations: (1) in the L, D and PD growth phases, reduce the level of intracellular ROS; and (2) late in the ST growth phase, elevate the level of intracellular ROS but permit to sustain it below a critically high level of 50 AU (Figures 4.40 and 4.41).

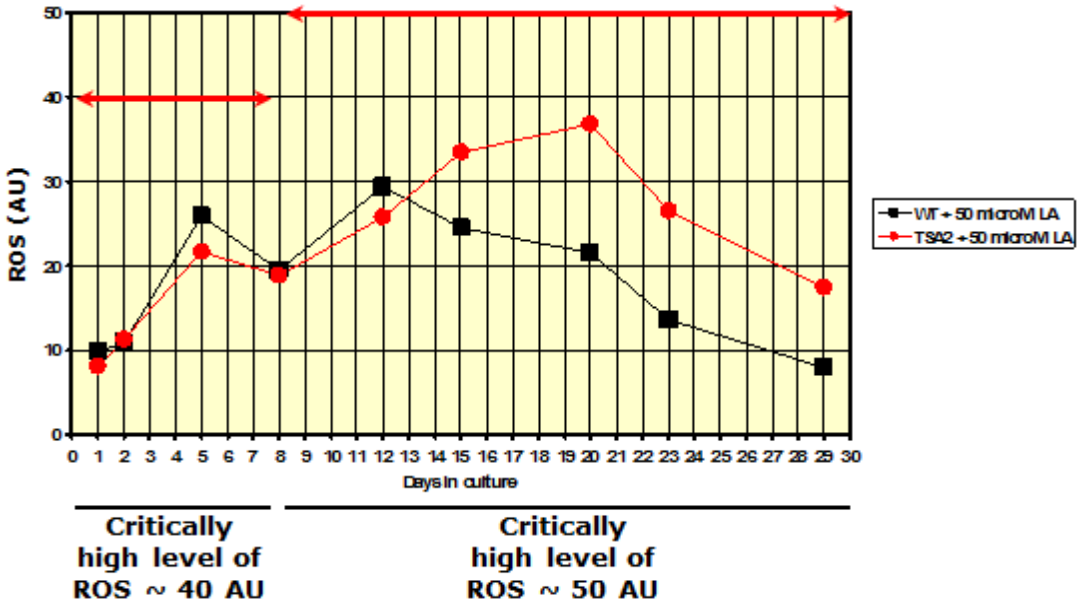

Figure 4.37. The *tsa2Δ* mutation, which enhances the ability of LCA to extend longevity, alters the age-dependent dynamics of ROS production.

Wild-type and *tsa2Δ* cells were cultured in the nutrient-rich YP medium initially containing 0.2% glucose and supplemented with LCA added at the final concentration of 50 μM. The levels of intracellular ROS were measured as described in "Materials and Methods". Red lines denote the levels of ROS that are critically high for the L, D and PD growth phases (days 1 to 7; 40 AU) or for the ST growth phase (Days 7 to 29; 50 AU).

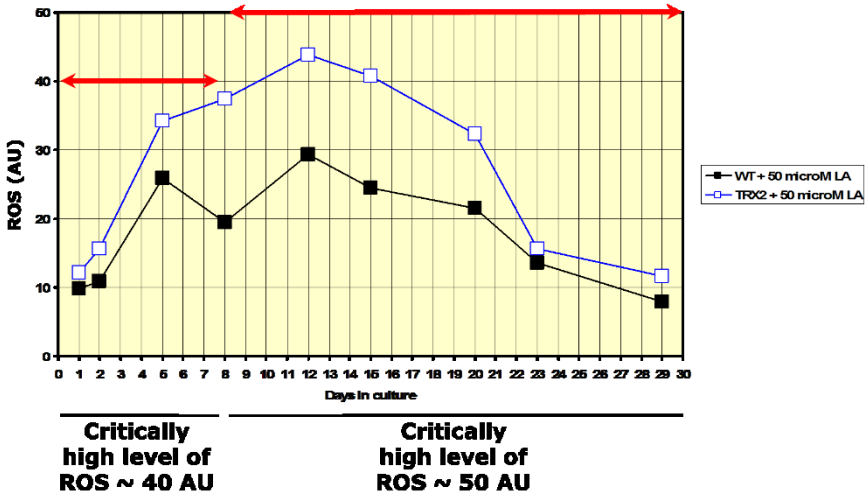

Figure 4.38. The *trx2Δ* mutation, which enhances the ability of LCA to extend longevity, alters the age-dependent dynamics of ROS production.

Wild-type and *trx2Δ* cells were cultured in the nutrient-rich YP medium initially containing 0.2% glucose and supplemented with LCA added at the final concentration of 50 μM. The levels of intracellular ROS were measured as described in ″Materials and Methods″. Red lines denote the levels of ROS that are critically high for the L, D and PD growth phases (days 1 to 7; 40 AU) or for the ST growth phase (Days 7 to 29; 50 AU).

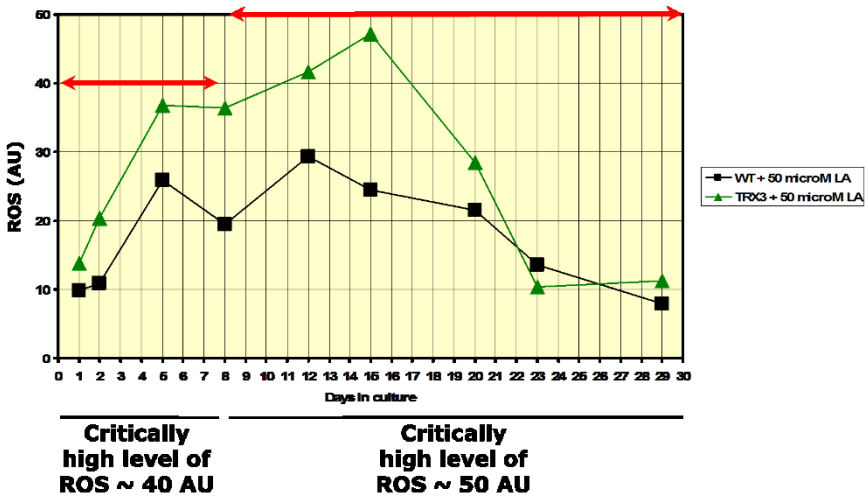

Figure 4.39. The *trx3Δ* mutation, which enhances the ability of LCA to extend longevity, alters the age-dependent dynamics of ROS production.

Wild-type and *trx3Δ* cells were cultured in the nutrient-rich YP medium initially containing 0.2% glucose and supplemented with LCA added at the final concentration of 50 μM. The levels of intracellular ROS were measured

as described in ″Materials and Methods″. Red lines denote the levels of ROS that are critically high for the L, D and PD growth phases (days 1 to 7; 40 AU) or for the ST growth phase (Days 7 to 29; 50 AU).

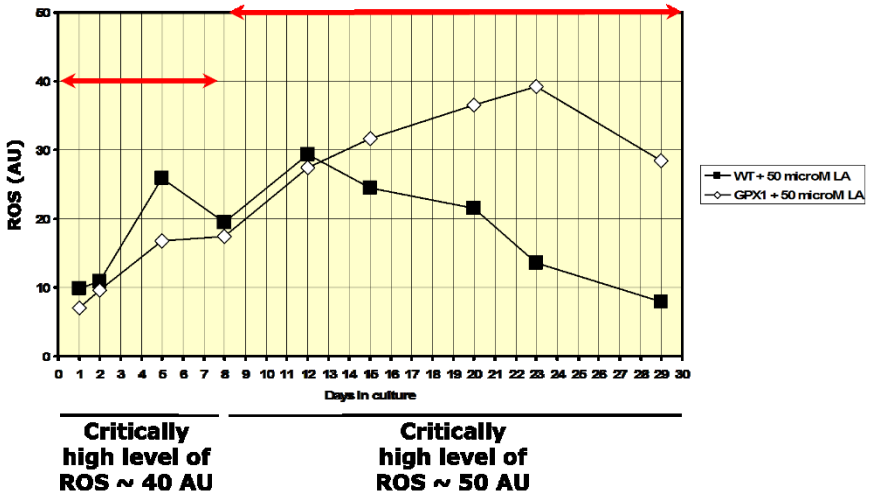

Figure 4.40. The *gpx1Δ* mutation, which enhances the ability of LCA to extend longevity, alters the age-dependent dynamics of ROS production.

Wild-type and *gpx1Δ* cells were cultured in the nutrient-rich YP medium initially containing 0.2% glucose and supplemented with LCA added at the final concentration of 50 μM. The levels of intracellular ROS were measured as described in ″Materials and Methods″. Red lines denote the levels of ROS that are critically high for the L, D and PD growth phases (days 1 to 7; 40 AU) or for the ST growth phase (Days 7 to 29; 50 AU).

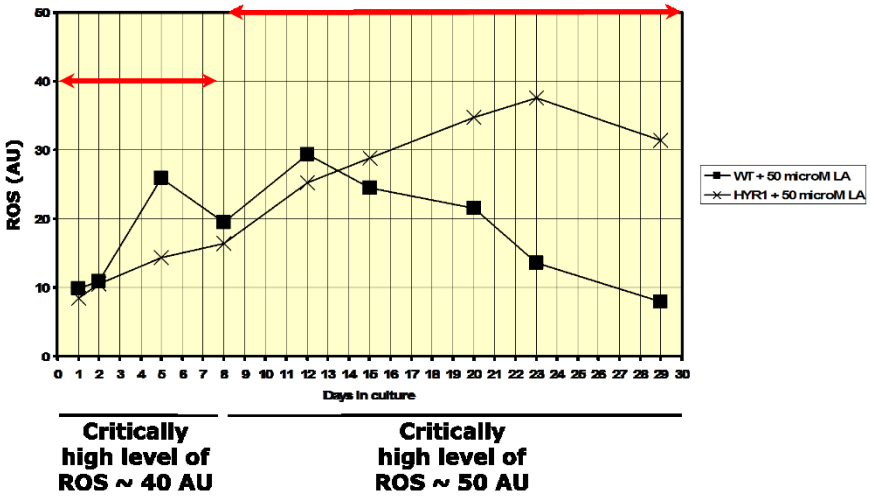

Figure 4.41. The *hyr1Δ* mutation, which enhances the ability of LCA to extend longevity, alters the age-dependent dynamics of ROS production.

Wild-type and *hyr1Δ* cells were cultured in the nutrient-rich YP medium initially containing 0.2% glucose and supplemented with LCA added at the final concentration of 50 μM. The levels of intracellular ROS were measured as described in ″Materials and Methods″. Red lines denote the levels of ROS that are critically high for the L, D and PD growth phases (days 1 to 7; 40 AU) or for the ST growth phase (Days 7 to 29; 50 AU).

4.4 Conclusions

In sum, findings described in this Chapter provide conclusive evidence in strong support of my hypothesis in which the longevity-extending potential of LCA is due in part to its ability to alter the age-related dynamics of mitochondrially produced ROS in both chronologically ″young″ and ″old″ cells, thus reducing the damaging effect of these ROS in ″young″ cells and amplifying their ″hormetic″ effect in ″old″ cells.

5 LCA accumulated in yeast mitochondria orchestrates a development of an anti-aging cellular pattern by causing age-related changes in cellular proteome

5.1 Introduction

The composition, morphology and functional state of mitochondria have been implicated in cell growth, division, differentiation, homeostasis, metabolism, stress response, signaling, immune response, aging, survival and death in evolutionarily distant eukaryotes; these cellular organelles are therefore central to the physiology, health and disease of eukaryotic organisms across phyla [3, 9, 10, 18, 19, 21, 23]. Mitochondria are indispensable for many vital cellular processes, including the following: (1) the synthesis of most cellular ATP via oxidative phosphorylation coupled to the electron transfer chain (ETC) in the inner mitochondrial membrane [3, 10]; (2) the generation of the tricarboxylic acid (TCA) cycle intermediates, some of which are used for the synthesis of amino acids, lipids and heme in mitochondria [3, 18, 19]; (3) the maintenance of a metabolic status-specific NAD^+/NADH ratio, AMP/ATP ratio, level of acetyl-CoA and level of *S*-adenosylmethionine; these mitochondria-derived metabolites modulate activities of several protein sensors governing energy-producing cellular metabolism and are also used for acetylation and methylation of numerous non-mitochondrial proteins involved in many cellular processes [3, 19, 23, 35]; (4) the synthesis and assembly of iron-sulfur clusters (ISC), inorganic cofactors of many mitochondrial, nuclear and cytosolic proteins playing essential roles in vital cellular processes [57]; (5) the formation of reactive oxygen species (ROS); these by-products of mitochondrial respiration play critical roles in regulating cell proliferation, differentiation, metabolism, signaling, immune response, aging, survival and death [18, 19, 41, 44, 47, 50, 53]; (6) the proteolytic degradation of unfolded proteins accumulated in mitochondria above a toxic threshold; the efflux of the resulting peptides from the mitochondria elicits a specific transcriptional response in the nucleus, thus reducing the number of unfolded proteins in mitochondria below the toxic threshold [18, 53, 70, 71, 73]; (7) the efflux of cytochrome *c* and other pro-apoptotic proteins from mitochondria to initiate a programmed form of apoptotic cell death as well as to modulate various non-apoptotic cellular processes, including cell cycle progression, differentiation, metabolism, autophagy, inflammation, immunity and regulated necrotic death [3, 9, 10, 12, 13, 16, 23]; (8) the assembly and disassembly of various multi-protein complexes on the outer mitochondrial surface; these dynamic multi-protein complexes have been implicated in cell

differentiation, signaling, metabolism, immune response, hypoxic response and death, as well as in mitochondrial fusion, fission, motility, inheritance, DNA maintenance and autophagic degradation [3, 9, 16, 21, 24, 93 - 97, 99]; (9) the establishment of zones of close apposition between the outer mitochondrial membrane and the mitochondria-associated membrane (MAM) domains of the endoplasmic reticulum (ER), plasma membrane, peroxisomes, vacuoles and autophagosomes; the MAM domains have been implicated in maintaining the homeostasis of intracellular Ca^{2+}, sustaining membrane phospholipid homeostasis, controlling mitochondrial biogenesis and morphology, regulating mitochondrial division and movement, controlling ER stress, influencing ROS and ATP production, orchestrating autophagosome biogenesis during non-selective and mitochondria-selective forms of autophagy, impinging on immune signaling and inflammation, and defining cell susceptibility to a programmed form of apoptotic death [3, 16, 21, 24, 25, 27, 28, 106, 108, 109]; and (10) the communication of mitochondria with lysosomes and peroxisomes via small mitochondria-derived vesicles, which contribute to mitochondrial quality control and peroxisome biogenesis (respectively) [120, 121].

All these findings support the view that mitochondria operate as signaling organelles that are intimately integrated with other cellular compartments in orchestrating many vital processes within eukaryotic cells [3, 16, 21, 24, 27, 28, 97, 99, 109]. A challenge is to uncover molecular mechanisms through which certain changes in the molecular composition of mitochondria influence their role as a signaling compartment that integrates cellular responses to various physiological conditions. A recent discovery by the Titorenko laboratory that exogenously added lithocholic bile acid (LCA) extends yeast chronological lifespan, accumulates in mitochondria and alters the mitochondrial membrane lipidome [193] provided an opportunity to explore how LCA-driven, longevity-extending changes in the composition of mitochondrial membrane phospholipids impact the ability of mitochondria to function as signaling organelles in aging. As a first step towards attaining our objective, in the studies described in this Chapter of my thesis I used quantitative mass spectrometry to investigate the effect of LCA on the age-related dynamics of alterations in levels of mitochondrial proteins and proteins in cellular locations outside of mitochondria.

5.2 Materials and methods

5.2.1 Strains and media

The wild-type strain *Saccharomyces cerevisiae* BY4742 (*MATα his3Δ1 leu2Δ0 lys2Δ0 ura3Δ0*) was used in this study. The composition of YEPD (0.2% glucose) medium was as follows: 1% yeast extract, 2% peptone, 0.2% glucose. Cells were cultured at 30^{o}C with rotational shaking at 200 rpm in Erlenmeyer flasks at a ″flask volume/medium volume″ ratio of 5:1.

5.2.2 A plating assay for the analysis of chronological lifespan

Cells were grown in YEPD (0.2% glucose) medium at 30^{o}C with rotational shaking at 200 rpm in Erlenmeyer flasks at a flask volume/medium volume ratio of 5:1. A sample of cells was removed from each culture at various time points. A fraction of the cell sample was diluted in order to determine the total number of cells per ml of culture using a hemacytometer. 10 µl of serial dilutions (1:10 to 1:10^{3}) of cells were applied to the hemacytometer, where each large square is calibrated to hold 0.1 µl. The number of cells in 4 large squares was then counted and an average was taken in order to ensure greater accuracy. The concentration of cells was calculated as follows: number of cells per large square x dilution factor x 10 x 1,000 = total number of cells per ml of culture. A second fraction of the cell sample was diluted and serial dilutions (1:10^{2} to 1:10^{5}) of cells were plated onto YEPD (2% glucose) plates in triplicate in order to count the number of viable cells per ml of each culture. 100 µl of diluted culture was plated onto each plate. After a 48-h incubation at 30^{o}C, the number of colonies per plate was counted. The number of colony forming units (CFU) equals to the number of viable cells in a sample. Therefore, the number of viable cells was calculated as follows: number of colonies x dilution factor x 10 = number of viable cells per ml. For each culture assayed, % viability of the cells was calculated as follows: number of viable cells per ml / total number of cells per ml x 100%. The % viability of cells in mid-logarithmic phase was set at 100% viability for that particular culture. The life span curves for wild-type and some of the mutant strains were also validated using a LIVE/DEAD yeast viability kit (Invitrogen) following the manufacturer's instructions for stationary-phase cultures.

5.2.3 Pharmacological manipulation of chronological lifespan

Chronological lifespan analysis was performed as described above in this section. The lithocholic (LCA) [#L6250] bile acid was from Sigma. The stock solution of LCA in DMSO was made on the day of adding this compound to cell cultures. LCA was added to growth medium at the final concentration of 50 μM immediately following cell inoculation into the medium. The final concentration of DMSO in yeast cultures supplemented with LCA (and in the corresponding control cultures supplemented with drug vehicle) was 1% (v/v).

5.2.4 Isolation of crude mitochondrial fraction from yeast cells

5.2.4.1 Reagents

1. Dithiothreitol (DTT) buffer [100 mM Tris-H2SO4, 10 mM dithiothreitol]
2. Zymolyase 100T from *Arthrobacter luteus* (MP Biomedicals)
3. Zymolyase buffer [1.2 M sorbitol, 20 mM potassium phosphate]
4. Homogenization buffer [0.6 M sorbitol, 10 mM Tris-HCl (pH 7.4), 1 mM EDTA, 0.2% (w/v) BSA]
5. SEM buffer [250 mM sucrose, 1 mM EDTA, 10 mM Mops (pH 7.2)]

5.2.4.2 Procedure

Cell cultures were combined in pre-weighed centrifuge bottles and cells were pelleted at 3,000 × g for 5 min at room temperature using a Beckman JA-10 rotor. The cells were washed twice with distilled water, followed by the determination of their wet weight. The cell pellets were resuspended in 2 ml/g DTT buffer and incubated on a shaker at 80 rpm for 20 min at 30ºC. The cells were pelleted as per initial centrifugation, washed in 7 ml/g Zymolyase buffer without Zymolyase and pelleted once more. The cells were incubated on a shaker at 80 rpm for 45 min at 30ºC with 1 mg/g (wet weight) of Zymolyase-100T in 7 ml/g Zymolyase buffer. Zymolyase was used because of its well-known strong lytic activity required to digest yeast cell wall. The spheroplasts obtained were then spun down at 2,200 × g for 8 min at 4ºC. All subsequent steps were carried out on ice or at 4°C with the use of cut pipette tips to avoid breaking organelles. The spheroplasts were resuspended in 6.5 ml/g ice-cold homogenization buffer and washed by centrifugation at 2,200 × g for 8 min at 4ºC. The spheroplasts were then mechanically homogenized with 15 strokes in 6.5 ml/g ice-cold homogenization buffer to disrupt yeast plasma

membrane for releasing organelles and cytoplasm. Following the homogenization, the cell debris was pelleted by centrifuging at 1,500 × g for 5 min at 4ºC using a Beckman JA-17 rotor. The resulting lysate supernatant was subjected to centrifugation twice at 3000 × g for 5 min at 4ºC to pellet the nuclei and 12,000 × g for 15 min at 4ºC. The newly obtained pellet contains mostly mitochondria, but also the endoplasmic reticulum (ER), Golgi, peroxisomes, lysosomes and vacuoles, whereas the supernatant contains the cytosol, microsomes from the ER and vacuoles. The pellet was resuspended in 6.5 ml/g in ice-cold homogenizing buffer, spun down for 5 min at 3,000 × g at 4ºC to obtain a supernatant containing mitochondria, which was then subjected to a spin at 12, 000 × g for 15 min at 4ºC. The resulting pellet was resuspended in 3 ml of SEM to be overlaid onto a sucrose gradient.

5.2.5 Purification of S. cerevisiae mitochondria devoid of microsomal and cytosolic contaminations

5.2.5.1 Reagents

1. SEM buffer [250 mM sucrose, 1 mM EDTA, 10 mM Mops (pH 7.2)]
2. EM buffer [10 mM Mops (pH 7.2), 1 mM EDTA]

5.2.5.2 Procedure

In order to purify yeast mitochondria from the crude mitochondrial fraction, an equilibrium density-gradient centrifugation was performed. Yeast mitochondria have a density of 1.18 g/cm^3 whereas 10% and 50% sucrose respectively have a density of 1.10 g/cm^3 and 1.30 g/cm^3. To prepare a sucrose density gradient for the purification of mitochondria, 1.5 ml of 60% sucrose in EM buffer was overlaid with 4 ml of 32%, 1.5 ml of 23% and 1.5 ml of 15% sucrose in EM buffer, followed by 3 ml of the crude mitochondrial suspension. The sucrose density gradient containing the mitochondrial suspension was subjected to centrifugation in a Beckman SW41 Ti swinging-bucket rotor at 134,000 × g for 60 min at 4ºC. The mitochondrial band, which was easily distinguishable, appeared at the interface between 60% and 32% sucrose. Fractions of 1 ml were recovered using a cut pipette tip and placed in 1.5 ml Eppendorf tubes and frozen at -80ºC until use. In order to quickly freeze the mitochondrial fractions, the fractions were immersed, with the aid of long tweezers, in a beaker of isopropyl alcohol kept in the -80ºC freezer.

5.2.6 Analysis of proteins by mass spectrometry

Proteins were resolved by SDS-PAGE and visualized by silver staining [245]. Protein bands were excised from the gel, reduced, alkylated and in-gel digested with trypsin [245]. The proteins were identified by matrix-assisted laser desorption/ionization mass spectrometric (MALDI MS) peptide mapping [246], using a Micromass M@LDI time-of-flight (TOF) mass spectrometer (Waters). Database searching using peptide masses was performed with the Mascot web-based search engine. For evaluating relative levels of individual proteins recovered in total cell lysates or purified mitochondria, a selected protein band was excised from the silver-stained gel and placed into an Eppendorf tube. A band of BSA containing 2 μg of this protein, which was also excised from the silver-stained gel, was added to each of the protein bands to be analyzed. Protein bands were reduced, alkylated and in-gel digested with trypsin [245]. The desalted peptide mixture was added to the surface of a MALDI target plate and allowed to air dry. The sample spot was then overlaid with MALDI matrix solution containing the Angiotensin I peptide standard (1:1 ratio). The presence of Angiotensin I in the sample carrying the analyzed mixture of peptides provided an additional estimate of the mass measurement accuracy after calibration, giving an opportunity to calculate the value of peptide mass tolerance for each individual mass spectrum. After the desalted peptide mixture was analyzed by MALDI-TOF, the monoisotopic masses of recovered BSA peptides and the intensities of their monoisotopic peaks were grouped separately from the masses and intensities of peptides originated from the protein of interest. These data provided an additional estimate of the mass measurement accuracy and were used for the quantitation of relative levels of the same protein recovered in different samples. For evaluating relative levels of the protein of interest found in the samples to be compared, a ratio "the intensity of the monoisotopic peak of a peptide originated from the protein of interest/the intensity of the monoisotopic peak of a BSA peptide with the monoisotopic mass closest to the mass of the peptide of interest" was calculated for each peptide originated from the protein of interest. Based on these data, the average value for relative levels of the protein of interest found in the two compared samples was calculated. The method for evaluating relative levels of the protein of interest recovered in different samples was validated by calculating relative levels of several standard proteins in the samples supplemented with different quantities of each of these proteins. Relative levels of proteins in cells or mitochondria of cells cultured in the presence of LCA (fold difference relative to those in the absence of LCA) are represented in the figures.

5.2.7 Statistical analysis

Statistical analysis was performed using Microsoft Excel's (2010) Analysis ToolPack-VBA. All data are presented as mean ± SEM. The *p* values were calculated using an unpaired two-tailed *t* test.

5.3 Results

5.3.1 LCA elicits age-related changes in mitochondrial proteome

I hypothesized that LCA accumulated in mitochondria of chronologically aging yeast may alter not only the membrane lipidome of these organelles [193] but also their proteome. To test this hypothesis, I used quantitative mass spectrometry to compare proteins that were recovered in mitochondria purified from wild-type (WT) cells cultured in the presence of LCA or in its absence. I found that LCA alters the age-related dynamics of changes in levels of numerous mitochondrial proteins implicated in many essential mitochondrial functions (Figure 5.1 and Appendix 1), including the following: (1) various enzymes of the TCA cycle (The Saccharomyces Genome Database (SGD): http://www.yeastgenome.org/); (2) Icl1p and Mls1p, enzymes of the glyoxylate cycle in mitochondria [157, 158]; (3) various protein components of the ETC [247]; (4) Aat1p, Gdh3p, Ilv5p, Ilv6p and Lys12p, enzymes involved in the biosynthesis of several amino acids, including aspartate, asparagine, threonine, glycine, isoleucine, glutamate, leucine, valine and lysine [248, 249]; (5) the Cox10p, Cyc3p and Hem14p proteins implicated in heme synthesis and attachment [250, 251]; (6) the Grx5p protein involved in the synthesis and assembly of ISCs, indispensable inorganic cofactors of various mitochondrial, nuclear and cytosolic proteins [57, 252]; (7) Pos5p, an enzyme catalyzing the synthesis of NADPH from NADH [253, 254]; (8) key protein components of reactive oxygen species (ROS) detoxification in mitochondria [247]; (9) stress response proteins that have been implicated in mitochondrial protein import, folding and stress protection [247]; (10) the Mia40p and Tim23p components of a machinery involved in protein import into the inner membrane, intermembrane space and matrix of mitochondria [250, 255, 256]; (11) the Caf4p and Mdv1p protein components of mitochondrial fission machinery [9]; (12) proteins that are essential for the synthesis, processing and translation of various mitochondrial RNA species [247]; and (13) various mtDNA-binding proteins with essential roles in mitochondrial nucleoid replication, maintenance, protection from damage and inheritance [247].

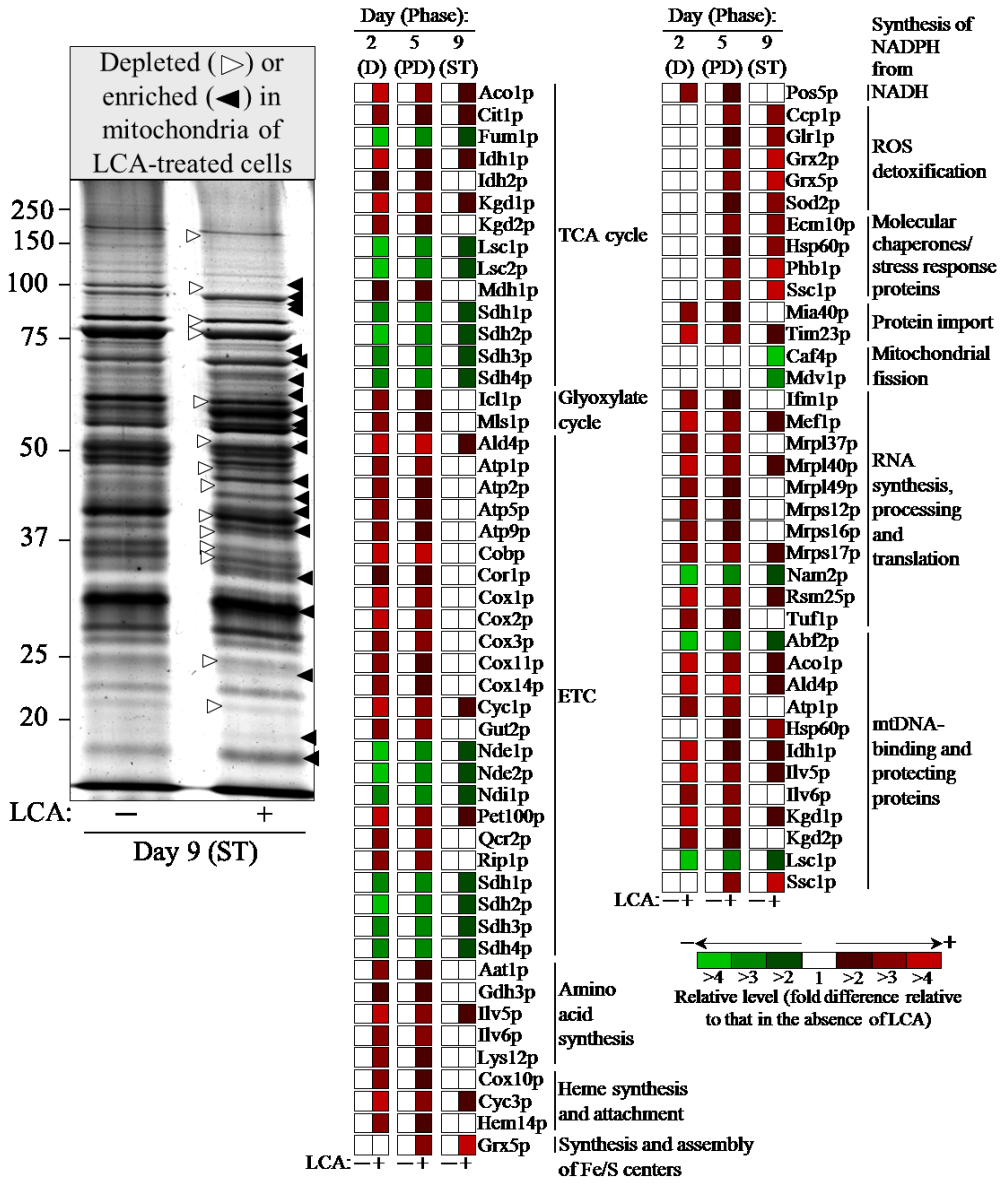

Figure 5.1. LCA alters the age-related dynamics of changes in levels of numerous mitochondrial proteins implicated in many essential mitochondrial functions.

Wild-type cells were cultured in the nutrient-rich YP medium initially containing 0.2% glucose, with 50 μM LCA or without it. Mitochondria were purified from cells recovered on days 2, 5 and 9 of culturing (D, PD and ST growth phases, respectively) as described in ″Materials and Methods″. Mass spectrometry-based identification and quantitation of proteins recovered in purified mitochondria were performed as described in ″Materials and Methods″. Relative levels of proteins in mitochondria of cells cultured in the presence of LCA (fold difference relative to those in the absence of LCA) are shown. Abbreviations: D, diauxic growth phase; ETC, the mitochondrial electron transport chain; mtDNA, mitochondrial DNA; PD, post-diauxic growth phase; ROS, reactive oxygen species; ST, stationary growth phase; TCA, the tricarboxylic acid cycle in mitochondria.

With the help of the SPELL online search engine [257], I used each of these mitochondrial proteins as a query for analyzing extensive datasets of gene expression profiles in yeast mutants that lack (1) various transcription factors; (2) protein components of several signaling pathways known to be modulated by mitochondria; or (3) mitochondrial proteins shown to be essential for modulating these signaling pathways. Such bioinformatic analysis revealed that the mitochondrial proteins whose levels were altered in an age-related fashion in yeast cells cultured with LCA can be divided into two regulons, each modulated by a different kind of mitochondrial dysfunction. I call these two regulons a partial mitochondrial dysfunction (PMD) regulon and an oxidative stress (OS) regulon (Figure 5.2). Based on expression profiles of the genes encoding mitochondrial proteins composing the PMD regulon and taking into consideration published data on regulation of such proteins in response to certain mitochondrial dysfunctions, it can be divided into six ″clusters″ (Figure 5.2). Each of these clusters denotes a distinct type of partial mitochondrial dysfunction that elicits a different signaling pathway governed by a distinct set of transcription factors. The PMD regulon includes the following clusters: (1) *rho*^{0} cluster (which is governed by Rtg2p, a sensor of an age-related reduction of mitochondrial membrane potential) [18, 158, 258 - 262]; (2) S1 cluster [18, 258, 260, 261]; (3) general TCA cycle dysfunction cluster [18, 258 - 261]; (4) *kgd1Δ*, *kgd2Δ* or *lpd1Δ* cluster [18, 259 - 261]; (5) *yme1Δ mdl1Δ* cluster [18, 261]; and (6) *afo1Δ* cluster (which is governed by Sfp1p, a transcription activator of genes encoding cytoplasmic ribosomal proteins) [18, 172]. The OS regulon includes the following clusters: (1) a cluster governed by the transcription factor Yap1p, a primary determinant in the antioxidant response of yeast cells [263 - 269]; (2) a cluster governed by the transcription factors Msn2p/Msn4p, which are required for expression of numerous genes in response to thermal, oxidative and other types of stress [262, 267 - 270]; (3) a cluster governed by the transcription factor Skn7p, which is involved in the osmotic and oxidative stress responses [263 - 269]; and (4) a cluster governed by Hog1p, a mitogen-activated protein kinase orchestrating an osmosensing signal transduction pathway in yeast [269, 271, 272].

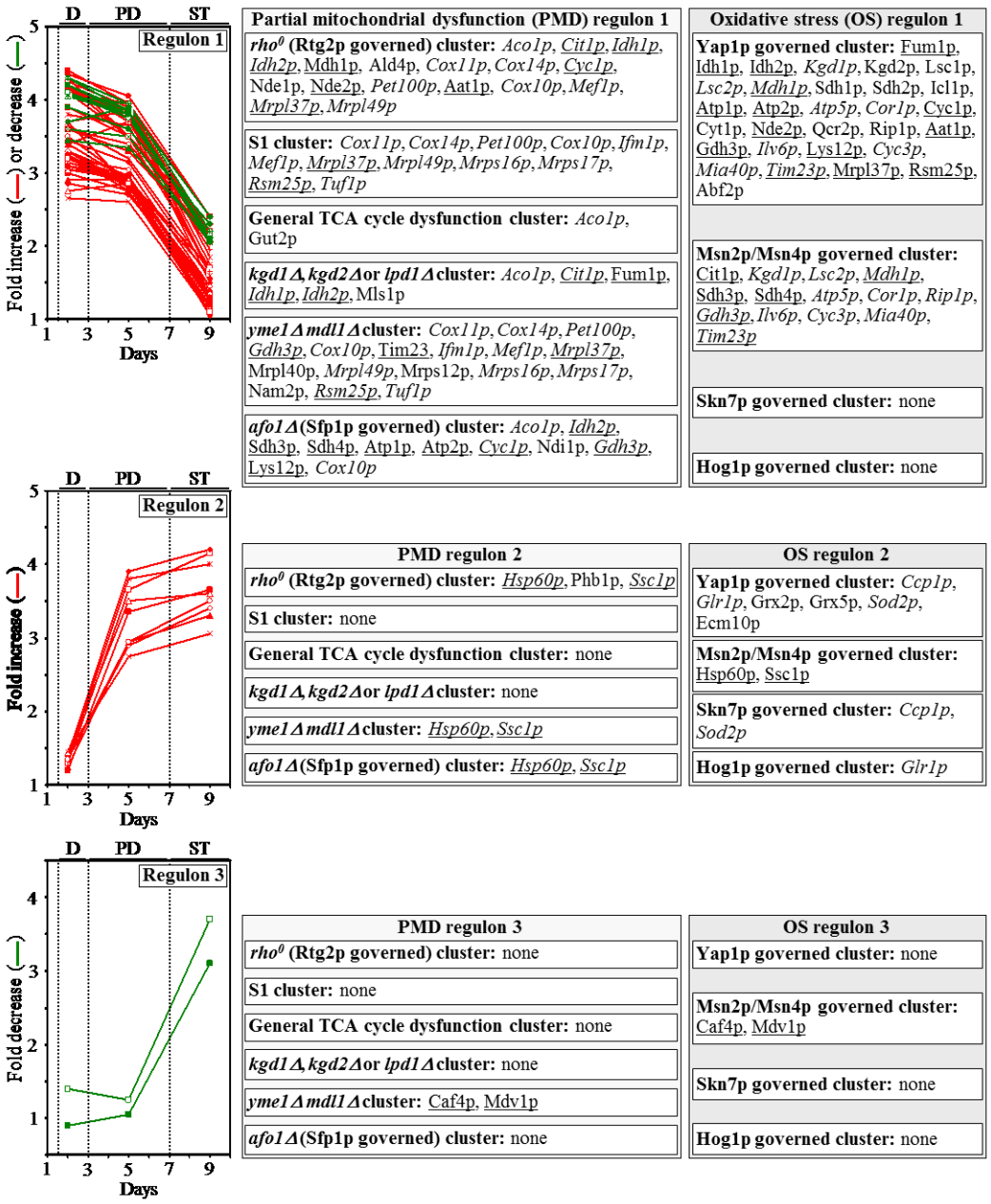

Figure 5.2. The mitochondrial proteins whose levels are altered in an age-related fashion in yeast cells cultured with LCA can be divided into two regulons called a partial mitochondrial dysfunction (PMD) regulon and an oxidative stress (OS) regulon.

Each regulon is modulated by a different kind of mitochondrial dysfunction. Based on expression profiles of the genes encoding mitochondrial proteins composing the PMD and OS regulons and considering published data on regulation of such proteins in response to certain mitochondrial dysfunctions, each regulon can be divided into several ″clusters″. Each cluster denotes a distinct type of partial mitochondrial dysfunction that elicits a different signaling pathway mediated by a distinct set of transcription factors. Because mitochondrial proteins constituting the PMD and OS regulons exhibit three different patterns of the age-related dynamics of changes in their cellular levels,

each of these regulons is separated into regulons ″type 1″, ″type 2″ and ″type 3″. The names of proteins that belong to more than one PMD or OS regulon are italicized; the names of proteins that are members of both a PMD regulon and an OS regulon are underlined. Abbreviations: D, diauxic growth phase; PD, post-diauxic growth phase; ST, stationary growth phase.

It needs to be emphasized that mitochondrial proteins constituting the PMD and OS regulons exhibit three different patterns of the age-related dynamics of changes in their cellular levels; to underscore the existence of such differences in expression, we separated each of the PMD and OS regulons into regulons ″type 1″, ″type 2″ and ″type 3″ (Figure 5.2 and Appendix 1). The cellular levels of mitochondrial proteins comprising the PMD and OS regulons type 1 remained nearly unchanged during diauxic (D) and post-diauxic (PD) growth phases but underwent a 2-3 fold increase or decrease during the subsequent stationary (ST) growth phase (Figure 5.2; PMD regulon 1 and OS regulon 1). Furthermore, the cellular levels of mitochondrial proteins comprising the PMD and OS regulons type 2 elevated by 2-3 folds during D and PD growth phases but remained almost unaltered during the following ST growth phase (Figure 5.2; PMD regulon 2 and OS regulon 2). Moreover, the cellular levels of mitochondrial proteins comprising the PMD and OS regulons type 3 remained nearly the same during the most of D and PD growth phases but underwent a 3-4 fold reduction during the subsequent ST growth phase (Figure 5.2; PMD regulon 3 and OS regulon 3). Noteworthy, the expression of genes encoding mitochondrial proteins that belong to the PMD regulons type 1, 2 and 3 is known to be regulated by the transcription factors Rtg1p/Rtg2p/Rtg3p, Sfp1p and Aft1p [18, 172, 262]. The expression of genes coding for mitochondrial proteins that belong to the OS regulons type 1, 2 and 3 has been shown to be under the control of the transcription factors Yap1p, Msn2p/Msn4p, Skn7p and Hog1p [263 - 268, 270, 271].

5.3.2 LCA causes age-related changes in cellular proteome

Age-related alterations in the rates and efficiencies of several processes within mitochondria are known to modulate the capacity of these organelles to make and release certain molecular signals; outside mitochondria, such signals have been shown to cause changes in the rates and efficiencies of longevity-defining processes in other cellular locations [3, 16, 18, 19, 21, 24, 27, 28, 71, 262]. Of note, I found that a treatment of yeast cells with LCA alters the age-related

chronology of these mitochondrial processes [19, 139, 155, 184, 193, 218]. I therefore hypothesized that LCA may impact not only the levels of numerous mitochondrial proteins but also the levels of proteins in cellular locations outside mitochondria. To validate this hypothesis, I used quantitative mass spectrometry to compare proteins that were recovered in total lysates of WT cells cultured in the presence of LCA or in its absence. This quantitative analysis of cellular proteins confirmed the data of such analysis for proteins recovered in purified mitochondria; indeed, I found that LCA alters the age-related dynamics of changes in levels of many mitochondrial proteins known for their essential roles in vital mitochondrial functions and aging in yeast (compare Figures 5.1 and 5.3, as well as Appendices 1 and 2). Moreover, I found that LCA causes age-related changes in levels of numerous proteins known to be located outside of mitochondria and shown to be involved in various cellular processes (Figure 5.3 and Appendix 2). These cellular processes include the following: (1) glycogen degradation; (2) the glycolytic pathway; (3) the pentose phosphate pathway; (4) pyruvate conversion to acetyl-CoA; (5) the maintenance of redox balance between NAD and NADH with the help of carnitine and glycerol-3-phosphate shuttles; (6) ROS detoxification; (7) stress response; (8) glutathione synthesis; (9) gluconeogenesis; (10) ethanol formation; (11) the synthesis and hydrolytic degradation of triacylglycerols (TAG) and ergosteryl esters (EE), the two major neutral lipids; (12) the synthesis of various amino acids; (13) nucleotide synthesis; (14) the assembly of the 40S and 60S ribosomal subunits from numerous protein components whose levels were altered by LCA; and (15) proteasomal and vacuolar protein degradation [18, 19, 145, 155, 158, 214, 247].

I then subjected cellular proteins whose levels were changed in yeast grown in a medium supplemented with LCA to bioinformatic analysis with the help of the SPELL online search engine [257], as described above for mitochondrial proteins. Just as my bioinformatic analysis of mitochondrial proteins revealed (see above), I found that each of the cellular proteins whose level was altered in yeast cultured with LCA belongs to the following two multi-clustered regulons: (1) the PMD regulon, which consisted of the *rho*^{0} (Rtg2p governed) cluster, S1 cluster, general TCA cycle dysfunction cluster, *kgd1Δ*, *kgd2Δ* or *lpd1Δ* cluster, *yme1Δ mdl1Δ* cluster, and *afo1Δ* (Sfp1p governed) cluster [18, 19, 158, 172, 258 - 262]; and (2) the OS regulon, which included the Yap1p governed cluster, Msn2p/Msn4p governed cluster, Skn7p governed cluster

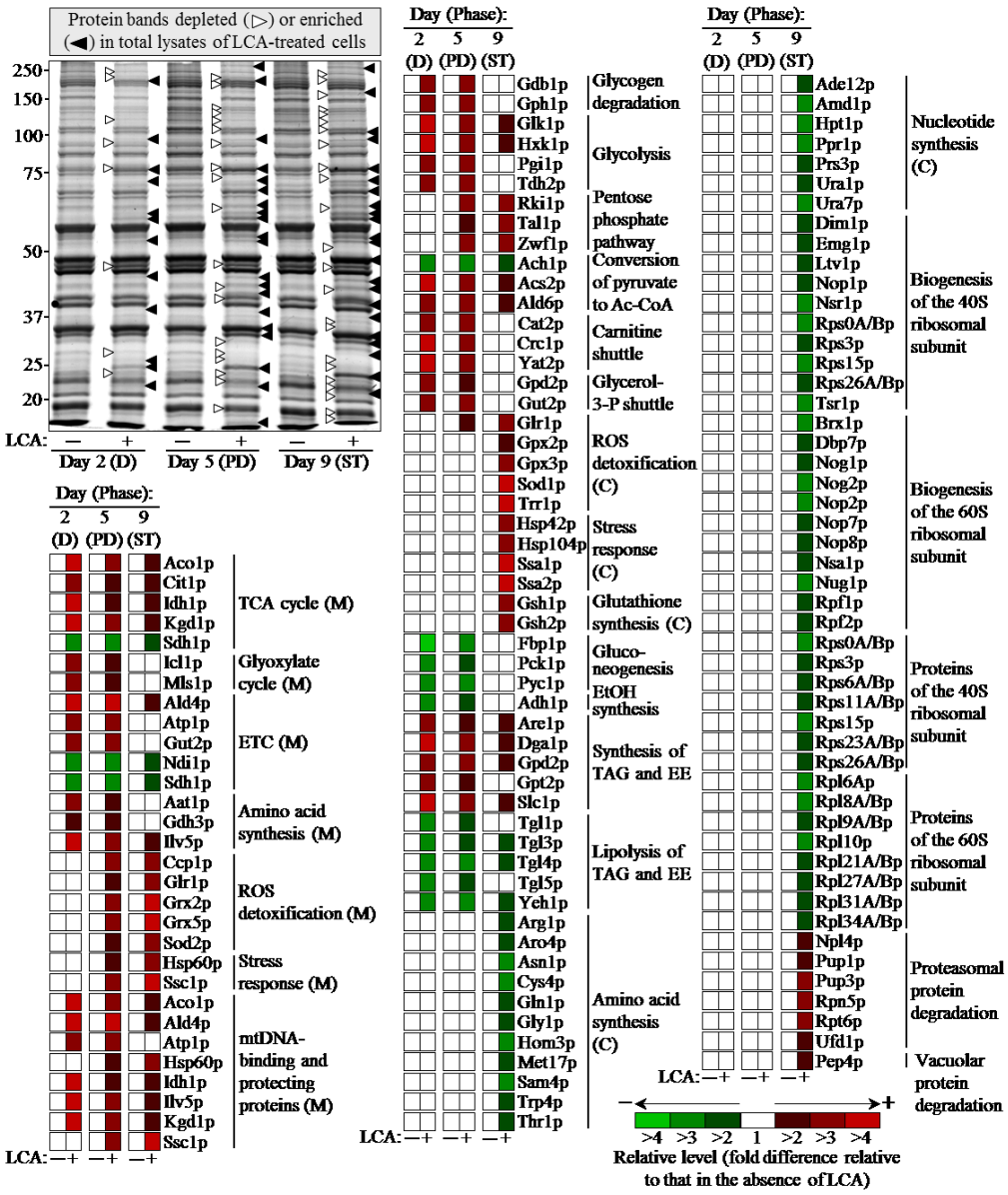

Figure 5.3. LCA alters the age-related dynamics of changes in levels of many mitochondrial proteins and numerous proteins located outside of mitochondria; these mitochondrial and non-mitochondrial proteins have been implicated in various cellular processes.

Wild-type cells were cultured in the nutrient-rich YP medium initially containing 0.2% glucose, with 50 μM LCA or without it. Cells were recovered on days 2, 5 and 9 of culturing (D, PD and ST growth phases, respectively). Mass spectrometry-based identification and quantitation of proteins recovered in total lysates of yeast cells were performed as described in ″Materials and Methods″. Relative levels of proteins in cells cultured in the presence of LCA (fold difference relative to those in the absence of LCA) are shown. Abbreviations: C, cytosol; D, diauxic growth phase; EE, ergosteryl esters; ETC, the mitochondrial electron transport chain; M, mitochondria; mtDNA, mitochondrial DNA; PD, post-diauxic growth phase; ROS, reactive oxygen species; ST, stationary growth phase; TAG, triacylglycerols; TCA, the tricarboxylic acid cycle in mitochondria.

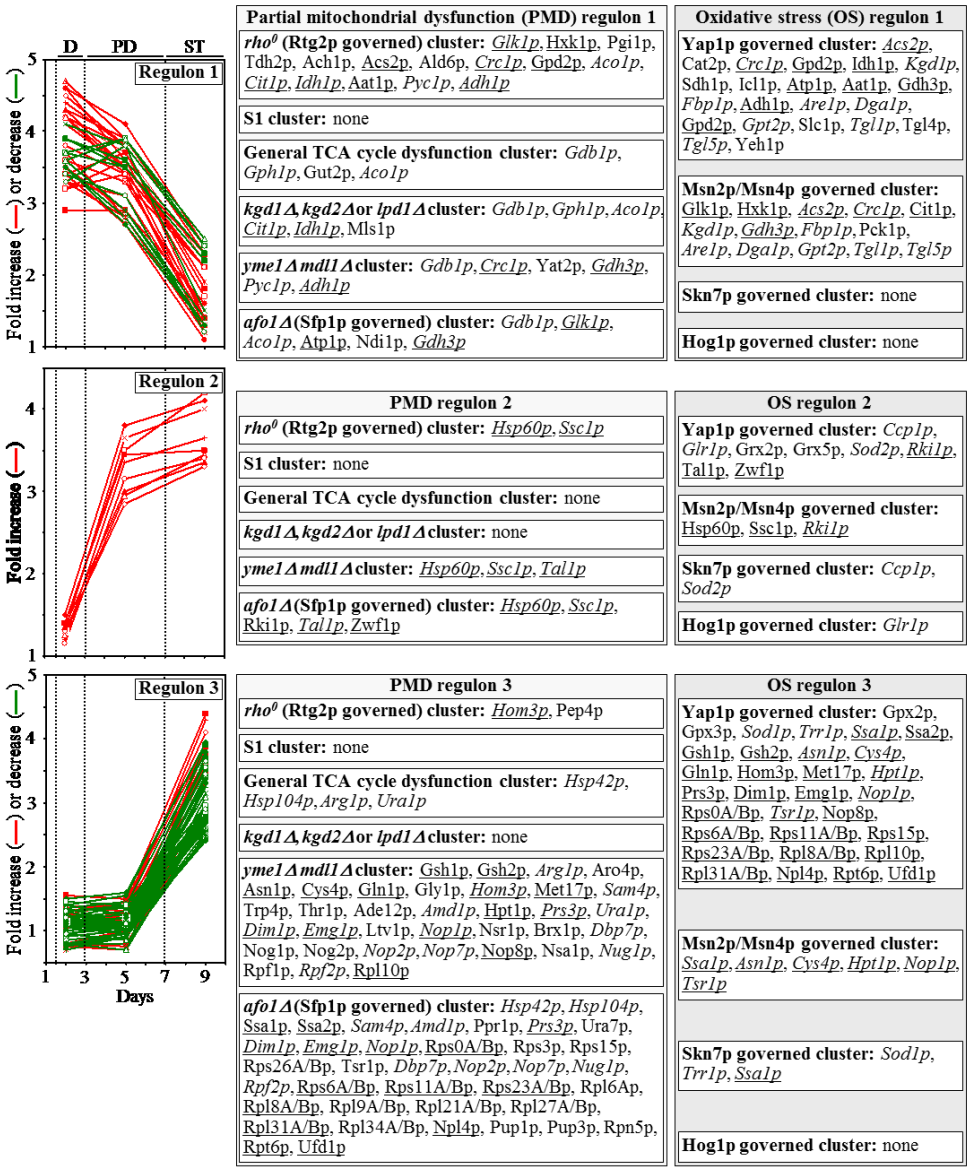

Figure 5.4. Each of the cellular proteins whose level is changed in yeast cultured with LCA belongs to the following two multi-clustered regulons, each modulated by a different kind of mitochondrial dysfunction.

(1) the partial mitochondrial dysfunction (PMD) regulon, which consisted of the *rho*^{0} (Rtg2p governed) cluster, S1 cluster, general TCA cycle dysfunction cluster, *kgd1Δ*, *kgd2Δ* or *lpd1Δ* cluster, *yme1Δ mdl1Δ* cluster, and *afo1Δ* (Sfp1p governed) cluster; and 2) the oxidative stress (OS) regulon, which included the Yap1p governed cluster, Msn2p/Msn4p governed cluster, Skn7p governed cluster and Hog1p governed cluster. Each cluster denotes a distinct type of partial mitochondrial dysfunction that elicits a different signaling pathway governed by a distinct set of transcription factors. Because cellular proteins that belong to the PMD and OS regulons display three different patterns of age-related changes in their levels, each of these regulons is separated into regulons ″type 1″, ″type 2″ and ″type 3″. The names of cellular proteins that belong to more than one PMD or OS regulon are italicized; the

names of cellular proteins that are members of both a PMD regulon and an OS regulon are underlined. Abbreviations: D, diauxic growth phase; PD, post-diauxic growth phase; ST, stationary growth phase.

and Hog1p governed cluster (Figure 5.4) [18, 19, 262 - 268, 270 - 272]. I also found that, akin to mitochondrial proteins constituting the PMD and OS regulons, cellular proteins that belong to each of them displays either of the following three patterns of age-related changes in their levels: (1) the levels of cellular proteins that belong to the PMD and OS regulons type 1 remained nearly unchanged during D and PD growth phases but underwent a 3-4 fold rise or reduction during the subsequent ST growth phase (Figure 5.4; PMD regulon 1 and OS regulon 1); (2) the levels of cellular proteins that belong to the PMD and OS regulons type 2 increased by 3-4 folds during D and PD growth phases but remained almost unaltered during the following ST growth phase (Figure 5.4; PMD regulon 2 and OS regulon 2); and (3) the levels of cellular proteins that belong to the PMD and OS regulons type 3 remained practically the same during the most of D and PD growth phases but underwent a 2-4 fold reduction or rise during the subsequent ST growth phase (Figure 5.4; PMD regulon 3 and OS regulon 3). Moreover, I noted that: (1) similar to mitochondrial proteins constituting the three different PMD regulons, the expression of genes for cellular proteins that belong to the PMD regulons type 1, 2 and 3 has been shown to be governed by the transcription factors Rtg1p/Rtg2p/Rtg3p, Sfp1p and Aft1p [18, 172, 262]; and (2) akin to mitochondrial proteins constituting the three different OS regulons, the expression of genes for cellular proteins that belong to the OS regulons type 1, 2 and 3 is known to be controlled by the transcription factors Yap1p, Msn2p/Msn4p, Skn7p and Hog1p [263 - 268, 270 - 272].

5.3.3 Longevity extension by LCA requires a distinct set of transcription factors

I found that gene-deletion mutations eliminating either the Rtg1p, Rtg2p, Rtg3p, Sfp1p, Yap1p, Msn2p/Msn4p, Skn7p or Hog1p transcription factor(s) significantly reduce the extent to which LCA extends yeast longevity (Figures 5.5 and 5.6); all these factors are known to cause a development of an anti-aging cellular pattern by activating specific transcriptional programs in the nucleus [18, 19, 172, 261 - 268, 270 - 272]. In contrast, a single-gene-deletion mutation eliminating the transcription factor Aft1p increased the longevity-extending efficiency of LCA (Figures 5.5 and 5.6); this factor has been shown to respond to reduced levels of cellular ISCs by eliciting a pro-aging transcriptional program in the nucleus [18, 19, 56, 60]. In sum, these findings suggest that, by

establishing a specific pattern of an age-related expression of numerous nuclear genes encoding mitochondrial and non-mitochondrial proteins that belong to the PMD or OS regulons of type 1, 2 or 3, each of these transcription factors plays an essential role in longevity extension by LCA.

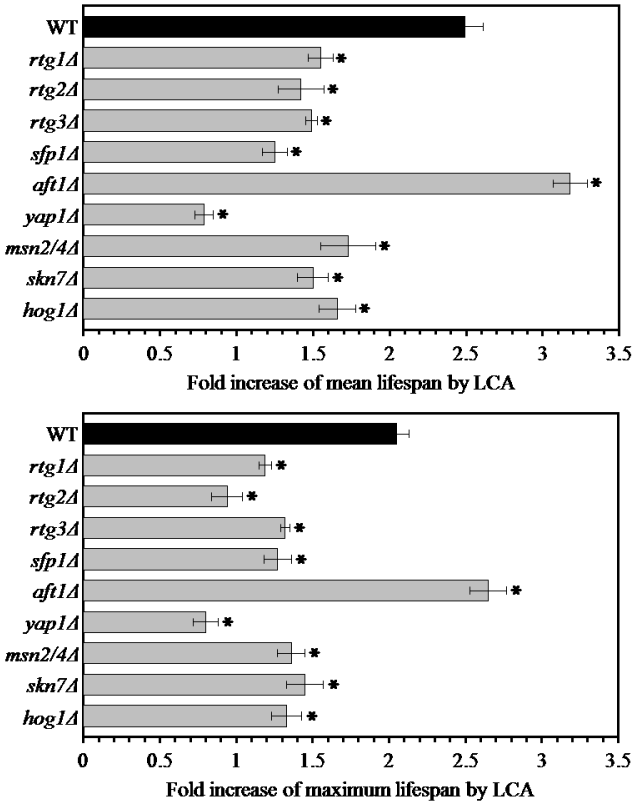

Figure 5.5. Gene-deletion mutations eliminating the Rtg1p, Rtg2p, Rtg3p, Sfp1p, Aft1p, Yap1p, Msn2p/Msn4p, Skn7p or Hog1p transcription factor significantly alter the extent to which LCA extends yeast longevity.

Wild-type and mutant cells lacking one (or two, as in case of *msn2/4Δ* mutant cells) of the above transcription factors were cultured in the nutrient-rich YP medium initially containing 0.2% glucose, with 50 μM LCA or without it. The chronological lifespans were measured as described in ″Materials and Methods″. Data are presented as means ± SEM (n = 4-6; *p < 0.01).

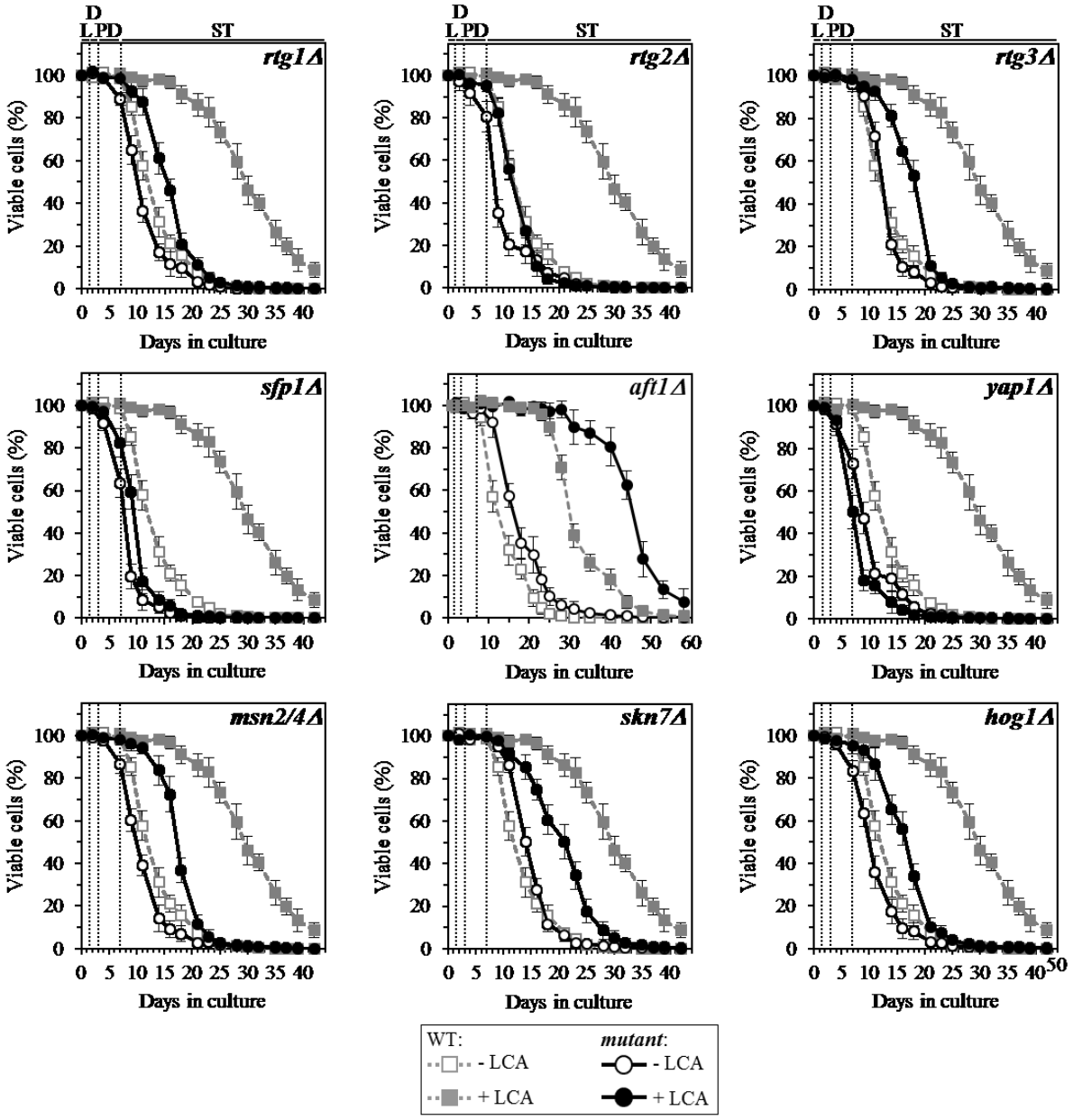

Figure 5.6. Gene-deletion mutations eliminating the Rtg1p, Rtg2p, Rtg3p, Sfp1p, Aft1p, Yap1p, Msn2p/Msn4p, Skn7p or Hog1p transcription factor significantly alter the extent to which LCA extends yeast longevity.

Wild-type and mutant cells lacking one (or two, as in case of *msn2/4Δ* mutant cells) of these transcription factors were cultured in the nutrient-rich YP medium initially containing 0.2% glucose, with 50 μM LCA or without it. The chronological lifespans were measured as described in ″Materials and Methods″. Survival curves of chronologically aging yeast are shown; data are presented as means ± SEM (n = 4-6).

5.4 Discussion

This study and my recent published data [193] suggest that LCA-driven changes in mitochondrial lipidome alter mitochondrial proteome and functionality, thereby enabling mitochondria to function as signaling organelles that orchestrate an establishment of an anti-aging transcriptional program for many longevity-defining nuclear genes (Figure 5.7). It is conceivable that the reduced mitochondrial membrane potential seen in chronologically ″young″ yeast cells cultured with LCA [193] triggers the mitochondrial retrograde (RTG) signaling pathway of cellular aging regulation (Figure 5.7); the Rtg2p protein component of this pathway is known to respond to a decline in mitochondrial membrane potential by stimulating nuclear import of the Rtg1p-Rtg3p heterodimeric transcription factor, which in the nucleus triggers an anti-aging transcriptional program [18, 19, 262]. Furthermore, the observed in chronologically ″old″ yeast cells cultured with LCA reduction in the levels of several protein components of the large and small subunits of mitochondrial ribosome (Figures 5.1 and 5.2) is likely to activate the so-called back-signaling pathway (Figure 5.7); in response to reduced levels of mitochondrial ribosomal proteins this pathway is known to trigger an anti-aging transcriptional program which in the nucleus is activated by the transcription factor Sfp1p [18, 19, 172]. Moreover, it is plausible that the observed in chronologically ″old″ yeast cells cultured with LCA rise in the levels of proteins involved in the synthesis and assembly of ISCs in mitochondria (Figures 5.1 and 5.2) may diminish activity and/or nuclear import of Aft1p (Figure 5.7), a transcription factor known to respond to reduced levels of cellular ISCs by driving a pro-aging transcriptional program in the nucleus [18, 19, 56, 60]. It is also conceivable that the observed in chronologically ″young″ and ″old″ yeast cells cultured with LCA significant changes in the levels of numerous mitochondrial and non-mitochondrial proteins comprising the *yme1Δ mdl1Δ* cluster of the PMD regulon (Figures 5.1 to 5.4) activate a distinct retrograde response signaling pathway that triggers an anti-aging transcriptional program in the nucleus (Figure 5.7); this pathway is known to be elicited in response to a simultaneous lack of the mitochondrial i-AAA protease Yme1p and the mitochondrial ABC-transporter Mdl1p involved in peptide export from mitochondria [18, 19, 261]. Finally, the observed ability of LCA to amplify the ″hormetic″, anti-aging effect of mitochondrially generated ROS by enabling to maintain their levels in chronologically ″old″ yeast cells relatively high but below a cytotoxic threshold [19, 193] is likely to delay aging by activating Yap1p, Msn2p/Msn4p, Skn7p or Hog1p (Figure 5.7); these transcription factors are

known to respond to ″hormetic″ levels of ROS by triggering an anti-aging transcriptional program in the nucleus [18, 19, 263 - 268, 270 - 272].

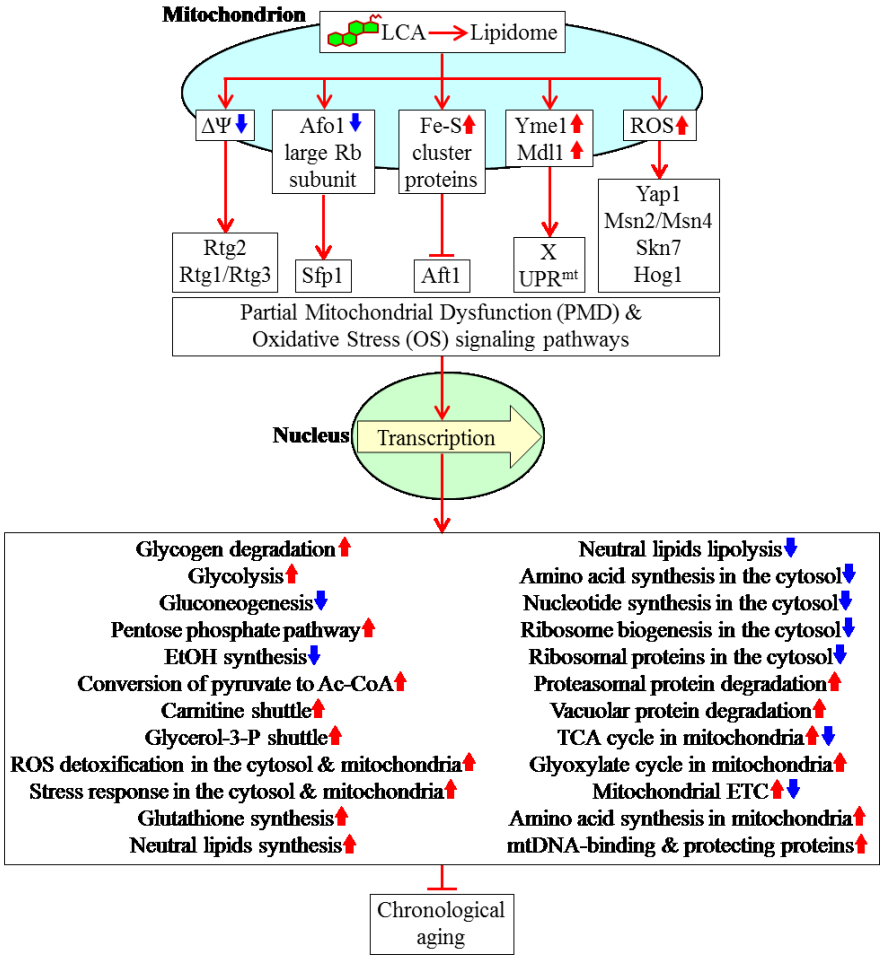

Figure 5.7. A model for how LCA-driven changes in mitochondrial lipidome alter mitochondrial proteome and functionality, thereby enabling mitochondria to function as signaling organelles modulating transcription of many longevity-defining nuclear genes.

See text for details. Abbreviations: Ac-CoA, acetyl-CoA; ETC, the mitochondrial electron transport chain; mtDNA, mitochondrial DNA; ROS, reactive oxygen species; ST, stationary growth phase; TCA, the tricarboxylic acid cycle in mitochondria.

Moreover, this study and published data from the Titorenko laboratory [19, 20, 139, 155, 159, 184, 193, 214, 218] suggest the following model for how LCA-driven changes in mitochondrial proteome and functionality early and late in life of chronologically aging yeast cause a stepwise development of an anti-aging cellular pattern and its maintenance throughout lifespan (Figure 5.8).

Early in life of a chronologically aging yeast cell, during the D phase of growth, LCA within the inner and outer membranes of mitochondria reduces the capacities of coupled mitochondrial respiration, mitochondrial membrane potential and mitochondrial ROS production (Figure 5.8) - likely by decreasing the levels of the ″upstream″ protein components (i.e. Ndi1p, Nde1p, Nde2p and Sdh1p-Sdh4p) of the mitochondrial ETC and increasing the levels of its ″downstream″ protein components (i.e. cytochrome *c* as well as respiratory complexes III, IV and V) (Figures 5.1 to 5.4). By differentially altering the levels of proteins involved in the mitochondrial TCA cycle (Figures 5.1 to 5.4), LCA increases the efficiencies with which some of the intermediates of this cycle are converted into amino acids, NADPH and heme within mitochondria (Figure 5.8); the rates of such conversion during D growth phase are further elevated by the LCA-elicited rise in the levels of mitochondrial enzymes catalyzing the key reactions of the conversion (Figures 5.1 to 5.4). The rise in the levels of proteins known to be essential for the synthesis, processing and translation of various mitochondrial RNA species, which is observed in mitochondria of cultured with LCA cells during D growth phase (Figures 5.1 to 5.4), improves mitochondrial functionality by stimulating these processes within mitochondria (Figure 5.8). Furthermore, the elevated levels of mitochondrial components involved in protein import into the inner membrane, intermembrane space and matrix of mitochondria (Figures 5.1 to 5.4) accelerate these processes during D growth phase, thus further improving mitochondrial functionality (Figure 5.8). Additionally, by increasing the levels of mtDNA-binding proteins during D growth phase (Figures 5.1 to 5.4), LCA stabilizes the mitochondrial nucleoid and protects it from oxidative and other forms of age-related damage (Figure 5.8). During the D phase of growth, LCA within the inner and outer mitochondrial membranes also elevates the levels of mitochondrial membrane proteins required for acetyl-CoA uptake by mitochondria (Figures 5.1 to 5.4); moreover, the altered functionality of these mitochondria triggers several mitochondria-to-nucleus signaling pathways that differentially affect cellular levels of non-mitochondrial proteins involved in various metabolic pathways for carbohydrates and lipids (Figures 5.1 to 5.4). The resulting remodeling of these pathways in yeast cells cultured in the presence of LCA (1) stimulates glycogen degradation, glycolysis, acetyl-CoA formation in the cytosol and neutral lipids synthesis in the ER – thus increasing the levels of NADH, ATP and neutral lipids; and (2) inhibits ethanol formation from acetaldehyde, acyl-CoA conversion to acetate, gluconeogenetic metabolism of pyruvate and the lipolytic

conversion of neutral lipids into fatty acids – thereby further stimulating acetyl-CoA formation in the cytosol, from which it is then transported with the increased efficiency into mitochondria to improve their functionality (Figure 5.8) [18,19].

During the subsequent PD phase of growth, LCA within the inner and outer mitochondrial membranes not only maintains its ability to decrease the levels of the ″upstream″ protein components of the mitochondrial ETC and to increase the levels of its ″downstream″ protein components but also elevates the level of the mitochondrial cytochrome-*c* peroxidase Ccp1p (Figures 5.1 to 5.4) – thus enabling to sustain reduced capacities of coupled mitochondrial respiration, mitochondrial membrane potential and mitochondrial ROS production (Figure 5.8). By increasing the levels of stress response proteins implicated in mitochondrial protein import, folding, stress protection and membrane proteins biogenesis (Figures 5.1 to 5.4), LCA stimulates all these longevity-defining processes in mitochondria of yeast cells that have entered the PD phase of growth (Figure 5.8). Furthermore, a sustained ability of LCA to increase the levels of mtDNA-binding proteins during PD growth phase (Figures 5.1 to 5.4) enables it to support mitochondrial nucleoid stability and protection from age-related damage (Figure 5.8). Moreover, by increasing the levels of numerous mitochondrial proteins integrated into a network of antioxidant scavenger reactions for ROS decomposition (Figures 5.1 to 5.4), LCA attenuates oxidative damage to mitochondrial proteins, lipids and nucleic acids (Figure 5.8). In addition, the altered functionality of mitochondria in cells cultured with LCA triggers mitochondria-to-nucleus signaling that during PD growth phase increases the levels of non-mitochondrial proteins involved in the pentose phosphate pathway (Figures 5.1 to 5.4); this pathway is known to generate NADPH, the primary source of cellular reducing equivalents required for the reductive synthesis of fatty acids, sterols and some amino acids as well as for the protection of numerous thiol-containing cytosolic, nuclear and mitochondrial proteins from oxidative damage (Figure 5.8) [19, 191].

During ST phase, LCA within mitochondria maintains its ability to elevate the levels of many mitochondrial proteins involved in antioxidant scavenger reactions for ROS decomposition (Figures 5.1 to 5.4), thus reducing the extent of oxidative damage to mitochondrial proteins, lipids and nucleic acids (Figure 5.8). In addition, LCA attenuates mitochondrial fragmentation during ST phase by reducing the levels of the Caf4p and Mdv1p protein components of mitochondrial fission machinery (Figures 5.1 to 5.4) - thus delaying an age-related form of

programmed apoptotic cell death (Figure 5.8). During ST phase, the altered functionality of mitochondria in yeast cultured in the presence of LCA also stimulates several mitochondria-to-nucleus signaling pathways that differentially affect cellular levels of many non-mitochondrial proteins involved in various longevity-defining processes (Figures 5.1 to 5.4). The resulting remodeling of these processes outside mitochondria (1) reduces the extent of oxidative damage to cytosolic proteins; (2) stimulates protein folding, unfolding and refolding in the cytosol; (3) promotes vacuolar and proteasomal protein degradation; (4) slows down amino acid and nucleotide synthesis in the cytosol; and (5) decelerates protein synthesis in the cytosol by attenuating the assembly of the 40S and 60S ribosomal subunits (Figure 5.8).

In the future, it would be important to further explore the following key aspects of the mechanism we proposed here, through which yeast mitochondria function as signaling organelles orchestrating a stepwise development of a longevity-defining cellular pattern. First, it would be intriguing to investigate how several genetic interventions known to cause various changes in the mitochondrial membrane lipidome [273 - 276] might influence the ability of LCA (1) to extend longevity of chronologically aging yeast; (2) to elicit a characteristic set of age-related changes in mitochondrial proteome and functionality; and (3) to cause a distinct kind of age-related alterations in the levels of proteins outside mitochondria. Second, it would be interesting to elucidate how genetic interventions known to alter mitochondrial membrane potential, mitochondrial ribosomal proteins, mitochondrial synthesis and assembly of ISCs, mitochondrial protein degradation and peptide efflux, or mitochondrial ROS [18, 19], would impact the capability of LCA to trigger a characteristic pattern of age-related changes in the concentrations of proteins located outside of mitochondria. Third, it would be important to use quantitative mass spectrometry-based metabolomics to investigate the characteristic anti-aging ″metabolic signature″ driven by LCA, for which we could compare to our data from proteomic analyses.

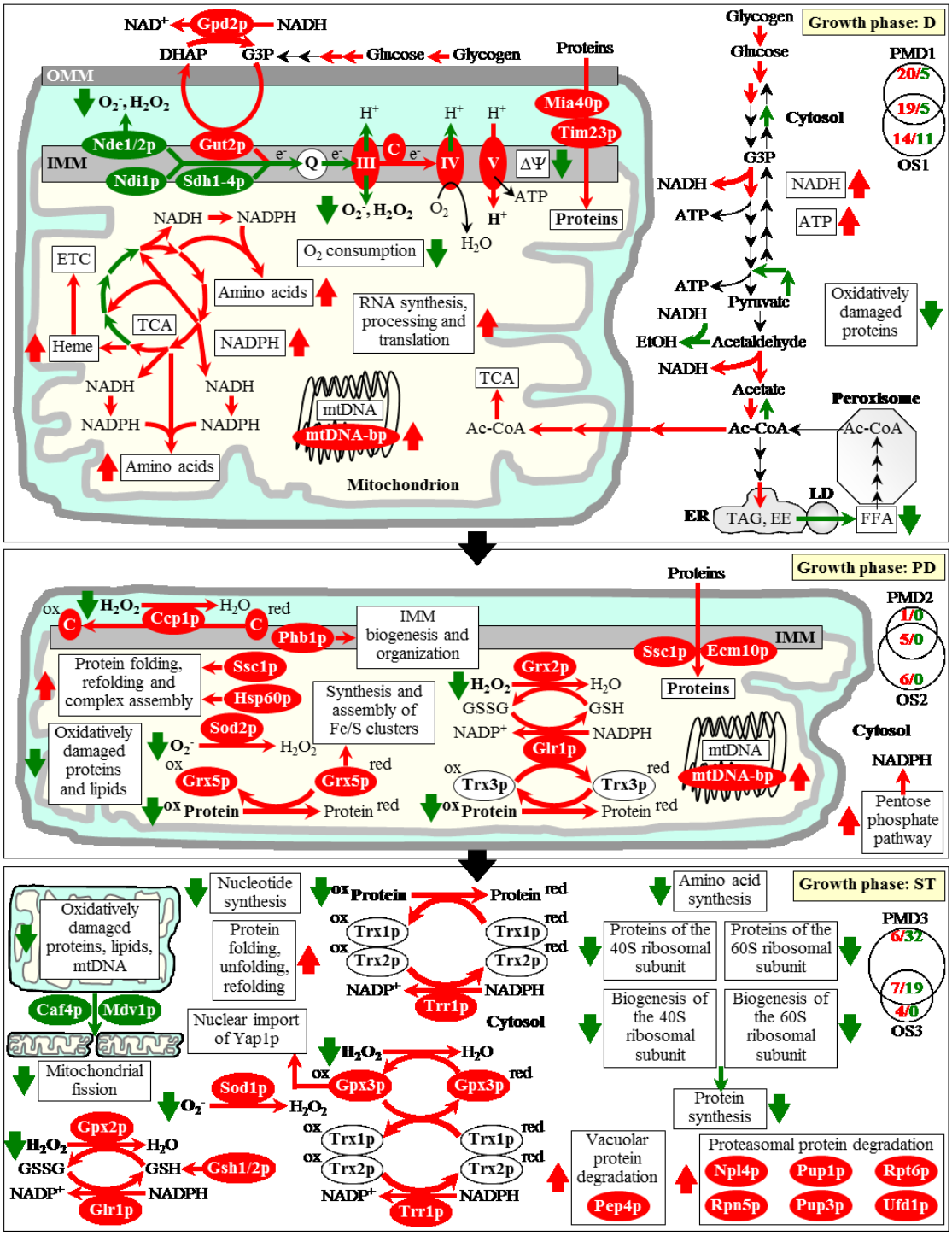

Figure 5.8. A model for how LCA-driven changes in mitochondrial proteome and functionality early and late in life of chronologically aging yeast orchestrate a stepwise development of an anti-aging cellular pattern and its maintenance throughout lifespan.

From the data of proteomic analysis (Figures 5.1-5.4) and based on the data of biochemical and cell biological analyses [19, 20, 139, 155, 159, 184, 193, 210, 211, 214, 218], I inferred an outline of metabolic pathways and processes that were activated (red arrows) or inhibited (green arrows) in cells cultured with exogenous LCA. Arrows next to the names

of metabolites, proteins or processes denote those of them whose concentrations or efficiencies were elevated (red arrows) or reduced (green arrows) in cells cultured with exogenous LCA. Abbreviations: Ac-CoA, acetyl-CoA; D, diauxic growth phase; EE, ethyl esters; ER, endoplasmic reticulum; EtOH, ethanol; ETC, the mitochondrial electron transport chain; FFA, free fatty acids; IMM, inner mitochondrial membrane; LD, lipid droplets; mtDNA, mitochondrial DNA; OMM, outer mitochondrial membrane; PD, post-diauxic growth phase; ST, stationary growth phase; TAG, triacylglycerols; TCA, the tricarboxylic acid cycle in mitochondria. See text for details.

5.5 Conclusions

Using quantitative mass spectrometry in the studies described in this Chapter of my thesis, I demonstrated that LCA alters the age-related dynamics of changes in levels of many mitochondrial proteins, as well as numerous proteins in cellular locations outside of mitochondria. These proteins belong to two regulons, each modulated by a different mitochondrial dysfunction; I call them a partial mitochondrial dysfunction regulon and an oxidative stress regulon. I found that proteins constituting these regulons (1) can be divided into several ″clusters″, each of which denotes a distinct type of partial mitochondrial dysfunction that elicits a different signaling pathway mediated by a discrete set of transcription factors; (2) exhibit three different patterns of the age-related dynamics of changes in their cellular levels; and (3) are encoded by genes whose expression is regulated by the transcription factors Rtg1p/Rtg2p/Rtg3p, Sfp1p, Aft1p, Yap1p, Msn2p/Msn4p, Skn7p and Hog1p, each of which is essential for longevity extension by LCA. My findings suggest that LCA-driven changes in the mitochondrial lipidome alter the mitochondrial proteome and functionality, thereby enabling mitochondria to operate as signaling organelles that orchestrate the establishment of an anti-aging transcriptional program for many longevity-defining nuclear genes. Based on these findings, I proposed a model for how such LCA-driven changes early and late in life of chronologically aging yeast cause a stepwise development of an anti-aging cellular pattern and its maintenance throughout lifespan.

6 Mitophagy delays yeast chronological aging because it maintains a healthy population of functional mitochondria

6.1 Introduction

Mitophagy is a key mechanism of mitochondrial quality and quantity control responsible for the autophagic degradation of aged, dysfunctional, damaged or excessive mitochondria [277, 278]. Mitophagy in mammalian cells is known to be indispensable for several vital biological processes underlying organismal aging, development and differentiation, including (1) selective degradation of depolarized mitochondria in dopaminergic neurons in the substantia nigra, a PINK1/Parkin-dependent process impaired in autosomal recessive forms of Parkinson's disease; (2) massive elimination of mitochondria driven by Nix, a protein in the outer mitochondrial membrane, during reticulocyte-to-erythrocyte maturation; and (3) selective clearance of surplus mitochondria during white adipose tissue differentiation in an Atg5/Atg7-dependent manner [278 – 281]. In contrast, the physiological roles of mitophagy in yeast remain unknown. To examine the importance of mitophagy in yeast chronological aging, I investigated how the single-gene-deletion mutation *atg32Δ*, eliminating a mitochondrial receptor for selective autophagic removal of mitochondria [213, 278] impacts the chronological lifespan of yeast cultured under CR conditions. I also evaluated how the *atg32Δ*-dependent mutational block of mitophagy influences the efficiency with which LCA extends longevity of chronologically aging yeast. In addition, I examined how the *atg32Δ* mutation influences mitochondrial morphology and function in yeast cells cultured with or without LCA.

6.2 Materials and methods

6.2.1 Strains and media

The wild-type strain *Saccharomyces cerevisiae* BY4742 (*MATα his3Δ1 leu2Δ0 lys2Δ0 ura3Δ0*) and mutant strains *atg32Δ* (*MATα his3Δ1 leu2Δ0 lys2Δ0 ura3Δ0 atg32Δ::kanMX4*) and *atg36Δ* (*MATα his3Δ1 leu2Δ0 lys2Δ0 ura3Δ0 atg36Δ::kanMX4*) were used in this study. The composition of YEPD (0.2% glucose) medium was as follows: 1% yeast extract, 2% peptone, 0.2% glucose. Cells were cultured at 30°C with rotational shaking at 200 rpm in Erlenmeyer flasks at a ″flask volume/medium volume″ ratio of 5:1.

6.2.2 A plating assay for the analysis of chronological lifespan

Cells were grown in YEPD (0.2% glucose) medium at 30^{o}C with rotational shaking at 200 rpm in Erlenmeyer flasks at a flask volume/medium volume ratio of 5:1. A sample of cells was removed from each culture at various time points. A fraction of the cell sample was diluted in order to determine the total number of cells per ml of culture using a hemacytometer. 10 µl of serial dilutions (1:10 to 1:10^{3}) of cells were applied to the hemacytometer, where each large square is calibrated to hold 0.1 µl. The number of cells in 4 large squares was then counted and an average was taken in order to ensure greater accuracy. The concentration of cells was calculated as follows: number of cells per large square x dilution factor x 10 x 1,000 = total number of cells per ml of culture. A second fraction of the cell sample was diluted and serial dilutions (1:10^{2} to 1:10^{5}) of cells were plated onto YEPD (2% glucose) plates in triplicate in order to count the number of viable cells per ml of each culture. 100 µl of diluted culture was plated onto each plate. After a 48-h incubation at 30^{o}C, the number of colonies per plate was counted. The number of colony forming units (CFU) equals to the number of viable cells in a sample. Therefore, the number of viable cells was calculated as follows: number of colonies x dilution factor x 10 = number of viable cells per ml. For each culture assayed, % viability of the cells was calculated as follows: number of viable cells per ml / total number of cells per ml x 100%. The % viability of cells in mid-logarithmic phase was set at 100% viability for that particular culture. The life span curves for wild-type and some of the mutant strains were also validated using a LIVE/DEAD yeast viability kit (Invitrogen) following the manufacturer's instructions for stationary-phase cultures.

6.2.3 Pharmacological manipulation of chronological lifespan

Chronological lifespan analysis was performed as described above in this section. The lithocholic (LCA) [#L6250] bile acid was from Sigma. The stock solution of LCA in DMSO was made on the day of adding this compound to cell cultures. LCA was added to growth medium at the final concentration of 50 µM immediately following cell inoculation into the medium. The final concentration of DMSO in yeast cultures supplemented with LCA (and in the corresponding control cultures supplemented with drug vehicle) was 1% (v/v).

6.2.4 Monitoring the formation of ROS

Wild-type and mutant cells grown in YEPD (0.2% glucose) were tested microscopically for the production of ROS by incubation with dihydrorhodamine 123 (DHR). In the cell, this nonfluorescent compound can be oxidized to the fluorescent chromophore rhodamine 123 by ROS. Cells were also probed with a fluorescent counterstain Calcofluor White M2R (CW), which stains the yeast cell walls fluorescent blue. CW was added to each sample in order to label all cells for their proper visualization. DHR was stored in the dark at –20^{o}C as 50 µl aliquots of a 1 mg/ml solution in ethanol. CW was stored in the dark at –20^{o}C as the 5 mM stock solution in anhydrous DMSO (dimethylsulfoxide).

The concurrent staining of cells with DHR and CW was carried out as follows. The required amounts of the 50 µl DHR aliquots (1 mg/ml) and of the 5 mM stock solution of CW were taken out of the freezer and warmed to room temperature. The solutions of DHR and CW were then centrifuged at 21,000 x g for 5 min in order to clear them of any aggregates of fluorophores. For cell cultures with a titre of ~ 10^7 cells/ml, 100 µl was taken out of the culture to be treated. If the cell titre was lower, proportionally larger volumes were used. 6 µl of the 1 mg/ml DHR and 1 µl of the 5 mM CW solutions were added to each 100 µl aliquot of culture. After a 2-h incubation in the dark at room temperature, the samples were centrifuged at 21,000 x g for 5 min. Pellets were resuspended in 10 µl of PBS buffer (20 mM KH_2PO_4/KOH, pH 7.5, and 150 mM NaCl). Each sample was then supplemented with 5 µl of mounting medium, added to a microscope slide, covered with a coverslip, and sealed using nail polish. Once the slides were prepared, they were visualized under the Zeiss Axioplan fluorescence microscope mounted with a SPOT Insight 2 megapixel color mosaic digital camera. Several pictures of the cells on each slide were taken, with two pictures taken of each frame. One of the two pictures was of the cells seen through a rhodamine filter in order to detect cells dyed with DHR. The second picture was of the cells seen through a DAPI filter in order to visualize CW, and therefore all the cells present in the frame.

For evaluating the percentage of DHR-positive cells, the UTHSCSA Image Tool (Version 3.0) software was used to calculate both the total number of cells and the number of stained cells. Fluorescence of individual DHR-positive cells in arbitrary units was determined by using the UTHSCSA Image Tool software (Version 3.0). In each of 3-5 independent experiments, the value of median fluorescence was calculated by analyzing at least 800-1000 cells that were

collected at each time point. The median fluorescence values were plotted as a function of the number of days cells were cultured.

6.2.5 Monitoring the mitochondrial membrane potential (ΔΨ)

Rhodamine 123 (R123) (Invitrogen) staining for monitoring the mitochondrial membrane potential (ΔΨ) was performed according to established procedure (Invitrogen manual for the Yeast Mitochondrial Stain Sampler Kit). Images were collected with a Zeiss Axioplan fluorescence microscope (Zeiss) mounted with a SPOT Insight 2 megapixel color mosaic digital camera (Spot Diagnostic Instruments). For evaluating the percentage of R123-positive cells, the UTHSCSA Image Tool (Version 3.0) software was used to calculate both the total number of cells and the number of stained cells. Fluorescence of individual R123-positive cells in arbitrary units was determined by using the UTHSCSA Image Tool software (Version 3.0). In each of 3-6 independent experiments, the value of median fluorescence was calculated by analyzing at least 800-1000 cells that were collected at each time point. The median fluorescence values were plotted as a function of the number of days cells were cultured.

6.2.6 Immunofluorescence microscopy

Cell cultures were fixed in 3.7% formaldehyde for 45 min at room temperature. The cells were washed in solution B (100 mM KH_2PO_4/KOH pH 7.5, 1.2 M sorbitol), treated with Zymolyase 100T (MP Biomedicals, 1 μg Zymolyase 100T/1 mg cells) for 30 min at 30^{o}C and then processed as previously described (Pringle *et al*., 1991). Monoclonal antibody raised against porin (Invitrogen, 0.25 μg/μl in TBSB buffer [20 mM Tris/HCl pH 7.5, 150 mM NaCl, 1 mg/ml BSA]) was used as a primary antibody. Alexa Fluor 568 goat anti-mouse IgG (Invitrogen, 2 μg/μl in TBSB buffer) was used as a secondary antibody. The labeled samples were mounted in mounting solution (16.7 mM Tris/HCl pH 9.0, 1.7 mg/ml p-phenylenediamine, 83% glycerol). Images were collected with a Zeiss Axioplan fluorescence microscope (Zeiss) mounted with a SPOT Insight 2 megapixel color mosaic digital camera (Spot Diagnostic Instruments).

6.2.7 Oxygen consumption assay

The rate of oxygen consumption by yeast cells recovered at various time points was measured continuously in a 2-ml stirred chamber using a custom-designed biological oxygen

monitor (Science Technical Center of Concordia University) equipped with a Clark-type oxygen electrode. 1 ml of YEPD medium supplemented with 0.2% glucose was added to the electrode for approximately 5 minutes to obtain a baseline. Cultured cells of a known titre were spun down at 3,000 x g for 5 minutes. The resulting pellet was resuspended in YEPD medium supplemented with 0.2% glucose and then added to the electrode with the medium that was used to obtain a baseline. The resulting slope was used to calculate the rate of oxygen consumption in O_2% x min^{-1} x 10^9 cells.

6.2.8 Measurement of the frequency of nuclear mutations

The frequency of spontaneous point mutations in the *CAN1* gene of nuclear DNA was evaluated by measuring the frequency of mutations that caused resistance to the antibiotic canavanine. A sample of cells was removed from each culture at various time-points. Cells were plated in triplicate onto YNB (0.67% Yeast Nitrogen Base without amino acids [#DF0919153; Fisher Scientific]) plates containing 2% glucose and supplemented with L-canavanine (50 mg/L), histidine, leucine, lysine and uracil (#C1625, #H8125, #L8912, #L5751 and #U0750, respectively; all from Sigma). In addition, serial dilutions of each sample were plated in triplicate onto YP plates containing 2% glucose for measuring the number of viable cells. The number of CFU was counted after 4 d of incubation at 30^{o}C. For each culture, the frequency of mutations that caused resistance to canavanine was calculated as follows: number of CFU per ml on YNB plates containing 2% glucose, L-canavanine (50 mg/L), histidine, leucine, lysine and uracil/number of CFU per ml on YP plates containing 2% glucose.

6.2.9 Measurement of the frequency of mitochondrial mutations affecting mitochondrial components

The frequency of spontaneous single-gene (*mit*$^-$ and *syn*$^-$) and deletion (*rho*$^-$ and *rho*^{o}) mutations in mtDNA affecting essential mitochondrial components was evaluated by measuring the fraction of respiratory-competent (*rho*$^+$) yeast cells remaining in their aging population. *rho*$^+$ cells maintained intact their mtDNA and their nuclear genes encoding essential mitochondrial components. Therefore, *rho*$^+$ cells were able to grow on glycerol, a non-fermentable carbon source. In contrast, mutant cells deficient in mitochondrial respiration were unable to grow on glycerol. These mutant cells carried mutations in mtDNA (including single-gene *mit*$^-$ and *syn*$^-$

mutations or large deletions *rho*$^-$) or completely lacked this DNA (*rho*^{o} mutants). Serial dilutions of cell samples removed from different phases of growth were plated in triplicate onto YP plates containing either 2% glucose or 3% glycerol (#BP229-4; Fisher Scientific) as carbon source. Plates were incubated at 30^{o}C. The number of CFU on YP plates containing 2% glucose was counted after 2 d of incubation, whereas the number of CFU on YP plates containing 3% glycerol was counted after 6 d of incubation. For each culture, the percentage of respiratory-deficient (*mit*$^-$, *syn*$^-$, *rho*$^-$, *rho*^{o} and *pet*$^-$) cells was calculated as follows: 100 – [(number of CFU per ml on YP plates containing 3% glycerol/number of CFU per ml on YP plates containing 2% glucose)] × 100.

The frequency of spontaneous point mutations in the *rib2* and *rib3* loci of mtDNA was evaluated by measuring the frequency of mtDNA mutations that caused resistance to the antibiotic erythromycin. These mutations impair only mtDNA. A sample of cells was removed from each culture at various time-points. Cells were plated in triplicate onto YP plates containing 3% glycerol and erythromycin (1 mg/ml) [#227330050; Acros Organics]. In addition, serial dilutions of each sample were plated in triplicate onto YP plates containing 3% glycerol as carbon source for measuring the number of respiratory-competent (*rho*$^+$) cells. The number of CFU was counted after 6 d of incubation at 30^{o}C. For each culture, the frequency of mutations that caused resistance to erythromycin was calculated as follows: number of CFU per ml on YP plates containing 3% glycerol and erythromycin/number of CFU per ml on YP plates containing 3% glycerol.

6.2.10 Isolation of crude mitochondrial fraction from yeast cells

6.2.10.1 Reagents

1. Dithiothreitol (DTT) buffer [100 mM Tris-H2SO4, 10 mM dithiothreitol]
2. Zymolyase 100T from *Arthrobacter luteus* (MP Biomedicals)
3. Zymolyase buffer [1.2 M sorbitol, 20 mM potassium phosphate]
4. Homogenization buffer [0.6 M sorbitol, 10 mM Tris-HCl (pH 7.4), 1 mM EDTA, 0.2% (w/v) BSA]
5. SEM buffer [250 mM sucrose, 1 mM EDTA, 10 mM Mops (pH 7.2)]

6.2.10.2 Procedure

Cell cultures were combined in pre-weighed centrifuge bottles and cells were pelleted at 3,000 × g for 5 min at room temperature using a Beckman JA-10 rotor. The cells were washed twice with distilled water, followed by the determination of their wet weight. The cell pellets were resuspended in 2 ml/g DTT buffer and incubated on a shaker at 80 rpm for 20 min at 30ºC. The cells were pelleted as per initial centrifugation, washed in 7 ml/g Zymolyase buffer without Zymolyase and pelleted once more. The cells were incubated on a shaker at 80 rpm for 45 min at 30ºC with 1 mg/g (wet weight) of Zymolyase-100T in 7 ml/g Zymolyase buffer. Zymolyase was used because of its well-known strong lytic activity required to digest yeast cell wall. The spheroplasts obtained were then spun down at 2,200 × g for 8 min at 4ºC. All subsequent steps were carried out on ice or at 4°C with the use of cut pipette tips to avoid breaking organelles. The spheroplasts were resuspended in 6.5 ml/g ice-cold homogenization buffer and washed by centrifugation at 2,200 × g for 8 min at 4ºC. The spheroplasts were then mechanically homogenized with 15 strokes in 6.5 ml/g ice-cold homogenization buffer to disrupt yeast plasma membrane for releasing organelles and cytoplasm. Following the homogenization, the cell debris was pelleted by centrifuging at 1,500 × g for 5 min at 4ºC using a Beckman JA-17 rotor. The resulting lysate supernatant was subjected to centrifugation twice at 3000 × g for 5 min at 4ºC to pellet the nuclei and 12,000 × g for 15 min at 4ºC. The newly obtained pellet contains mostly mitochondria, but also the endoplasmic reticulum (ER), Golgi, peroxisomes, lysosomes and vacuoles, whereas the supernatant contains the cytosol, microsomes from the ER and vacuoles. The pellet was resuspended in 6.5 ml/g in ice-cold homogenizing buffer, spun down for 5 min at 3,000 × g at 4ºC to obtain a supernatant containing mitochondria, which was then subjected to a spin at 12, 000 × g for 15 min at 4ºC. The resulting pellet was resuspended in 3 ml of SEM to be overlaid onto a sucrose gradient.

6.2.11 Purification of S. cerevisiae mitochondria devoid of microsomal and cytosolic contaminations

6.2.11.1 Reagents

1. SEM buffer [250 mM sucrose, 1 mM EDTA, 10 mM Mops (pH 7.2)]
2. EM buffer [10 mM Mops (pH 7.2), 1 mM EDTA]

6.2.11.2 Procedure

In order to purify yeast mitochondria from the crude mitochondrial fraction, an equilibrium density-gradient centrifugation was performed. Yeast mitochondria have a density of 1.18 g/cm^3 whereas 10% and 50% sucrose respectively have a density of 1.10 g/cm^3 and 1.30 g/cm^3. To prepare a sucrose density gradient for the purification of mitochondria, 1.5 ml of 60% sucrose in EM buffer was overlaid with 4 ml of 32%, 1.5 ml of 23% and 1.5 ml of 15% sucrose in EM buffer, followed by 3 ml of the crude mitochondrial suspension. The sucrose density gradient containing the mitochondrial suspension was subjected to centrifugation in a Beckman SW41 Ti swinging-bucket rotor at 134,000 × g for 60 min at 4ºC. The mitochondrial band, which was easily distinguishable, appeared at the interface between 60% and 32% sucrose. Fractions of 1 ml were recovered using a cut pipette tip and placed in 1.5 ml Eppendorf tubes and frozen at -80ºC until use. In order to quickly freeze the mitochondrial fractions, the fractions were immersed, with the aid of long tweezers, in a beaker of isopropyl alcohol kept in the -80ºC freezer.

6.2.12 Blue-native gel electrophoresis (BN-PAGE)

6.2.12.1 Equipment

1. Hoefer SE 400 vertical slab gel electrophoresis unit
2. Bio Rad Power Pac 3000 Power supply

6.2.12.2 Reagents

1. 4% acrylamide running gel [1.5 ml AB (acrylamide/bis-acrylamide)-3 mix, 6 ml gel buffer 3×, 10.4 ml distilled water, 100 µl APS, 10 µl TEMED]
2. 13% acrylamide running gel
3. 3.5% acrylamide sample gel
4. Solubilization buffer A [50 mM sodium chloride, 50 mM imidazole/HCl, 2 mM 6-aminohexanoic acid, 1 mM EDTA, pH 7.0]
5. Coomassie blue G-250 dye stock [5% wt/vol in 500 mM 6-aminohexanoic acid]
6. Cathode buffer B [50 mM Tricine, 7.5 mM imidazole, 0.02% Coomassie blue G-250, pH 7.0]

7. Cathode buffer B/10 [50 mM Tricine, 7.5 mM imidazole, 0.002% Coomassie blue G-250, pH 7.0]
8. Anode buffer [25 mM imidazole, pH 7.0]

6.2.12.3 Procedure

Mitochondria protein aliquots of 400 μg were pelleted by centrifugation at 50,000 × g for 30 min using a Beckman MLS-50 rotor. The mitochondria pellet was resuspended in 40 μl of solubilization buffer A and the mitochondria membranes were homogenized by twirling a tiny spatula. The detergent digitonin at 20% (3.0 g/g; *i.e.*, 6 μl) was added to the homogenate, which was incubated for 10 min at room temperature. The sample was subsequently centrifuged at 20,000 × g for 20 min at room temperature. To the resulting supernatant, 5 μl of 5% Coomassie blue G-250 dye in 50% glycerol was added at an 8 g/g detergent/dye ratio (*i.e.*, 3 μl). The sample containing solubilized mitochondrial membrane was loaded to a 0.16 × 0.5 cm well of a gradient separation gel with dimensions 1.5 × 14 × 15 cm composed of 4% and 13% acrylamide mixture with a sample gel of 3.5% acrylamide. Urease at 1mg/ml was also loaded on an adjacent well and used as a molecular marker (10 μl urease, 10 μl buffer A, 2.4 μl 50 % glycerol, 1.6 μl 5% Coomassie blue G-250). BN-PAGE was performed at 4°C under the following conditions: 300 ml of Cathode buffer B in the upper chamber and 300 ml of Anode buffer in the lower chamber were used and the power supply set at constant 100 V, 15 mA, 400 W until the sample entered the gradient gel. Electrophoresis was then continued at 500 V and 15 mA until the blue running front moved about a third of the total running distance. At this point, Cathode Buffer B was replaced with 300 ml of Cathode buffer B/10 for better detection of faint protein bands and electrophoresis was continued for a total of 4 h or until the blue running front was 1 cm from the bottom of the gel. Once electrophoresis was completed the blue native gel stained with Coomassie blue G-250 was photographed, documented and stored at 4°C.

6.2.13 Tricine-SDS-PAGE

6.2.13.1 Equipment

1. Hoefer SE 400 vertical slab gel electrophoresis unit
2. Bio Rad Power Pac 3000 Power supply

6.2.13.2 Reagents

1. 10%T, 3%C Tricine-SDS running gel
2. 10% acrylamide native stacking gel
3. Anode buffer 10× [1.0 M Tris, 0.225 M HCl, pH 8.9]
4. Cathode buffer 10× [1.0 M Tris, 1.0 M Tricine, 1% SDS, pH 8.25]
5. Precision Plus Protein™ Unstained standards 10 - 250 kD (Bio-Rad)

6.2.13.3 Procedure

A 0.5-cm gel strip was cut from the 1st dimension (1D) BN-PAGE gel and placed on a glass plate with the top of the strip to the left and the bottom of the strip to the right. The strip was soaked with 5 ml of a solution containing 1% SDS and 1% mercaptoethanol for 2 h at room temperature. Following the incubation, the strip was thoroughly rinsed with water and squeezed in between 1.5-mm spacers and 18 × 16 cm glass plates. A 30-ml separating gel mixture composed of 10%T, 3%C Tricine-SDS was poured in between the glass plates leaving a gap of 0.5 cm from the native gel strip. After polymerization, a 0.5-cm spacer was inserted between the plates, and placed to the right of the gel to create a well to load protein markers. In order to fill the 0.5-cm gap between the running gel and the native strip, as well as the space between the native gel and the spacers, 5 ml of a 10% acrylamide native gel mixture was used, and Unstained protein molecular markers (Bio-Rad) were loaded to the far right of the gel for reference. Electrophoresis was performed at constant 200 V, 50 mA, 400 W for 3 h at room temperature.

6.2.14 Silver stain after 1D-BN-PAGE followed by 2D-Tricine-SDS-PAGE

Protein bands are then visualized by silver staining using the Silver Stain Plus Kit from Bio-Rad.

6.2.14.1 Reagents

1. Fixative solution [200 ml methanol, 40 ml acetic acid, 40 ml Fixative Enhancer solution, 120 ml distilled water]
2. Staining solution [35 ml distilled water, 5 ml Silver complex solution, 5 ml Reduction Moderator solution, 5 ml Image Development solution, 50 ml Development Accelerator solution]

3. Stop solution [5% acetic acid]

6.2.14.2 Procedure

Once electrophoresis was completed, the gel was incubated in 400 ml of 50% methanol on a shaker at 55 rpm for 2 h. The gel was then incubated in 200 ml of the Fixative solution for 20 min and washed twice with 200 ml of distilled water for 10 min. The gel was then immersed in 100 ml of the Staining Solution composed of Silver complex, Reduction Moderator, Image Development and Development Accelerator solutions. Once the desired staining intensity was reached, development was immediately stopped by incubating the silver stained gel in 400 ml of 5% acetic acid for 15 min, which was followed by a rinse with 400 ml of distilled water for 5 min. The gel was then photographed, documented and stored at 4°C in 400 ml of distilled water.

6.2.15 In-gel digestion of proteins separated by 2D-Tricine-SDS-PAGE

6.2.15.1 Reagents

1. 30 mM Potassium Ferricyanide
2. 100 mM Sodium Thiosulfate
3. 100mM Ammonium Bicarbonate (ABC)
4. 10 mM Dithiothreitol (DTT) [in 5ml of 100mM Ammonium Bicarbonate (ABC)]
5. 55 mM Iodoacetamide (IAA) [in 5ml of 100mM Ammonium Bicarbonate (ABC)]
6. Trypsin, Proteomics Grade (Sigma Aldrich)

6.2.15.2 Procedure

Once the individual mitochondrial proteins were separated, each band on the 1D BN-2D Tricine-SDS gel was cut out with a razor blade and the gel piece was placed in 0.5-ml siliconized Eppendorf tubes. The bands were washed with distilled water and destained with 50 µl of a 1:1 mixture of 20 mM potassium ferricyanide and 100 mM sodium thiosulfate for 20 min in the dark with occasional vortexing. The destaining solution was removed and the bands were washed twice with distilled water. The bands were then incubated in 50 µl of acetonitrile (ACN) for 5 min at 37°C, after which ACN was removed and the bands were dried at 37°C. Next, the destained bands were incubated in 50 µl of 10 mM dithiothreitol for 30 min at 37°C to reduce thiol groups in peptides. DTT was discarded and the bands were incubated in 50 µl of 55 mM

iodoacetamide for 20 min at 37°C in the dark to remove the residual DTT. IAA was removed and the bands were incubated in 50 µl of a 1:1 mixture of 100 mM ABC and 50% acetonitrile for 10 min at 37°C. The mixture was discarded and the bands were incubated twice in 50 µl of CAN under the same conditions and dried at 37°C. The trypsin and trypsin buffer were prepared as follows: (1) 1.6 ml of a 1:1 mixture of 100 mM ABC and 10mM $CaCl_2$ were used to resuspend 20 µg of trypsin; and (2) for protein digest, 50 µl of trypsin solution (1 mg/ml) was added to the bands, which were then incubated overnight at 37°C.

6.2.16 Extracting peptides from yeast mitochondrial proteins digested with trypsin

The following day, the samples were spun down and the supernatants containing peptides were transferred to new 0.5-ml siliconized Eppendorf tubes. To extract more peptides, the gel pieces were subjected to several washes and treatments at room temperature; the supernatants were conserved and combined with the first set to extracted peptides. For the first extraction, the bands were initially incubated in 50 µl of 25 mM ABC for 10 min and then in 50 µl of ACN for 10 min. The samples were spun down and the supernatant were added to the first set of extracted peptides. For the second extraction, the bands were incubated in 50 µl of 5% formic acid for 10 min and then in 50 µl of ACN for 10 min. The samples were spun down and the supernatant were combined with the first set of extracted peptides. The gel pieces were no longer used and discarded. To prevent possible oxidation during storage, 12.5 µl of 100 mM DTT was added to each set of peptides. The peptides were completely dried in a Speed-Vac at medium temperature settings (37°C) for 2 h and stored at -20°C until MS analysis.

6.2.17 Sample preparation for MS analysis

Dried peptides were resuspended in 20 µl of 5% ACN. For each recovered protein band, an aliquot of 10 µl of dried peptides in 5% ACN was diluted 2-fold in Nano pure water for MS analysis. Samples can be stored at -20°C until being subjected to MS analysis.

6.2.18 MS analysis

Individual proteins composing each band were then identified by reverse phase high performance liquid chromatography coupled to mass spectrometry (RP-HPLC/MS) using an

LTQ Orbitrap. 3-µl aliquots of peptides were separated in ACN gradient using a 100-µM capillary column packed with C18 mobile phase.

6.2.19 Analysis using the Thermo Proteome Discoverer application and SEQUEST

Once acquiring time was completed using the LTQ Orbitrap, the raw mass spectrometry data file obtained by Xcalibur were analyzed using the Thermo Scientific Xcalibur Proteome Discoverer application (version 1.3) hereafter referred to as the Proteome Discoverer. The Proteome Discoverer was used to identify individual protein components of the isolated mitochondrial respiratory complexes and supercomplexes by comparing the raw data of mass spectra of digested fragments to the mass spectra of peptides within the Uniprot FASTA database. The analysis by the Proteome Discoverer coupled to the FASTA database was enabled by using the peak-finding search engine SEQUEST. The SEQUEST engine processes MS data using a peak-finding algorithm to search the raw data for generating a peak probability list with relative protein abundances.

6.2.19.1 SEQUEST search wizard within the Proteome Discoverer application

6.2.19.1.1 Raw file and Scan Range Selection Parameters

The raw file was selected and the Base peak ion chromatogram appeared to reveal: (1) the "Intensity (counts)" corresponding to the intensity of the largest peak in the spectrum; and (2) the "Time (min)" showing the retention time (RT). The following algorithm and settings were used:

Lower RT Limit (min): The beginning of the RT of the scan range of interest: 10 min.

Upper RT Limit (min): The end of the retention time of the scan range of interest: 18 min.

Scan Extraction Parameters

First mass: The mass of the first precursor ion in the range of ion fragments to search for in the database: 350 Daltons (Da).

Last mass: The mass of the last precursor ion in the range of ion fragments to search for in the database: 5000 Daltons (Da).

Activation type: The fragmentation method to use for activating the scan: Collision Induced Dissociation (CID).

Unrecognized charge replacement: Specifies the charge number of the precursor ions: Automatic (Default), assigns a charge number of +2 and +3 to the spectrum.

Intensity threshold: Specifies the intensity threshold below which ions are filtered out. The default value of 0.0 was used.

Minimum ion count: The minimum ion count corresponds to the minimum number of ions that must be present in an MS/MS spectrum for it to be included in a search. The default value of 1 was used.

S/N threshold: The signal-to-noise threshold is the intensity of the signal to the intensity of the background noise. The use of this threshold filters out low-intensity ions that function as a noise. The value of 1.5 was used.

Database: Uniprot_sprot FASTA

Enzyme: Trypsin

Missed Cleavages: The maximum number of internal cleavage sites per peptide fragment that is acceptable for an enzyme to miss during proteolytic digest. The default value of 2 was used.

Precursor mass tolerance: The precursor mass tolerance value used for finding peptide candidates. The possible range of values is 0.01 to 5000 ppm. The default value of 10 ppm was used.

Fragment mass tolerance: The default mass tolerance value of 0.8 Da was used for matching fragment peaks. The possible range of values was 0.0001 to 2.0 Da.

Ions series calculated: Specifies the ion factors for a, b, c, x, y, and z ions for the experiment type. The possible range is 0 through 1.0 for all ion factors. The ion factors used are b ions: 1 and y ions :1.

Search against decoy database: Specifies if the application uses a decoy database in the search; the "yes" was used.

Target FDR (strict): Specifies a strict target false discovery rate (FDR) for peptide matches with high confidence. The possible value range of 0.0 to 1.0 was used. The default value of 0.01 (1% FDR) was used.

Target FDR (relaxed): Specifies a relaxed target false discovery rate (FDR) for peptide matches with moderate confidence. The possible value range from 0.0 to 1.0 was used. The default value of 0.05 (5% FDR) was used.

6.2.19.1.2 Identification of yeast mitochondria complexes and supercomplexes using the Thermo Proteome Search Results Report

Protein Results Parameters

The protein page displays all the proteins and their corresponding peptides found in the sample during the database search. For each protein, the report shows the following results:

Accession: The unique identifier was assigned to the protein by the Uniprot FASTA database.

Description: The name and description of the protein of the identifier appeared in the corresponding Accession column.

Score: The SEQUEST protein score is the sum of all peptide XCorr values above the specified score threshold. The score threshold was calculated as "0.8 + *peptide charge* * *peptide relevance factor*", where *peptide relevance factor* has a default value of 0.4. For each spectrum, only the highest-scoring match was used. For each spectrum and sequence, the Proteome Discoverer application uses only the highest scored peptide.

Coverage: Represents the percentage of the protein sequence covered by the identified peptides.

 # *Proteins:* Represents the number of identified proteins in the protein group of a master protein. When the Protein Grouping setting is disabled, the #Proteins is always equal to 1.

 # *Unique Peptides:* Represents the number of peptide sequences unique to a protein.

 # *Peptides:* Represents the number of different peptide sequences identified in the protein.

 # *PSMs:* The peptide spectrum matches (PSMs) value corresponds to the total number of identified peptide sequences for the protein, including those that have been identified redundantly.

 # *AAs:* Represents the number of amino acid in the sequence length of the protein.

MW ^{kDa}: Represents the calculated molecular weight of the protein.

Calc. pI: Represents the theoretically calculated isoelectric point, *i.e.* the pH value at which a particular molecule carries no net electrical charge.

Peptides Results Parameters: For each identified peptide, the report shows the following results:

Protein Descriptions: Identifies a protein associated with the peptides. This description is taken from the Uniprot FASTA file.

 # *Proteins:* Represents the total number of proteins in which this peptide can be found.

Probability: Represents the probability score for the peptide.

SpScore (search-dependent): Represents the raw value of the preliminary score of the SEQUEST algorithm.

XCorr (search-dependent): Scores the number of fragment ions that are common to two different peptides with the same precursor mass; calculates the cross-correlation score for all candidate peptides queried from the database.

Δ Score: A measure of the difference between the top two scores for the peptides identified by that spectrum; the Proteome Discoverer application calculates this score as follows: ΔScore = Score(Rank N Peptide) – Score(Rank 1 Peptide)/Score(Rank 1 Peptide).

ΔCn: Represents the normalized score difference between the currently selected PSM and the highest-scoring PSM for that spectrum.

 # Missed Cleavages: Represents the number of cleavage sites in a peptide sequence that trypsin did not cleave, excluding the cases where the presence of proline prevents trypsin from cleaving the peptide bond.

Peptides Matched: Represents the number of peptides included in the precursor mass tolerance window set for the search.

Charge: Represents the charge state of the peptide.

Intensity: Represents the intensity of the precursor ion.

MH+ ^{Da}: Represents the protonated monoisotopic mass of the peptide, in Daltons.

ΔM ^{ppm}: Represents the difference between the theoretical mass of the peptide and the experimental mass of the precursor ion.

RT ^{min}: Represents the retention time when the peptide was observed, in minutes.

Xcalibur is a registered trademark of Thermo Fisher Scientific Inc. in the United States. SEQUEST is a registered trademark of the University of Washington in the United States.

6.2.20 Immunodetection of carbonyl groups in oxidatively damaged cellular proteins

Total cell lysates were made by vortexing the cells in ice-cold TCL buffer (25 mM MOPS/KOH, pH 7.2, 150 mM NaCl, 50 mM DTT, and 1% CHAPS) with glass beads three times for 1 min. Lysates were then centrifuged for 5 min at 21,000 × g at 4^{o}C, and the supernatants of total cell lysates were collected. The carbonyl groups of proteins recovered in total cell lysates were derivatized to 2,4-dinitrophenylhydrazones using the OxyBlot^{TM} Protein

Oxidation Detection Kit (Chemicon), according to the manufacturer's instructions. Briefly, total cellular proteins were denatured by adding 12% SDS to an equal volume of the total cell lysate containing 10 μg of protein. Denatured proteins were incubated with 2,4-dinitrophenylhydrazine for 15 min at room temperature. Proteins were separated by 12.5% SDS-PAGE. Immunoblotting using a Trans-Blot SD semi-dry electrophoretic transfer system (Bio-Rad) was performed as described [230]. The derivatized carbonyl groups were detected with a 2,4-dinitrophenyl-specific antibody (Chemicon) and the Amersham ECL Western Blotting System (GE Healthcare).

6.2.21 Miscellaneous procedures

Protein concentration in samples of purified mitochondria was determined with an RC DC protein assay kit (#500-0122; Bio-Rad) following the manufacturer's instructions.

SDS-PAGE and immunoblotting using a Trans-Blot SD semi-dry electrophoretic transfer system (#170-3940; Bio-Rad) were performed as previously described [230]. Blots were decorated with monoclonal antibodies raised against porin (#459500; Invitrogen) or polyclonal antisera raised against cytochrome *c* (kind gift of Dr. Roland Lill, Philipps Universität Marburg), cytochrome *c*1, subunit II of cytochrome *c* oxidase or alpha and beta subunits of the mitochondrial F1ATPase (all three antisera were kind gifts of Dr. Carla Koehler, University of California, Los Angeles). Antigen-antibody complexes were detected by enhanced chemiluminescence using an Amersham ECL Plus Western Blotting Detection Reagents (#RPN2132; GE Healthcare).

State III and IV respiratory rates measurement using NADH as a respiratory substrate of external NADH:quinone oxidoreductase or succinate as a respiratory substrate of complex II, as well as uncoupled respiratory rates (UC) measurement in the presence of the uncoupler CCCP and a respiratory substrate (NADH or succinate) were performed by polarography of purified mitochondria according to established procedures [282]. The ratios of state III rate/state IV rate (i.e., RCR), state III rate/UC rate and ADP/O (i.e., the stoichiometry of coupled oxidation and phosphorylation) were calculated as previously described [283]. Enzymatic activities of NADH:decylubiquinone oxidoreductase (NQR; an impaired in proton pumping across the IMM analog of the respiratory complex I in higher eukaryotes) [284], succinate:decylubiquinone-2,6-dichlorophenolindophenol oxidoreductase (the respiratory complex II) [285], ubiquinol:cytochrome *c* oxidoreductase (the respiratory complex III) [286], cytochrome *c* oxidase (the respiratory complex

IV) [287] and F_1F_0-ATP synthase (the respiratory complex V) [288] were determined by established methods.

Electron microscopy followed by morphometric analyses of the resulting images [289] were performed according to established procedures. Preparation of cellular extracts and microanalytic biochemical assays for measuring ATP were performed as previously described [233].

6.2.22 Statistical analysis

Statistical analysis was performed using Microsoft Excel's (2010) Analysis ToolPack-VBA. All data are presented as mean ± SEM. The *p* values were calculated using an unpaired two-tailed *t* test.

6.3 Results

6.3.1 Mitophagy is a longevity assurance process

As a first step towards addressing a role of selective autophagic mitochondrial removal in sustaining essential biological processes in yeast, I evaluated the importance of mitophagy in longevity assurance. I compared the chronological lifespan (CLS) of wild-type (WT) strain to that of the single-gene-deletion mutant strain *atg32Δ*, which is impaired only in the mitophagic pathway of selective autophagy but not in other pathways of selective or non-selective autophagy [213, 278]. Both yeast strains were cultured in the nutrient-rich YP (1% yeast extract and 2% peptone) medium initially containing low (0.2%) concentration of glucose, a fermentable carbon source. Importantly, yeast cells grown under these longevity-extending caloric restriction (CR) conditions are not starving [145]. I found that the *atg32Δ* mutation substantially shortens both the mean and maximum CLS of yeast limited in calorie supply (Figure 6.1). Thus, mitophagy is an essential longevity assurance process in chronologically aging yeast grown under CR.

The essential role of mitophagy in regulating yeast longevity under CR conditions is limited to this form of selective autophagy. Indeed, I found that the single-gene-deletion mutation *atg36Δ*, known to impair only the pexophagic pathway of selective autophagy but not mitophagic or any other pathways of selective or non-selective autophagy [290], did not influence the mean or maximum CLS of yeast limited in calorie supply (Figure 6.2).

6.3.2 Mitophagy is required for longevity extension by LCA

We revealed that LCA extends the CLS of yeast grown under CR on 0.2% glucose [155]. To assess a role of selective autophagic mitochondrial removal in longevity extension by LCA, I tested if this bile acid added to growth medium at the time of cell inoculation is able to extend longevity of the mitophagy-deficient *atg32Δ* mutant. As I found, the *atg32Δ* mutation abolishes the ability of LCA to increase both the mean and maximum CLS of yeast limited in calorie supply (Figure 6.1). Hence, mitophagy is required for longevity extension by LCA in chronologically aging yeast grown under CR on 0.2% glucose. Unlike mitophagy, the pexophagic form of selective autophagy is not obligatory for the ability of LCA to extend longevity of chronologically aging yeast under CR conditions. In fact, the exclusive impairment of pexophagy by the single-gene-deletion mutation *atg36Δ* did not compromise the longevity-extending efficacy of LCA in yeast limited in calorie supply (Figure 6.2).

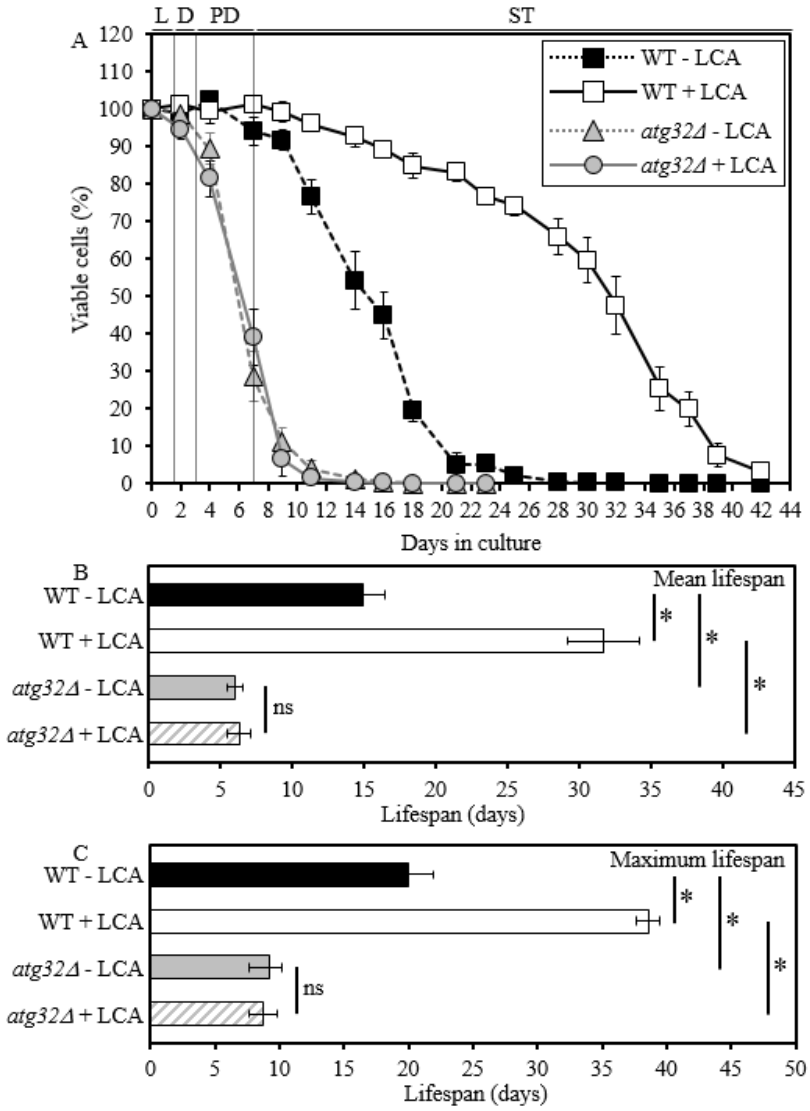

Figure 6.1. Under CR conditions, the *atg32Δ*-dependent mutational block of mitophagy substantially shortens yeast CLS and abolishes the longevity-extending effect of LCA.

WT and *atg32Δ* strains were cultured in the nutrient-rich YP medium initially containing 0.2% glucose in the presence or absence of 50 μM LCA. Effect of the *atg32Δ* mutation and LCA on survival (A) and on the mean (B) and maximum (C) lifespans of chronologically aging yeast grown under CR conditions on 0.2% glucose. Data are presented as means ± SEM (n = 6-8; *$p < 0.01$). Abbreviations: Diauxic (D), logarithmic (L), post-diauxic (PD) or stationary (ST) growth phase.

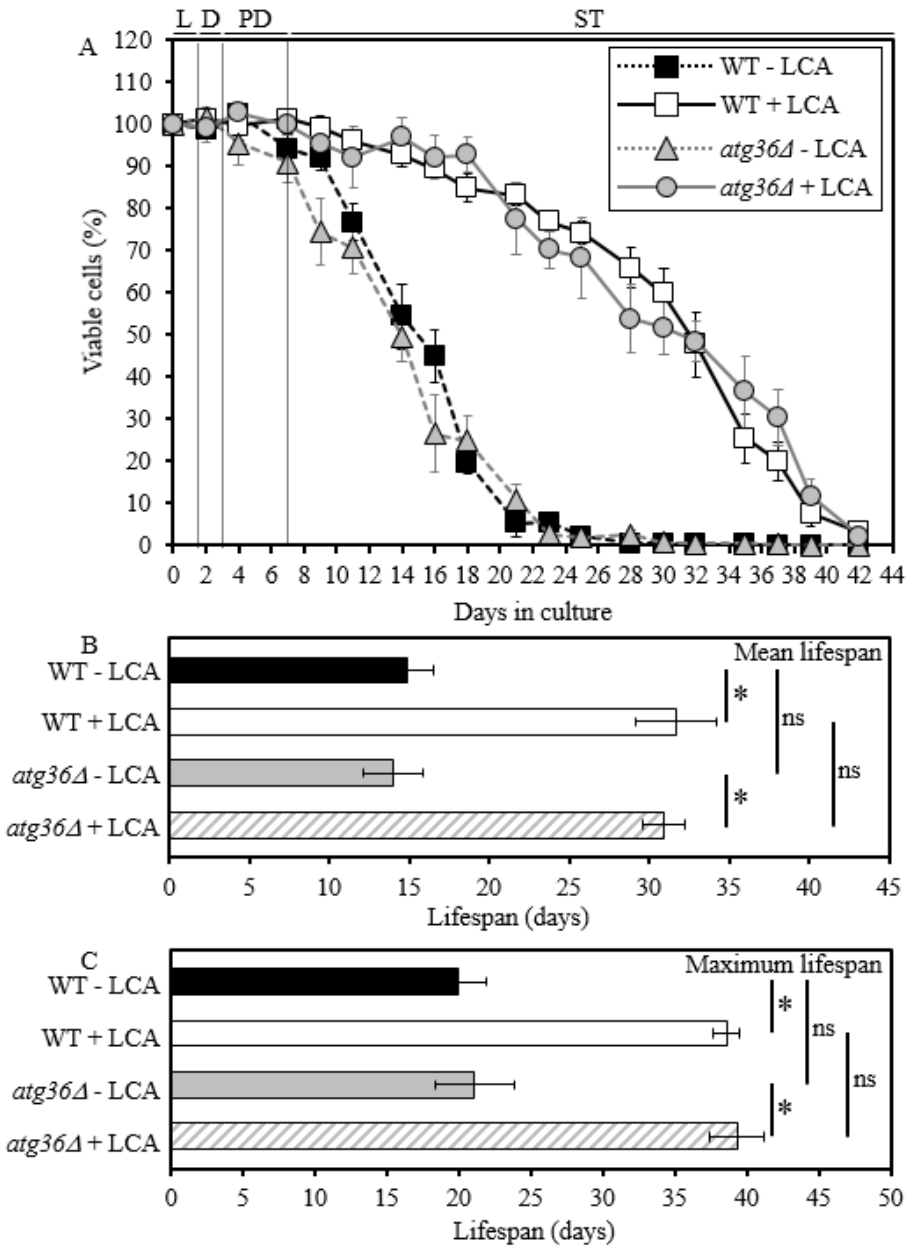

Figure 6.2. Under CR conditions, the *atg36Δ*-dependent mutational block of pexophagy does not alter yeast CLS and does not compromise the longevity-extending efficacy of LCA.

WT and *atg36Δ* strains were cultured in the nutrient-rich YP medium initially containing 0.2% glucose in the presence or absence of 50 μM LCA. Effect of the *atg36Δ* mutation and LCA on survival (A) and on the mean (B) and maximum (C) lifespans of chronologically aging yeast grown under CR conditions on 0.2% glucose. Data are presented as means ± SEM (n = 5-6; *p < 0.01; ns, not significant). Abbreviations: Diauxic (D), logarithmic (L), post-diauxic (PD) or stationary (ST) growth phase.

6.3.3 Macromitophagy defines the size and number of mitochondria, their shape and morphology, and their ability to exist as a network

To provide a mechanistic insight into the demonstrated essential role of mitophagy in defining longevity of chronologically aging yeast under CR conditions, I used electron microscopy (EM) to compare the age-related dynamics of changes in the size, number and morphology of mitochondria in WT cells to that in mitophagy-deficient *atg32Δ* cells. I found that in cells grown under CR on 0.2% glucose and recovered at different periods of CLS, the *atg32Δ* mutation (1) results in accumulation of greatly enlarged mitochondria (Figures 6.3A and 6.3B); (2) substantially increases the number of mitochondria (Figures 6.3A and 6.3C); (3) alters mitochondrial morphology by elevating the proportion of round-shaped mitochondria, especially in cells entered PD growth phase and recovered on day 4 of cell culturing (Figure 6.3A); and (4) reduces the length of mitochondrial cristae and alters their morphological appearance (Figure 6.3A). Furthermore, my indirect immunofluorescence microscopy analysis of cells grown under CR on 0.2% glucose and recovered at different periods of CLS revealed that the *atg32Δ* mutation also causes massive fragmentation of the elaborate mitochondrial network seen in WT cells (Figures 6.3B and 6.3E).

In sum, my microscopical analyses suggest that under CR conditions mitophagy is required to maintain a network of mitochondria, perhaps by selectively eliminating individual mitochondria segregated from this network due to certain changes in the morphology of their cristae. One could envisage that the inability of mitophagy-deficient *atg32Δ* cells to eliminate these morphologically distinct (and possibly dysfunctional) mitochondria following their segregation from the mitochondrial network may result in their progressive accumulation with age, thereby leading to the establishment of a pro-aging cellular pattern and ultimately shortening yeast longevity.

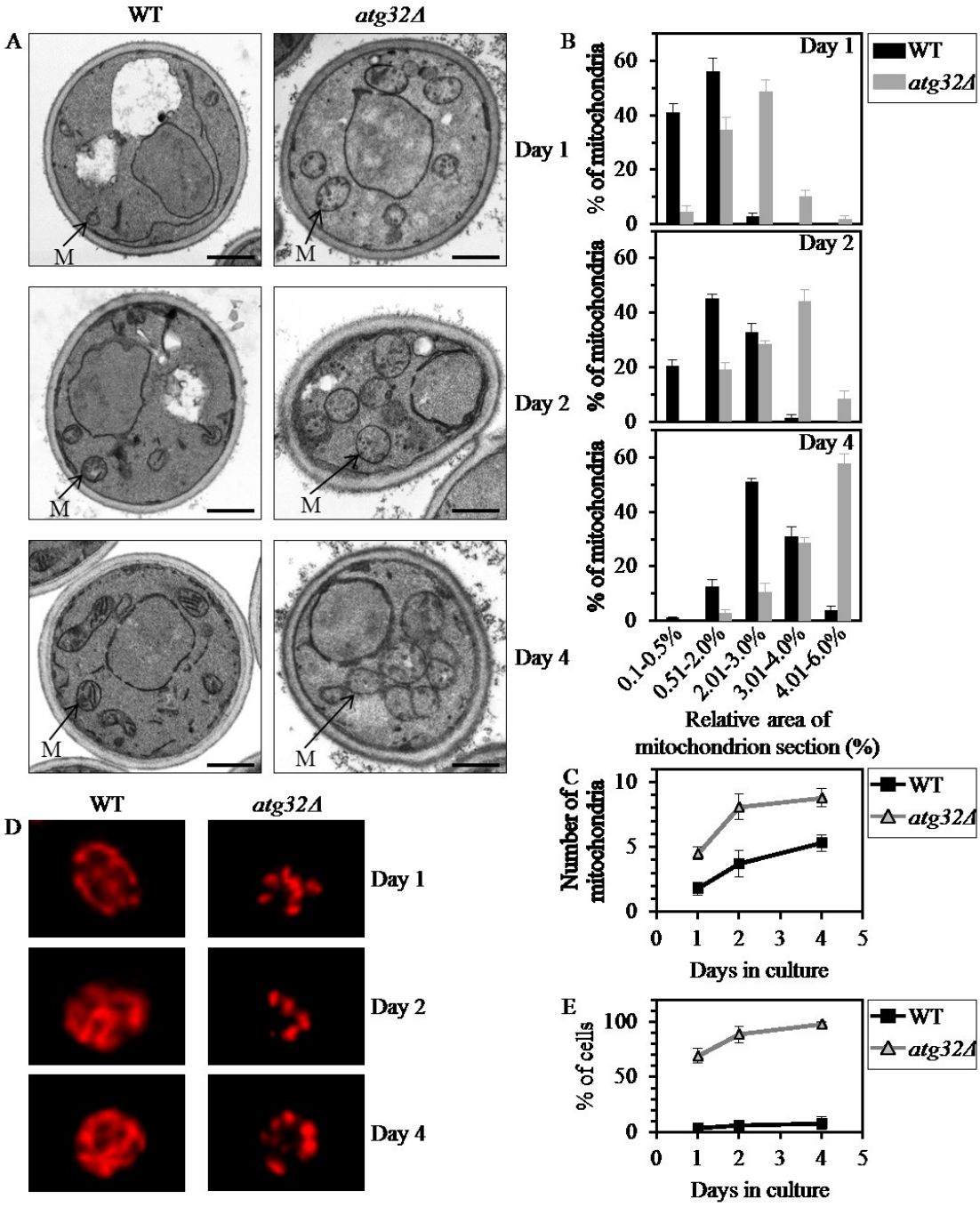

Figure 6.3. Under CR conditions, the *atg32Δ*-dependent mutational block of mitophagy alters the age-related dynamics of changes in mitochondrial size, number, shape, morphology and network appearance.

WT and *atg32Δ* strains were cultured in the nutrient-rich YP medium initially containing 0.2% glucose. (A) Transmission electron micrographs of WT and *atg32Δ* cells recovered on day 1, 2 or 4 of cell culturing. M, mitochondrion. Bar, 1 μm. (B) Percentage of mitochondria in WT and *atg32Δ* cells having the indicated relative area of mitochondrion section. The relative area of mitochondrion section was calculated as (area of mitochondrion section/area of cell section) × 100. Data are presented as means ± SEM (at least 100 cells of each strain were used

for morphometric analysis at each time-point). (C) Numbers of mitochondria in WT and *atg32Δ* cells. The data of morphometric analysis are expressed as the number of mitochondria per μm^3 of cell section ± SEM (at least 100 cells of each strain were used for morphometric analysis at each time-point). (D) Morphology of mitochondria in WT and *atg32Δ* cells recovered on day 1, 2 or 4 of cell culturing. Mitochondria were visualized by indirect immunofluorescence microscopy using monoclonal anti-porin primary antibodies and Alexa Fluor 568-conjugated goat anti-mouse IgG secondary antibodies. (E) The percentage of cells exhibiting fragmented mitochondria was calculated. At least 800 cells of each strain were used for quantitation at each time-point. Data are presented as mean ± SEM (n = 3).

6.3.4 Macromitophagy sustains a healthy population of functional mitochondria

Based on my finding that mitophagy plays an essential role in preserving the mitochondrial network in CR yeast, I hypothesized that this form of selective autophagy is required for sustaining a healthy population of functional mitochondria in chronologically aging cells. To test the validity of my hypothesis, I assessed the age-related dynamics of changes in several vital mitochondrial functions during chronological aging of WT and *atg32Δ* yeast cells. I found that in cells cultured under CR on 0.2% glucose and recovered at different periods of CLS, the *atg32Δ* mutation (1) leads to accumulation of dysfunctional mitochondria exhibiting reduced respiration (Figure 6.4A); (2) causes a build-up of dysfunctional mitochondria having a reduced electrochemical potential across the inner mitochondrial membrane (IMM) (Figure 6.4B); (3) triggers a release of cytochrome *c* from the intermediate space of mitochondria into the cytosol (Figure 6.4C), known to be a hallmark event of mitochondrial outer membrane permeabilization (MOMP) [10]; and (4) reduces the cellular level of ATP (Figure 6.4D), which under CR conditions is produced mainly in mitochondria [189]. All these changes in vital mitochondrial functions were observed in mitophagy-deficient *atg32Δ* cells as early as after 2 days of culturing (Figure 6.4).

These findings suggest that under CR conditions mitophagy is required to sustain a healthy network of functional mitochondria that actively respire, exhibit high electrochemical potential across the IMM, maintain outer mitochondrial membrane impermeability to proteins and efficiently synthesize ATP. Thus, it is conceivable that in chronologically aging yeast limited in calorie supply mitophagy selectively eliminates dysfunctional mitochondria impaired in vital mitochondrial functions that define longevity.

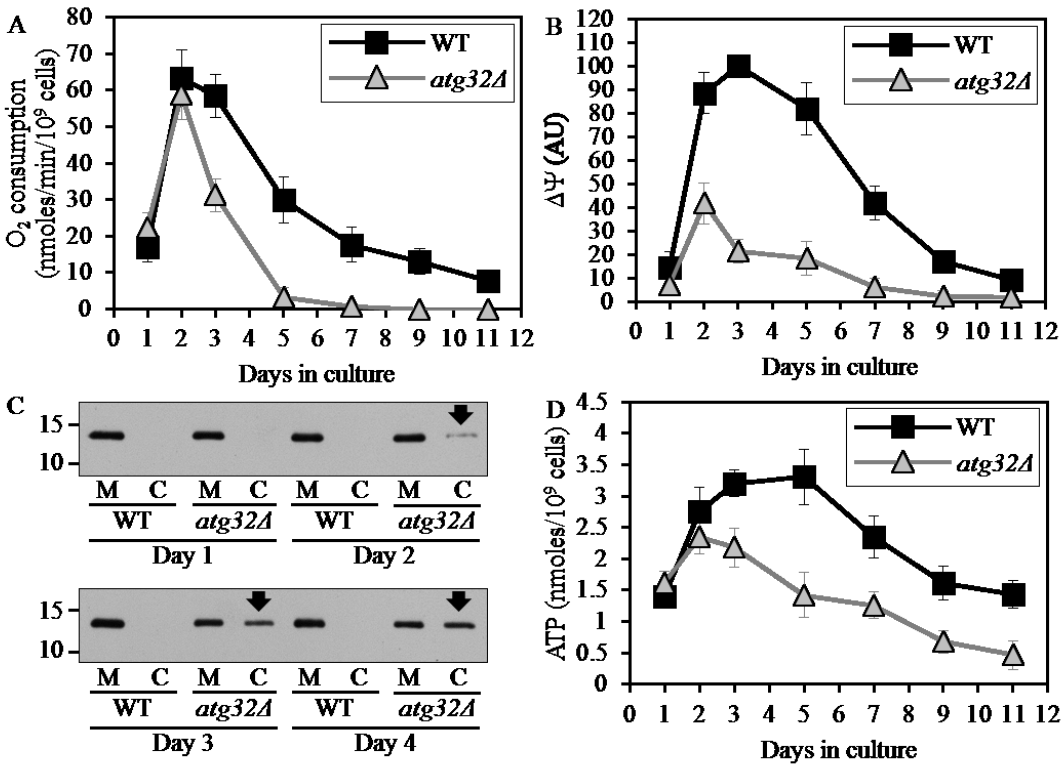

Figure 6.4. Under CR conditions, the *atg32Δ*-dependent mutational block of mitophagy alters the age-related chronology of changes in vital mitochondrial functions.

WT and *atg32Δ* strains were cultured in the nutrient-rich YP medium initially containing 0.2% glucose. Effect of the *atg36Δ* mutation on the rate of oxygen consumption by cells (A), electrochemical potential across the IMM (ΔΨ) (B), level of cytochrome *c* in purified mitochondria (marked as ″M″) and the cytosolic fraction (marked as ″C″) (C), and cellular level of ATP (D). Data in A, B and D are presented as means ± SEM (n = 6-9).

6.3.5 Mitophagy maintains a population of mitochondria whose inner membrane exhibits abundant respiratory and non-respiratory protein supercomplexes of distinct compositions

A body of recent evidence supports the view that, instead of existing as separate units freely moving within the IMM, individual respiratory protein complexes are assembled into supramolecular structures known as respiratory supercomplexes or respirasomes [235, 236]. Some changes in such supramolecular organization of respiratory protein complexes may cause detrimental alterations of the mitochondrial respiratory chain, thereby eliciting certain age-related pathologies [237]. I therefore hypothesized that the observed inability of prematurely aging under CR conditions *atg32Δ* cells to sustain a healthy population of functional mitochondria

(Figure 6.4) may be caused in part by some changes in the abundance and/or composition of certain respiratory protein supercomplexes. To validate this hypothesis, I purified mitochondria from WT and *atg32Δ* cells, used digitonin to solubilize protein complexes from the inner membrane of these mitochondria, and separated the solubilized protein complexes on a linear 4-13% acrylamide gradient gel for first-dimension blue native PAGE (1-D BN-PAGE). This gradient gel is known to resolve protein complexes within the mass range of 100 kDa - 3 MDa [238]. My 1-D BN-PAGE analysis revealed that in cells cultured under CR on 0.2% glucose and recovered on day 4 of culturing, the *atg32Δ* mutation reduces the levels of several protein complexes in the IMM, including complexes 2, 3, 4 and 5 (Figure 6.5A). Because the molecular masses of all these and other protein complexes resolved by 1-D BN-PAGE exceeded 545 kDa, a molecular mass of the largest commercially available urease tetramer marker protein (Figure 6.5A), they represent very large protein supercomplexes assembled from several protein complexes [284]. Noteworthy, my separation of denatured monomeric membrane proteins from purified mitochondria by SDS-PAGE and their subsequent quantitative analysis by immunoblotting revealed that the *atg32Δ* mutation does not cause significant changes to the total levels of the respiratory complexes III, IV or V (Figures 6.5B and 6.5C). Hence, the observed reduction of the levels of protein supercomplexes 2, 3, 4 and 5 in the IMM of *atg32Δ* cells (Figure 6.5A) was not due to a decrease in the total amounts of the respiratory complexes III, IV or V. It is conceivable therefore that in the IMM of *atg32Δ* cells a significant portion of these protein supercomplexes undergo a remodeling caused by their complete or partial dissociation into individual proteins or small protein subcomplexes.

To define the composition of each of the protein supercomplexes recovered by 1-D BN-PAGE (Figure 6.5A), I resolved their individual protein components by second-dimension tricine-SDS-PAGE (2-D SDS-PAGE), visualized these components by silver staining and identified them by mass spectrometry. I found that, in addition to one or more kinds of individual respiratory complexes, many protein supercomplexes in the IMM of WT cells contain one or more proteins that have not been traditionally viewed as components associated (even transiently) with the mitochondrial respiratory chain. These novel protein components of respiratory protein supercomplexes in the IMM of WT cells include: (1) the ADP-ATP carrier protein Aac2p, a component of supercomplexes 1, 2, 4 and 6; (2) the mitochondrial porin Por1p, a component of supercomplexes 1, 2 and 8; (3) the Pda1p, Pdb1p, Lat1p and Lpd1p subunits of

the mitochondrial pyruvate dehydrogenase complex, components of the supercomplex 1; (4) the mitochondrial external NADH dehydrogenase Nde1p, a component of the supercomplex 1; (5) the Kgd1p subunit of the mitochondrial alpha-ketoglutarate dehydrogenase complex, a component of the supercomplex 2; (6) the Ald4p isoform of acetaldehyde dehydrogenase, a component of the supercomplex 8; and (7) the Idh1p and Idh2p isoforms of isocitrate dehydrogenase, a component of the supercomplex 8 (Figure 6.6A; Appendix 3). Moreover, the protein supercomplex 5 in the IMM of WT cells is a non-respiratory supercomplex composed of many molecules of Yme2p (Figure 6.6A; Appendix 3), an integral IMM protein with a role in maintaining mitochondrial nucleoid structure and number. It should be stressed that the *atg32Δ* mutation not only eliminates this non-respiratory supercomplex 5 but also causes a dissociation of several proteins or protein complexes from supercomplexes 1, 2, 3, 4, 6, 7 and 8. Some of these dissociated in *atg32Δ* cells proteins or protein complexes are known as components of the mitochondrial respiratory chain, including (1) Ndi1p, a dissociated from the supercomplex 1 oxidoreductase that (akin to the mitochondrial respiratory complex I in higher eukaryotes) transfers electrons from NADH to ubiquinone in the respiratory chain but (unlike respiratory complex I in higher eukaryotes) does not pump protons; (2) the respiratory complex III, which dissociates from supercomplexes 3, 7 and 8; (3) the respiratory complex IV, which dissociates from the supercomplex 7; and (4) the respiratory complex V, which dissociates from supercomplexes 4, 6 and 8 (Figures 6.6A and 6.6B; Appendix 3). Other of the dissociated in *atg32Δ* cells proteins or protein complexes have not been traditionally viewed as components associated (even transiently) with the mitochondrial respiratory chain; they include (1) dissociated from the supercomplex 1 subunits Pda1p, Pdb1p, Lat1p and Lpd1p of the mitochondrial pyruvate dehydrogenase complex; (2) a dissociated from the supercomplex 1 mitochondrial external NADH dehydrogenase Nde1p; and (3) a dissociated from the supercomplex 2 subunit Kgd1p of the mitochondrial alpha-ketoglutarate dehydrogenase complex (Figures 6.6A and 6.6B; Appendix 3).

In sum, these data suggest that under CR conditions mitophagy is required to sustain a population of mitochondria whose inner membrane exhibits abundant protein supercomplexes, each composed of a distinct set of respiratory and non-respiratory protein complexes. Thus, in chronologically aging yeast limited in calorie supply mitophagy selectively eliminates mitochondria whose inner membrane (1) has reduced levels of respiratory and non-respiratory

protein supercomplexes 2, 3, 4 and 5 due to their complete dissociation into individual proteins or small protein subcomplexes; (2) accumulates respiratory and non-respiratory protein supercomplexes 1, 3, 4, 6, 7 and 8 that lack one or more respiratory complexes; (3) amasses respiratory and non-respiratory protein supercomplexes 1, 2 and 8 that lack proteins not traditionally viewed as components associated with the mitochondrial respiratory chain; and/or (4) has diminished level of the non-respiratory protein supercomplex 5 composed of many molecules of Yme2p, an integral IMM protein involved in maintaining mitochondrial nucleoid structure and number.

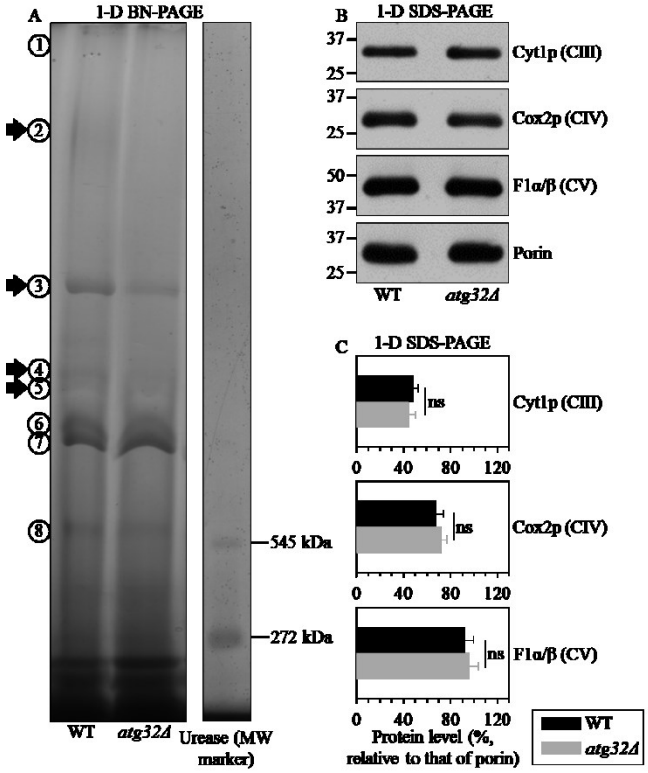

Figure 6.5. Under CR conditions, the *atg32Δ* mutation reduces the levels of several large protein supercomplexes in the IMM, likely due to their dissociation into individual proteins or small protein subcomplexes.

WT and *atg32Δ* strains were cultured in the nutrient-rich YP medium initially containing 0.2% glucose. Mitochondria were purified from WT and *atg32Δ* cells recovered on day 4 of culturing. (A) Digitonin-solubilized protein complexes from the inner membrane of these mitochondria were separated on a linear 4-13% acrylamide gradient gel for first-dimension blue native PAGE (1-D BN-PAGE). Arrows mark the positions of protein supercomplexes 2, 3, 4 and 5 whose levels were reduced in the IMM of *atg32Δ* cells. (B and C) Equal quantities (10 μg) of protein from these mitochondria were subjected to first-dimension SDS-PAGE (1-D SDS-PAGE) and analyzed by quantitative immunoblotting with antibodies to porin (loading control), Cyt1p (cytochrome *c*1, a

component of the respiratory complex III), Cox2p (subunit II of cytochrome *c* oxidase, a component of the respiratory complex IV) or F1α/β (alpha and beta subunits of the mitochondrial F1ATPase, the respiratory complex V). Data in C are presented as means ± SEM (n = 3-4; ns, not significant).

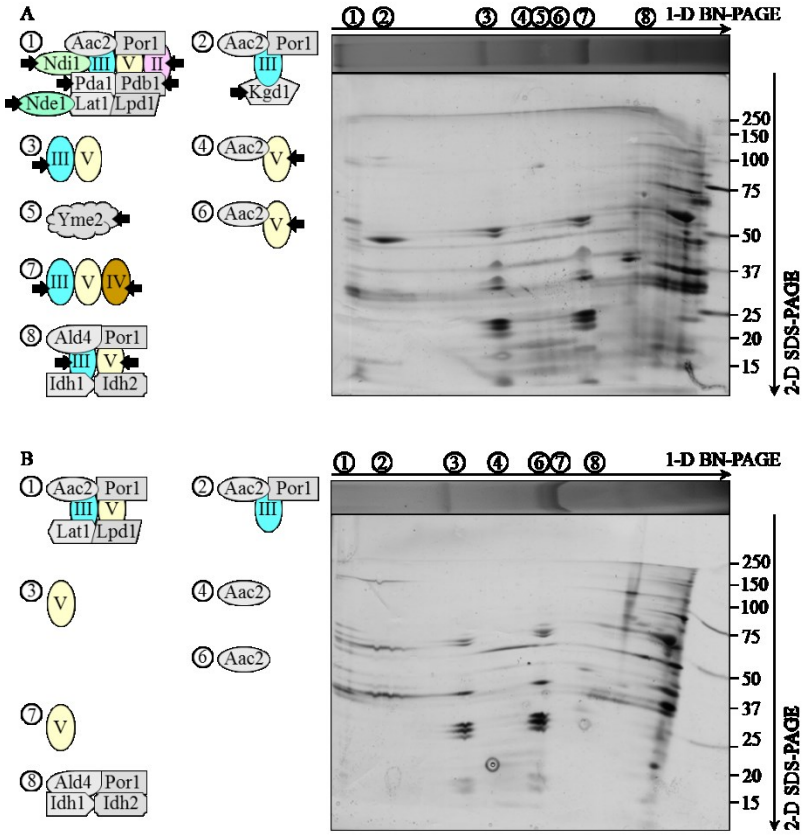

Figure 6.6. Under CR conditions, the *atg32Δ* mutation eliminates the non-respiratory protein supercomplex 5 in the IMM and alters compositions of other protein supercomplexes recovered by 1-D BN-PAGE.

WT and *atg32Δ* strains were cultured in the nutrient-rich YP medium initially containing 0.2% glucose. Mitochondria were purified from WT and *atg32Δ* cells recovered on day 4 of culturing. Digitonin-solubilized protein supercomplexes from the inner membrane of mitochondria purified from WT (A) or *atg32Δ* (B) cells were separated by first-dimension blue native PAGE (1-D BN-PAGE) and then resolved by second-dimension tricine-SDS-PAGE (2-D SDS-PAGE). Following silver staining, the separated by 2-D SDS-PAGE proteins were identified by mass spectrometry. Arrows in A mark the non-respiratory protein supercomplex 5 lacking in the IMM of *atg32Δ* cells as well as individual proteins or respiratory protein complexes dissociated from other protein supercomplexes in the IMM of these mutant cells.

6.3.6 Mitophagy preserves a population of mitochondria that efficiently couple electron transport to ATP synthesis and exhibit high and balanced activities of all five oxidative phosphorylation (OXPHOS) complexes

I sought to investigate whether the mitophagy-deficient *atg32Δ* cells in which we observed reduced abundance and altered composition of the major respiratory and non-respiratory protein supercomplexes (Figures 6.5 and 6.6) have an impact on the functional state of the electron transport and OXPHOS system in the IMM of these prematurely aging mutant cells.

To attain this objective, I used polarography of mitochondria purified from WT and *atg32Δ* cells for measuring the following three kinds of respiratory rate: (1) the rate of state III (also called ADP-stimulated state) respiration [282, 283], which was assessed immediately following addition of 50 μM ADP to mitochondria supplemented with a respiratory substrate; (2) the rate of state IV (also known as resting, basal or ADP-independent state) respiration [283, 287], which was monitored after the exogenously added ADP was entirely converted to ATP; and (3) the rate of uncoupled (UC) respiration [283, 288], which was determined after addition of the uncoupler carbonyl cyanide m-chlorophenylhydrazone (CCCP) to mitochondria incubated with a respiratory substrate in the absence of exogenous ADP. In these polarographic assays, the rates of state III, state IV and UC respiration were measured using NADH as a respiratory substrate of external NADH:quinone oxidoreductase or succinate as a respiratory substrate of complex II.

I found that the *atg32Δ* mutation significantly reduces the rates of state IV (Figures 6.7D and 6.7E) and UC (Figures 6.7G and 6.7H) respiration in the presence of NADH or succinate as a respiratory substrate. Both these respiratory rates are known to reflect the capacity of the electron transport chain (ETC) in the IMM [282, 283]. Thus, in cells grown under CR conditions on 0.2% glucose mitophagy is required to preserve a population of mitochondria that exhibit high capacity of electron transport along the respiratory chain.

I also found that the *atg32Δ* mutation considerably decreases (1) the rate of state III respiration (Figures 6.7A and 6.7B); (2) the state III rate/state IV rate ratio (known as the respiratory control ratio, RCR) (Figures 6.7J and 6.7K); (3) the state III rate/UC rate ratio (Figures 6.7M and 6.7N); and (4) the ADP/O ratio (i.e., the number ATP molecules synthesized per oxygen atom reduced) (Figures 6.7P and 6.7Q). All these parameters are known to reflect the extent of the functional and physical integrity of the IMM; the ADP/O ratio is also a direct

measure of the efficacy of coupling between ADP phosphorylation and electron transport along the respiratory chain [282, 283, 288]. I therefore concluded that in yeast cells limited in calorie supply macromitophagy is obligatory for sustaining a population of mitochondria that (1) preserve the functional and physical integrity of the IMM; and (2) efficiently couple electron transport to ATP synthesis.

To get insight into the effect of the observed in mitophagy-deficient *atg32Δ* cells reduced abundance and altered composition of the major respiratory and non-respiratory protein supercomplexes on the functional state of each of the five OXPHOS protein complexes, I measured their enzymatic activities in mitochondria purified from WT and *atg32Δ* cells grown under CR conditions on 0.2% glucose. As I found, the *atg32Δ* mutation causes a significant reduction in enzymatic activities of NADH:decylubiquinone oxidoreductase (NQR; an analog of the respiratory complex I in higher eukaryotes that is impaired in proton pumping across the IMM), succinate:decylubiquinone-2,6-dichlorophenolindophenol oxidoreductase (the respiratory complex II), ubiquinol:cytochrome c oxidoreductase (the respiratory complex III), cytochrome *c* oxidase (the respiratory complex IV) and F1F0-ATP synthase (the respiratory complex V) (Figures 6.7C, 6.7F, 6.7I, 6.7L and 6.7O). Noteworthy, the extent of such reduction for the respiratory complexes IV and V substantially exceeded that for NQR as well as for the respiratory complexes II and III (Figure 6.7R). Hence, in yeast cells limited in calorie supply mitophagy is needed for maintaining a population of mitochondria that display high and balanced activities of all five OXPHOS complexes.

Altogether, my polarographic and enzymatic assays in mitochondria purified from WT and *atg32Δ* cells suggest that in chronologically aging yeast under CR conditions, mitophagy may selectively eliminate mitochondria whose inner membrane exhibits (1) a compromised functional and physical integrity of the IMM; (2) disproportionally reduced activities of the five OXPHOS complexes; (3) a low capacity of electron transport along the respiratory chain; and (4) a reduced efficacy of coupling between ADP phosphorylation and electron transport.

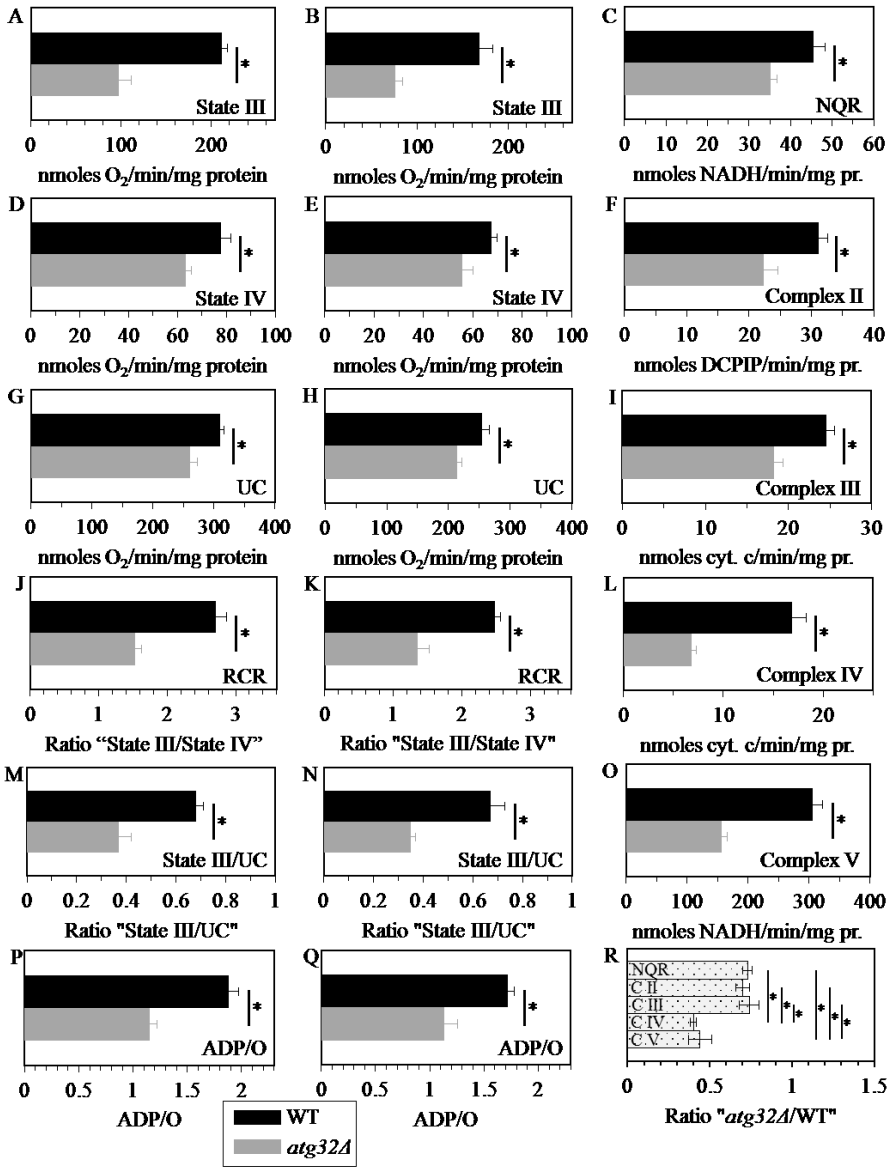

Figure 6.7. Under CR conditions, the *atg32Δ* mutation reduces capacity of the mitochondrial ETC, lowers the efficacy of coupling between ADP phosphorylation and electron transport, compromises the integrity of the IMM, and disproportionally decreases activities of all OXPHOS enzymes.

WT and *atg32Δ* strains were cultured in the nutrient-rich YP medium initially containing 0.2% glucose. Mitochondria were purified from WT and *atg32Δ* cells recovered on day 4 of culturing. The rates of state III (A and B), state IV (D and E) and UC (G and H) respiration were measured using NADH (A, D and G) or succinate (B, E and H) as a respiratory substrate. The ratios of state III rate/state IV rate (RCR; J and K), state III rate/UC rate (M and N) and ADP/O (P and Q) were determined using NADH (J, M and P) or succinate (K, N and Q) as a respiratory substrate. Enzymatic activities of the OXPHOS enzymes NADH:decylubiquinone oxidoreductase (NQR; C), succinate:decylubiquinone-2,6-dichlorophenolindophenol oxidoreductase (complex II) (F), ubiquinol:cytochrome *c* oxidoreductase (complex III) (I), cytochrome *c* oxidase (complex IV) (L) and F_1F_0-ATP synthase (complex V) (O)

were assessed. For each of these OXPHOS enzymes, the ratio "activity in mitochondria of *atg32Δ* strain/activity in mitochondria of WT strain" was calculated (R).

6.3.7 Mitophagy sustains a population of mitochondria that generate low levels of ROS and exhibit only a minor oxidative damage to mitochondrial macromolecules

The available literature supports the view that the multifactorial functional state of the mitochondrial ETC and OXPHOS system in the inner membrane of yeast mitochondria (rather than just the total number of electrons transported along the respiratory chain) determines the rate of mitochondrial ROS production, thereby modulating the extent of oxidative cellular damage and other vital processes defining yeast longevity [185, 186, 291 – 293]. It is well established that the functional state of the mitochondrial ETC and coupled OXPHOS system in yeast is influenced in part by the rate of mitochondrial respiration, capacity of electron flow through the respiratory chain, number and activity of individual OXPHOS enzymes, and relative levels of the five OXPHOS complexes [185, 186, 188, 291, 292]. I demonstrated that in yeast limited in calorie supply, the *atg32Δ*-dependent mutational block of mitophagy reduces mitochondrial respiration, decreases capacity of the mitochondrial ETC, lowers the efficacy of coupling between ADP phosphorylation and electron transport, and disproportionally lessens activities of all OXPHOS enzymes (Figures 6.4A and 6.7). This observation prompted me to investigate if the longevity-shortening *atg32Δ* mutation alters the age-related dynamics of changes in mitochondrially generated ROS and/or impacts the extent of oxidative damage to mitochondrial macromolecules. I found that in chronologically aging yeast cultured under CR on 0.2% glucose and recovered at different periods of CLS, the *atg32Δ* mutation elevates the level of mitochondrially produced ROS (Figure 6.8A). Furthermore, my comparative analysis of mitochondria purified from WT and *atg32Δ* mutant cells limited in calorie supply revealed that this mutation increases the extent of oxidative carbonylation of mitochondrial proteins (Figures 6.8B and 6.9) and elevates the levels of oxidatively damaged mitochondrial membrane lipids (Figure 6.8C). I also observed that *atg32Δ* mutant cells grown under CR on 0.2% glucose exhibited augmented, as compared to WT cells, frequencies of deletion (*rho*$^{-}$ and *rho*^{0}) and point (*rib2* and *rib3*) mutations in mitochondrial DNA (mtDNA) (Figures 6.8D and 6.8E) - likely due to an elevated extent of oxidative damage to mtDNA in these mutant cells.

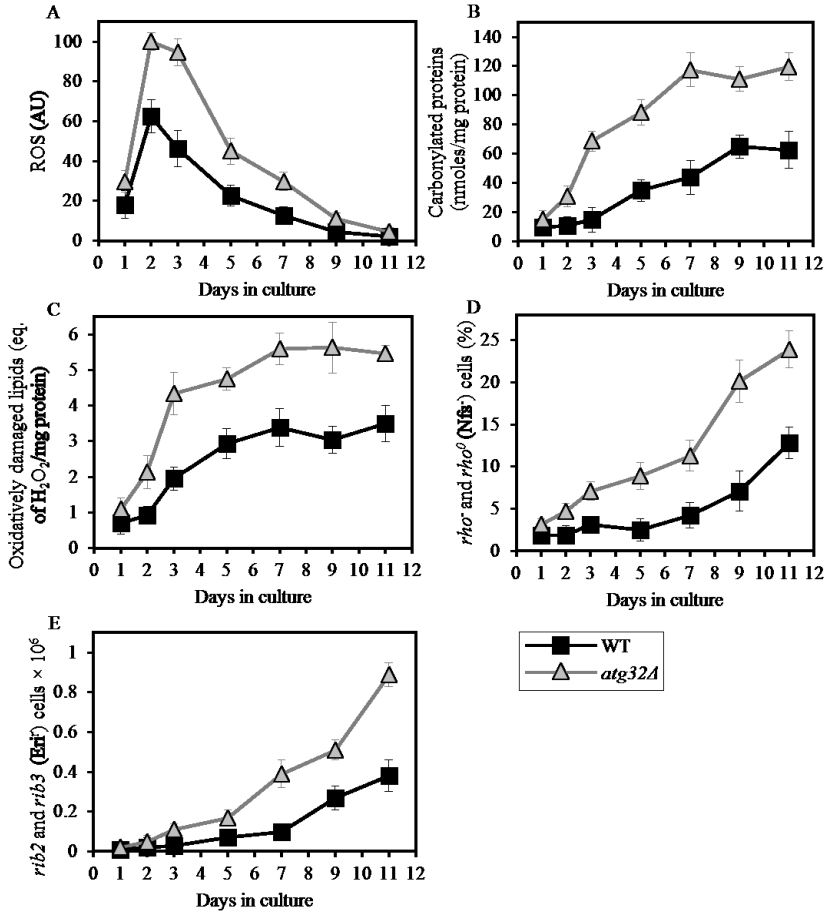

Figure 6.8. Under CR conditions, the *atg32Δ* mutation increases the level of mitochondrially produced ROS, elevates the extent of oxidative damage to mitochondrial proteins and membrane lipids, and rises the frequencies of mutations in mtDNA.

WT and *atg32Δ* strains were cultured in the nutrient-rich YP medium initially containing 0.2% glucose. (A) The dynamics of age-dependent changes in the intracellular levels of ROS during chronological aging of yeast. ROS were visualized using dihydrorhodamine 123 (DHR). At least 1,000 cells were used for quantitation of DHR staining for each of 4 independent experiments. Data are presented as mean ± SEM. (B and C) Carbonylated proteins (B) and oxidatively damaged membrane lipids (C) in purified mitochondria were determined as described in ″Materials and Methods″. Data are presented as mean ± SEM (n = 2-3). (D) The percentage of respiratory-deficient cells unable to grow in medium containing 3% glycerol because they carried large mtDNA deletions (*rho*$^-$) or lacked mtDNA (*rho*^{o}). Data are presented as mean ± SEM (n = 5). (E) The frequencies of *rib2* and *rib3* point mutations in mtDNA caused resistance to erythromycin. Data are presented as mean ± SEM (n = 4).

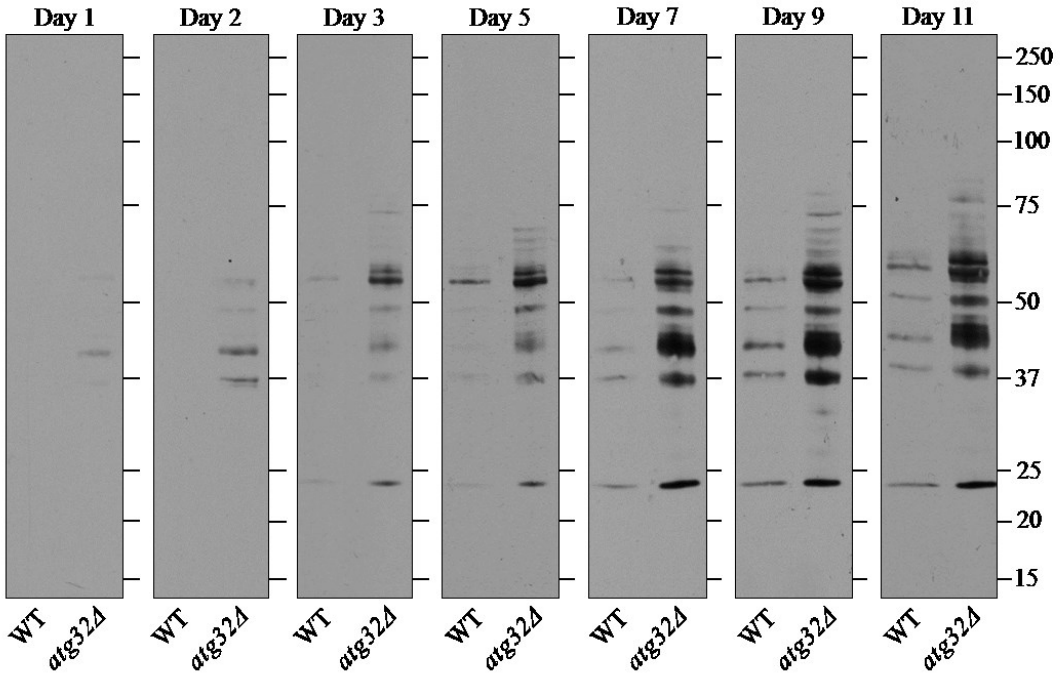

Figure 6.9. Under CR conditions, the *atg32Δ* mutation elevates the extent of oxidative damage to mitochondrial proteins.

WT and *atg32Δ* strains were cultured in the nutrient-rich YP medium initially containing 0.2% glucose. Immunodetection of carbonyl groups in oxidatively damaged proteins of purified mitochondria was performed as described in ″Materials and Methods″.

Taken together, these findings suggest that under CR conditions mitophagy is required to sustain a population of mitochondria that generate low levels of ROS and exhibit only minor oxidative damage to mitochondrial proteins, membrane lipids and DNA. Thus, it is conceivable that in chronologically aging yeast limited in calorie supply, mitophagy selectively eliminates mitochondria producing excessively high concentrations of ROS and accumulating elevated levels of macromolecules oxidatively damaged due to their exposure to mitochondrial ROS. One could predict that the inability of mitophagy-deficient *atg32Δ* cells to eliminate these oxidatively impaired (and therefore dysfunctional) mitochondria may result in their progressive accumulation with age, thereby shortening yeast longevity.

6.4 Discussion and Conclusions

CR is a diet in which only calorie availability is limited but the supply of amino acids, nucleotides, vitamins and other nutrients is not compromised [294]. This dietary intervention is known for its robust longevity-extending and health-improving effects across species [294 – 298], although recent findings in mice and primates initiated an intense debate over some of the beneficial effects attributed to CR [299, 300]. In this Chapter of my thesis, I provide the first evidence that selective autophagic mitochondrial removal plays a pivotal role in longevity extension by a CR diet in chronologically aging yeast; such a diet was implemented by culturing yeast cells in a nutrient-rich medium initially containing low (0.2%) concentration of glucose, a fermentable carbon source. It should be emphasized that under these longevity-extending CR conditions yeast cells are not starving but undergo an extensive remodeling of their metabolism in order to match the level of ATP produced under longevity-shortening non-CR conditions [145, 214]. Moreover, the findings presented in this Chapter of my thesis also revealed that in chronologically aging yeast limited in calorie supply, mitophagy is essential for longevity extension by LCA. This bile acid is a potent anti-aging intervention previously shown to act in synergy with CR to enable a significant further extension of yeast lifespan under CR conditions by modulating so-called "housekeeping" longevity pathways [155, 184]. In sum, these findings imply that mitophagy is a longevity assurance process that in chronologically aging yeast underlies the synergistic beneficial effects of anti-aging dietary and pharmacological interventions (i.e., CR and LCA) on lifespan.

The data presented in this Chapter of my thesis suggest that mitophagy can maintain survival of chronologically aging yeast limited in calorie supply by controlling a compendium of vital cellular processes known for their essential roles in defining longevity, as outlined below.

First, in short-lived *atg32Δ* cells we observed significant reduction in the level of ATP, which implies that mitophagy can selectively eliminate mitochondria incapable of producing this universal energy source in quantities sufficient to drive pro-longevity cellular processes. The diminished mitochondrial ATP production we see in mitophagy-deficient *atg32Δ* cells is likely due to their demonstrated inability to sustain a population of functional mitochondria whose inner membranes exhibit abundant protein supercomplexes, each composed of a distinct set of respiratory and non-respiratory protein complexes. It is conceivable that these *atg32Δ* cells accumulate mitochondria that exhibit (1) a decreased respiration rate; (2) a reduced

electrochemical potential across the IMM; (3) an impaired functional and physical integrity of the IMM; (4) disproportionally lowered activities of all five OXPHOS complexes; (5) a reduced capacity of electron transport along the respiratory chain; and (6) a low efficacy of coupling between ADP phosphorylation and electron transport. Within these prematurely aging *atg32Δ* cells, the build-up of these dysfunctional mitochondria can be progressively accelerated by the age-related accumulation of mitochondria that (1) generate high levels of ROS; (2) display a major oxidative damage to mitochondrial proteins and lipids; and (3) exhibit increased frequencies of mtDNA mutations likely caused by excessive levels of mitochondrial ROS.

Second, in prematurely aging *atg32Δ* cells, the substantial rise of ROS in mitochondria, the major cellular site of ROS formation as by-products of respiration [39, 243, 301], implies that mitophagy can selectively eliminate mitochondria incapable of maintaining intracellular ROS concentration below a toxic threshold. Because both mitochondrial membranes are permeable to the hydrogen peroxide form of ROS [39, 243, 301], the elevated ROS production by mitochondria accumulating in mitophagy-deficient *atg32Δ* cells is likely to accelerate yeast aging by causing an excessive oxidative damage to extramitochondrial cellular macromolecules. To test the validity of this hypothesis, I am currently investigating an impact of the *atg32Δ* mutation on the levels of oxidatively damaged proteins, lipids and nucleic acids that reside outside mitochondria.

Third, in short-lived *atg32Δ* cells, we observed massive fragmentation of the elaborate mitochondrial network, reduction of the electrochemical potential across the IMM, release of cytochrome *c* from the intermediate space of mitochondria into the cytosol and an elevated level of ROS, implying that mitophagy can selectively eliminate mitochondria that exhibit MOMP and the so-called mitochondrial permeability transition (MPT). MOMP is known to trigger apoptotic cell death, whereas MPT promotes necrotic cell death [10, 302]. One could anticipate that the early loss of viability by prematurely aging *atg32Δ* cells demonstrated in this chapter may be due to their accelerated apoptotic or necrotic death controlled by mitochondria. It should be emphasized that both these cell death modalities have been shown to define yeast longevity [145, 155, 184, 209, 303]. It is conceivable, therefore, that mitophagy can maintain survival of chronologically aging yeast limited in calorie supply by eliminating only mitochondria capable of triggering an age-related form of apoptotic or necrotic cell death initiated by MOMP and/or MPT. A challenge for the future will be to use chronologically aging yeast under CR conditions as a valuable model for

elucidating the impact of the *atg32Δ* mutation on the spatiotemporal dynamics of various hallmark events characteristic of apoptotic and necrotic modes of cell death.

Fourth, in *atg32Δ* cells grown under CR conditions, we observed substantial reduction of both mitochondrial respiration and the electrochemical potential across the IMM, which has been shown to stimulate activity of the cAMP-dependent protein kinase A (PKA) in WT yeast cells cultured under conditions of amino acid starvation [304]. PKA is known to govern several longevity-defining processes in chronologically aging yeast [137]. If activated, this nutrient-sensory protein kinase (1) inhibits a housekeeping, anti-aging process of non-selective macroautophagy [304 – 306]; (2) activates a pro-aging process of protein synthesis in the cytosol (Smets et al., 2010); and (3) inhibits nuclear import of Msn2p and Msn4p, thus turning off an anti-aging transcriptional program driven by these two stress response transcriptional activators [307, 308]. One could predict that mitophagy can maintain survival of chronologically aging yeast limited in calorie supply by eliminating mitochondria exhibiting a decreased respiration rate and a reduced electrochemical potential across the IMM, thereby attenuating PKA signalling to establish a pro-longevity cellular pattern. It would be important to test the validity of this hypothesis in the near future by assessing the effects of the *atg32Δ* mutation on non-selective autophagy, protein synthesis in the cytosol, nuclear import of Msn2p and Msn4p, and transcriptional pattern in yeast cultured under CR conditions.

Another challenge for the future will be to establish which of the numerous morphological and physiological features (exhibited by dysfunctional mitochondria that amass in *atg32Δ* cells) direct only a population of dysfunctional mitochondria for selective mitophagic destruction in WT cells limited in calorie supply. It would be also important to investigate if in WT cells grown under CR, only a pool of Atg32p confined to dysfunctional mitochondria is subjected to phosphorylation, as it has been seen in yeast undergoing mitophagy triggered in response to nitrogen starvation [309, 310]. Moreover, it remains to be seen which of the mitophagy-linked proteins other than Atg32p (a number of such proteins have been identified in the genome-wide screens as products of genes essential for mitophagy [212, 213]) are involved in macromitophagy in chronologically aging WT cells limited in calorie supply.

7 Integration of peroxisomes into an endomembrane system that governs cellular aging

7.1 Introduction

A growing body of evidence implies that, in addition to the well known roles of the peroxisome in housing fatty acid oxidation and maintaining hydrogen peroxide homeostasis [311 – 313], this organelle is actively involved in organizing the processes of development, differentiation and morphogenesis in evolutionarily distant organisms. In mammalian and plant cells, the rate of fatty acid metabolism and the efficiency of ROS and reactive nitrogen species (RNS) turnover within the peroxisome define the dynamics of changes in the levels of signaling lipids, ROS and RNS outside this organelle [314 – 317]. Following their release from the peroxisome, these signaling molecules bind and activate a distinct set of transcription factors that respond by causing global changes in gene expression to initiate certain developmental and differentiation programs [316 – 329]. Thus, the peroxisome functions as an intracellular signaling compartment that can orchestrate important developmental decisions from inside the cell by modulating the extra-peroxisomal concentrations of several potent cellular messengers [330 – 333]. Furthermore, the peroxisome can operate as an organizing platform for several developmental and differentiation programs by compartmentalizing the initial steps of plasmalogen biosynthesis in mammalian and nematode cells, providing acetyl-CoA for the biosynthesis of melanin and glycerol in fungal cells, and carrying out the oxidative decomposition of very long-chain fatty acids, phytanic acid and pristanic acid in mammalian cells [331, 334 – 346]. Moreover, while the peroxisome-associated pools of several bifunctional proteins with dual subcellular localization operate in peroxisome biogenesis and function, their pools in other organelles organize certain processes of development, differentiation and morphogenesis in mammalian, plant and yeast cells [330, 347 - 357]. In addition, the peroxisome provides a template for the formation of the Woronin body, a specialized subcellular compartment that in the filamentous fungi *Neurospora crassa* and *Aspergillus oryzae* is essential for a multistep process in cell morphogenesis initiated by physical damage to hyphae 358 – 363. In human cells, the peroxisome can also serve as an intracellular platform for the development of the human immunodeficiency virus and rotavirus [364, 365].

Recent findings have broadened a spectrum of complex biological processes that depend on the functional integrity of the peroxisome. Emergent evidence supports the view that such peroxisome-confined metabolic processes as fatty acid oxidation, ROS turnover and anaplerotic

replenishment of TCA cycle intermediates play essential roles in defining the replicative and chronological age of a eukaryotic cell [157]. Peroxisomal fatty acid oxidation has been shown to regulate cellular aging because it operates as a system controller that modulates levels of non-esterified fatty acids and diacylglycerol by governing lipid dynamics in peroxisomes, lipid bodies and the ER [145, 153, 157]; non-esterified fatty acids are known to accelerate the age-related necrotic and apoptotic cell death mechanisms, whereas the diacylglycerol-activated protein kinase C signaling sensitizes cells to age-related stresses [366 – 370]. Furthermore, peroxisomal fatty acid oxidation and anaplerotic reactions have been demonstrated to delay cellular aging by potentiating the mitochondrial retrograde (RTG) signaling pathway of longevity regulation [136, 157, 259, 371 – 375]. Moreover, ROS homeostasis and the extent of macromolecular oxidative damage within the peroxisome govern several anti-aging processes confined to this organelle [157, 376 – 383].

The peroxisome defines the replicative and chronological age of a eukaryotic cell not only by operating as a system controller that modulates levels of non-esterified fatty acids and diacylglycerol, replenishes TCA cycle intermediates destined for mitochondria, and contributes to the maintenance of peroxisomal ROS homeostasis and macromolecular oxidative damage. Recent studies have revealed that this organelle can also regulate cellular aging via its communication with other cellular compartments. This dynamic communication involves the establishment of extensive physical contact between peroxisomes and lipid bodies, maintenance of an ER to peroxisome connectivity system, exchange of certain metabolites between peroxisomes and other cellular compartments, and bidirectional flow of some protein and lipid constituents between peroxisomes and other organelles. In this Chapter of my thesis I summarize the evidence that peroxisomes are dynamically integrated into an endomembrane system that governs cellular aging. I discuss various strategies through which peroxisomes are integrated into this endomembrane system, critically evaluate the molecular mechanisms underlying each of these strategies, and analyze the age-related dynamics of communications between peroxisomes and other cellular compartments composing the longevity-defining endomembrane system. I also outline recent progress in understanding how communications between peroxisomes and other cellular compartments within this system influence the development of a pro- or anti-aging cellular pattern. Based on the available evidence, I propose a model for the integration of peroxisomes into the endomembrane system governing cellular aging.

7.2 A role for cytosol-to-peroxisome targeting of Pnc1p in regulating yeast longevity

Support for a distinctive mechanism that underlies the essential role of peroxisomes in regulating cellular aging comes from the observation that Pnc1p, a pyrazinamidase/nicotinamidase 1 that converts nicotinamide to nicotinic acid in the NAD^+ salvage pathway [384], is targeted from the cytosol to the peroxisome in response to CR and various mild stresses [385]. CR and all of these other "hormetic" stimuli - the term "hormesis" refers to a beneficial defense response of an organism to a low-intensity biological stress [244, 386 – 388] - increase the lifespan of replicatively aging yeast in a Pnc1p-dependent manner [385]. Peroxisomal import of Pnc1p under conditions of such longevity-extending hormesis requires the peroxisomal targeting signal 2 (PTS2) shuttling receptor Pex7p and the peroxin Pex6p, but does not rely on the PTS1 receptor Pex5p [385]. Such specific peroxisomal targeting of Pnc1p, one of the key regulators of replicative aging in yeast [389], in response to their exposure to various anti-aging exogenous factors suggests that Pnc1p in the peroxisome could modulate some longevity-related processes confined to this organelle. What are these processes?

The established function of Pnc1p in the nucleus - an organelle to which this protein is also sorted from the cytosol in yeast exposed to CR and other hormetic stimuli [385] - provides a useful hint on the nature of peroxisome-confined processes that could be modulated by Pnc1p under these longevity-extending conditions. In the nucleus, Pnc1p depletes the level of nicotinamide, a strong non-competitive inhibitor of the NAD^+-dependent protein deacetylase Sir2p required for lifespan extension in yeast under CR conditions [390]. The resulting Pnc1p-driven activation of Sir2p delays replicative aging by suppressing recombination at the ribosomal DNA (rDNA) locus, thereby decreasing the efficiency of extrachromosomal rDNA circle (ERC) formation in the nucleolus [389]. It should be stressed that two of the four members of the Sir2p family of NAD^+-dependent protein deacetylases (*i.e.*, sirtuins) in yeast - called Hst3p and Hst4p for being Homologs of SIR Two proteins - drive the metabolism of fatty acids by activating acyl-CoA synthetases for their short-chain species [391]. By converting short-chain fatty acids into their corresponding acyl-CoA forms, acyl-CoA synthetases enable their cellular and intracellular

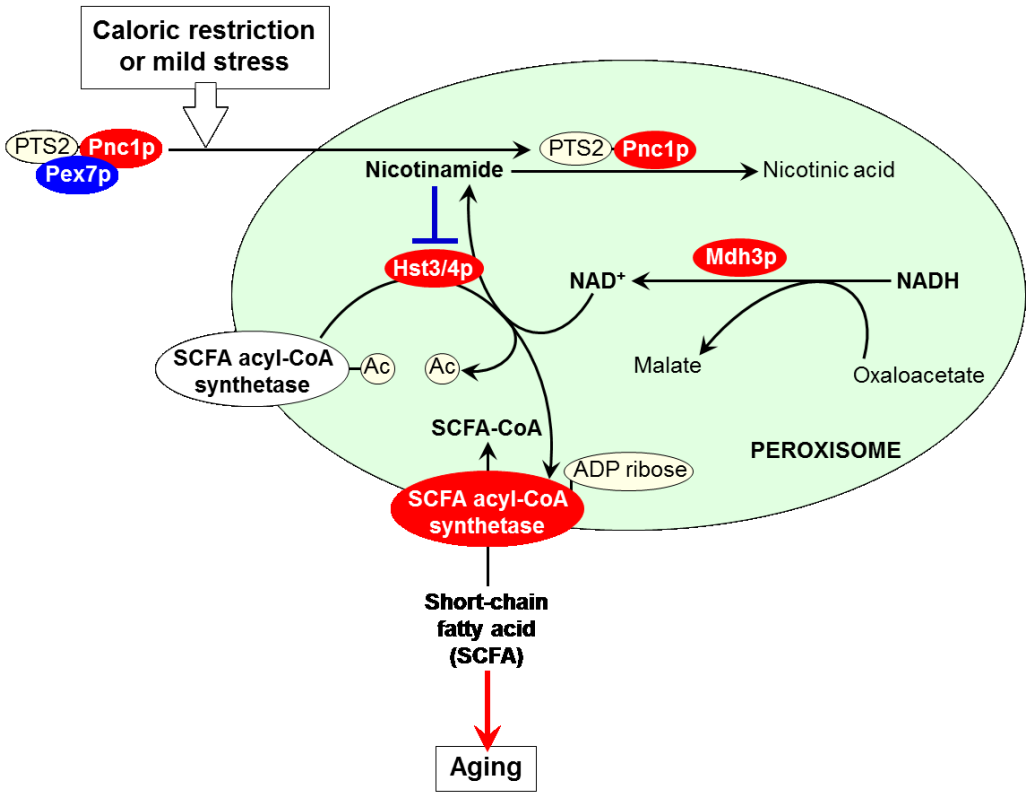

Figure 7.1. A proposed role for cytosol-to-peroxisome targeting of Pnc1p in regulating longevity of replicatively aging yeast.

If exposed to caloric restriction (CR) and other hormetic anti-aging stimuli, yeast cells respond by targeting Pnc1p - a pyrazinamidase/nicotinamidase 1 that converts nicotinamide to nicotinic acid in the NAD^+ salvage pathway - not only to the nucleus but also to the peroxisome. The delivery of Pnc1p to the peroxisome depends on the peroxisomal targeting signal 2 (PTS2) shuttling receptor Pex7p. Inside the peroxisome, Pnc1p activates the sirtuins Hst3p and Hst4p by reducing the concentration of their non-competitive inhibitor nicotinamide. Using NAD^+ generated by the peroxisomal malate dehydrogenase Mdh3p as a co-substrate in protein deacetylation and ADP-ribosylation reactions, the activated Hst3p and Hst4p stimulate acyl-CoA synthetases required for peroxisomal transport and oxidation of short-chain fatty acids (SCFA). By reducing the levels of these fatty acids in the cytosol, peroxisomes contribute to the beneficial effect of CR and other hormetic stimuli on longevity. See text for details.

transport and metabolism [391]. It has been proposed that both Hst3p and Hst4p activate these acyl-CoA synthetases by deacetylating them and cleaving NAD^+ in each reaction cycle [391]. Because sirtuins are also known for their NAD^+-dependent ADP-ribosylation activity [392, 393], a possibility that Hst3p and Hst4p activate acyl-CoA synthetases for short-chain fatty acids in ADP-ribosylation reactions is also feasible. Altogether, these findings suggest the following hypothesis for a role of cytosol-to-peroxisome targeting of Pnc1p in regulating longevity of

replicatively aging yeast (Figure 7.1). In response to their exposure to CR and other hormetic anti-aging stimuli, yeast cells target Pnc1p not only to the nucleus but also to the peroxisome. Following its PTS2- and Pex7p-dependent import into the peroxisome, Pnc1p depletes the level of nicotinamide, a strong non-competitive inhibitor of Hst3p and Hst4p. As a co-substrate in protein deacetylation and/or ADP-ribosylation reactions, each of these sirtuins could use NAD^+ known to be generated by the peroxisomal malate dehydrogenase Mdh3p [394]. The Pnc1p-dependent depletion of nicotinamide activates Hst3p and Hst4p; in turn, these sirtuins stimulate acyl-CoA synthetases required for peroxisomal transport and oxidation of short-chain fatty acids (Figure 7.1). I hypothesize that, by depleting the levels of these fatty acids in the cytosol and/or oxidizing them, peroxisomes make an important contribution to the longevity-extending effect of CR and other hormetic stimuli. A critical evaluation of the above hypothesis will require testing of the localization of Hst3p and Hst4p to the peroxisome, either permanent or triggered in response to CR and mild stresses. Another key challenge for the future will be to evaluate the ability of peroxisomal acyl-CoA synthetases to undergo reversible deacetylation and/or ADP-ribosylation in an Hst3p- and/or Hst4p-dependent fashion following exposure of yeast to these longevity-extending stimuli.

7.3 The peroxin Pex6p contributes to the maintenance of age asymmetry between the mother and daughter yeast cells with respect to segregation of functional mitochondria

Several peroxisomal proteins are known to possess dual subcellular localization and function [330, 395, 396]. While the major, peroxisome-bound portion of each of these proteins controls essential processes confined to this organelle, their pools in other organellar compartments govern certain developmental, differentiation and morphogenetic programs [330, 396]. The emergeing compendium of these bifunctional peroxisomal proteins with dual subcellular localization is on a fast-growing list of the so-called "moonlighting proteins" [397 – 403]. By analyzing the information on dynamic changes in metabolic status and/or organelle functional state within one subcellular location and then moving to other location(s) for initiating an adequate response to such changes, these moonlighting proteins integrate various cellular activities in space and time [398 – 400, 402 – 405].

The peroxin Pex6p is an AAA ATPase (ATPase associated with various cellular activities) whose peroxisome-associated pool has been implicated in peroxisomal protein import [406 – 408]. In the yeast *Yarrowia lipolytica* Pex6p is a moonlighting protein whose minor portion is confined to the ER [347, 348]. The ER-associated Pex6p is an essential component of protein machinery that orchestrates the dimorphic transition from a round yeast form to a filamentous (mycelial) form [330, 347]. Pex6p, along with other ER components of this machinery, governs this cell polarization and differentiation program by driving the delivery of mycelium-specific proteins from the ER to the cell surface [347].

Recently, a list of the "extra-curricular" activities of Pex6p has been updated by including to it the essential role that this peroxin plays in regulating yeast longevity. Because the yeast *Saccharomyces cerevisiae* reproduces by asymmetric cell division, replicatively "young" mother cells retain such "senescence factors" (also called "aging factors") as ERCs, oxidatively damaged proteins, protein aggregates and dysfunctional mitochondria (Figure 7.2A) [408 – 415]. Their budding progeny therefore retains the full replicative capacity by not inheriting ERCs or damaged/aggregated proteins and receiving only functional mitochondria [411 – 413]. In replicatively "old" mother cells, this age asymmetry between the mother and daughter cells is lost. As a result, the daughters inherit all four of the known senescence factors (Figure 7.2A) [408, 412, 413]. It should be stressed that the overexpression of Pex6p suppresses the lack of age asymmetry between mother and daughter cells in a strain carrying a point mutation in the nuclear gene *ATP2* encoding the ß-subunit of the F_1 sector of mitochondrial F_0, F_1- ATP synthase [417, 418]. Moreover, not only Pex6p - along with yet-to-be-identified cytosolic proteins - facilitates the import of Atp2p into mitochondria, but it also drives the segregation of functional mitochondria to daughter cells [418]. Therefore, it is conceivable that Pex6p could operate as one of the "filters" sequestering dysfunctional mitochondria in the mother cell and/or segregating functional mitochondria to the daughter cell (Figures 7.2B and 7.2C). The challenge remains to define the mechanisms underlying the ability of Pex6p to facilitate mitochondrial import of Atp2p and to maintain the age-related asymmetrical segregation of functional mitochondria between mother and daughter cells. Another key challenge for the future will be to establish the mechanism for delivery of Pex6p from peroxisomes to mitochondria. Importantly, not only the biogenesis of these two organelles is governed by common transcriptional pathways, but they also share

several key components of their division machineries and are linked through mitochondria-to-peroxisome vesicular traffic (Figures 7.2B and 7.2C) [116, 136, 375, 396, 419, 420].

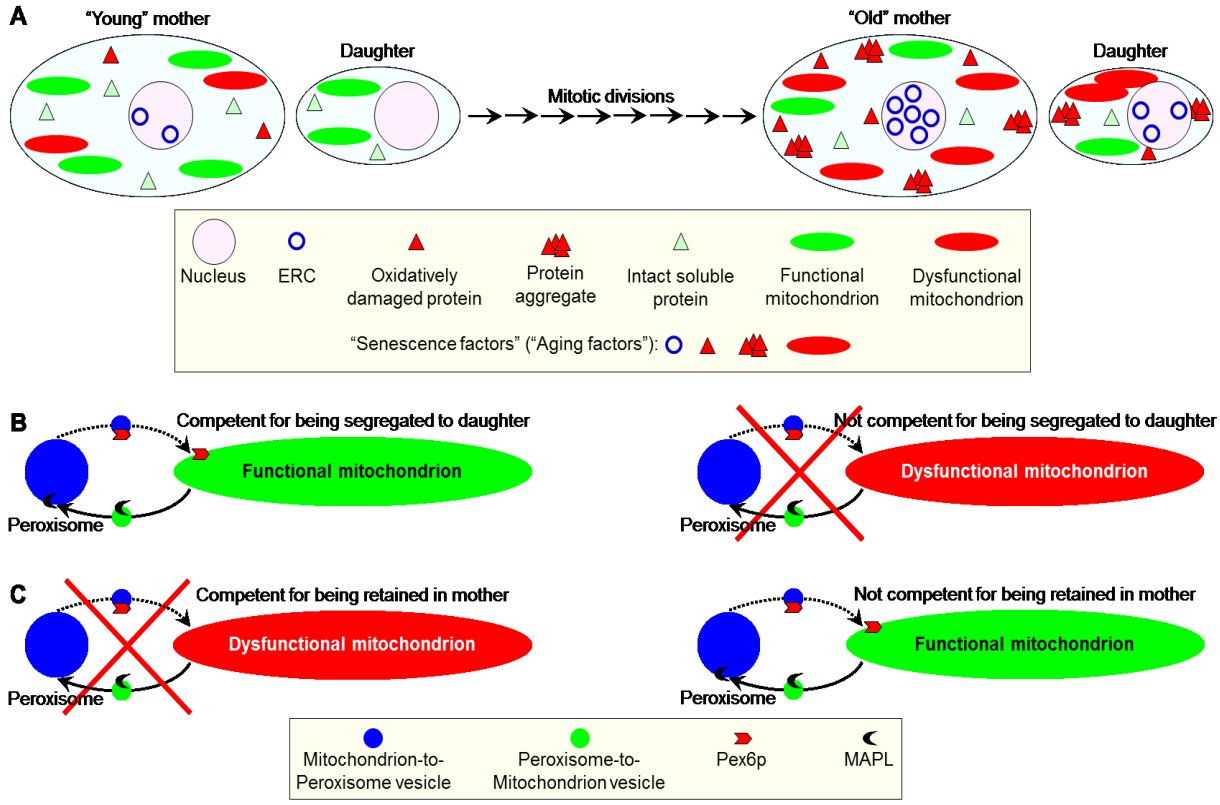

Figure 7.2. A proposed role for the mainly peroxisomal protein Pex6p in sequestering dysfunctional mitochondria in the mother cell of replicatively aging yeast and/or segregating functional mitochondria to the daughter cell.

(A) In the reproducing by asymmetric cell division yeast *Saccharomyces cerevisiae*, the budding progeny of replicatively "young" mother cells retains the full replicative capacity by not inheriting such "senescence factors" (also called "aging factors") as extrachromosomal rDNA circles (ERC), oxidatively damaged proteins, protein aggregates and dysfunctional mitochondria. In contrast, the daughters of replicatively "old" mother cells inherit these senescence factors. (B, C) A peroxisome-associated pool of the peroxin Pex6p has been long known for its essential role in peroxisomal protein import. An "extra-curricular" activity of this protein consists in driving the segregation of functional mitochondria to daughter cells. Pex6p could operate as a "filter" sequestering dysfunctional mitochondria in the mother cell (B) and/or segregating functional mitochondria to the daughter cell (C). The mechanism underlying such function of Pex6p may involve a recently discovered vesicular traffic between peroxisomes and mitochondria. See text for details.

7.4 Two mechanisms for preventing the segregation of dysfunctional, oxidatively damaged peroxisomes to the daughter yeast cell during mitosis

Not only do peroxisomes in replicatively aging yeast contribute to selective segregation of functional mitochondria to the daughter cell, but they also possess a protein machine that governs their own distribution between mother and daughter cells. Recent studies suggested two mechanisms by which this protein machine may operate in preventing the inheritance of dysfunctional, oxidatively damaged peroxisomes by the daughter cell during mitosis.

In *S. cerevisiae*, the inheritance of peroxisomes by daughter cells relies on the peroxisomal protein Inp2p [421]. By acting as a receptor for the class V myosin motor Myo2p, Inp2p tags peroxisomes for their segregation to the daughter cell [422]. It is conceivable that such Inp2p-dependent tagging of peroxisomes plays a longevity-extending role by enabling the inheritance of only functional peroxisomes by daughter cells. Importantly, the phosphorylation of Inp2p makes it susceptible to degradation, thereby impairing the segregation of Inp2p-less peroxisomes to the daughter cell [422, 423]. One could therefore speculate that such phosphorylation and degradation target mainly Inp2p on dysfunctional, oxidatively damaged peroxisomes for sequestering them in the mother cell.

In another yeast species, *Y. lipolytica*, the inheritance of only newly formed from the ER template peroxisomes may prevent the segregation of their oxidatively damaged, "old" counterparts to the daughter cell during mitosis [423]. By possessing a dual role in the formation of new peroxisomes from the ER template and in the recruitment of the class V myosin motor Myo2p to their membranes, the peroxins Pex3p and Pex3Bp may enable the selective segregation of these newly formed peroxisomes to the daughter cell, thereby allowing to retain the entire population of dysfunctional, oxidatively damaged peroxisomes in the mother cell [423].

The challenge remains to define the molecular mechanisms underlying the proposed selectivity in 1) phosphorylating Inp2p only on dysfunctional, oxidatively damaged peroxisomes; and 2) targeting Myo2p only to the ER-confined pool of Pex3p.

7.5 A model for the integration of peroxisomes into an endomembrane system that governs cellular aging

The evidence summarized here and elsewhere [157, 330, 396] implies that peroxisomes contribute to the regulation of cellular aging via several different mechanisms. In each of these

mechanisms, peroxisomes communicate with other organelles by establishing extensive physical contact with lipid bodies, maintaining the ER-peroxisome connectivity, exchanging certain metabolites, and/or being involved in the bidirectional flow of some of their protein and lipid constituents. Thus, peroxisomes are dynamically integrated into an endomembrane system that governs cellular aging. I propose a model for such integration (Figure 7.3). The central tenet of this model is that the age-dependent efficiency of protein import into the peroxisome modulates the dynamics of its communication with other cellular compartments, thereby influencing several longevity regulation pathways that rely on such communication. The overall efficiency of peroxisomal protein import is defined by the efficiencies of binding of Pex5p and Pex7p – the PTS1 and PTS2 cytosolic shuttling receptors, respectively – to their cargo proteins in the cytosol, translocation of the receptor-cargo complexes across the peroxisomal membrane, and receptor recycling [407, 408]. Importantly, the efficiencies of all these processes are reduced with age [157, 377, 424]. In the proposed model, if the overall efficiency of protein import into peroxisomes is actively maintained at a sufficiently high level, these organelles trigger certain anti-aging processes within the endomembrane system governing cellular aging (Figure 7.3). Conversely, if the overall efficiency of peroxisomal protein import is lower than this critical level, peroxisomes promote the development of a pro-aging pattern within this endomembrane system (Figure 7.3).

The model envisions that the efficient Pex5p-dependent peroxisomal import of the ROS scavenging enzymes catalase (Cta1p in yeast) and peroxiredoxin (PrxAp in mammals and Pmp20p in yeast) in replicatively and chronologically "young" cells aids in minimizing the oxidative damage to peroxisomal proteins and membrane lipids (Figure 7.3) [157, 326, 327]. At the surface of the peroxisome, quality control of the Pex5p-driven protein import in these cells is governed by the receptor accumulation and degradation in the absence of recycling (RADAR) pathway for the recycling of Pex5p [157, 407, 425]. Inside the peroxisome, the insulin degrading enzyme (IDE), peroxisomal Lon (pLon) protease and peroxisome-associated protein degradation

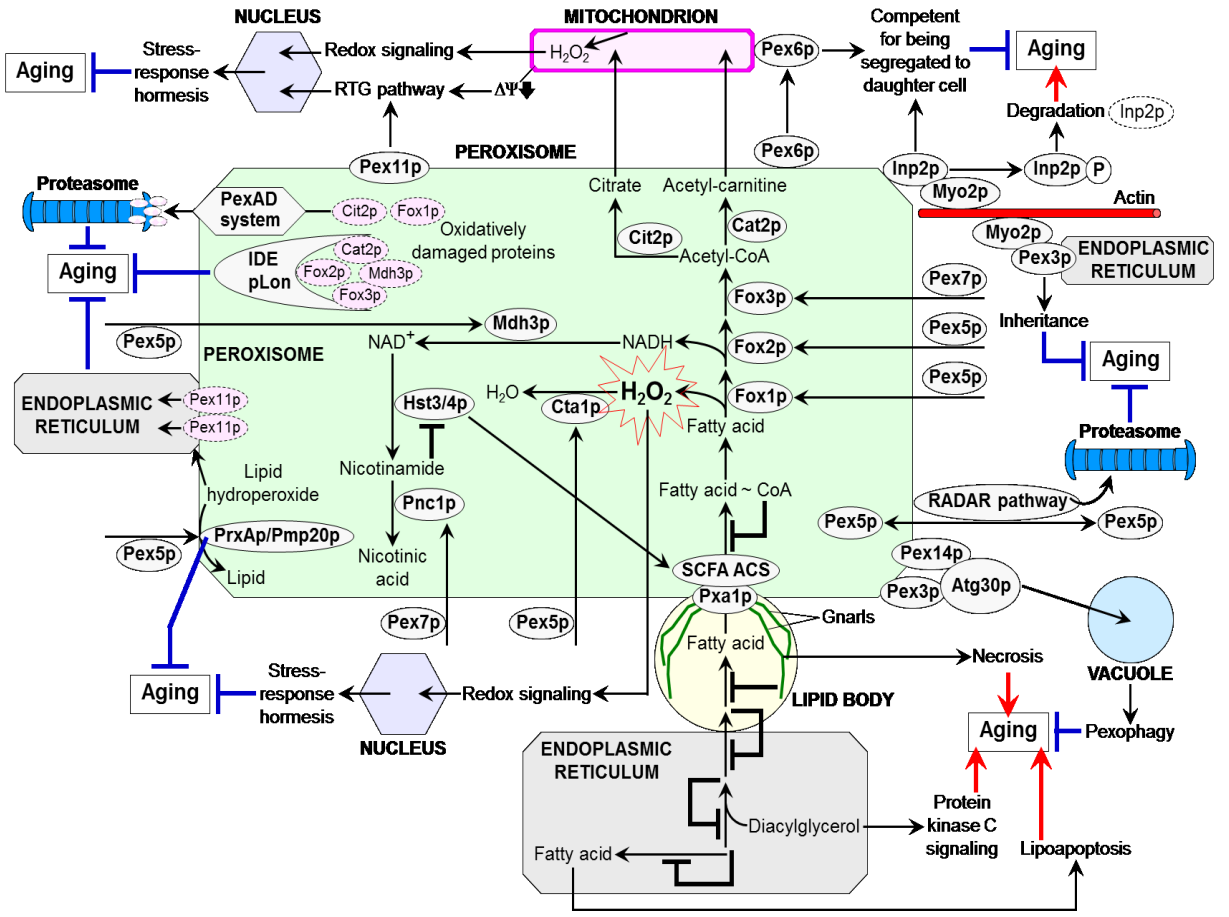

Figure 7.3. A model for the dynamic integration of peroxisomes into an endomembrane system governing cellular aging.

Several mechanisms underlie the essential contribution of peroxisomes to the regulation of cellular aging. Each of these mechanisms relies on a network of communications between peroxisomes and other organelles through the maintenance of the endoplasmic reticulum-peroxisome connectivity, establishment of the extensive physical contact with lipid bodies, exchange of certain metabolites, and/or the bidirectional flow of some of their proteins and lipids. Thus, peroxisomes are dynamically integrated into an endomembrane system that governs cellular aging. By modulating the dynamics of communication between peroxisomes and other cellular compartments, the age-dependent efficiency of peroxisomal protein import influences a compendium of longevity regulation pathways relying on such communication. Peroxisomes promote the development of a pro-aging pattern within an endomembrane system governing cellular aging if the overall efficiency of peroxisomal protein import is actively maintained at a sufficiently high level. Conversely, peroxisomes trigger certain pro-aging processes within this endomembrane system if the overall efficiency of peroxisomal protein import is lower than this critical level. See text for details. IDE, insulin degrading enzyme; PexAD, peroxisome-associated protein degradation; pLon, peroxisomal Lon protease; RADAR, receptor accumulation and degradation in the absence of recycling; RTG, retrograde; SCFA ACS, short-chain fatty acid acetyl-CoA synthetase; ΔΨ, electrochemical potential across the inner mitochondrial membrane.

(PexAD) system carry out the degradation of oxidatively damaged peroxisomal matrix proteins that are incapable of supporting the anti-aging processes orchestrated by functionally active peroxisomes [376, 378, 380, 381]. A healthy population of such peroxisomes in "young" cells is also sustained by pexophagy, an autophagy-related process in which dysfunctional peroxisomes carrying oxidatively damaged proteins are selectively degraded following their sequestration by vacuoles of yeast and plant cells or lysosomes of mammalian cells (Figure 7.3) [378, 426, 427]. In plant cells exposed to oxidative stress, the ER-peroxisome connectivity enables the retro-flow of oxidatively damaged matrix proteins as well as of membrane proteins and lipids to the ER - thereby contributing to the maintenance of a healthy population of functionally active peroxisomes [382, 383].

In the proposed model, peroxisomes in "young" cells not only actively avoid the oxidative damage to their protein and lipid constituents but also operate as a signaling platform that, by maintaining ROS concentration at a certain "optimal" level, delays cellular aging by inducing stress-response hormesis (Figure 7.3) [157]. At such a level, ROS are unable to elicit substantial oxidative damage to cellular macromolecules but can activate several redox signaling networks known to elevate the abundance and/or activity of stress-protecting and other anti-aging proteins [39, 243, 428].

Furthermore, the PTS1 and PTS2 cytosolic shuttling receptors Pex5p and Pex7p drive peroxisomal import of Fox1p, Fox2p and Fox3p [429]. The efficient import of these core enzymes of fatty acid β-oxidation into peroxisomes of "young" cells increases the efficacy with which they decompose fatty acids derived from triacylglycerols that are synthesized in the ER and deposited within lipid bodies [145, 153, 430, 431]. Due to such accelerated peroxisomal fatty acid oxidation and the resulting decrease in the concentrations of non-esterified fatty acids and diacylglycerol, "young" cells escape the premature death by resisting lipid-induced necrosis and apoptosis and by sustaining stress resistance through the attenuation of diacylglycerol-activated protein kinase C signaling (Figure 7.3) [145, 153, 157]. Another way for the longevity-extending acceleration of peroxisomal fatty acid oxidation in "young" cells is the governed by sirtuins Hst3p and Hst4p stimulation of acyl-CoA synthetases that are required for peroxisomal transport and oxidation of short-chain fatty acids. This anti-aging process is driven by the efficient Pex5p-

and Pex7p-dependent peroxisomal import of Mdh3p and Pnc1p for synthesizing a substrate and decomposing an inhibitor of the sirtuins, respectively (Figure 7.3).

Moreover, the longevity-extending ability of peroxisomes to promote the anti-aging RTG signaling pathway of peroxisomes-mitochondria, mitochondria-nucleus and nucleus-peroxisomes communications in "young" cells is enhanced by the highly efficient peroxisomal import of Fox1p, Fox2p, Fox3p, Cit2p and Cat2p in these cells (Figure 7.3) [157]. Fox1p, Fox2p and Fox3p are involved in the peroxisomal oxidation of fatty acid to acetyl-CoA following their Pex5p- and Pex7p-dependent delivery to peroxisomes, whereas the citrate synthase Cit2p and acetyl-carnitine synthase Cat2p are imported into these organelles with the help of Pex5p to catalyze the anaplerotic conversion of acetyl-CoA to citrate and acetyl-carnitine (Figure 7.3) [157, 259, 373, 428]. The longevity-extending RTG signaling pathway in "young" cells is further amplified through the Pex11p-driven proliferation of peroxisomes and the resulting increase in the effectiveness with which the confined to these organelles fatty acid oxidation and anaplerotic reactions replenish TCA cycle intermediates destined for mitochondria (Figure 7.3) [157, 375, 408]. It should be emphasized that, by maintaining the functionality of mitochondria in "young" cells, the peroxisome-driven RTG pathway controls the homeostasis of mitochondrial ROS [157]. This enables the ROS-dependent activation of several redox signaling networks aimed at increasing the levels of stress-protecting and other anti-aging proteins or post-translationally activating some of them (Figure 7.3) [39, 243, 427]. In the proposed model, the segregation of functional mitochondria to the "young" daughter cell and/or the sequestration of dysfunctional mitochondria in the "old" mother cell in replicatively aging yeast are/is driven in part by the delivery of the peroxin Pex6p from peroxisomes to mitochondria through a mechanism that remains to be established (Figure 7.3) [416, 417].

According to the proposed model, *S. cerevisiae* Inp2p - a peroxisome-specific receptor for the class V myosin motor Myo2p - tags peroxisomes for their segregation to the "young" daughter cell in a process that may play a life-extending role by enabling the inheritance of only functional peroxisomes (Figure 7.3) [421, 422]. Furthermore, by possessing a dual role in the formation of new peroxisomes from the ER template and in the recruitment of Myo2p to their membranes, the *Y. lipolytica* peroxins Pex3p and Pex3Bp may enable the inheritance of only newly formed from the ER template peroxisomes thus preventing the segregation of their oxidatively damaged, "old" counterparts to the daughter cell during mitosis (Figure 7.3) [422].

The proposed model envisions that the overall efficiency of peroxisomal protein import gradually decreases with replicative and chronological age (Figure 7.3). A steady, age-related increase in the concentration of peroxisome-confined proteins that are oxidatively damaged by peroxisomally produced ROS could be the driving force for such deterioration of peroxisomal protein import efficiency. The Pex5p-dependent peroxisomal import of catalase - due to the age-dependent decline in the efficiency of its binding to Pex5p and in the extent of Pex5p recycling - is the most sensitive to oxidative damage peroxisomal process [377, 423]. The resulting deceleration of catalase import into peroxisomes increases the extent of oxidative damage to their proteins and lipids, thereby initiating the "deterioration spiral" that eventually lowers the overall efficiency of peroxisomal protein import below a critical level. Consequently, the role of peroxisomes in the regulation of cellular aging is switching from being a platform for activating a compendium of anti-aging processes within the endomembrane system governing cellular aging to becoming a platform for the development of a pro-aging pattern within this endomembrane system [157]. Specifically, the RADAR pathway, IDE and pLon proteases, PexAD system, and pexophagy eventually fail due to the progressive, age-dependent accumulation of oxidatively damaged proteins and lipids in peroxisomes. Thus, cellular aging coincides with the build-up of dysfunctional peroxisomes that are unable anymore to support the anti-aging processes within the endomembrane system governing such aging. Among these impaired anti-aging processes are (1) the peroxisome- and mitochondria-driven pathways of stress response hormesis; (2) the Hst3p/Hst4p-dependent stimulation of acyl-CoA synthetases for peroxisomal transport and oxidation of short-chain fatty acids; (3) the RTG signaling pathway of peroxisomes-mitochondria, mitochondria-nucleus and nucleus-peroxisomes communications; (4) the Pex6p-dependent sequestration of dysfunctional mitochondria in the "old" mother cell and/or segregation of functional mitochondria to the "young" daughter cell; and (5) the Inp2p-, Pex3p- and Pex3Bp-dependent segregation of functional peroxisomes to the "young" daughter cell (Figure 7.3). Moreover, the model foresees that, by being unable to maintain low levels of non-esterified fatty acids and diacylglycerol, the dysfunctional, oxidatively damaged peroxisomes accumulated in aged cells (1) activate the longevity-shortening necrotic and apoptotic cell death mechanisms induced by non-esterified fatty acids ; and (2) are unable to attenuate the diacylglycerol-activated protein kinase C signaling that reduces stress resistance (Figure 7.3).

7.6 Conclusions

Growing evidence supports the view that peroxisomes govern cellular aging via several different mechanisms involving their dynamic communication with other cellular compartments. An important conceptual advance in our understanding of the inherent complexity of cellular aging is that the age-related dynamics of communications between peroxisomes and various other organelles modulates a compendium of longevity regulation pathways. It is conceivable therefore that the peroxisome is dynamically integrated into an endomembrane system governing cellular aging. Much progress has recently been made in defining how communications between peroxisomes and other cellular compartments influence the development of a pro- or anti-aging pattern within this endomembrane system. The challenge remains to define the molecular mechanisms underlying the integration of peroxisomes into the endomembrane system governing cellular aging. Future work will aim at understanding how peroxisomes switch their role in the regulation of cellular aging from being a platform for activating a compendium of anti-aging processes confined to this endomembrane system in "young" cells to becoming a platform for the development of a pro-aging pattern within this endomembrane system in "old" cells. This knowledge will provide greater insight into the mechanisms underlying longevity regulation and is expected to reveal novel targets for anti-aging pharmaceuticals that can extend longevity by modulating the age-related dynamics of communications between peroxisomes and other cellular compartments.

8 Future Directions

In this thesis, I have presented yeast mitochondria as a signaling platform through which longevity-defining cellular patterns can be established. Further investigation into the effects of changes in the mitochondrial lipidome (through genetic manipulation [273 – 276]) will provide valuable insight on how LCA is able to extend lifespan, alter the mitochondrial proteome and function, and affect specific age-related proteins outside the mitochondrion. Furthermore, employing a quantitative, mass spectrometry-based metabolomic analysis of LCA-treated yeast cells will allow us to characterize the metabolomic signature of the anti-aging effect that LCA induces.

With respect to cell death mechanisms, it would interesting to use the *atg32Δ* mutat yeast strain under CR conditions to uncover the impact on various hallmark events that are characteristic of apoptotic and necrotic modes of cell death. In addition, the effects of the *atg32Δ* mutation on several processes, including non-selective autophagy, protein synthesis in the cytosol, nuclear import of Msn2p and Msn4p, and transcriptional pattern in yeast cultured under CR conditions would provide greater insight.

In characterizing the *atg32Δ* mutation, I have presented several morphological and physiological features that amass over time and are exhibited by dysfunctional mitochondria. Going forward, teasing out which of these features specific to dysfunctional mitochondria result in their selection for mitophagy would help to provide insight on this process of selective degradation. In this regard, the phosphorylation state of Atg32p is an interesting target for further investigation, in light of dysfunctional mitochondria with phosphorylated Atg32p being selected for mitophagy, in response to nitrogen starvation [309, 310]. While Atg32p is essential for mitophagy [212, 213], it is currently unclear which other mitophagy-linked proteins or ATG genes are involved in macromitophagy and how altering these proteins would impact mitophagy.

Looking at the interplay between peroxisomes and mitochondria, another challenge is to establish the mechanism through which Pex6p is shuttled from peroxisomes to mitochondria. This is of particular interest, considering that the biogenesis of both peroxisomes and mitochondria share not only common transcriptional pathways, but also key components of their division machineries and are also linked through mitochondria-to-peroxisome vesicular traffic [116, 136, 375, 396, 419, 420].

Finally, it would be useful to examine the ability of peroxisomes to play alternating roles withing the endomembrane system in cellular aging, whether activating anti-aging processes in "young" cells or stimulating a pro-aging pattern in "old" cells. By harnessing this information, we can gain a better understanding of life-extending mechanisms at play with respect to cellular aging. In turn, this could lead to the possibility of discovering novel targets for therapeutic use, which would ultimately attenuate age-related diseases and disorders by modulating the dynamic crosstalk between mitochondria, peroxisomes and other cellular compartments.

9 References

1. McBride, H. M., Neuspiel, M. & Wasiak, S. Mitochondria: More Than Just a Powerhouse. *Current Biology* **16,** R551–R560 (2006).
2. Breitenbach, M. *et al.* The role of mitochondria in the aging processes of yeast. *Subcell. Biochem.* **57,** 55–78 (2012).
3. Nunnari, J. & Suomalainen, A. Mitochondria: in sickness and in health. *Cell* **148,** 1145–1159 (2012).
4. Vafai, S. B. & Mootha, V. K. Mitochondrial disorders as windows into an ancient organelle. *Nature* **491,** 374–383 (2012).
5. Pagliarini, D. J. & Rutter, J. Hallmarks of a new era in mitochondrial biochemistry. *Genes Dev.* **27,** 2615–2627 (2013).
6. Lane, N. *Power, sex, suicide: mitochondria and the meaning of life*. (Oxford University Press, 2006).
7. Hill, B. G. *et al.* Integration of cellular bioenergetics with mitochondrial quality control and autophagy. *Biol. Chem.* **393,** 1485–1512 (2012).
8. Huang, H. & Frohman, M. A. Lipid signaling on the mitochondrial surface. *Biochim. Biophys. Acta* **1791,** 839–844 (2009).
9. Westermann, B. Mitochondrial fusion and fission in cell life and death. *Nat. Rev. Mol. Cell Biol.* **11,** 872–884 (2010).
10. Green, D. R., Galluzzi, L. & Kroemer, G. Mitochondria and the autophagy-inflammation-cell death axis in organismal aging. *Science* **333,** 1109–1112 (2011).
11. Collins, Y. *et al.* Mitochondrial redox signalling at a glance. *J. Cell. Sci.* **125,** 801–806 (2012).

12. Galluzzi, L., Kepp, O. & Kroemer, G. Mitochondria: master regulators of danger signalling. *Nat. Rev. Mol. Cell Biol.* **13,** 780–788 (2012).

13. Galluzzi, L., Kepp, O., Trojel-Hansen, C. & Kroemer, G. Non-apoptotic functions of apoptosis-regulatory proteins. *EMBO Rep.* **13,** 322–330 (2012).

14. Gao, Q. & Frohman, M. A. Roles for the lipid-signaling enzyme MitoPLD in mitochondrial dynamics, piRNA biogenesis, and spermatogenesis. *BMB Rep* **45,** 7–13 (2012).

15. Perier, C. & Vila, M. Mitochondrial biology and Parkinson's disease. *Cold Spring Harb Perspect Med* **2,** a009332 (2012).

16. Tait, S. W. G. & Green, D. R. Mitochondria and cell signalling. *J. Cell. Sci.* **125,** 807–815 (2012).

17. Andersen, J. L. & Kornbluth, S. The tangled circuitry of metabolism and apoptosis. *Mol. Cell* **49,** 399–410 (2013).

18. Leonov, A. & Titorenko, V. I. A network of interorganellar communications underlies cellular aging. *IUBMB Life* **65,** 665–674 (2013).

19. Arlia-Ciommo, A., Leonov, A., Piano, A., Svistkova, V. & Titorenko, V. Cell-autonomous mechanisms of chronological aging in the yeast Saccharomyces cerevisiae. *Microbial Cell* **1,** 163–178 (2014).

20. Arlia-Ciommo, A., Piano, A., Leonov, A., Svistkova, V. & Titorenko, V. I. Quasi-programmed aging of budding yeast: a trade-off between programmed processes of cell proliferation, differentiation, stress response, survival and death defines yeast lifespan. *Cell Cycle* **13,** 3336–3349 (2014).

21. Chandel, N. S. Mitochondria as signaling organelles. *BMC Biol.* **12,** 34 (2014).

22. Friedman, J. R. & Nunnari, J. Mitochondrial form and function. *Nature* **505,** 335–343

(2014).

23. Green, D. R., Galluzzi, L. & Kroemer, G. Cell biology. Metabolic control of cell death. *Science* **345,** 1250256 (2014).
24. Kasahara, A. & Scorrano, L. Mitochondria: from cell death executioners to regulators of cell differentiation. *Trends Cell Biol.* **24,** 761–770 (2014).
25. Kaufman, R. J. & Malhotra, J. D. Calcium trafficking integrates endoplasmic reticulum function with mitochondrial bioenergetics. *Biochim. Biophys. Acta* **1843,** 2233–2239 (2014).
26. Labbé, K., Murley, A. & Nunnari, J. Determinants and functions of mitochondrial behavior. *Annu. Rev. Cell Dev. Biol.* **30,** 357–391 (2014).
27. Naon, D. & Scorrano, L. At the right distance: ER-mitochondria juxtaposition in cell life and death. *Biochim. Biophys. Acta* **1843,** 2184–2194 (2014).
28. Van Vliet, A. R., Verfaillie, T. & Agostinis, P. New functions of mitochondria associated membranes in cellular signaling. *Biochim. Biophys. Acta* **1843,** 2253–2262 (2014).
29. Finley, L. W. S. & Haigis, M. C. The coordination of nuclear and mitochondrial communication during aging and calorie restriction. *Ageing Res. Rev.* **8,** 173–188 (2009).
30. Anderson, K. A. & Hirschey, M. D. Mitochondrial protein acetylation regulates metabolism. *Essays Biochem.* **52,** 23–35 (2012).
31. He, W., Newman, J. C., Wang, M. Z., Ho, L. & Verdin, E. Mitochondrial sirtuins: regulators of protein acylation and metabolism. *Trends Endocrinol. Metab.* **23,** 467–476 (2012).
32. Sack, M. N. & Finkel, T. Mitochondrial metabolism, sirtuins, and aging. *Cold Spring Harb Perspect Biol* **4,** (2012).

33. Wellen, K. E. & Thompson, C. B. A two-way street: reciprocal regulation of metabolism and signalling. *Nat. Rev. Mol. Cell Biol.* **13,** 270–276 (2012).

34. Andreux, P. A., Houtkooper, R. H. & Auwerx, J. Pharmacological approaches to restore mitochondrial function. *Nat Rev Drug Discov* **12,** 465–483 (2013).

35. Kaelin, W. G. & McKnight, S. L. Influence of metabolism on epigenetics and disease. *Cell* **153,** 56–69 (2013).

36. Burkewitz, K., Zhang, Y. & Mair, W. B. AMPK at the nexus of energetics and aging. *Cell Metab.* **20,** 10–25 (2014).

37. Cerutti, R. *et al.* NAD(+)-dependent activation of Sirt1 corrects the phenotype in a mouse model of mitochondrial disease. *Cell Metab.* **19,** 1042–1049 (2014).

38. Eisenberg, T. *et al.* Nucleocytosolic depletion of the energy metabolite acetyl-coenzyme a stimulates autophagy and prolongs lifespan. *Cell Metab.* **19,** 431–444 (2014).

39. Giorgio, M., Trinei, M., Migliaccio, E. & Pelicci, P. G. Hydrogen peroxide: a metabolic by-product or a common mediator of ageing signals? *Nat. Rev. Mol. Cell Biol.* **8,** 722–728 (2007).

40. Dai, D.-F., Chiao, Y. A., Marcinek, D. J., Szeto, H. H. & Rabinovitch, P. S. Mitochondrial oxidative stress in aging and healthspan. *Longev Healthspan* **3,** 6 (2014).

41. Stuart, J. A., Maddalena, L. A., Merilovich, M. & Robb, E. L. A midlife crisis for the mitochondrial free radical theory of aging. *Longev Healthspan* **3,** 4 (2014).

42. Sena, L. A. & Chandel, N. S. Physiological roles of mitochondrial reactive oxygen species. *Mol. Cell* **48,** 158–167 (2012).

43. Schieber, M. & Chandel, N. S. ROS function in redox signaling and oxidative stress. *Curr. Biol.* **24,** R453–462 (2014).

44. Hekimi, S., Lapointe, J. & Wen, Y. Taking a 'good' look at free radicals in the aging process. *Trends Cell Biol.* **21,** 569–576 (2011).

45. Ray, P. D., Huang, B.-W. & Tsuji, Y. Reactive oxygen species (ROS) homeostasis and redox regulation in cellular signaling. *Cell. Signal.* **24,** 981–990 (2012).

46. Kawagishi, H. & Finkel, T. Unraveling the truth about antioxidants: ROS and disease: finding the right balance. *Nat. Med.* **20,** 711–713 (2014).

47. Ristow, M. Unraveling the truth about antioxidants: mitohormesis explains ROS-induced health benefits. *Nat. Med.* **20,** 709–711 (2014).

48. Schroeder, E. A. & Shadel, G. S. Alternative mitochondrial fuel extends life span. *Cell Metab.* **15,** 417–418 (2012).

49. Hwang, A. B. *et al.* Feedback regulation via AMPK and HIF-1 mediates ROS-dependent longevity in Caenorhabditis elegans. *Proc. Natl. Acad. Sci. U.S.A.* **111,** E4458–4467 (2014).

50. Schieber, M. & Chandel, N. S. TOR signaling couples oxygen sensing to lifespan in C. elegans. *Cell Rep* **9,** 9–15 (2014).

51. Xu, S. & Chisholm, A. D. C. elegans epidermal wounding induces a mitochondrial ROS burst that promotes wound repair. *Dev. Cell* **31,** 48–60 (2014).

52. Yee, C., Yang, W. & Hekimi, S. The intrinsic apoptosis pathway mediates the pro-longevity response to mitochondrial ROS in C. elegans. *Cell* **157,** 897–909 (2014).

53. Yun, J. & Finkel, T. Mitohormesis. *Cell Metab.* **19,** 757–766 (2014).

54. Lill, R. & Mühlenhoff, U. Maturation of iron-sulfur proteins in eukaryotes: mechanisms, connected processes, and diseases. *Annu. Rev. Biochem.* **77,** 669–700 (2008).

55. Sheftel, A., Stehling, O. & Lill, R. Iron-sulfur proteins in health and disease. *Trends*

Endocrinol. Metab. **21,** 302–314 (2010).

56. Xu, X. M. & Møller, S. G. Iron-sulfur clusters: biogenesis, molecular mechanisms, and their functional significance. *Antioxid. Redox Signal.* **15,** 271–307 (2011).
57. Lill, R. *et al.* The role of mitochondria in cellular iron-sulfur protein biogenesis and iron metabolism. *Biochim. Biophys. Acta* **1823,** 1491–1508 (2012).
58. Beilschmidt, L. K. & Puccio, H. M. Mammalian Fe-S cluster biogenesis and its implication in disease. *Biochimie* **100,** 48–60 (2014).
59. Stehling, O., Wilbrecht, C. & Lill, R. Mitochondrial iron-sulfur protein biogenesis and human disease. *Biochimie* **100,** 61–77 (2014).
60. Veatch, J. R., McMurray, M. A., Nelson, Z. W. & Gottschling, D. E. Mitochondrial dysfunction leads to nuclear genome instability via an iron-sulfur cluster defect. *Cell* **137,** 1247–1258 (2009).
61. Gari, K. *et al.* MMS19 links cytoplasmic iron-sulfur cluster assembly to DNA metabolism. *Science* **337,** 243–245 (2012).
62. Gottschling, D. E. Molecular biology. Fragile delivery to the genome. *Science* **337,** 160–161 (2012).
63. Stehling, O. *et al.* MMS19 assembles iron-sulfur proteins required for DNA metabolism and genomic integrity. *Science* **337,** 195–199 (2012).
64. Haynes, C. M. & Ron, D. The mitochondrial UPR - protecting organelle protein homeostasis. *J. Cell. Sci.* **123,** 3849–3855 (2010).
65. Haynes, C. M., Yang, Y., Blais, S. P., Neubert, T. A. & Ron, D. The matrix peptide exporter HAF-1 signals a mitochondrial UPR by activating the transcription factor ZC376.7 in C. elegans. *Mol. Cell* **37,** 529–540 (2010).

66. Kirstein-Miles, J. & Morimoto, R. I. Peptides signal mitochondrial stress. *Cell Metab.* **11,** 177–178 (2010).

67. Baker, B. M. & Haynes, C. M. Mitochondrial protein quality control during biogenesis and aging. *Trends Biochem. Sci.* **36,** 254–261 (2011).

68. Nargund, A. M., Pellegrino, M. W., Fiorese, C. J., Baker, B. M. & Haynes, C. M. Mitochondrial import efficiency of ATFS-1 regulates mitochondrial UPR activation. *Science* **337,** 587–590 (2012).

69. Vögtle, F.-N. & Meisinger, C. Sensing mitochondrial homeostasis: the protein import machinery takes control. *Dev. Cell* **23,** 234–236 (2012).

70. Haynes, C. M., Fiorese, C. J. & Lin, Y.-F. Evaluating and responding to mitochondrial dysfunction: the mitochondrial unfolded-protein response and beyond. *Trends Cell Biol.* **23,** 311–318 (2013).

71. Pellegrino, M. W., Nargund, A. M. & Haynes, C. M. Signaling the mitochondrial unfolded protein response. *Biochim. Biophys. Acta* **1833,** 410–416 (2013).

72. Hill, S. & Van Remmen, H. Mitochondrial stress signaling in longevity: a new role for mitochondrial function in aging. *Redox Biol* **2,** 936–944 (2014).

73. Mottis, A., Jovaisaite, V. & Auwerx, J. The mitochondrial unfolded protein response in mammalian physiology. *Mamm. Genome* **25,** 424–433 (2014).

74. Hashimoto, Y. *et al.* A rescue factor abolishing neuronal cell death by a wide spectrum of familial Alzheimer's disease genes and Abeta. *Proc. Natl. Acad. Sci. U.S.A.* **98,** 6336–6341 (2001).

75. Tajima, H. *et al.* Evidence for in vivo production of Humanin peptide, a neuroprotective factor against Alzheimer's disease-related insults. *Neurosci. Lett.* **324,** 227–231 (2002).

76. Guo, B. *et al.* Humanin peptide suppresses apoptosis by interfering with Bax activation. *Nature* **423,** 456–461 (2003).

77. Ikonen, M. *et al.* Interaction between the Alzheimer's survival peptide humanin and insulin-like growth factor-binding protein 3 regulates cell survival and apoptosis. *Proc. Natl. Acad. Sci. U.S.A.* **100,** 13042–13047 (2003).

78. Harada, M. *et al.* N-Formylated humanin activates both formyl peptide receptor-like 1 and 2. *Biochem. Biophys. Res. Commun.* **324,** 255–261 (2004).

79. Zhai, D. *et al.* Humanin binds and nullifies Bid activity by blocking its activation of Bax and Bak. *J. Biol. Chem.* **280,** 15815–15824 (2005).

80. Lee, C., Yen, K. & Cohen, P. Humanin: a harbinger of mitochondrial-derived peptides? *Trends Endocrinol. Metab.* **24,** 222–228 (2013).

81. Yen, K., Lee, C., Mehta, H. & Cohen, P. The emerging role of the mitochondrial-derived peptide humanin in stress resistance. *J. Mol. Endocrinol.* **50,** R11–19 (2013).

82. Rabiet, M.-J., Huet, E. & Boulay, F. Human mitochondria-derived N-formylated peptides are novel agonists equally active on FPR and FPRL1, while Listeria monocytogenes-derived peptides preferentially activate FPR. *Eur. J. Immunol.* **35,** 2486–2495 (2005).

83. Hauser, C. J. *et al.* Mitochondrial damage associated molecular patterns from femoral reamings activate neutrophils through formyl peptide receptors and P44/42 MAP kinase. *J Orthop Trauma* **24,** 534–538 (2010).

84. Raoof, M., Zhang, Q., Itagaki, K. & Hauser, C. J. Mitochondrial peptides are potent immune activators that activate human neutrophils via FPR-1. *J Trauma* **68,** 1328–1332; discussion 1332–1334 (2010).

85. Zhang, Q. *et al.* Circulating mitochondrial DAMPs cause inflammatory responses to injury.

Nature **464,** 104–107 (2010).

86. Nakahira, K. *et al.* Autophagy proteins regulate innate immune responses by inhibiting the release of mitochondrial DNA mediated by the NALP3 inflammasome. *Nat. Immunol.* **12,** 222–230 (2011).

87. Tschopp, J. Mitochondria: Sovereign of inflammation? *Eur. J. Immunol.* **41,** 1196–1202 (2011).

88. Mathew, A. *et al.* Degraded mitochondrial DNA is a newly identified subtype of the damage associated molecular pattern (DAMP) family and possible trigger of neurodegeneration. *J. Alzheimers Dis.* **30,** 617–627 (2012).

89. Sun, S. *et al.* Mitochondrial DAMPs increase endothelial permeability through neutrophil dependent and independent pathways. *PLoS ONE* **8,** e59989 (2013).

90. Sutendra, G. *et al.* A nuclear pyruvate dehydrogenase complex is important for the generation of acetyl-CoA and histone acetylation. *Cell* **158,** 84–97 (2014).

91. Durieux, J., Wolff, S. & Dillin, A. The cell-non-autonomous nature of electron transport chain-mediated longevity. *Cell* **144,** 79–91 (2011).

92. Taylor, R. C., Berendzen, K. M. & Dillin, A. Systemic stress signalling: understanding the cell non-autonomous control of proteostasis. *Nat. Rev. Mol. Cell Biol.* **15,** 211–217 (2014).

93. Esseltine, J. L. & Scott, J. D. AKAP signaling complexes: pointing towards the next generation of therapeutic targets? *Trends Pharmacol. Sci.* **34,** 648–655 (2013).

94. Koshiba, T. Mitochondrial-mediated antiviral immunity. *Biochim. Biophys. Acta* **1833,** 225–232 (2013).

95. Taylor, S. S., Zhang, P., Steichen, J. M., Keshwani, M. M. & Kornev, A. P. PKA: lessons learned after twenty years. *Biochim. Biophys. Acta* **1834,** 1271–1278 (2013).

96. Giménez-Cassina, A. *et al.* Regulation of hepatic energy metabolism and gluconeogenesis by BAD. *Cell Metab.* **19,** 272–284 (2014).

97. Liu, L., Sakakibara, K., Chen, Q. & Okamoto, K. Receptor-mediated mitophagy in yeast and mammalian systems. *Cell Res.* **24,** 787–795 (2014).

98. Pourcelot, M. & Arnoult, D. Mitochondrial dynamics and the innate antiviral immune response. *FEBS J.* **281,** 3791–3802 (2014).

99. Westermann, B. Mitochondrial inheritance in yeast. *Biochim. Biophys. Acta* **1837,** 1039–1046 (2014).

100. Rowland, A. A. & Voeltz, G. K. Endoplasmic reticulum-mitochondria contacts: function of the junction. *Nat. Rev. Mol. Cell Biol.* **13,** 607–625 (2012).

101. Helle, S. C. J. *et al.* Organization and function of membrane contact sites. *Biochim. Biophys. Acta* **1833,** 2526–2541 (2013).

102. Kornmann, B. The molecular hug between the ER and the mitochondria. *Curr. Opin. Cell Biol.* **25,** 443–448 (2013).

103. Daniele, T. & Schiaffino, M. V. Organelle biogenesis and interorganellar connections: Better in contact than in isolation. *Commun Integr Biol* **7,** e29587 (2014).

104. Elbaz-Alon, Y. *et al.* A dynamic interface between vacuoles and mitochondria in yeast. *Dev. Cell* **30,** 95–102 (2014).

105. Hönscher, C. *et al.* Cellular metabolism regulates contact sites between vacuoles and mitochondria. *Dev. Cell* **30,** 86–94 (2014).

106. Klecker, T., Böckler, S. & Westermann, B. Making connections: interorganelle contacts orchestrate mitochondrial behavior. *Trends Cell Biol.* **24,** 537–545 (2014).

107. Marchi, S., Patergnani, S. & Pinton, P. The endoplasmic reticulum-mitochondria

connection: one touch, multiple functions. *Biochim. Biophys. Acta* **1837,** 461–469 (2014).

108. Prinz, W. A. Bridging the gap: membrane contact sites in signaling, metabolism, and organelle dynamics. *J. Cell Biol.* **205,** 759–769 (2014).
109. Van der Laan, M., Bohnert, M., Wiedemann, N. & Pfanner, N. Role of MINOS in mitochondrial membrane architecture and biogenesis. *Trends Cell Biol.* **22,** 185–192 (2012).
110. Hamasaki, M. *et al.* Autophagosomes form at ER-mitochondria contact sites. *Nature* **495,** 389–393 (2013).
111. Böckler, S. & Westermann, B. Mitochondrial ER contacts are crucial for mitophagy in yeast. *Dev. Cell* **28,** 450–458 (2014).
112. Lahiri, S. *et al.* A conserved endoplasmic reticulum membrane protein complex (EMC) facilitates phospholipid transfer from the ER to mitochondria. *PLoS Biol.* **12,** e1001969 (2014).
113. Schlattner, U. *et al.* Mitochondrial cardiolipin/phospholipid trafficking: the role of membrane contact site complexes and lipid transfer proteins. *Chem. Phys. Lipids* **179,** 32–41 (2014).
114. Tamura, Y., Sesaki, H. & Endo, T. Phospholipid transport via mitochondria. *Traffic* **15,** 933–945 (2014).
115. Tatsuta, T., Scharwey, M. & Langer, T. Mitochondrial lipid trafficking. *Trends Cell Biol.* **24,** 44–52 (2014).
116. Neuspiel, M. *et al.* Cargo-selected transport from the mitochondria to peroxisomes is mediated by vesicular carriers. *Curr. Biol.* **18,** 102–108 (2008).
117. Braschi, E. *et al.* Vps35 mediates vesicle transport between the mitochondria and

peroxisomes. *Curr. Biol.* **20,** 1310–1315 (2010).

118. Soubannier, V. *et al.* A vesicular transport pathway shuttles cargo from mitochondria to lysosomes. *Curr. Biol.* **22,** 135–141 (2012).

119. Soubannier, V., Rippstein, P., Kaufman, B. A., Shoubridge, E. A. & McBride, H. M. Reconstitution of mitochondria derived vesicle formation demonstrates selective enrichment of oxidized cargo. *PLoS ONE* **7,** e52830 (2012).

120. Mohanty, A. & McBride, H. M. Emerging roles of mitochondria in the evolution, biogenesis, and function of peroxisomes. *Front Physiol* **4,** 268 (2013).

121. Sugiura, A., McLelland, G.-L., Fon, E. A. & McBride, H. M. A new pathway for mitochondrial quality control: mitochondrial-derived vesicles. *EMBO J.* **33,** 2142–2156 (2014).

122. Calvo, S. E. & Mootha, V. K. The mitochondrial proteome and human disease. *Annu Rev Genomics Hum Genet* **11,** 25–44 (2010).

123. Koopman, W. J. H., Willems, P. H. G. M. & Smeitink, J. A. M. Monogenic mitochondrial disorders. *N. Engl. J. Med.* **366,** 1132–1141 (2012).

124. Schiff, M., Bénit, P., Jacobs, H. T., Vockley, J. & Rustin, P. Therapies in inborn errors of oxidative metabolism. *Trends Endocrinol. Metab.* **23,** 488–495 (2012).

125. Ylikallio, E. & Suomalainen, A. Mechanisms of mitochondrial diseases. *Ann. Med.* **44,** 41–59 (2012).

126. Lin, M. T. & Beal, M. F. Mitochondrial dysfunction and oxidative stress in neurodegenerative diseases. *Nature* **443,** 787–795 (2006).

127. Fulda, S., Galluzzi, L. & Kroemer, G. Targeting mitochondria for cancer therapy. *Nat Rev Drug Discov* **9,** 447–464 (2010).

128. Szendroedi, J., Phielix, E. & Roden, M. The role of mitochondria in insulin resistance and type 2 diabetes mellitus. *Nat Rev Endocrinol* **8,** 92–103 (2012).

129. Costa, V. & Scorrano, L. Shaping the role of mitochondria in the pathogenesis of Huntington's disease. *EMBO J.* **31,** 1853–1864 (2012).

130. Wallace, D. C. Mitochondria and cancer. *Nat. Rev. Cancer* **12,** 685–698 (2012).

131. Olszewska, A. & Szewczyk, A. Mitochondria as a pharmacological target: magnum overview. *IUBMB Life* **65,** 273–281 (2013).

132. Bratic, A. & Larsson, N.-G. The role of mitochondria in aging. *J. Clin. Invest.* **123,** 951–957 (2013).

133. López-Otín, C., Blasco, M. A., Partridge, L., Serrano, M. & Kroemer, G. The hallmarks of aging. *Cell* **153,** 1194–1217 (2013).

134. Barros, M. H., da Cunha, F. M., Oliveira, G. A., Tahara, E. B. & Kowaltowski, A. J. Yeast as a model to study mitochondrial mechanisms in ageing. *Mech. Ageing Dev.* **131,** 494–502 (2010).

135. Pan, Y. Mitochondria, reactive oxygen species, and chronological aging: a message from yeast. *Exp. Gerontol.* **46,** 847–852 (2011).

136. Jazwinski, S. M. The Retrograde Response and Other Pathways of Interorganelle Communication in Yeast Replicative Aging. *Subcell. Biochem.* **57,** 79–100 (2012).

137. Longo, V. D., Shadel, G. S., Kaeberlein, M. & Kennedy, B. Replicative and chronological aging in Saccharomyces cerevisiae. *Cell Metab.* **16,** 18–31 (2012).

138. Jazwinski, S. M. The retrograde response: when mitochondrial quality control is not enough. *Biochim. Biophys. Acta* **1833,** 400–409 (2013).

139. Burstein, M. T. & Titorenko, V. I. A mitochondrially targeted compound delays aging in

yeast through a mechanism linking mitochondrial membrane lipid metabolism to mitochondrial redox biology. *Redox Biol* **2,** 305–307 (2014).

140. Mirisola, M. G. & Longo, V. D. A radical signal activates the epigenetic regulation of longevity. *Cell Metab.* **17,** 812–813 (2013).
141. Steinkraus, K. A., Kaeberlein, M. & Kennedy, B. K. Replicative aging in yeast: the means to the end. *Annu. Rev. Cell Dev. Biol.* **24,** 29–54 (2008).
142. Steffen, K. K., Kennedy, B. K. & Kaeberlein, M. Measuring replicative life span in the budding yeast. *J Vis Exp* (2009). doi:10.3791/1209
143. Kaeberlein, M. Lessons on longevity from budding yeast. *Nature* **464,** 513–519 (2010).
144. Denoth Lippuner, A., Julou, T. & Barral, Y. Budding yeast as a model organism to study the effects of age. *FEMS Microbiol. Rev.* **38,** 300–325 (2014).
145. Goldberg, A. A. *et al.* Effect of calorie restriction on the metabolic history of chronologically aging yeast. *Exp. Gerontol.* **44,** 555–571 (2009).
146. Longo, V. D. & Fabrizio, P. Chronological Aging in Saccharomyces cerevisiae. *Subcell. Biochem.* **57,** 101–121 (2012).
147. Piper, P. W. Maximising the yeast chronological lifespan. *Subcell. Biochem.* **57,** 145–159 (2012).
148. Weissman, J., Guthrie, C. & Fink, G. R. *Guide to yeast genetics: functional genomics, proteomics, and other systems analysis*. (Elsevier/Academic, 2010).
149. Botstein, D. & Fink, G. R. Yeast: an experimental organism for 21st Century biology. *Genetics* **189,** 695–704 (2011).
150. Sutphin, G. L., Olsen, B. A., Kennedy, B. K. & Kaeberlein, M. Genome-wide analysis of yeast aging. *Subcell. Biochem.* **57,** 251–289 (2012).

151. Richard, V. R., Bourque, S. D. & Titorenko, V. I. Metabolomic and lipidomic analyses of chronologically aging yeast. *Methods Mol. Biol.* **1205,** 359–373 (2014).

152. Eisenberg, T. *et al.* Induction of autophagy by spermidine promotes longevity. *Nat. Cell Biol.* **11,** 1305–1314 (2009).

153. Goldberg, A. A. *et al.* A novel function of lipid droplets in regulating longevity. *Biochem. Soc. Trans.* **37,** 1050–1055 (2009).

154. Fontana, L., Partridge, L. & Longo, V. D. Extending healthy life span--from yeast to humans. *Science* **328,** 321–326 (2010).

155. Goldberg, A. A. *et al.* Chemical genetic screen identifies lithocholic acid as an anti-aging compound that extends yeast chronological life span in a TOR-independent manner, by modulating housekeeping longevity assurance processes. *Aging (Albany NY)* **2,** 393–414 (2010).

156. Kapahi, P. *et al.* With TOR, less is more: a key role for the conserved nutrient-sensing TOR pathway in aging. *Cell Metab.* **11,** 453–465 (2010).

157. Titorenko, V. I. & Terlecky, S. R. Peroxisome metabolism and cellular aging. *Traffic* **12,** 252–259 (2011).

158. Beach, A. *et al.* Integration of peroxisomes into an endomembrane system that governs cellular aging. *Front Physiol* **3,** 283 (2012).

159. Beach, A. & Titorenko, V. I. Essential roles of peroxisomally produced and metabolized biomolecules in regulating yeast longevity. *Subcell. Biochem.* **69,** 153–167 (2013).

160. De Cabo, R., Carmona-Gutierrez, D., Bernier, M., Hall, M. N. & Madeo, F. The search for antiaging interventions: from elixirs to fasting regimens. *Cell* **157,** 1515–1526 (2014).

161. Nyström, T. & Liu, B. Protein quality control in time and space - links to cellular aging.

FEMS Yeast Res. **14,** 40–48 (2014).

162. Sinclair, D. A. & Guarente, L. Small-molecule allosteric activators of sirtuins. *Annu. Rev. Pharmacol. Toxicol.* **54,** 363–380 (2014).
163. Hughes, A. L. & Gottschling, D. E. An early age increase in vacuolar pH limits mitochondrial function and lifespan in yeast. *Nature* **492,** 261–265 (2012).
164. Jazwinski, S. M. & Kriete, A. The yeast retrograde response as a model of intracellular signaling of mitochondrial dysfunction. *Front Physiol* **3,** 139 (2012).
165. McFaline-Figueroa, J. R. *et al.* Mitochondrial quality control during inheritance is associated with lifespan and mother-daughter age asymmetry in budding yeast. *Aging Cell* **10,** 885–895 (2011).
166. Fehrmann, S. *et al.* Aging yeast cells undergo a sharp entry into senescence unrelated to the loss of mitochondrial membrane potential. *Cell Rep* **5,** 1589–1599 (2013).
167. Knorre, D. A., Popadin, K. Y., Sokolov, S. S. & Severin, F. F. Roles of mitochondrial dynamics under stressful and normal conditions in yeast cells. *Oxid Med Cell Longev* **2013,** 139491 (2013).
168. Faculty of Bioengineering and Bioinformatics, Moscow State University, Vorobyevy Gory 1, Moscow, Russia *et al.* Early manifestations of replicative aging in the yeast Saccharomyces cerevisiae. *Microbial Cell* **1,** 37–42 (2014).
169. Higuchi, R. *et al.* Actin dynamics affect mitochondrial quality control and aging in budding yeast. *Curr. Biol.* **23,** 2417–2422 (2013).
170. Nyström, T. & Liu, B. The mystery of aging and rejuvenation - a budding topic. *Curr. Opin. Microbiol.* **18,** 61–67 (2014).
171. Vevea, J. D., Swayne, T. C., Boldogh, I. R. & Pon, L. A. Inheritance of the fittest

mitochondria in yeast. *Trends Cell Biol.* **24,** 53–60 (2014).

172. Heeren, G. *et al.* The mitochondrial ribosomal protein of the large subunit, Afo1p, determines cellular longevity through mitochondrial back-signaling via TOR1. *Aging (Albany NY)* **1,** 622–636 (2009).
173. Chen, X. J. The search for nonconventional mitochondrial determinants of aging. *Mol. Cell* **42,** 271–273 (2011).
174. Perocchi, F. *et al.* Assessing systems properties of yeast mitochondria through an interaction map of the organelle. *PLoS Genet.* **2,** e170 (2006).
175. Merz, S. & Westermann, B. Genome-wide deletion mutant analysis reveals genes required for respiratory growth, mitochondrial genome maintenance and mitochondrial protein synthesis in Saccharomyces cerevisiae. *Genome Biol.* **10,** R95 (2009).
176. Caballero, A. *et al.* Absence of mitochondrial translation control proteins extends life span by activating sirtuin-dependent silencing. *Mol. Cell* **42,** 390–400 (2011).
177. Yang, J.-S. *et al.* Spatial and functional organization of mitochondrial protein network. *Sci Rep* **3,** 1403 (2013).
178. Koppen, M. & Langer, T. Protein degradation within mitochondria: versatile activities of AAA proteases and other peptidases. *Crit. Rev. Biochem. Mol. Biol.* **42,** 221–242 (2007).
179. Baker, M. J., Tatsuta, T. & Langer, T. Quality control of mitochondrial proteostasis. *Cold Spring Harb Perspect Biol* **3,** (2011).
180. Delaney, J. R. *et al.* Stress profiling of longevity mutants identifies Afg3 as a mitochondrial determinant of cytoplasmic mRNA translation and aging. *Aging Cell* **12,** 156–166 (2013).
181. Kissová, I., Deffieu, M., Manon, S. & Camougrand, N. Uth1p is involved in the autophagic degradation of mitochondria. *J. Biol. Chem.* **279,** 39068–39074 (2004).

182. Bhatia-Kiššová, I. & Camougrand, N. Mitophagy in yeast: actors and physiological roles. *FEMS Yeast Res.* **10,** 1023–1034 (2010).

183. Welter, E. *et al.* Uth1 is a mitochondrial inner membrane protein dispensable for post-log-phase and rapamycin-induced mitophagy. *FEBS J.* **280,** 4970–4982 (2013).

184. Burstein, M. T. *et al.* Lithocholic acid extends longevity of chronologically aging yeast only if added at certain critical periods of their lifespan. *Cell Cycle* **11,** 3443–3462 (2012).

185. Bonawitz, N. D., Chatenay-Lapointe, M., Pan, Y. & Shadel, G. S. Reduced TOR signaling extends chronological life span via increased respiration and upregulation of mitochondrial gene expression. *Cell Metab.* **5,** 265–277 (2007).

186. Pan, Y. & Shadel, G. S. Extension of chronological life span by reduced TOR signaling requires down-regulation of Sch9p and involves increased mitochondrial OXPHOS complex density. *Aging (Albany NY)* **1,** 131–145 (2009).

187. Pan, Y., Schroeder, E. A., Ocampo, A., Barrientos, A. & Shadel, G. S. Regulation of yeast chronological life span by TORC1 via adaptive mitochondrial ROS signaling. *Cell Metab.* **13,** 668–678 (2011).

188. Ocampo, A., Liu, J., Schroeder, E. A., Shadel, G. S. & Barrientos, A. Mitochondrial respiratory thresholds regulate yeast chronological life span and its extension by caloric restriction. *Cell Metab.* **16,** 55–67 (2012).

189. Fraenkel, D. G. *Yeast intermediary metabolism*. (Cold Spring Harbor Laboratory Press, 2011).

190. Cai, L. & Tu, B. P. Driving the cell cycle through metabolism. *Annu. Rev. Cell Dev. Biol.* **28,** 59–87 (2012).

191. Brandes, N. *et al.* Time line of redox events in aging postmitotic cells. *Elife* **2,** e00306

(2013).

192. Kyryakov, P. *et al.* Caloric restriction extends yeast chronological lifespan by altering a pattern of age-related changes in trehalose concentration. *Front Physiol* **3,** 256 (2012).

193. Beach, A. *et al.* Mitochondrial membrane lipidome defines yeast longevity. *Aging (Albany NY)* **5,** 551–574 (2013).

194. Schroeder, E. A., Raimundo, N. & Shadel, G. S. Epigenetic silencing mediates mitochondria stress-induced longevity. *Cell Metab.* **17,** 954–964 (2013).

195. Schroeder, E. A. & Shadel, G. S. Crosstalk between mitochondrial stress signals regulates yeast chronological lifespan. *Mech. Ageing Dev.* **135,** 41–49 (2014).

196. Broach, J. R. Nutritional control of growth and development in yeast. *Genetics* **192,** 73–105 (2012).

197. De Virgilio, C. The essence of yeast quiescence. *FEMS Microbiol. Rev.* **36,** 306–339 (2012).

198. Crespo, J. L., Powers, T., Fowler, B. & Hall, M. N. The TOR-controlled transcription activators GLN3, RTG1, and RTG3 are regulated in response to intracellular levels of glutamine. *Proc. Natl. Acad. Sci. U.S.A.* **99,** 6784–6789 (2002).

199. Powers, R. W., Kaeberlein, M., Caldwell, S. D., Kennedy, B. K. & Fields, S. Extension of chronological life span in yeast by decreased TOR pathway signaling. *Genes Dev.* **20,** 174–184 (2006).

200. Jewell, J. L., Russell, R. C. & Guan, K.-L. Amino acid signalling upstream of mTOR. *Nat. Rev. Mol. Cell Biol.* **14,** 133–139 (2013).

201. Conrad, M. *et al.* Nutrient sensing and signaling in the yeast Saccharomyces cerevisiae. *FEMS Microbiol. Rev.* **38,** 254–299 (2014).

202. Shimobayashi, M. & Hall, M. N. Making new contacts: the mTOR network in metabolism and signalling crosstalk. *Nat. Rev. Mol. Cell Biol.* **15,** 155–162 (2014).

203. Swinnen, E., Ghillebert, R., Wilms, T. & Winderickx, J. Molecular mechanisms linking the evolutionary conserved TORC1-Sch9 nutrient signalling branch to lifespan regulation in Saccharomyces cerevisiae. *FEMS Yeast Res.* **14,** 17–32 (2014).

204. Wissing, S. *et al.* An AIF orthologue regulates apoptosis in yeast. *J. Cell Biol.* **166,** 969–974 (2004).

205. Büttner, S. *et al.* Endonuclease G regulates budding yeast life and death. *Mol. Cell* **25,** 233–246 (2007).

206. Eisenberg, T., Büttner, S., Kroemer, G. & Madeo, F. The mitochondrial pathway in yeast apoptosis. *Apoptosis* **12,** 1011–1023 (2007).

207. Pereira, C. *et al.* Mitochondria-dependent apoptosis in yeast. *Biochim. Biophys. Acta* **1783,** 1286–1302 (2008).

208. Madeo, F. *et al.* Caspase-dependent and caspase-independent cell death pathways in yeast. *Biochem. Biophys. Res. Commun.* **382,** 227–231 (2009).

209. Carmona-Gutierrez, D. *et al.* Apoptosis in yeast: triggers, pathways, subroutines. *Cell Death Differ.* **17,** 763–773 (2010).

210. Sheibani, S. *et al.* Macromitophagy, neutral lipids synthesis, and peroxisomal fatty acid oxidation protect yeast from 'liponecrosis', a previously unknown form of programmed cell death. *Cell Cycle* **13,** 138–147 (2014).

211. Richard, V. R. *et al.* Mechanism of liponecrosis, a distinct mode of programmed cell death. *Cell Cycle* **13,** 3707–3726 (2014).

212. Kanki, T., Wang, K., Cao, Y., Baba, M. & Klionsky, D. J. Atg32 is a mitochondrial protein

that confers selectivity during mitophagy. *Dev. Cell* **17,** 98–109 (2009).

213. Okamoto, K., Kondo-Okamoto, N. & Ohsumi, Y. Mitochondria-anchored receptor Atg32 mediates degradation of mitochondria via selective autophagy. *Dev. Cell* **17,** 87–97 (2009).
214. Beach, A. & Titorenko, V. I. In search of housekeeping pathways that regulate longevity. *Cell Cycle* **10,** 3042–3044 (2011).
215. Richard, V. R. *et al.* Macromitophagy is a longevity assurance process that in chronologically aging yeast limited in calorie supply sustains functional mitochondria and maintains cellular lipid homeostasis. *Aging (Albany NY)* **5,** 234–269 (2013).
216. Cheng, X. & Ivessa, A. S. The migration of mitochondrial DNA fragments to the nucleus affects the chronological aging process of Saccharomyces cerevisiae. *Aging Cell* **9,** 919–923 (2010).
217. Cheng, X. & Ivessa, A. S. Accumulation of linear mitochondrial DNA fragments in the nucleus shortens the chronological life span of yeast. *Eur. J. Cell Biol.* **91,** 782–788 (2012).
218. Arlia-Ciommo, A., Piano, A., Svistkova, V., Mohtashami, S. & Titorenko, V. I. Mechanisms underlying the anti-aging and anti-tumor effects of lithocholic bile acid. *Int J Mol Sci* **15,** 16522–16543 (2014).
219. Beach, A. *et al.* Lithocholic bile acid accumulated in yeast mitochondria orchestrates a development of an anti-aging cellular pattern by causing age-related changes in cellular proteome. *Cell Cycle* **Submitted,** (2015).
220. Bourque, S. D. & Titorenko, V. I. A quantitative assessment of the yeast lipidome using electrospray ionization mass spectrometry. *J Vis Exp* (2009). doi:10.3791/1513
221. Richard, V. R. *et al.* Macromitophagy is a longevity assurance process that in chronologically aging yeast limited in calorie supply sustains functional mitochondria and

maintains cellular lipid homeostasis. *Aging (Albany NY)* **5,** 234–269 (2013).

222. Rieder, S. E. & Emr, S. D. Isolation of subcellular fractions from the yeast Saccharomyces cerevisiae. *Curr Protoc Cell Biol* **Chapter 3,** Unit 3.8 (2001).

223. Gregg, C., Kyryakov, P. & Titorenko, V. I. Purification of mitochondria from yeast cells. *J Vis Exp* (2009). doi:10.3791/1417

224. Wiley, S. E., Rardin, M. J. & Dixon, J. E. Chapter 13 Localization and function of the 2Fe-2S outer mitochondrial membrane protein mitoNEET. *Meth. Enzymol.* **456,** 233–246 (2009).

225. Gurtovenko, A. A. & Anwar, J. Modulating the structure and properties of cell membranes: the molecular mechanism of action of dimethyl sulfoxide. *J Phys Chem B* **111,** 10453–10460 (2007).

226. Goldberg, A. A. *et al.* Lithocholic bile acid selectively kills neuroblastoma cells, while sparing normal neuronal cells. *Oncotarget* **2,** 761–782 (2011).

227. Osman, C., Voelker, D. R. & Langer, T. Making heads or tails of phospholipids in mitochondria. *J. Cell Biol.* **192,** 7–16 (2011).

228. Böttinger, L. *et al.* Phosphatidylethanolamine and cardiolipin differentially affect the stability of mitochondrial respiratory chain supercomplexes. *J. Mol. Biol.* **423,** 677–686 (2012).

229. Claypool, S. M. & Koehler, C. M. The complexity of cardiolipin in health and disease. *Trends Biochem. Sci.* **37,** 32–41 (2012).

230. Titorenko, V. I., Smith, J. J., Szilard, R. K. & Rachubinski, R. A. Pex20p of the yeast Yarrowia lipolytica is required for the oligomerization of thiolase in the cytosol and for its targeting to the peroxisome. *J. Cell Biol.* **142,** 403–420 (1998).

231. Szilard, R. K., Titorenko, V. I., Veenhuis, M. & Rachubinski, R. A. Pay32p of the yeast Yarrowia lipolytica is an intraperoxisomal component of the matrix protein translocation machinery. *J. Cell Biol.* **131,** 1453–1469 (1995).

232. Fabrizio, P. *et al.* SOD2 functions downstream of Sch9 to extend longevity in yeast. *Genetics* **163,** 35–46 (2003).

233. Lin, S. S., Manchester, J. K. & Gordon, J. I. Enhanced gluconeogenesis and increased energy storage as hallmarks of aging in Saccharomyces cerevisiae. *J. Biol. Chem.* **276,** 36000–36007 (2001).

234. Gómez, L. A. & Hagen, T. M. Age-related decline in mitochondrial bioenergetics: does supercomplex destabilization determine lower oxidative capacity and higher superoxide production? *Semin. Cell Dev. Biol.* **23,** 758–767 (2012).

235. Vonck, J. & Schäfer, E. Supramolecular organization of protein complexes in the mitochondrial inner membrane. *Biochim. Biophys. Acta* **1793,** 117–124 (2009).

236. Lenaz, G. & Genova, M. L. Structure and organization of mitochondrial respiratory complexes: a new understanding of an old subject. *Antioxid. Redox Signal.* **12,** 961–1008 (2010).

237. Lenaz, G. & Genova, M. L. Supramolecular organisation of the mitochondrial respiratory chain: a new challenge for the mechanism and control of oxidative phosphorylation. *Adv. Exp. Med. Biol.* **748,** 107–144 (2012).

238. Wittig, I., Braun, H.-P. & Schägger, H. Blue native PAGE. *Nat Protoc* **1,** 418–428 (2006).

239. Nicholls, D. Mitochondrial bioenergetics, aging, and aging-related disease. *Sci Aging Knowledge Environ* **2002,** pe12 (2002).

240. Newmeyer, D. D. & Ferguson-Miller, S. Mitochondria: releasing power for life and

unleashing the machineries of death. *Cell* **112,** 481–490 (2003).

241. Balaban, R. S., Nemoto, S. & Finkel, T. Mitochondria, oxidants, and aging. *Cell* **120,** 483–495 (2005).

242. Storz, P. Mitochondrial ROS--radical detoxification, mediated by protein kinase D. *Trends Cell Biol.* **17,** 13–18 (2007).

243. D'Autréaux, B. & Toledano, M. B. ROS as signalling molecules: mechanisms that generate specificity in ROS homeostasis. *Nat. Rev. Mol. Cell Biol.* **8,** 813–824 (2007).

244. Rattan, S. I. S. Hormesis in aging. *Ageing Res. Rev.* **7,** 63–78 (2008).

245. Shevchenko, A. *et al.* Linking genome and proteome by mass spectrometry: large-scale identification of yeast proteins from two dimensional gels. *Proc. Natl. Acad. Sci. U.S.A.* **93,** 14440–14445 (1996).

246. Jiménez, C. R., Huang, L., Qiu, Y. & Burlingame, A. L. Searching sequence databases over the internet: protein identification using MS-Fit. *Curr Protoc Protein Sci* **Chapter 16,** Unit 16.5 (2001).

247. Costanzo, M. C. *et al.* New mutant phenotype data curation system in the Saccharomyces Genome Database. *Database (Oxford)* **2009,** bap001 (2009).

248. Aris, J. P. *et al.* Amino Acid Homeostasis and Chronological Longevity in Saccharomyces cerevisiae. *Subcell. Biochem.* **57,** 161–186 (2012).

249. Ljungdahl, P. O. & Daignan-Fornier, B. Regulation of amino acid, nucleotide, and phosphate metabolism in Saccharomyces cerevisiae. *Genetics* **190,** 885–929 (2012).

250. Fox, T. D. Mitochondrial protein synthesis, import, and assembly. *Genetics* **192,** 1203–1234 (2012).

251. Soto, I. C., Fontanesi, F., Liu, J. & Barrientos, A. Biogenesis and assembly of eukaryotic

cytochrome c oxidase catalytic core. *Biochim. Biophys. Acta* **1817,** 883–897 (2012).

252. Rodríguez-Manzaneque, M. T., Tamarit, J., Bellí, G., Ros, J. & Herrero, E. Grx5 is a mitochondrial glutaredoxin required for the activity of iron/sulfur enzymes. *Mol. Biol. Cell* **13,** 1109–1121 (2002).
253. Strand, M. K. *et al.* POS5 gene of Saccharomyces cerevisiae encodes a mitochondrial NADH kinase required for stability of mitochondrial DNA. *Eukaryotic Cell* **2,** 809–820 (2003).
254. Murray, D. B., Haynes, K. & Tomita, M. Redox regulation in respiring Saccharomyces cerevisiae. *Biochim. Biophys. Acta* **1810,** 945–958 (2011).
255. Dudek, J., Rehling, P. & van der Laan, M. Mitochondrial protein import: common principles and physiological networks. *Biochim. Biophys. Acta* **1833,** 274–285 (2013).
256. Pareek, G., Krishnamoorthy, V. & D'Silva, P. Molecular insights revealing interaction of Tim23 and channel subunits of presequence translocase. *Mol. Cell. Biol.* **33,** 4641–4659 (2013).
257. Hibbs, M. A. *et al.* Exploring the functional landscape of gene expression: directed search of large microarray compendia. *Bioinformatics* **23,** 2692–2699 (2007).
258. Hughes, T. R. *et al.* Functional discovery via a compendium of expression profiles. *Cell* **102,** 109–126 (2000).
259. Traven, A., Wong, J. M., Xu, D., Sopta, M. & Ingles, C. J. Interorganellar communication. Altered nuclear gene expression profiles in a yeast mitochondrial dna mutant. *J. Biol. Chem.* **276,** 4020–4027 (2001).
260. McCammon, M. T., Epstein, C. B., Przybyla-Zawislak, B., McAlister-Henn, L. & Butow, R. A. Global transcription analysis of Krebs tricarboxylic acid cycle mutants reveals an

alternating pattern of gene expression and effects on hypoxic and oxidative genes. *Mol. Biol. Cell* **14,** 958–972 (2003).

261. Arnold, I., Wagner-Ecker, M., Ansorge, W. & Langer, T. Evidence for a novel mitochondria-to-nucleus signalling pathway in respiring cells lacking i-AAA protease and the ABC-transporter Mdl1. *Gene* **367,** 74–88 (2006).
262. Jazwinski, S. M. The Retrograde ResponseRetrograde Response and Other Pathways of Interorganelle CommunicationInterorganelle Communication in Yeast Replicative Aging. *Subcell. Biochem.* **57,** 79–100 (2012).
263. Lee, J. *et al.* Yap1 and Skn7 control two specialized oxidative stress response regulons in yeast. *J. Biol. Chem.* **274,** 16040–16046 (1999).
264. Temple, M. D., Perrone, G. G. & Dawes, I. W. Complex cellular responses to reactive oxygen species. *Trends Cell Biol.* **15,** 319–326 (2005).
265. Brombacher, K., Fischer, B. B., Rüfenacht, K. & Eggen, R. I. L. The role of Yap1p and Skn7p-mediated oxidative stress response in the defence of Saccharomyces cerevisiae against singlet oxygen. *Yeast* **23,** 741–750 (2006).
266. Rodrigues-Pousada, C., Menezes, R. A. & Pimentel, C. The Yap family and its role in stress response. *Yeast* **27,** 245–258 (2010).
267. Aung-Htut, M. T., Ayer, A., Breitenbach, M. & Dawes, I. W. Oxidative stresses and ageing. *Subcell. Biochem.* **57,** 13–54 (2012).
268. Morano, K. A., Grant, C. M. & Moye-Rowley, W. S. The response to heat shock and oxidative stress in Saccharomyces cerevisiae. *Genetics* **190,** 1157–1195 (2012).
269. Engelberg, D., Perlman, R. & Levitzki, A. Transmembrane signaling in Saccharomyces cerevisiae as a model for signaling in metazoans: state of the art after 25 years. *Cell. Signal.*

26, 2865–2878 (2014).

270. Galdieri, L., Mehrotra, S., Yu, S. & Vancura, A. Transcriptional regulation in yeast during diauxic shift and stationary phase. *OMICS* **14,** 629–638 (2010).

271. Barbosa, A. D. *et al.* Activation of the Hog1p kinase in Isc1p-deficient yeast cells is associated with mitochondrial dysfunction, oxidative stress sensitivity and premature aging. *Mech. Ageing Dev.* **133,** 317–330 (2012).

272. Brewster, J. L. & Gustin, M. C. Hog1: 20 years of discovery and impact. *Sci Signal* **7,** re7 (2014).

273. Horvath, S. E. & Daum, G. Lipids of mitochondria. *Prog. Lipid Res.* **52,** 590–614 (2013).

274. Schlattner, U. *et al.* Mitochondrial cardiolipin/phospholipid trafficking: the role of membrane contact site complexes and lipid transfer proteins. *Chem. Phys. Lipids* **179,** 32–41 (2014).

275. Tamura, Y., Sesaki, H. & Endo, T. Phospholipid transport via mitochondria. *Traffic* **15,** 933–945 (2014).

276. Tatsuta, T., Scharwey, M. & Langer, T. Mitochondrial lipid trafficking. *Trends Cell Biol.* **24,** 44–52 (2014).

277. Yen, W.-L. & Klionsky, D. J. How to live long and prosper: autophagy, mitochondria, and aging. *Physiology (Bethesda)* **23,** 248–262 (2008).

278. Kanki, T., Klionsky, D. J. & Okamoto, K. Mitochondria autophagy in yeast. *Antioxid. Redox Signal.* **14,** 1989–2001 (2011).

279. Youle, R. J. & Narendra, D. P. Mechanisms of mitophagy. *Nat. Rev. Mol. Cell Biol.* **12,** 9–14 (2011).

280. Hirota, Y., Kang, D. & Kanki, T. The physiological role of mitophagy: new insights into

phosphorylation events. *Int J Cell Biol* **2012,** 354914 (2012).

281. Lee, J., Giordano, S. & Zhang, J. Autophagy, mitochondria and oxidative stress: cross-talk and redox signalling. *Biochem. J.* **441,** 523–540 (2012).
282. Claypool, S. M., Oktay, Y., Boontheung, P., Loo, J. A. & Koehler, C. M. Cardiolipin defines the interactome of the major ADP/ATP carrier protein of the mitochondrial inner membrane. *J. Cell Biol.* **182,** 937–950 (2008).
283. Li, Z. & Graham, B. H. Measurement of mitochondrial oxygen consumption using a Clark electrode. *Methods Mol. Biol.* **837,** 63–72 (2012).
284. Schägger, H. & Pfeiffer, K. Supercomplexes in the respiratory chains of yeast and mammalian mitochondria. *EMBO J.* **19,** 1777–1783 (2000).
285. Stroh, A. *et al.* Assembly of respiratory complexes I, III, and IV into NADH oxidase supercomplex stabilizes complex I in Paracoccus denitrificans. *J. Biol. Chem.* **279,** 5000–5007 (2004).
286. Krause, F. *et al.* Supramolecular organization of cytochrome c oxidase- and alternative oxidase-dependent respiratory chains in the filamentous fungus Podospora anserina. *J. Biol. Chem.* **279,** 26453–26461 (2004).
287. Barrientos, A. In vivo and in organello assessment of OXPHOS activities. *Methods* **26,** 307–316 (2002).
288. Fontanesi, F., Diaz, F. & Barrientos, A. Evaluation of the mitochondrial respiratory chain and oxidative phosphorylation system using yeast models of OXPHOS deficiencies. *Curr Protoc Hum Genet* **Chapter 19,** Unit19.5 (2009).
289. Guo, T. *et al.* A signal from inside the peroxisome initiates its division by promoting the remodeling of the peroxisomal membrane. *J. Cell Biol.* **177,** 289–303 (2007).

290. Motley, A. M., Nuttall, J. M. & Hettema, E. H. Pex3-anchored Atg36 tags peroxisomes for degradation in Saccharomyces cerevisiae. *EMBO J.* **31,** 2852–2868 (2012).

291. Barros, M. H., Bandy, B., Tahara, E. B. & Kowaltowski, A. J. Higher respiratory activity decreases mitochondrial reactive oxygen release and increases life span in Saccharomyces cerevisiae. *J. Biol. Chem.* **279,** 49883–49888 (2004).

292. Bonawitz, N. D., Rodeheffer, M. S. & Shadel, G. S. Defective mitochondrial gene expression results in reactive oxygen species-mediated inhibition of respiration and reduction of yeast life span. *Mol. Cell. Biol.* **26,** 4818–4829 (2006).

293. Bonawitz, N. D. & Shadel, G. S. Rethinking the mitochondrial theory of aging: the role of mitochondrial gene expression in lifespan determination. *Cell Cycle* **6,** 1574–1578 (2007).

294. Masoro, E. J. *Caloric restriction a key to understanding and modulating aging*. (Elsevier, 2002). at <http://site.ebrary.com/id/10190339>

295. Mair, W. & Dillin, A. Aging and survival: the genetics of life span extension by dietary restriction. *Annu. Rev. Biochem.* **77,** 727–754 (2008).

296. Colman, R. J. *et al.* Caloric restriction delays disease onset and mortality in rhesus monkeys. *Science* **325,** 201–204 (2009).

297. Fabrizio, P. & Wei, M. Conserved role of medium acidification in chronological senescence of yeast and mammalian cells. *Aging (Albany NY)* **3,** 1127–1129 (2011).

298. Leontieva, O. V. & Blagosklonny, M. V. Yeast-like chronological senescence in mammalian cells: phenomenon, mechanism and pharmacological suppression. *Aging (Albany NY)* **3,** 1078–1091 (2011).

299. Liao, C.-Y., Rikke, B. A., Johnson, T. E., Diaz, V. & Nelson, J. F. Genetic variation in the murine lifespan response to dietary restriction: from life extension to life shortening. *Aging*

Cell **9,** 92–95 (2010).

300. Mattison, J. A. *et al.* Impact of caloric restriction on health and survival in rhesus monkeys from the NIA study. *Nature* **489,** 318–321 (2012).
301. Barrientos, A. Complementary roles of mitochondrial respiration and ROS signaling on cellular aging and longevity. *Aging (Albany NY)* **4,** 578–579 (2012).
302. Vandenabeele, P., Galluzzi, L., Vanden Berghe, T. & Kroemer, G. Molecular mechanisms of necroptosis: an ordered cellular explosion. *Nat. Rev. Mol. Cell Biol.* **11,** 700–714 (2010).
303. Eisenberg, T., Carmona-Gutierrez, D., Büttner, S., Tavernarakis, N. & Madeo, F. Necrosis in yeast. *Apoptosis* **15,** 257–268 (2010).
304. Graef, M. & Nunnari, J. Mitochondria regulate autophagy by conserved signalling pathways. *EMBO J.* **30,** 2101–2114 (2011).
305. Yorimitsu, T., Zaman, S., Broach, J. R. & Klionsky, D. J. Protein kinase A and Sch9 cooperatively regulate induction of autophagy in Saccharomyces cerevisiae. *Mol. Biol. Cell* **18,** 4180–4189 (2007).
306. Stephan, J. S., Yeh, Y.-Y., Ramachandran, V., Deminoff, S. J. & Herman, P. K. The Tor and PKA signaling pathways independently target the Atg1/Atg13 protein kinase complex to control autophagy. *Proc. Natl. Acad. Sci. U.S.A.* **106,** 17049–17054 (2009).
307. Smets, B. *et al.* Life in the midst of scarcity: adaptations to nutrient availability in Saccharomyces cerevisiae. *Curr. Genet.* **56,** 1–32 (2010).
308. Medvedik, O., Lamming, D. W., Kim, K. D. & Sinclair, D. A. MSN2 and MSN4 link calorie restriction and TOR to sirtuin-mediated lifespan extension in Saccharomyces cerevisiae. *PLoS Biol.* **5,** e261 (2007).
309. Aoki, Y. *et al.* Phosphorylation of Serine 114 on Atg32 mediates mitophagy. *Mol. Biol.*

Cell **22,** 3206–3217 (2011).

310. Mao, K., Wang, K., Zhao, M., Xu, T. & Klionsky, D. J. Two MAPK-signaling pathways are required for mitophagy in Saccharomyces cerevisiae. *J. Cell Biol.* **193,** 755–767 (2011).
311. Poirier, Y., Antonenkov, V. D., Glumoff, T. & Hiltunen, J. K. Peroxisomal beta-oxidation--a metabolic pathway with multiple functions. *Biochim. Biophys. Acta* **1763,** 1413–1426 (2006).
312. Wanders, R. J. A. & Waterham, H. R. Biochemistry of mammalian peroxisomes revisited. *Annu. Rev. Biochem.* **75,** 295–332 (2006).
313. Schlüter, A., Real-Chicharro, A., Gabaldón, T., Sánchez-Jiménez, F. & Pujol, A. PeroxisomeDB 2.0: an integrative view of the global peroxisomal metabolome. *Nucleic Acids Res.* **38,** D800–805 (2010).
314. Desvergne, B. & Wahli, W. Peroxisome proliferator-activated receptors: nuclear control of metabolism. *Endocr. Rev.* **20,** 649–688 (1999).
315. Corpas, F. J., Barroso, J. B. & del Río, L. A. Peroxisomes as a source of reactive oxygen species and nitric oxide signal molecules in plant cells. *Trends Plant Sci.* **6,** 145–150 (2001).
316. Del Río, L. A., Sandalio, L. M., Corpas, F. J., Palma, J. M. & Barroso, J. B. Reactive oxygen species and reactive nitrogen species in peroxisomes. Production, scavenging, and role in cell signaling. *Plant Physiol.* **141,** 330–335 (2006).
317. Nyathi, Y. & Baker, A. Plant peroxisomes as a source of signalling molecules. *Biochim. Biophys. Acta* **1763,** 1478–1495 (2006).
318. Kersten, S., Desvergne, B. & Wahli, W. Roles of PPARs in health and disease. *Nature* **405,** 421–424 (2000).

319. Desikan, R., A-H-Mackerness, S., Hancock, J. T. & Neill, S. J. Regulation of the Arabidopsis transcriptome by oxidative stress. *Plant Physiol.* **127,** 159–172 (2001).

320. Hu, J. *et al.* A role for peroxisomes in photomorphogenesis and development of Arabidopsis. *Science* **297,** 405–409 (2002).

321. Ma, L. *et al.* Genomic evidence for COP1 as a repressor of light-regulated gene expression and development in Arabidopsis. *Plant Cell* **14,** 2383–2398 (2002).

322. Michalik, L. *et al.* PPAR expression and function during vertebrate development. *Int. J. Dev. Biol.* **46,** 105–114 (2002).

323. Baker, A., Graham, I. A., Holdsworth, M., Smith, S. M. & Theodoulou, F. L. Chewing the fat: beta-oxidation in signalling and development. *Trends Plant Sci.* **11,** 124–132 (2006).

324. Michalik, L. & Wahli, W. Involvement of PPAR nuclear receptors in tissue injury and wound repair. *J. Clin. Invest.* **116,** 598–606 (2006).

325. Bonekamp, N. A., Völkl, A., Fahimi, H. D. & Schrader, M. Reactive oxygen species and peroxisomes: struggling for balance. *Biofactors* **35,** 346–355 (2009).

326. Antonenkov, V. D., Grunau, S., Ohlmeier, S. & Hiltunen, J. K. Peroxisomes are oxidative organelles. *Antioxid. Redox Signal.* **13,** 525–537 (2010).

327. Ivashchenko, O. *et al.* Intraperoxisomal redox balance in mammalian cells: oxidative stress and interorganellar cross-talk. *Mol. Biol. Cell* **22,** 1440–1451 (2011).

328. Li, A. *et al.* Transcriptome analysis of H2O2-treated wheat seedlings reveals a H2O2-responsive fatty acid desaturase gene participating in powdery mildew resistance. *PLoS ONE* **6,** e28810 (2011).

329. Neher, M. D., Weckbach, S., Huber-Lang, M. S. & Stahel, P. F. New insights into the role of peroxisome proliferator-activated receptors in regulating the inflammatory response after

tissue injury. *PPAR Res* **2012,** 728461 (2012).

330. Titorenko, V. I. & Rachubinski, R. A. The peroxisome: orchestrating important developmental decisions from inside the cell. *J. Cell Biol.* **164,** 641–645 (2004).
331. Terlecky, S. R. & Titorenko, V. I. *Emergent Functions of the Peroxisome*. (Research Signpost, 2009).
332. Thoms, S., Grønborg, S. & Gärtner, J. Organelle interplay in peroxisomal disorders. *Trends Mol Med* **15,** 293–302 (2009).
333. Dixit, E. *et al.* Peroxisomes are signaling platforms for antiviral innate immunity. *Cell* **141,** 668–681 (2010).
334. Powers, J. M. & Moser, H. W. Peroxisomal disorders: genotype, phenotype, major neuropathologic lesions, and pathogenesis. *Brain Pathol.* **8,** 101–120 (1998).
335. Motley, A. M., Hettema, E. H., Ketting, R., Plasterk, R. & Tabak, H. F. Caenorhabditis elegans has a single pathway to target matrix proteins to peroxisomes. *EMBO Rep.* **1,** 40–46 (2000).
336. Thines, E., Weber, R. W. & Talbot, N. J. MAP kinase and protein kinase A-dependent mobilization of triacylglycerol and glycogen during appressorium turgor generation by Magnaporthe grisea. *Plant Cell* **12,** 1703–1718 (2000).
337. Gould, S. G., Valle, D. & Raymond, G. V. in *The Metabolic and Molecular Bases of Inherited Disease* 3181–3217 (McGraw-Hill, 2001).
338. Kimura, A., Takano, Y., Furusawa, I. & Okuno, T. Peroxisomal metabolic function is required for appressorium-mediated plant infection by Colletotrichum lagenarium. *Plant Cell* **13,** 1945–1957 (2001).
339. Petriv, O. I., Pilgrim, D. B., Rachubinski, R. A. & Titorenko, V. I. RNA interference of

peroxisome-related genes in C. elegans: a new model for human peroxisomal disorders. *Physiol. Genomics* **10,** 79–91 (2002).

340. Wang, Z.-Y. *et al.* The molecular biology of appressorium turgor generation by the rice blast fungus Magnaporthe grisea. *Biochem. Soc. Trans.* **33,** 384–388 (2005).
341. Asakura, M., Okuno, T. & Takano, Y. Multiple contributions of peroxisomal metabolic function to fungal pathogenicity in Colletotrichum lagenarium. *Appl. Environ. Microbiol.* **72,** 6345–6354 (2006).
342. Imazaki, A. *et al.* Contribution of peroxisomes to secondary metabolism and pathogenicity in the fungal plant pathogen Alternaria alternata. *Eukaryotic Cell* **9,** 682–694 (2010).
343. Van Veldhoven, P. P. Biochemistry and genetics of inherited disorders of peroxisomal fatty acid metabolism. *J. Lipid Res.* **51,** 2863–2895 (2010).
344. Goh, J. *et al.* The PEX7-mediated peroxisomal import system is required for fungal development and pathogenicity in Magnaporthe oryzae. *PLoS ONE* **6,** e28220 (2011).
345. Mast, F. D. *et al.* A Drosophila model for the Zellweger spectrum of peroxisome biogenesis disorders. *Dis Model Mech* **4,** 659–672 (2011).
346. Bhadauria, V., Banniza, S., Vandenberg, A., Selvaraj, G. & Wei, Y. Peroxisomal alanine: glyoxylate aminotransferase AGT1 is indispensable for appressorium function of the rice blast pathogen, Magnaporthe oryzae. *PLoS ONE* **7,** e36266 (2012).
347. Titorenko, V. I., Ogrydziak, D. M. & Rachubinski, R. A. Four distinct secretory pathways serve protein secretion, cell surface growth, and peroxisome biogenesis in the yeast Yarrowia lipolytica. *Mol. Cell. Biol.* **17,** 5210–5226 (1997).
348. Titorenko, V. I. & Rachubinski, R. A. Mutants of the yeast Yarrowia lipolytica defective in protein exit from the endoplasmic reticulum are also defective in peroxisome biogenesis.

Mol. Cell. Biol. **18,** 2789–2803 (1998).

349. Lin, Y., Sun, L., Nguyen, L. V., Rachubinski, R. A. & Goodman, H. M. The Pex16p homolog SSE1 and storage organelle formation in Arabidopsis seeds. *Science* **284,** 328–330 (1999).

350. Footitt, S. *et al.* Control of germination and lipid mobilization by COMATOSE, the Arabidopsis homologue of human ALDP. *EMBO J.* **21,** 2912–2922 (2002).

351. Gavva, N. R. *et al.* NAPP2, a peroxisomal membrane protein, is also a transcriptional corepressor. *Genomics* **79,** 423–431 (2002).

352. Geuze, H. J. *et al.* Involvement of the endoplasmic reticulum in peroxisome formation. *Mol. Biol. Cell* **14,** 2900–2907 (2003).

353. Lin, Y., Cluette-Brown, J. E. & Goodman, H. M. The peroxisome deficient Arabidopsis mutant sse1 exhibits impaired fatty acid synthesis. *Plant Physiol.* **135,** 814–827 (2004).

354. Slabas, A. R., Ndimba, B., Simon, W. J. & Chivasa, S. Proteomic analysis of the Arabidopsis cell wall reveals unexpected proteins with new cellular locations. *Biochem. Soc. Trans.* **32,** 524–528 (2004).

355. Karnik, S. K. & Trelease, R. N. Arabidopsis peroxin 16 coexists at steady state in peroxisomes and endoplasmic reticulum. *Plant Physiol.* **138,** 1967–1981 (2005).

356. Ashibe, B., Hirai, T., Higashi, K., Sekimizu, K. & Motojima, K. Dual subcellular localization in the endoplasmic reticulum and peroxisomes and a vital role in protecting against oxidative stress of fatty aldehyde dehydrogenase are achieved by alternative splicing. *J. Biol. Chem.* **282,** 20763–20773 (2007).

357. Freitag, J., Ast, J. & Bölker, M. Cryptic peroxisomal targeting via alternative splicing and stop codon read-through in fungi. *Nature* **485,** 522–525 (2012).

358. Jedd, G. & Chua, N. H. A new self-assembled peroxisomal vesicle required for efficient resealing of the plasma membrane. *Nat. Cell Biol.* **2,** 226–231 (2000).

359. Tenney, K. *et al.* Hex-1, a gene unique to filamentous fungi, encodes the major protein of the Woronin body and functions as a plug for septal pores. *Fungal Genet. Biol.* **31,** 205–217 (2000).

360. Liu, F. *et al.* Making two organelles from one: Woronin body biogenesis by peroxisomal protein sorting. *J. Cell Biol.* **180,** 325–339 (2008).

361. Escaño, C. S. *et al.* Disruption of the Aopex11-1 gene involved in peroxisome proliferation leads to impaired Woronin body formation in Aspergillus oryzae. *Eukaryotic Cell* **8,** 296–305 (2009).

362. Jedd, G. Fungal evo-devo: organelles and multicellular complexity. *Trends Cell Biol.* **21,** 12–19 (2011).

363. Liu, F., Lu, Y., Pieuchot, L., Dhavale, T. & Jedd, G. Import oligomers induce positive feedback to promote peroxisome differentiation and control organelle abundance. *Dev. Cell* **21,** 457–468 (2011).

364. Cohen, G. B., Rangan, V. S., Chen, B. K., Smith, S. & Baltimore, D. The human thioesterase II protein binds to a site on HIV-1 Nef critical for CD4 down-regulation. *J. Biol. Chem.* **275,** 23097–23105 (2000).

365. Mohan, K. V. K., Som, I. & Atreya, C. D. Identification of a type 1 peroxisomal targeting signal in a viral protein and demonstration of its targeting to the organelle. *J. Virol.* **76,** 2543–2547 (2002).

366. Spitaler, M. & Cantrell, D. A. Protein kinase C and beyond. *Nat. Immunol.* **5,** 785–790 (2004).

367. Low, C. P., Liew, L. P., Pervaiz, S. & Yang, H. Apoptosis and lipoapoptosis in the fission yeast Schizosaccharomyces pombe. *FEMS Yeast Res.* **5,** 1199–1206 (2005).

368. Feng, H., Ren, M., Chen, L. & Rubin, C. S. Properties, regulation, and in vivo functions of a novel protein kinase D: Caenorhabditis elegans DKF-2 links diacylglycerol second messenger to the regulation of stress responses and life span. *J. Biol. Chem.* **282,** 31273–31288 (2007).

369. Bener Aksam, E. *et al.* Absence of the peroxiredoxin Pmp20 causes peroxisomal protein leakage and necrotic cell death. *Free Radic. Biol. Med.* **45,** 1115–1124 (2008).

370. Jungwirth, H. *et al.* Loss of peroxisome function triggers necrosis. *FEBS Lett.* **582,** 2882–2886 (2008).

371. Chelstowska, A. & Butow, R. A. RTG genes in yeast that function in communication between mitochondria and the nucleus are also required for expression of genes encoding peroxisomal proteins. *J. Biol. Chem.* **270,** 18141–18146 (1995).

372. Kos, W., Kal, A. J., van Wilpe, S. & Tabak, H. F. Expression of genes encoding peroxisomal proteins in Saccharomyces cerevisiae is regulated by different circuits of transcriptional control. *Biochim. Biophys. Acta* **1264,** 79–86 (1995).

373. Epstein, C. B. *et al.* Genome-wide responses to mitochondrial dysfunction. *Mol. Biol. Cell* **12,** 297–308 (2001).

374. Jazwinski, S. M. The retrograde response links metabolism with stress responses, chromatin-dependent gene activation, and genome stability in yeast aging. *Gene* **354,** 22–27 (2005).

375. Liu, Z. & Butow, R. A. Mitochondrial retrograde signaling. *Annu. Rev. Genet.* **40,** 159–185 (2006).

376. Morita, M. *et al.* Insulin-degrading enzyme exists inside of rat liver peroxisomes and degrades oxidized proteins. *Cell Struct. Funct.* **25,** 309–315 (2000).

377. Legakis, J. E. *et al.* Peroxisome senescence in human fibroblasts. *Mol. Biol. Cell* **13,** 4243–4255 (2002).

378. Aksam, E. B. *et al.* A peroxisomal lon protease and peroxisome degradation by autophagy play key roles in vitality of Hansenula polymorpha cells. *Autophagy* **3,** 96–105 (2007).

379. Koepke, J. I., Wood, C. S., Terlecky, L. J., Walton, P. A. & Terlecky, S. R. Progeric effects of catalase inactivation in human cells. *Toxicol. Appl. Pharmacol.* **232,** 99–108 (2008).

380. Aksam, E. B., de Vries, B., van der Klei, I. J. & Kiel, J. A. K. W. Preserving organelle vitality: peroxisomal quality control mechanisms in yeast. *FEMS Yeast Res.* **9,** 808–820 (2009).

381. Lingard, M. J., Monroe-Augustus, M. & Bartel, B. Peroxisome-associated matrix protein degradation in Arabidopsis. *Proc. Natl. Acad. Sci. U.S.A.* **106,** 4561–4566 (2009).

382. Mathur, J. Rapid peroxisomal responses to ROS suggest an alternative mechanistic model for post-biogenesis peroxisomal life cycle in plants. *Plant Signal Behav* **4,** 787–789 (2009).

383. Sinclair, A. M., Trobacher, C. P., Mathur, N., Greenwood, J. S. & Mathur, J. Peroxule extension over ER-defined paths constitutes a rapid subcellular response to hydroxyl stress. *Plant J.* **59,** 231–242 (2009).

384. Ghislain, M., Talla, E. & François, J. M. Identification and functional analysis of the Saccharomyces cerevisiae nicotinamidase gene, PNC1. *Yeast* **19,** 215–224 (2002).

385. Anderson, R. M., Bitterman, K. J., Wood, J. G., Medvedik, O. & Sinclair, D. A. Nicotinamide and PNC1 govern lifespan extension by calorie restriction in Saccharomyces cerevisiae. *Nature* **423,** 181–185 (2003).

386. Gems, D. & Partridge, L. Stress-response hormesis and aging: ‘that which does not kill us makes us stronger’. *Cell Metab.* **7,** 200–203 (2008).

387. Calabrese, V. *et al.* Hormesis, cellular stress response and vitagenes as critical determinants in aging and longevity. *Mol. Aspects Med.* **32,** 279–304 (2011).

388. Calabrese, V. *et al.* Cellular stress responses, hormetic phytochemicals and vitagenes in aging and longevity. *Biochim. Biophys. Acta* **1822,** 753–783 (2012).

389. Su-Ju, L. & Sinclair, D. A. 17 Molecular Mechanisms of Aging: Insights from Budding Yeast. *Cold Spring Harbor Monograph Archive; Molecular Biology of Aging* **51,** 483–516 (2008).

390. Bitterman, K. J., Anderson, R. M., Cohen, H. Y., Latorre-Esteves, M. & Sinclair, D. A. Inhibition of silencing and accelerated aging by nicotinamide, a putative negative regulator of yeast sir2 and human SIRT1. *J. Biol. Chem.* **277,** 45099–45107 (2002).

391. Starai, V. J., Takahashi, H., Boeke, J. D. & Escalante-Semerena, J. C. Short-chain fatty acid activation by acyl-coenzyme A synthetases requires SIR2 protein function in Salmonella enterica and Saccharomyces cerevisiae. *Genetics* **163,** 545–555 (2003).

392. Haigis, M. C. & Guarente, L. P. Mammalian sirtuins--emerging roles in physiology, aging, and calorie restriction. *Genes Dev.* **20,** 2913–2921 (2006).

393. Haigis, M. C. & Sinclair, D. A. Mammalian sirtuins: biological insights and disease relevance. *Annu Rev Pathol* **5,** 253–295 (2010).

394. Kunze, M., Pracharoenwattana, I., Smith, S. M. & Hartig, A. A central role for the peroxisomal membrane in glyoxylate cycle function. *Biochim. Biophys. Acta* **1763,** 1441–1452 (2006).

395. Mast, F. D., Fagarasanu, A., Knoblach, B. & Rachubinski, R. A. Peroxisome biogenesis:

something old, something new, something borrowed. *Physiology (Bethesda)* **25,** 347–356 (2010).

396. Islinger, M., Grille, S., Fahimi, H. D. & Schrader, M. The peroxisome: an update on mysteries. *Histochem. Cell Biol.* **137,** 547–574 (2012).
397. Jeffery, C. J. Moonlighting proteins. *Trends Biochem. Sci.* **24,** 8–11 (1999).
398. Shi, Y. & Shi, Y. Metabolic enzymes and coenzymes in transcription--a direct link between metabolism and transcription? *Trends Genet.* **20,** 445–452 (2004).
399. Kim, J.-W. & Dang, C. V. Multifaceted roles of glycolytic enzymes. *Trends Biochem. Sci.* **30,** 142–150 (2005).
400. Gancedo, C. & Flores, C.-L. Moonlighting proteins in yeasts. *Microbiol. Mol. Biol. Rev.* **72,** 197–210, table of contents (2008).
401. Jeffery, C. J. Moonlighting proteins--an update. *Mol Biosyst* **5,** 345–350 (2009).
402. Flores, C.-L. & Gancedo, C. Unraveling moonlighting functions with yeasts. *IUBMB Life* **63,** 457–462 (2011).
403. Jeffery, C. J. Proteins with neomorphic moonlighting functions in disease. *IUBMB Life* **63,** 489–494 (2011).
404. Cho, Y.-H., Yoo, S.-D. & Sheen, J. Regulatory functions of nuclear hexokinase1 complex in glucose signaling. *Cell* **127,** 579–589 (2006).
405. Sen, N. *et al.* Nitric oxide-induced nuclear GAPDH activates p300/CBP and mediates apoptosis. *Nat. Cell Biol.* **10,** 866–873 (2008).
406. Titorenko, V. I. & Rachubinski, R. A. Spatiotemporal dynamics of the ER-derived peroxisomal endomembrane system. *Int Rev Cell Mol Biol* **272,** 191–244 (2009).
407. Ma, C., Agrawal, G. & Subramani, S. Peroxisome assembly: matrix and membrane protein

biogenesis. *J. Cell Biol.* **193,** 7–16 (2011).

408. Rucktäschel, R., Girzalsky, W. & Erdmann, R. Protein import machineries of peroxisomes. *Biochim. Biophys. Acta* **1808,** 892–900 (2011).

409. Jazwinski, S. M. Yeast longevity and aging--the mitochondrial connection. *Mech. Ageing Dev.* **126,** 243–248 (2005).

410. Erjavec, N., Larsson, L., Grantham, J. & Nyström, T. Accelerated aging and failure to segregate damaged proteins in Sir2 mutants can be suppressed by overproducing the protein aggregation-remodeling factor Hsp104p. *Genes Dev.* **21,** 2410–2421 (2007).

411. Erjavec, N., Cvijovic, M., Klipp, E. & Nyström, T. Selective benefits of damage partitioning in unicellular systems and its effects on aging. *Proc. Natl. Acad. Sci. U.S.A.* **105,** 18764–18769 (2008).

412. Henderson, K. A. & Gottschling, D. E. A mother's sacrifice: what is she keeping for herself? *Curr. Opin. Cell Biol.* **20,** 723–728 (2008).

413. Steinkraus, K. A., Kaeberlein, M. & Kennedy, B. K. Replicative aging in yeast: the means to the end. *Annu. Rev. Cell Dev. Biol.* **24,** 29–54 (2008).

414. Eldakak, A. *et al.* Asymmetrically inherited multidrug resistance transporters are recessive determinants in cellular replicative ageing. *Nat. Cell Biol.* **12,** 799–805 (2010).

415. Liu, B. *et al.* The polarisome is required for segregation and retrograde transport of protein aggregates. *Cell* **140,** 257–267 (2010).

416. Zhou, C. *et al.* Motility and segregation of Hsp104-associated protein aggregates in budding yeast. *Cell* **147,** 1186–1196 (2011).

417. Lai, C.-Y., Jaruga, E., Borghouts, C. & Jazwinski, S. M. A mutation in the ATP2 gene abrogates the age asymmetry between mother and daughter cells of the yeast

Saccharomyces cerevisiae. *Genetics* **162,** 73–87 (2002).

418. Seo, J.-G., Lai, C.-Y., Miceli, M. V. & Jazwinski, S. M. A novel role of peroxin PEX6: suppression of aging defects in mitochondria. *Aging Cell* **6,** 405–413 (2007).

419. Andrade-Navarro, M. A., Sanchez-Pulido, L. & McBride, H. M. Mitochondrial vesicles: an ancient process providing new links to peroxisomes. *Curr. Opin. Cell Biol.* **21,** 560–567 (2009).

420. Delille, H. K., Alves, R. & Schrader, M. Biogenesis of peroxisomes and mitochondria: linked by division. *Histochem. Cell Biol.* **131,** 441–446 (2009).

421. Fagarasanu, A., Fagarasanu, M., Eitzen, G. A., Aitchison, J. D. & Rachubinski, R. A. The peroxisomal membrane protein Inp2p is the peroxisome-specific receptor for the myosin V motor Myo2p of Saccharomyces cerevisiae. *Dev. Cell* **10,** 587–600 (2006).

422. Fagarasanu, A. *et al.* Myosin-driven peroxisome partitioning in S. cerevisiae. *J. Cell Biol.* **186,** 541–554 (2009).

423. Fagarasanu, A., Mast, F. D., Knoblach, B. & Rachubinski, R. A. Molecular mechanisms of organelle inheritance: lessons from peroxisomes in yeast. *Nat. Rev. Mol. Cell Biol.* **11,** 644–654 (2010).

424. Terlecky, S. R., Koepke, J. I. & Walton, P. A. Peroxisomes and aging. *Biochim. Biophys. Acta* **1763,** 1749–1754 (2006).

425. Léon, S. *et al.* Dynamics of the peroxisomal import cycle of PpPex20p: ubiquitin-dependent localization and regulation. *J. Cell Biol.* **172,** 67–78 (2006).

426. Farré, J.-C., Manjithaya, R., Mathewson, R. D. & Subramani, S. PpAtg30 tags peroxisomes for turnover by selective autophagy. *Dev. Cell* **14,** 365–376 (2008).

427. Manjithaya, R., Nazarko, T. Y., Farré, J.-C. & Subramani, S. Molecular mechanism and

physiological role of pexophagy. *FEBS Lett.* **584,** 1367–1373 (2010).

428. Veal, E. A., Day, A. M. & Morgan, B. A. Hydrogen peroxide sensing and signaling. *Mol. Cell* **26,** 1–14 (2007).

429. Hiltunen, J. K. *et al.* The biochemistry of peroxisomal beta-oxidation in the yeast Saccharomyces cerevisiae. *FEMS Microbiol. Rev.* **27,** 35–64 (2003).

430. Goodman, J. M. The gregarious lipid droplet. *J. Biol. Chem.* **283,** 28005–28009 (2008).

431. Kohlwein, S. D. Triacylglycerol homeostasis: insights from yeast. *J. Biol. Chem.* **285,** 15663–15667 (2010).

10 Appendices

10.1 Appendix 1. Relative levels of proteins recovered in mitochondria that were purified from wild-type cells cultured in the nutrient-rich YP medium initially containing 0.2% glucose, with 50 μM LCA or without it

Mitochondria were purified from cells recovered on days 2, 5 and 9 of culturing (D, PD and ST growth phases, respectively) as described in ″Materials and Methods″. Proteins were identified and quantified using MALDI MS peptide mapping as described in ″Materials and Methods″. Relative levels of proteins in mitochondria of cells cultured in the presence of LCA are presented as fold difference relative to those in the absence of LCA (n = 3).

Protein	NCBI accession no.	Function	Protein level	
			LCA concentration (μM)	
			50	0
Day 2 (D phase)				
Aco1p	NP_013407	Mitochondrial TCA cycle; mtDNA binding and protection	4.23 ± 0.38	1
Cit1p	NP_014398	Mitochondrial TCA cycle	3.14 ± 0.25	1
Fum1p	NP_015061	Mitochondrial TCA cycle	0.24 ± 0.09	1
Idh1p	NP_014361	Mitochondrial TCA cycle; mtDNA binding and protection	4.07 ± 0.25	1
Idh2p	NP_014779	Mitochondrial TCA cycle	2.18 ± 0.36	1
Kgd1p	NP_012141	Mitochondrial TCA cycle; mtDNA binding and protection	4.42 ± 0.19	1
Kgd2p	NP_010432	Mitochondrial TCA cycle; mtDNA binding and protection	3.25 ± 0.13	1
Lsc1p	NP_014785	Mitochondrial TCA cycle; mtDNA binding and protection	0.21 ± 0.06	1
Lsc2p	NP_011760	Mitochondrial TCA cycle	0.25 ± 0.11	1
Mdh1p	NP_012838	Mitochondrial TCA cycle	2.39 ± 0.42	1
Sdh1p	NP_012774	Mitochondrial TCA cycle and ETC	0.32 ± 0.27	1
Sdh2p	NP_013059	Mitochondrial TCA cycle and ETC	0.23 ± 0.13	1
Sdh3p	NP_012781	Mitochondrial TCA cycle and ETC	0.39 ± 0.05	1
Sdh4p	NP_010463	Mitochondrial TCA cycle and ETC	0.28 ± 0.07	1
Icl1p	NP_010991	Mitochondrial TCA cycle	3.17 ± 0.34	1
Mls1p	NP_014282	Mitochondrial TCA cycle	3.44 ± 0.22	1
Ald4p	NP_015019	Mitochondrial ETC; mtDNA binding and protection	4.37 ± 0.51	1
Atp1p	NP_009453	Mitochondrial ETC; mtDNA binding and protection	3.32 ± 0.39	1
Atp2p	NP_012655	Mitochondrial ETC	3.64 ± 0.43	1
Atp5p	NP_010584	Mitochondrial ETC	3.09 ± 0.17	1
Atp9p	NP_013816	Mitochondrial ETC	3.71 ± 0.32	1
Cobp	NP_015109	Mitochondrial ETC	4.29 ± 0.48	1
Cor1p	NP_009508	Mitochondrial ETC	2.25 ± 0.23	1
Cox1p	NP_009305	Mitochondrial ETC	4.17 ± 0.38	1
Cox2p	NP_009326	Mitochondrial ETC	4.36 ± 0.46	1
Cox3p	NP_009328	Mitochondrial ETC	3.22 ± 0.19	1
Cox11p	NP_015193	Mitochondrial ETC	3.44 ± 0.32	1
Cox14p	NP_013577	Mitochondrial ETC	3.65 ± 0.21	1

Cyc1p	NP_012582	Mitochondrial ETC	4.49 ± 0.58	1
Gut2p	NP_012111	Mitochondrial ETC	3.09 ± 0.17	1
Nde1p	NP_013865	Mitochondrial ETC	0.21 ± 0.06	1
Nde2p	NP_010198	Mitochondrial ETC	0.25 ± 0.12	1
Ndi1p	NP_013586	Mitochondrial ETC	0.30 ± 0.06	1
Pet100p	NP_010364	Mitochondrial ETC	4.33 ± 0.34	1
Qcr2p	NP_015517	Mitochondrial ETC	3.87 ± 0.42	1
Rip1p	NP_010890	Mitochondrial ETC	3.10 ± 0.28	1
Aat1p	NP_012816	Amino acid synthesis in mitochondria	3.74 ± 0.66	1
Gdh3p	NP_009339	Amino acid synthesis in mitochondria	2.46 ± 0.22	1
Ilv5p	NP_013459	Amino acid biosynthesis in mitochondria; mtDNA binding and protection	4.91 ± 0.50	1
Ilv6p	NP_009918	Amino acid biosynthesis in mitochondria; mtDNA binding and protection	3.48 ± 0.47	1
Lys12p	NP_012172	Amino acid biosynthesis in mitochondria	3.80 ± 0.35	1
Cox10p	NP_015153	Heme synthesis and attachment in mitochondria	3.57 ± 0.63	1
Cyc3p	NP_009361	Heme synthesis and attachment in mitochondria	4.17 ± 0.19	1
Hem14p	NP_010930	Heme synthesis and attachment in mitochondria	3.71 ± 0.47	1
Grx5p	NP_015266	Heme synthesis and attachment in mitochondria; ROS detoxification in mitochondria	1.09 ± 0.14	1
Pos5p	NP_015136	Synthesis of NADPH from NADH in mitochondria	3.20 ± 0.28	1
Ccp1p	NP_012992	ROS detoxification in mitochondria	0.92 ± 0.11	1
Glr1p	NP_015234	ROS detoxification in mitochondria	1.08 ± 0.06	1
Grx2p	NP_010801	ROS detoxification in mitochondria	1.04 ± 0.15	1
Sod2p	NP_011872	ROS detoxification in mitochondria	0.89 ± 0.13	1
Ecm10p	NP_010884	Molecular chaperone/stress response protein in mitochondria	0.97 ± 0.19	1
Hsp60p	NP_013360	Molecular chaperone/stress response protein in mitochondria; mtDNA binding and protection	1.13 ± 0.08	1
Phb1p	NP_011656	Molecular chaperone/stress response protein in mitochondria	0.85 ± 0.11	1
Ssc1p	NP_012579	Molecular chaperone/stress response protein in mitochondria; mtDNA binding and protection	0.92 ± 0.34	1
Mia40p	NP_012726	Protein import into mitochondria	3.07 ± 0.34	1
Tim23p	NP_014421	Protein import into mitochondria	4.23 ± 0.67	1
Caf4p	NP_012962	Mitochondrial fission	1.15 ± 0.13	1
Mdv1p	NP_012423	Mitochondrial fission	0.98 ± 0.12	1
Ifm1p	NP_014619	RNA synthesis, processing and translation in mitochondria	3.84 ± 0.56	1
Mef1p	NP_013170	RNA synthesis, processing and translation in mitochondria	4.40 ± 0.41	1
Mrpl37p	NP_009831	RNA synthesis, processing and translation in mitochondria	3.25 ± 0.24	1
Mrpl40p	NP_015152	RNA synthesis, processing and translation in mitochondria	4.57 ± 0.31	1
Mrpl49p	NP_012439	RNA synthesis, processing and translation in mitochondria	3.49 ± 0.53	1
Mrps12p	NP_014434	RNA synthesis, processing and translation in mitochondria	3.11 ± 0.19	1
Mrps16p	NP_015312	RNA synthesis, processing and translation in mitochondria	3.76 ± 0.44	1
Mrps17p	NP_013913	RNA synthesis, processing and translation in mitochondria	3.52 ± 0.32	1
Nam2p	NP_013488	RNA synthesis, processing and translation in mitochondria	0.23 ± 0.13	1
Rsm25p	NP_012179	RNA synthesis, processing and translation in mitochondria	4.16 ± 0.51	1
Tuf1p	NP_014830	RNA synthesis, processing and translation in mitochondria	3.27 ± 0.20	1
Abf2p	NP_013788	mtDNA binding and protection	0.27 ± 0.06	1
Day 5 (PD phase)				
Aco1p	NP_013407	Mitochondrial TCA cycle; mtDNA binding and protection	3.32 ± 0.43	1
Cit1p	NP_014398	Mitochondrial TCA cycle	2.14 ± 0.16	1
Fum1p	NP_015061	Mitochondrial TCA cycle	0.31 ± 0.14	1

Idh1p	NP_014361	Mitochondrial TCA cycle; mtDNA binding and protection	2.35 ± 0.27	1
Idh2p	NP_014779	Mitochondrial TCA cycle	2.43 ± 0.39	1
Kgd1p	NP_012141	Mitochondrial TCA cycle; mtDNA binding and protection	3.50 ± 0.23	1
Kgd2p	NP_010432	Mitochondrial TCA cycle; mtDNA binding and protection	2.27 ± 0.19	1
Lsc1p	NP_014785	Mitochondrial TCA cycle; mtDNA binding and protection	0.31 ± 0.12	1
Lsc2p	NP_011760	Mitochondrial TCA cycle	0.35 ± 0.08	1
Mdh1p	NP_012838	Mitochondrial TCA cycle	2.62 ± 0.56	1
Sdh1p	NP_012774	Mitochondrial TCA cycle and ETC	0.26 ± 0.10	1
Sdh2p	NP_013059	Mitochondrial TCA cycle and ETC	0.32 ± 0.17	1
Sdh3p	NP_012781	Mitochondrial TCA cycle and ETC	0.29 ± 0.07	1
Sdh4p	NP_010463	Mitochondrial TCA cycle and ETC	0.27 ± 0.13	1
Icl1p	NP_010991	Mitochondrial TCA cycle	2.34 ± 0.21	1
Mls1p	NP_014282	Mitochondrial TCA cycle	2.69 ± 0.34	1
Ald4p	NP_015019	Mitochondrial ETC; mtDNA binding and protection	4.19 ± 0.53	1
Atp1p	NP_009453	Mitochondrial ETC; mtDNA binding and protection	3.42 ± 0.30	1
Atp2p	NP_012655	Mitochondrial ETC	2.47 ± 0.45	1
Atp5p	NP_010584	Mitochondrial ETC	2.75 ± 0.19	1
Atp9p	NP_013816	Mitochondrial ETC	2.51 ± 0.28	1
Cobp	NP_015109	Mitochondrial ETC	4.67 ± 0.66	1
Cor1p	NP_009508	Mitochondrial ETC	2.16 ± 0.34	1
Cox1p	NP_009305	Mitochondrial ETC	3.30 ± 0.51	1
Cox2p	NP_009326	Mitochondrial ETC	3.72 ± 0.22	1
Cox3p	NP_009328	Mitochondrial ETC	3.58 ± 0.41	1
Cox11p	NP_015193	Mitochondrial ETC	2.21 ± 0.14	1
Cox14p	NP_013577	Mitochondrial ETC	2.33 ± 0.27	1
Cyc1p	NP_012582	Mitochondrial ETC	3.49 ± 0.34	1
Gut2p	NP_012111	Mitochondrial ETC	3.64 ± 0.41	1
Nde1p	NP_013865	Mitochondrial ETC	0.32 ± 0.15	1
Nde2p	NP_010198	Mitochondrial ETC	0.29 ± 0.10	1
Ndi1p	NP_013586	Mitochondrial ETC	0.26 ± 0.07	1
Pet100p	NP_010364	Mitochondrial ETC	3.21 ± 0.32	1
Qcr2p	NP_015517	Mitochondrial ETC	3.44 ± 0.53	1
Rip1p	NP_010890	Mitochondrial ETC	3.69 ± 0.41	1
Aat1p	NP_012816	Amino acid synthesis in mitochondria	2.48 ± 0.26	1
Gdh3p	NP_009339	Amino acid synthesis in mitochondria	2.15 ± 0.14	1
Ilv5p	NP_013459	Amino acid biosynthesis in mitochondria; mtDNA binding and protection	3.34 ± 0.33	1
Ilv6p	NP_009918	Amino acid biosynthesis in mitochondria; mtDNA binding and protection	3.47 ± 0.26	1
Lys12p	NP_012172	Amino acid biosynthesis in mitochondria	2.30 ± 0.42	1
Cox10p	NP_015153	Heme synthesis and attachment in mitochondria	2.57 ± 0.54	1
Cyc3p	NP_009361	Heme synthesis and attachment in mitochondria	3.64 ± 0.18	1
Hem14p	NP_010930	Heme synthesis and attachment in mitochondria	2.45 ± 0.23	1
Grx5p	NP_015266	Heme synthesis and attachment in mitochondria; ROS detoxification in mitochondria	3.27 ± 0.31	1
Pos5p	NP_015136	Synthesis of NADPH from NADH in mitochondria	2.33 ± 0.48	1
Ccp1p	NP_012992	ROS detoxification in mitochondria	3.44 ± 0.22	1
Glr1p	NP_015234	ROS detoxification in mitochondria	2.51 ± 0.19	1
Grx2p	NP_010801	ROS detoxification in mitochondria	3.38 ± 0.50	1
Sod2p	NP_011872	ROS detoxification in mitochondria	2.67 ± 0.34	1
Ecm10p	NP_010884	Molecular chaperone/stress response protein in mitochondria	3.27 ± 0.21	1

Hsp60p	NP_013360	Molecular chaperone/stress response protein in mitochondria; mtDNA binding and protection	2.23 ± 0.42	1
Phb1p	NP_011656	Molecular chaperone/stress response protein in mitochondria	3.54 ± 0.37	1
Ssc1p	NP_012579	Molecular chaperone/stress response protein in mitochondria; mtDNA binding and protection	3.49 ± 0.53	1
Mia40p	NP_012726	Protein import into mitochondria	2.36 ± 0.26	1
Tim23p	NP_014421	Protein import into mitochondria	3.67 ± 0.45	1
Caf4p	NP_012962	Mitochondrial fission	0.88 ± 0.17	1
Mdv1p	NP_012423	Mitochondrial fission	1.12 ± 0.08	1
Ifm1p	NP_014619	RNA synthesis, processing and translation in mitochondria	2.19 ± 0.23	1
Mef1p	NP_013170	RNA synthesis, processing and translation in mitochondria	3.38 ± 0.41	1
Mrpl37p	NP_009831	RNA synthesis, processing and translation in mitochondria	3.66 ± 0.34	1
Mrpl40p	NP_015152	RNA synthesis, processing and translation in mitochondria	3.27 ± 0.29	1
Mrpl49p	NP_012439	RNA synthesis, processing and translation in mitochondria	2.32 ± 0.18	1
Mrps12p	NP_014434	RNA synthesis, processing and translation in mitochondria	2.46 ± 0.32	1
Mrps16p	NP_015312	RNA synthesis, processing and translation in mitochondria	2.23 ± 0.25	1
Mrps17p	NP_013913	RNA synthesis, processing and translation in mitochondria	3.44 ± 0.11	1
Nam2p	NP_013488	RNA synthesis, processing and translation in mitochondria	0.30 ± 0.09	1
Rsm25p	NP_012179	RNA synthesis, processing and translation in mitochondria	3.56 ± 0.38	1
Tuf1p	NP_014830	RNA synthesis, processing and translation in mitochondria	2.47 ± 0.22	1
Abf2p	NP_013788	mtDNA binding and protection	0.28 ± 0.14	1
Day 9 (ST phase)				
Aco1p	NP_013407	Mitochondrial TCA cycle; mtDNA binding and protection	2.19 ± 0.12	1
Cit1p	NP_014398	Mitochondrial TCA cycle	2.27 ± 0.33	1
Fum1p	NP_015061	Mitochondrial TCA cycle	0.42 ± 0.17	1
Idh1p	NP_014361	Mitochondrial TCA cycle; mtDNA binding and protection	2.42 ± 0.31	1
Idh2p	NP_014779	Mitochondrial TCA cycle	1.13 ± 0.14	1
Kgd1p	NP_012141	Mitochondrial TCA cycle; mtDNA binding and protection	2.34 ± 0.29	1
Kgd2p	NP_010432	Mitochondrial TCA cycle; mtDNA binding and protection	0.91 ± 0.07	1
Lsc1p	NP_014785	Mitochondrial TCA cycle; mtDNA binding and protection	0.40 ± 0.19	1
Lsc2p	NP_011760	Mitochondrial TCA cycle	0.37 ± 0.11	1
Mdh1p	NP_012838	Mitochondrial TCA cycle	1.08 ± 0.24	1
Sdh1p	NP_012774	Mitochondrial TCA cycle and ETC	0.45 ± 0.16	1
Sdh2p	NP_013059	Mitochondrial TCA cycle and ETC	0.39 ± 0.08	1
Sdh3p	NP_012781	Mitochondrial TCA cycle and ETC	0.47 ± 0.13	1
Sdh4p	NP_010463	Mitochondrial TCA cycle and ETC	0.42 ± 0.10	1
Icl1p	NP_010991	Mitochondrial TCA cycle	1.14 ± 0.22	1
Mls1p	NP_014282	Mitochondrial TCA cycle	1.06 ± 0.16	1
Ald4p	NP_015019	Mitochondrial ETC; mtDNA binding and protection	2.42 ± 0.34	1
Atp1p	NP_009453	Mitochondrial ETC; mtDNA binding and protection	1.21 ± 0.27	1
Atp2p	NP_012655	Mitochondrial ETC	1.14 ± 0.11	1
Atp5p	NP_010584	Mitochondrial ETC	1.32 ± 0.36	1
Atp9p	NP_013816	Mitochondrial ETC	0.93 ± 0.18	1
Cobp	NP_015109	Mitochondrial ETC	1.17 ± 0.23	1
Cor1p	NP_009508	Mitochondrial ETC	1.09 ± 0.12	1
Cox1p	NP_009305	Mitochondrial ETC	1.27 ± 0.10	1
Cox2p	NP_009326	Mitochondrial ETC	1.12 ± 0.15	1
Cox3p	NP_009328	Mitochondrial ETC	1.31 ± 0.36	1
Cox11p	NP_015193	Mitochondrial ETC	0.93 ± 0.21	1
Cox14p	NP_013577	Mitochondrial ETC	0.88 ± 0.09	1
Cyc1p	NP_012582	Mitochondrial ETC	2.39 ± 0.31	1

Gut2p	NP_012111	Mitochondrial ETC	1.18 ± 0.14	1
Nde1p	NP_013865	Mitochondrial ETC	0.39 ± 0.11	1
Nde2p	NP_010198	Mitochondrial ETC	0.34 ± 0.18	1
Ndi1p	NP_013586	Mitochondrial ETC	0.42 ± 0.22	1
Pet100p	NP_010364	Mitochondrial ETC	2.46 ± 0.33	1
Qcr2p	NP_015517	Mitochondrial ETC	1.19 ± 0.21	1
Rip1p	NP_010890	Mitochondrial ETC	1.27 ± 0.13	1
Aat1p	NP_012816	Amino acid synthesis in mitochondria	0.92 ± 0.15	1
Gdh3p	NP_009339	Amino acid synthesis in mitochondria	0.87 ± 0.09	1
Ilv5p	NP_013459	Amino acid biosynthesis in mitochondria; mtDNA binding and protection	2.45 ± 0.21	1
Ilv6p	NP_009918	Amino acid biosynthesis in mitochondria; mtDNA binding and protection	1.19 ± 0.15	1
Lys12p	NP_012172	Amino acid biosynthesis in mitochondria	1.26 ± 0.27	1
Cox10p	NP_015153	Heme synthesis and attachment in mitochondria	0.91 ± 0.12	1
Cyc3p	NP_009361	Heme synthesis and attachment in mitochondria	2.33 ± 0.19	1
Hem14p	NP_010930	Heme synthesis and attachment in mitochondria	1.12 ± 0.11	1
Grx5p	NP_015266	Heme synthesis and attachment in mitochondria; ROS detoxification in mitochondria	4.67 ± 0.43	1
Pos5p	NP_015136	Synthesis of NADPH from NADH in mitochondria	1.08 ± 0.14	1
Ccp1p	NP_012992	ROS detoxification in mitochondria	3.61 ± 0.32	1
Glr1p	NP_015234	ROS detoxification in mitochondria	3.79 ± 0.41	1
Grx2p	NP_010801	ROS detoxification in mitochondria	4.75 ± 0.27	1
Sod2p	NP_011872	ROS detoxification in mitochondria	3.43 ± 0.18	1
Ecm10p	NP_010884	Molecular chaperone/stress response protein in mitochondria	3.51 ± 0.34	1
Hsp60p	NP_013360	Molecular chaperone/stress response protein in mitochondria; mtDNA binding and protection	3.90 ± 0.59	1
Phb1p	NP_011656	Molecular chaperone/stress response protein in mitochondria	4.49 ± 0.21	1
Ssc1p	NP_012579	Molecular chaperone/stress response protein in mitochondria; mtDNA binding and protection	4.56 ± 0.20	1
Mia40p	NP_012726	Protein import into mitochondria	0.88 ± 0.13	1
Tim23p	NP_014421	Protein import into mitochondria	2.37 ± 0.06	1
Caf4p	NP_012962	Mitochondrial fission	0.21 ± 0.10	1
Mdv1p	NP_012423	Mitochondrial fission	0.26 ± 0.11	1
Ifm1p	NP_014619	RNA synthesis, processing and translation in mitochondria	1.14 ± 0.19	1
Mef1p	NP_013170	RNA synthesis, processing and translation in mitochondria	2.63 ± 0.24	1
Mrpl37p	NP_009831	RNA synthesis, processing and translation in mitochondria	1.18 ± 0.07	1
Mrpl40p	NP_015152	RNA synthesis, processing and translation in mitochondria	2.46 ± 0.15	1
Mrpl49p	NP_012439	RNA synthesis, processing and translation in mitochondria	0.92 ± 0.09	1
Mrps12p	NP_014434	RNA synthesis, processing and translation in mitochondria	1.23 ± 0.21	1
Mrps16p	NP_015312	RNA synthesis, processing and translation in mitochondria	1.06 ± 0.12	1
Mrps17p	NP_013913	RNA synthesis, processing and translation in mitochondria	2.34 ± 0.18	1
Nam2p	NP_013488	RNA synthesis, processing and translation in mitochondria	0.40 ± 0.21	1
Rsm25p	NP_012179	RNA synthesis, processing and translation in mitochondria	2.79 ± 0.36	1
Tuf1p	NP_014830	RNA synthesis, processing and translation in mitochondria	1.17 ± 0.11	1
Abf2p	NP_013788	mtDNA binding and protection	0.39 ± 0.07	1

10.2 Appendix 2. Relative levels of proteins recovered in total lysates of wild-type cells cultured in the nutrient-rich YP medium initially containing 0.2% glucose, with 50 μM LCA or without it

For making total lysates, cells were collected at days 2, 5 and 9 of culturing (D, PD and ST growth phases, respectively). Proteins were identified and quantified using MALDI MS peptide mapping as described in ″Materials and Methods″. Relative levels of proteins in cells cultured with LCA are presented as fold difference relative to those without of LCA (n = 3).

Protein	NCBI accession no.	Function	Protein level	
			LCA concentration (μM)	
			50	0
Day 2 (D phase)				
Aco1p	NP_013407	Mitochondrial TCA cycle; mtDNA binding and protection	4.09 ± 0.21	1
Cit1p	NP_014398	Mitochondrial TCA cycle	3.45 ± 0.19	1
Idh1p	NP_014361	Mitochondrial TCA cycle; mtDNA binding and protection	4.31 ± 0.33	1
Kgd1p	NP_012141	Mitochondrial TCA cycle; mtDNA binding and protection	4.56 ± 0.61	1
Sdh1p	NP_012774	Mitochondrial TCA cycle and ETC	0.29 ± 0.12	1
Icl1p	NP_010991	Mitochondrial TCA cycle	3.24 ± 0.23	1
Mls1p	NP_014282	Mitochondrial TCA cycle	3.38 ± 0.37	1
Ald4p	NP_015019	Mitochondrial ETC; mtDNA binding and protection	4.41 ± 0.25	1
Atp1p	NP_009453	Mitochondrial ETC; mtDNA binding and protection	3.26 ± 0.11	1
Gut2p	NP_012111	Mitochondrial ETC	3.67 ± 0.54	1
Ndi1p	NP_013586	Mitochondrial ETC	0.28 ± 0.09	1
Aat1p	NP_012816	Amino acid synthesis in mitochondria	3.24 ± 0.22	1
Gdh3p	NP_009339	Amino acid synthesis in mitochondria	2.29 ± 0.16	1
Ilv5p	NP_013459	Amino acid biosynthesis in mitochondria; mtDNA binding and protection	4.42 ± 0.29	1
Ccp1p	NP_012992	ROS detoxification in mitochondria	0.93 ± 0.10	1
Glr1p	NP_015234	ROS detoxification in mitochondria	1.14 ± 0.18	1
Grx2p	NP_010801	ROS detoxification in mitochondria	1.06 ± 0.21	1
Grx5p	NP_015266	ROS detoxification in mitochondria	0.89 ± 0.07	1
Sod2p	NP_011872	ROS detoxification in mitochondria	0.97 ± 0.25	1
Hsp60p	NP_013360	Molecular chaperone/stress response protein in mitochondria; mtDNA binding and protection	1.21 ± 0.13	1
Ssc1p	NP_012579	Molecular chaperone/stress response protein in mitochondria; mtDNA binding and protection	0.86 ± 0.05	1
Gdb1p	NP_015510	Glycogen degradation	3.49 ± 0.24	1
Gph1p	NP_015486	Glycogen degradation	3.27 ± 0.38	1
Glk1p	NP_009890	Glycolysis	4.19 ± 0.16	1
Hxk1p	NP_116711	Glycolysis	4.46 ± 0.29	1
Pgi1p	NP_009755	Glycolysis	3.72 ± 0.53	1
Tdh2p	NP_012542	Glycolysis	3.35 ± 0.24	1
Rki1p	NP_014738	Pentose phosphate pathway	1.19 ± 0.11	1
Tal1p	NP_013458	Pentose phosphate pathway	1.07 ± 0.16	1
Zwf1p	NP_014158	Pentose phosphate pathway	0.92 ± 0.10	1

Ach1p	NP_009538	Conversion of pyruvate to Ac-CoA	0.28 ± 0.07	1
Acs2p	NP_013254	Conversion of pyruvate to Ac-CoA	1.16 ± 0.12	1
Ald6p	NP_015264	Conversion of pyruvate to Ac-CoA	0.89 ± 0.17	1
Cat2p	NP_013670	Carnitine shuttle	0.97 ± 0.09	1
Crc1p	NP_014743	Carnitine shuttle	1.13 ± 0.18	1
Yat2p	NP_010941	Carnitine shuttle	0.92 ± 0.06	1
Gpd2p	NP_014582	Glycerol-3-P shuttle	0.96 ± 0.11	1
Gpx2p	NP_009803	ROS detoxification in the cytosol	0.90 ± 0.09	1
Gpx3p	NP_012303	ROS detoxification in the cytosol	1.22 ± 0.15	1
Sod1p	NP_012638	ROS detoxification in the cytosol	1.11 ± 0.16	1
Trr1p	NP_010640	ROS detoxification in the cytosol	1.07 ± 0.23	1
Hsp42p	NP_010456	Molecular chaperone/stress response protein in the cytosol	0.88 ± 0.17	1
Hsp104p	NP_013074	Molecular chaperone/stress response protein in the cytosol	0.91 ± 0.06	1
Ssa1p	NP_009396	Molecular chaperone/stress response protein in the cytosol	1.15 ± 0.19	1
Ssa2p	NP_013076	Molecular chaperone/stress response protein in the cytosol	1.19 ± 0.21	1
Gsh1p	NP_012434	Glutathione synthesis in the cytosol	0.83 ± 0.09	1
Gsh2p	NP_014593	Glutathione synthesis in the cytosol	0.96 ± 0.14	1
Fbp1p	NP_013481	Gluconeogenesis in the cytosol	0.22 ± 0.17	1
Pck1p	NP_013023	Gluconeogenesis in the cytosol	0.29 ± 0.06	1
Pyc1p	NP_011453	Gluconeogenesis in the cytosol	0.32 ± 0.14	1
Adh1p	NP_014555	Ethanol synthesis in the cytosol	0.26 ± 0.07	1
Are1p	NP_009978	Synthesis of TAG and EE in the ER and lipid droplets	3.36 ± 0.25	1
Dga1p	NP_014888	Synthesis of TAG in the ER and lipid droplets	4.64 ± 0.41	1
Gpt2p	NP_012993	Synthesis of TAG in the ER and lipid droplets	3.67 ± 0.34	1
Slc1p	NP_010231	Synthesis of TAG in the ER and lipid droplets	4.79 ± 0.19	1
Tgl1p	NP_012782	Lipolysis of TAG and EE in lipid droplets	0.27 ± 0.12	1
Tgl3p	NP_014044	Lipolysis of TAG in lipid droplets	0.26 ± 0.05	1
Tgl4p	NP_013015	Lipolysis of TAG in lipid droplets	0.31 ± 0.16	1
Tgl5p	NP_014724	Lipolysis of TAG in lipid droplets	0.29 ± 0.11	1
Yeh1p	NP_013089	Lipolysis of TAG and EE in lipid droplets	0.32 ± 0.09	1
Arg1p	NP_014583	Amino acid synthesis in the cytosol	0.84 ± 0.15	1
Aro4p	NP_009808	Amino acid synthesis in the cytosol	1.16 ± 0.09	1
Asn1p	NP_015471	Amino acid synthesis in the cytosol	0.94 ± 0.13	1
Cys4p	NP_011671	Amino acid synthesis in the cytosol	0.97 ± 0.18	1
Gln1p	NP_015360	Amino acid synthesis in the cytosol	1.23 ± 0.10	1
Gly1p	NP_010868	Amino acid synthesis in the cytosol	0.91 ± 0.07	1
Hom3p	NP_010972	Amino acid synthesis in the cytosol	1.16 ± 0.15	1
Met17p	NP_013406	Amino acid synthesis in the cytosol	1.07 ± 0.19	1
Sam4p	NP_015050	Amino acid synthesis in the cytosol	1.12 ± 0.11	1
Trp4p	NP_010641	Amino acid synthesis in the cytosol	0.85 ± 0.09	1
Thr1p	NP_011890	Amino acid synthesis in the cytosol	0.93 ± 0.13	1
Ade12p	NP_014179	Nucleotide synthesis in the cytosol	0.96 ± 0.21	1
Amd1p	NP_013677	Nucleotide synthesis in the cytosol	1.19 ± 0.08	1
Hpt1p	NP_010687	Nucleotide synthesis in the cytosol	1.08 ± 0.17	1
Ppr1p	NP_013114	Nucleotide synthesis in the cytosol	0.91 ± 0.13	1
Prs3p	NP_011852	Nucleotide synthesis in the cytosol	0.88 ± 0.06	1
Ura1p	NP_012706	Nucleotide synthesis in the cytosol	0.95 ± 0.12	1
Ura7p	NP_009514	Nucleotide synthesis in the cytosol	1.21 ± 0.15	1
Dim1p	NP_015057	Biogenesis of the 40S ribosomal subunit	1.09 ± 0.21	1
Emg1p	NP_013287	Biogenesis of the 40S ribosomal subunit	1.14 ± 0.08	1

Ltv1p	NP_012779	Biogenesis of the 40S ribosomal subunit	0.83 ± 0.21	1
Nop1p	NP_010270	Biogenesis of the 40S ribosomal subunit	0.92 ± 0.13	1
Nsr1p	NP_011675	Biogenesis of the 40S ribosomal subunit	1.19 ± 0.11	1
Rps0A/Bp	NP_011730	Biogenesis of the 40S ribosomal subunit; a protein component of the 40S ribosomal subunit	0.90 ± 0.17	1
Rps3p	NP_014221	Biogenesis of the 40S ribosomal subunit; a protein component of the 40S ribosomal subunit	1.22 ± 0.07	1
Rps15p	NP_014602	Biogenesis of the 40S ribosomal subunit; a protein component of the 40S ribosomal subunit	1.05 ± 0.19	1
Rps26A/Bp	NP_011326	Biogenesis of the 40S ribosomal subunit; a protein component of the 40S ribosomal subunit	1.17 ± 0.22	1
Tsr1p	NP_010223	Biogenesis of the 40S ribosomal subunit	0.91 ± 0.13	1
Brx1p	NP_014565	Biogenesis of the 60S ribosomal subunit	0.82 ± 0.16	1
Dbp7p	NP_012949	Biogenesis of the 60S ribosomal subunit	1.24 ± 0.09	1
Nog1p	NP_015232	Biogenesis of the 60S ribosomal subunit	1.12 ± 0.27	1
Nog2p	NP_014451	Biogenesis of the 60S ribosomal subunit	0.90 ± 0.11	1
Nop2p	NP_014338	Biogenesis of the 60S ribosomal subunit	0.97 ± 0.19	1
Nop7p	NP_011617	Biogenesis of the 60S ribosomal subunit	1.18 ± 0.13	1
Nop8p	NP_014497	Biogenesis of the 60S ribosomal subunit	1.05 ± 0.22	1
Nsa1p	NP_011404	Biogenesis of the 60S ribosomal subunit	0.88 ± 0.13	1
Nug1p	NP_010921	Biogenesis of the 60S ribosomal subunit	1.26 ± 0.08	1
Rpf1p	NP_011956	Biogenesis of the 60S ribosomal subunit	0.92 ± 0.15	1
Rpf2p	NP_013007	Biogenesis of the 60S ribosomal subunit	1.14 ± 0.18	1
Rps6A/Bp	NP_015235	A protein component of the 40S ribosomal subunit	0.96 ± 0.21	1
Rps11A/Bp	NP_010308	A protein component of the 40S ribosomal subunit	1.22 ± 0.10	1
Rps23A/Bp	NP_015457	A protein component of the 40S ribosomal subunit	1.15 ± 0.24	1
Rpl6Ap	NP_013638	A protein component of the 60S ribosomal subunit	0.91 ± 0.19	1
Rpl8A/Bp	NP_011830	A protein component of the 60S ribosomal subunit	1.26 ± 0.13	1
Rpl9A/Bp	NP_011368	A protein component of the 60S ribosomal subunit	0.87 ± 0.11	1
Rpl10p	NP_013176	A protein component of the 60S ribosomal subunit	1.18 ± 0.15	1
Rpl21A/Bp	NP_009750	A protein component of the 60S ribosomal subunit	0.95 ± 0.23	1
Rpl27A/Bp	NP_011874	A protein component of the 60S ribosomal subunit	1.12 ± 0.17	1
Rpl31A/Bp	NP_010208	A protein component of the 60S ribosomal subunit	0.88 ± 0.20	1
Rpl34A/Bp	NP_010977	A protein component of the 60S ribosomal subunit	1.13 ± 0.05	1
Npl4p	NP_009729	Proteasomal protein degradation	1.17 ± 0.08	1
Pup1p	NP_014800	Proteasomal protein degradation	1.22 ± 0.13	1
Pup3p	NP_011020	Proteasomal protein degradation	0.95 ± 0.16	1
Rpn5p	NP_010134	Proteasomal protein degradation	0.98 ± 0.19	1
Rpt6p	NP_011467	Proteasomal protein degradation	0.87 ± 0.25	1
Ufd1p	NP_011562	Proteasomal protein degradation	1.11 ± 0.09	1
Pep4p	NP_015171	Vacuolar protein degradation	0.89 ± 0.13	1
Day 5 (PD phase)				
Aco1p	NP_013407	Mitochondrial TCA cycle; mtDNA binding and protection	3.43 ± 0.34	1
Cit1p	NP_014398	Mitochondrial TCA cycle	2.35 ± 0.17	1
Idh1p	NP_014361	Mitochondrial TCA cycle; mtDNA binding and protection	2.78 ± 0.21	1
Kgd1p	NP_012141	Mitochondrial TCA cycle; mtDNA binding and protection	3.36 ± 0.11	1
Sdh1p	NP_012774	Mitochondrial TCA cycle and ETC	0.27 ± 0.07	1
Icl1p	NP_010991	Mitochondrial TCA cycle	2.54 ± 0.31	1
Mls1p	NP_014282	Mitochondrial TCA cycle	2.79 ± 0.19	1
Ald4p	NP_015019	Mitochondrial ETC; mtDNA binding and protection	4.71 ± 0.62	1
Atp1p	NP_009453	Mitochondrial ETC; mtDNA binding and protection	3.65 ± 0.40	1

Gut2p	NP_012111	Mitochondrial ETC	3.28 ± 0.14	1
Ndi1p	NP_013586	Mitochondrial ETC	0.26 ± 0.11	1
Aat1p	NP_012816	Amino acid synthesis in mitochondria	2.77 ± 0.33	1
Gdh3p	NP_009339	Amino acid synthesis in mitochondria	2.49 ± 0.24	1
Ilv5p	NP_013459	Amino acid biosynthesis in mitochondria; mtDNA binding and protection	3.67 ± 0.14	1
Ccp1p	NP_012992	ROS detoxification in mitochondria	3.34 ± 0.21	1
Glr1p	NP_015234	ROS detoxification in mitochondria	2.55 ± 0.19	1
Grx2p	NP_010801	ROS detoxification in mitochondria	3.79 ± 0.35	1
Grx5p	NP_015266	ROS detoxification in mitochondria	3.42 ± 0.27	1
Sod2p	NP_011872	ROS detoxification in mitochondria	2.67 ± 0.16	1
Hsp60p	NP_013360	Molecular chaperone/stress response protein in mitochondria; mtDNA binding and protection	2.39 ± 0.11	1
Ssc1p	NP_012579	Molecular chaperone/stress response protein in mitochondria; mtDNA binding and protection	3.63 ± 0.24	1
Gdb1p	NP_015510	Glycogen degradation	3.40 ± 0.31	1
Gph1p	NP_015486	Glycogen degradation	3.55 ± 0.17	1
Glk1p	NP_009890	Glycolysis	3.74 ± 0.46	1
Hxk1p	NP_116711	Glycolysis	3.39 ± 0.13	1
Pgi1p	NP_009755	Glycolysis	3.68 ± 0.28	1
Tdh2p	NP_012542	Glycolysis	3.85 ± 0.11	1
Rki1p	NP_014738	Pentose phosphate pathway	3.21 ± 0.19	1
Tal1p	NP_013458	Pentose phosphate pathway	2.53 ± 0.32	1
Zwf1p	NP_014158	Pentose phosphate pathway	3.44 ± 0.23	1
Ach1p	NP_009538	Conversion of pyruvate to Ac-CoA	0.27 ± 0.09	1
Acs2p	NP_013254	Conversion of pyruvate to Ac-CoA	3.59 ± 0.17	1
Ald6p	NP_015264	Conversion of pyruvate to Ac-CoA	3.68 ± 0.31	1
Cat2p	NP_013670	Carnitine shuttle	3.75 ± 0.25	1
Crc1p	NP_014743	Carnitine shuttle	3.29 ± 0.07	1
Yat2p	NP_010941	Carnitine shuttle	3.38 ± 0.19	1
Gpd2p	NP_014582	Glycerol-3-P shuttle	2.77 ± 0.42	1
Gpx2p	NP_009803	ROS detoxification in the cytosol	0.93 ± 0.13	1
Gpx3p	NP_012303	ROS detoxification in the cytosol	1.22 ± 0.24	1
Sod1p	NP_012638	ROS detoxification in the cytosol	1.18 ± 0.07	1
Trr1p	NP_010640	ROS detoxification in the cytosol	0.87 ± 0.11	1
Hsp42p	NP_010456	Molecular chaperone/stress response protein in the cytosol	0.96 ± 0.09	1
Hsp104p	NP_013074	Molecular chaperone/stress response protein in the cytosol	0.91 ± 0.15	1
Ssa1p	NP_009396	Molecular chaperone/stress response protein in the cytosol	1.33 ± 0.21	1
Ssa2p	NP_013076	Molecular chaperone/stress response protein in the cytosol	1.25 ± 0.33	1
Gsh1p	NP_012434	Glutathione synthesis in the cytosol	1.17 ± 0.18	1
Gsh2p	NP_014593	Glutathione synthesis in the cytosol	0.85 ± 0.12	1
Fbp1p	NP_013481	Gluconeogenesis in the cytosol	0.28 ± 0.11	1
Pck1p	NP_013023	Gluconeogenesis in the cytosol	0.39 ± 0.09	1
Pyc1p	NP_011453	Gluconeogenesis in the cytosol	0.27 ± 0.15	1
Adh1p	NP_014555	Ethanol synthesis in the cytosol	0.42 ± 0.20	1
Are1p	NP_009978	Synthesis of TAG and EE in the ER and lipid droplets	2.34 ± 0.31	1
Dga1p	NP_014888	Synthesis of TAG in the ER and lipid droplets	3.69 ± 0.44	1
Gpt2p	NP_012993	Synthesis of TAG in the ER and lipid droplets	2.48 ± 0.23	1
Slc1p	NP_010231	Synthesis of TAG in the ER and lipid droplets	3.77 ± 0.17	1
Tgl1p	NP_012782	Lipolysis of TAG and EE in lipid droplets	0.40 ± 0.19	1
Tgl3p	NP_014044	Lipolysis of TAG in lipid droplets	0.33 ± 0.08	1

Tgl4p	NP_013015	Lipolysis of TAG in lipid droplets	0.29 ± 0.13	1
Tgl5p	NP_014724	Lipolysis of TAG in lipid droplets	0.42 ± 0.10	1
Yeh1p	NP_013089	Lipolysis of TAG and EE in lipid droplets	0.27 ± 0.14	1
Arg1p	NP_014583	Amino acid synthesis in the cytosol	1.12 ± 0.21	1
Aro4p	NP_009808	Amino acid synthesis in the cytosol	0.87 ± 0.19	1
Asn1p	NP_015471	Amino acid synthesis in the cytosol	0.95 ± 0.23	1
Cys4p	NP_011671	Amino acid synthesis in the cytosol	1.24 ± 0.31	1
Gln1p	NP_015360	Amino acid synthesis in the cytosol	1.16 ± 0.08	1
Gly1p	NP_010868	Amino acid synthesis in the cytosol	1.07 ± 0.14	1
Hom3p	NP_010972	Amino acid synthesis in the cytosol	0.91 ± 0.11	1
Met17p	NP_013406	Amino acid synthesis in the cytosol	1.19 ± 0.20	1
Sam4p	NP_015050	Amino acid synthesis in the cytosol	0.85 ± 0.23	1
Trp4p	NP_010641	Amino acid synthesis in the cytosol	0.94 ± 0.12	1
Thr1p	NP_011890	Amino acid synthesis in the cytosol	0.97 ± 0.28	1
Ade12p	NP_014179	Nucleotide synthesis in the cytosol	1.23 ± 0.17	1
Amd1p	NP_013677	Nucleotide synthesis in the cytosol	1.16 ± 0.21	1
Hpt1p	NP_010687	Nucleotide synthesis in the cytosol	0.92 ± 0.14	1
Ppr1p	NP_013114	Nucleotide synthesis in the cytosol	1.12 ± 0.15	1
Prs3p	NP_011852	Nucleotide synthesis in the cytosol	1.19 ± 0.23	1
Ura1p	NP_012706	Nucleotide synthesis in the cytosol	0.84 ± 0.19	1
Ura7p	NP_009514	Nucleotide synthesis in the cytosol	0.95 ± 0.12	1
Dim1p	NP_015057	Biogenesis of the 40S ribosomal subunit	0.88 ± 0.09	1
Emg1p	NP_013287	Biogenesis of the 40S ribosomal subunit	1.22 ± 0.16	1
Ltv1p	NP_012779	Biogenesis of the 40S ribosomal subunit	1.06 ± 0.23	1
Nop1p	NP_010270	Biogenesis of the 40S ribosomal subunit	1.11 ± 0.26	1
Nsr1p	NP_011675	Biogenesis of the 40S ribosomal subunit	0.84 ± 0.11	1
Rps0A/Bp	NP_011730	Biogenesis of the 40S ribosomal subunit; a protein component of the 40S ribosomal subunit	1.15 ± 0.14	1
Rps3p	NP_014221	Biogenesis of the 40S ribosomal subunit; a protein component of the 40S ribosomal subunit	1.23 ± 0.18	1
Rps15p	NP_014602	Biogenesis of the 40S ribosomal subunit; a protein component of the 40S ribosomal subunit	0.92 ± 0.07	1
Rps26A/Bp	NP_011326	Biogenesis of the 40S ribosomal subunit; a protein component of the 40S ribosomal subunit	0.96 ± 0.15	1
Tsr1p	NP_010223	Biogenesis of the 40S ribosomal subunit	1.14 ± 0.23	1
Brx1p	NP_014565	Biogenesis of the 60S ribosomal subunit	1.21 ± 0.12	1
Dbp7p	NP_012949	Biogenesis of the 60S ribosomal subunit	1.06 ± 0.16	1
Nog1p	NP_015232	Biogenesis of the 60S ribosomal subunit	1.28 ± 0.07	1
Nog2p	NP_014451	Biogenesis of the 60S ribosomal subunit	0.94 ± 0.11	1
Nop2p	NP_014338	Biogenesis of the 60S ribosomal subunit	0.91 ± 0.23	1
Nop7p	NP_011617	Biogenesis of the 60S ribosomal subunit	0.86 ± 0.15	1
Nop8p	NP_014497	Biogenesis of the 60S ribosomal subunit	0.97 ± 0.19	1
Nsa1p	NP_011404	Biogenesis of the 60S ribosomal subunit	1.13 ± 0.21	1
Nug1p	NP_010921	Biogenesis of the 60S ribosomal subunit	1.19 ± 0.17	1
Rpf1p	NP_011956	Biogenesis of the 60S ribosomal subunit	1.08 ± 0.12	1
Rpf2p	NP_013007	Biogenesis of the 60S ribosomal subunit	0.94 ± 0.16	1
Rps6A/Bp	NP_015235	A protein component of the 40S ribosomal subunit	0.91 ± 0.27	1
Rps11A/Bp	NP_010308	A protein component of the 40S ribosomal subunit	0.83 ± 0.11	1
Rps23A/Bp	NP_015457	A protein component of the 40S ribosomal subunit	0.88 ± 0.13	1
Rpl6Ap	NP_013638	A protein component of the 60S ribosomal subunit	0.97 ± 0.19	1
Rpl8A/Bp	NP_011830	A protein component of the 60S ribosomal subunit	1.28 ± 0.15	1

Rpl9A/Bp	NP_011368	A protein component of the 60S ribosomal subunit	1.14 ± 0.18	1
Rpl10p	NP_013176	A protein component of the 60S ribosomal subunit	1.17 ± 0.22	1
Rpl21A/Bp	NP_009750	A protein component of the 60S ribosomal subunit	1.33 ± 0.14	1
Rpl27A/Bp	NP_011874	A protein component of the 60S ribosomal subunit	1.26 ± 0.10	1
Rpl31A/Bp	NP_010208	A protein component of the 60S ribosomal subunit	1.16 ± 0.23	1
Rpl34A/Bp	NP_010977	A protein component of the 60S ribosomal subunit	1.28 ± 0.11	1
Npl4p	NP_009729	Proteasomal protein degradation	1.20 ± 0.18	1
Pup1p	NP_014800	Proteasomal protein degradation	0.94 ± 0.14	1
Pup3p	NP_011020	Proteasomal protein degradation	1.17 ± 0.21	1
Rpn5p	NP_010134	Proteasomal protein degradation	1.31 ± 0.19	1
Rpt6p	NP_011467	Proteasomal protein degradation	1.24 ± 0.13	1
Ufd1p	NP_011562	Proteasomal protein degradation	1.16 ± 0.15	1
Pep4p	NP_015171	Vacuolar protein degradation	1.09 ± 0.27	1
Day 9 (ST phase)				
Aco1p	NP_013407	Mitochondrial TCA cycle; mtDNA binding and protection	2.53 ± 0.34	1
Cit1p	NP_014398	Mitochondrial TCA cycle	2.39 ± 0.26	1
Idh1p	NP_014361	Mitochondrial TCA cycle; mtDNA binding and protection	2.27 ± 0.18	1
Kgd1p	NP_012141	Mitochondrial TCA cycle; mtDNA binding and protection	2.44 ± 0.09	1
Sdh1p	NP_012774	Mitochondrial TCA cycle and ETC	0.41 ± 0.16	1
Icl1p	NP_010991	Mitochondrial TCA cycle	1.18 ± 0.19	1
Mls1p	NP_014282	Mitochondrial TCA cycle	1.23 ± 0.31	1
Ald4p	NP_015019	Mitochondrial ETC; mtDNA binding and protection	2.67 ± 0.43	1
Atp1p	NP_009453	Mitochondrial ETC; mtDNA binding and protection	0.89 ± 0.12	1
Gut2p	NP_012111	Mitochondrial ETC	0.94 ± 0.08	1
Ndi1p	NP_013586	Mitochondrial ETC	0.41 ± 0.15	1
Aat1p	NP_012816	Amino acid synthesis in mitochondria	1.24 ± 0.21	1
Gdh3p	NP_009339	Amino acid synthesis in mitochondria	1.09 ± 0.17	1
Ilv5p	NP_013459	Amino acid biosynthesis in mitochondria; mtDNA binding and protection	2.33 ± 0.13	1
Ccp1p	NP_012992	ROS detoxification in mitochondria	3.41 ± 0.25	1
Glr1p	NP_015234	ROS detoxification in mitochondria	3.28 ± 0.19	1
Grx2p	NP_010801	ROS detoxification in mitochondria	4.65 ± 0.43	1
Grx5p	NP_015266	ROS detoxification in mitochondria	4.34 ± 0.32	1
Sod2p	NP_011872	ROS detoxification in mitochondria	3.42 ± 0.09	1
Hsp60p	NP_013360	Molecular chaperone/stress response protein in mitochondria; mtDNA binding and protection	3.29 ± 0.15	1
Ssc1p	NP_012579	Molecular chaperone/stress response protein in mitochondria; mtDNA binding and protection	4.47 ± 0.21	1
Gdb1p	NP_015510	Glycogen degradation	0.87 ± 0.13	1
Gph1p	NP_015486	Glycogen degradation	1.15 ± 0.19	1
Glk1p	NP_009890	Glycolysis	2.42 ± 0.16	1
Hxk1p	NP_116711	Glycolysis	2.37 ± 0.31	1
Pgi1p	NP_009755	Glycolysis	1.19 ± 0.25	1
Tdh2p	NP_012542	Glycolysis	0.91 ± 0.14	1
Rki1p	NP_014738	Pentose phosphate pathway	3.76 ± 0.42	1
Tal1p	NP_013458	Pentose phosphate pathway	3.47 ± 0.29	1
Zwf1p	NP_014158	Pentose phosphate pathway	3.33 ± 0.12	1
Ach1p	NP_009538	Conversion of pyruvate to Ac-CoA	0.44 ± 0.08	1
Acs2p	NP_013254	Conversion of pyruvate to Ac-CoA	2.49 ± 0.24	1
Ald6p	NP_015264	Conversion of pyruvate to Ac-CoA	2.26 ± 0.17	1
Cat2p	NP_013670	Carnitine shuttle	0.93 ± 0.11	1

Crc1p	NP_014743	Carnitine shuttle	0.90 ± 0.23	1
Yat2p	NP_010941	Carnitine shuttle	1.32 ± 0.20	1
Gpd2p	NP_014582	Glycerol-3-P shuttle	1.15 ± 0.31	1
Gpx2p	NP_009803	ROS detoxification in the cytosol	2.56 ± 0.27	1
Gpx3p	NP_012303	ROS detoxification in the cytosol	3.43 ± 0.19	1
Sod1p	NP_012638	ROS detoxification in the cytosol	4.65 ± 0.36	1
Trr1p	NP_010640	ROS detoxification in the cytosol	4.79 ± 0.41	1
Hsp42p	NP_010456	Molecular chaperone/stress response protein in the cytosol	3.51 ± 0.13	1
Hsp104p	NP_013074	Molecular chaperone/stress response protein in the cytosol	3.34 ± 0.21	1
Ssa1p	NP_009396	Molecular chaperone/stress response protein in the cytosol	4.87 ± 0.33	1
Ssa2p	NP_013076	Molecular chaperone/stress response protein in the cytosol	4.28 ± 0.16	1
Gsh1p	NP_012434	Glutathione synthesis in the cytosol	3.65 ± 0.24	1
Gsh2p	NP_014593	Glutathione synthesis in the cytosol	3.37 ± 0.18	1
Fbp1p	NP_013481	Gluconeogenesis in the cytosol	1.24 ± 0.06	1
Pck1p	NP_013023	Gluconeogenesis in the cytosol	0.93 ± 0.11	1
Pyc1p	NP_011453	Gluconeogenesis in the cytosol	1.18 ± 0.14	1
Adh1p	NP_014555	Ethanol synthesis in the cytosol	0.97 ± 0.22	1
Are1p	NP_009978	Synthesis of TAG and EE in the ER and lipid droplets	2.52 ± 0.31	1
Dga1p	NP_014888	Synthesis of TAG in the ER and lipid droplets	2.34 ± 0.17	1
Gpt2p	NP_012993	Synthesis of TAG in the ER and lipid droplets	0.86 ± 0.26	1
Slc1p	NP_010231	Synthesis of TAG in the ER and lipid droplets	2.63 ± 0.20	1
Tgl1p	NP_012782	Lipolysis of TAG and EE in lipid droplets	1.13 ± 0.11	1
Tgl3p	NP_014044	Lipolysis of TAG in lipid droplets	0.39 ± 0.09	1
Tgl4p	NP_013015	Lipolysis of TAG in lipid droplets	0.41 ± 0.15	1
Tgl5p	NP_014724	Lipolysis of TAG in lipid droplets	0.91 ± 0.13	1
Yeh1p	NP_013089	Lipolysis of TAG and EE in lipid droplets	0.44 ± 0.18	1
Arg1p	NP_014583	Amino acid synthesis in the cytosol	0.43 ± 0.07	1
Aro4p	NP_009808	Amino acid synthesis in the cytosol	0.35 ± 0.16	1
Asn1p	NP_015471	Amino acid synthesis in the cytosol	0.27 ± 0.13	1
Cys4p	NP_011671	Amino acid synthesis in the cytosol	0.26 ± 0.05	1
Gln1p	NP_015360	Amino acid synthesis in the cytosol	0.44 ± 0.11	1
Gly1p	NP_010868	Amino acid synthesis in the cytosol	0.41 ± 0.17	1
Hom3p	NP_010972	Amino acid synthesis in the cytosol	0.30 ± 0.08	1
Met17p	NP_013406	Amino acid synthesis in the cytosol	0.45 ± 0.14	1
Sam4p	NP_015050	Amino acid synthesis in the cytosol	0.35 ± 0.10	1
Trp4p	NP_010641	Amino acid synthesis in the cytosol	0.47 ± 0.05	1
Thr1p	NP_011890	Amino acid synthesis in the cytosol	0.40 ± 0.12	1
Ade12p	NP_014179	Nucleotide synthesis in the cytosol	0.43 ± 0.16	1
Amd1p	NP_013677	Nucleotide synthesis in the cytosol	0.29 ± 0.04	1
Hpt1p	NP_010687	Nucleotide synthesis in the cytosol	0.30 ± 0.13	1
Ppr1p	NP_013114	Nucleotide synthesis in the cytosol	0.27 ± 0.08	1
Prs3p	NP_011852	Nucleotide synthesis in the cytosol	0.44 ± 0.11	1
Ura1p	NP_012706	Nucleotide synthesis in the cytosol	0.35 ± 0.20	1
Ura7p	NP_009514	Nucleotide synthesis in the cytosol	0.29 ± 0.16	1
Dim1p	NP_015057	Biogenesis of the 40S ribosomal subunit	0.43 ± 0.12	1
Emg1p	NP_013287	Biogenesis of the 40S ribosomal subunit	0.46 ± 0.09	1
Ltv1p	NP_012779	Biogenesis of the 40S ribosomal subunit	0.40 ± 0.14	1
Nop1p	NP_010270	Biogenesis of the 40S ribosomal subunit	0.35 ± 0.10	1
Nsr1p	NP_011675	Biogenesis of the 40S ribosomal subunit	0.31 ± 0.06	1
Rps0A/Bp	NP_011730	Biogenesis of the 40S ribosomal subunit; a protein	0.27 ± 0.12	1

		component of the 40S ribosomal subunit		
Rps3p	NP_014221	Biogenesis of the 40S ribosomal subunit; a protein component of the 40S ribosomal subunit	0.38 ± 0.17	1
Rps15p	NP_014602	Biogenesis of the 40S ribosomal subunit; a protein component of the 40S ribosomal subunit	0.26 ± 0.08	1
Rps26A/Bp	NP_011326	Biogenesis of the 40S ribosomal subunit; a protein component of the 40S ribosomal subunit	0.40± 0.08	1
Tsr1p	NP_010223	Biogenesis of the 40S ribosomal subunit	0.30 ± 0.11	1
Brx1p	NP_014565	Biogenesis of the 60S ribosomal subunit	0.32 ± 0.16	1
Dbp7p	NP_012949	Biogenesis of the 60S ribosomal subunit	0.39 ± 0.13	1
Nog1p	NP_015232	Biogenesis of the 60S ribosomal subunit	0.34 ± 0.06	1
Nog2p	NP_014451	Biogenesis of the 60S ribosomal subunit	0.26 ± 0.15	1
Nop2p	NP_014338	Biogenesis of the 60S ribosomal subunit	0.31 ± 0.10	1
Nop7p	NP_011617	Biogenesis of the 60S ribosomal subunit	0.44 ± 0.13	1
Nop8p	NP_014497	Biogenesis of the 60S ribosomal subunit	0.39 ± 0.08	1
Nsa1p	NP_011404	Biogenesis of the 60S ribosomal subunit	0.35 ± 0.14	1
Nug1p	NP_010921	Biogenesis of the 60S ribosomal subunit	0.31 ± 0.19	1
Rpf1p	NP_011956	Biogenesis of the 60S ribosomal subunit	0.47 ± 0.22	1
Rpf2p	NP_013007	Biogenesis of the 60S ribosomal subunit	0.39 ± 0.06	1
Rps6A/Bp	NP_015235	A protein component of the 40S ribosomal subunit	0.44 ± 0.14	1
Rps11A/Bp	NP_010308	A protein component of the 40S ribosomal subunit	0.35 ± 0.09	1
Rps23A/Bp	NP_015457	A protein component of the 40S ribosomal subunit	0.42 ± 0.11	1
Rpl6Ap	NP_013638	A protein component of the 60S ribosomal subunit	0.31 ± 0.15	1
Rpl8A/Bp	NP_011830	A protein component of the 60S ribosomal subunit	0.27 ± 0.13	1
Rpl9A/Bp	NP_011368	A protein component of the 60S ribosomal subunit	0.40 ± 0.22	1
Rpl10p	NP_013176	A protein component of the 60S ribosomal subunit	0.28 ± 0.10	1
Rpl21A/Bp	NP_009750	A protein component of the 60S ribosomal subunit	0.42 ± 0.17	1
Rpl27A/Bp	NP_011874	A protein component of the 60S ribosomal subunit	0.36 ± 0.06	1
Rpl31A/Bp	NP_010208	A protein component of the 60S ribosomal subunit	0.37 ± 0.15	1
Rpl34A/Bp	NP_010977	A protein component of the 60S ribosomal subunit	0.40 ± 0.11	1
Npl4p	NP_009729	Proteasomal protein degradation	2.75 ± 0.32	1
Pup1p	NP_014800	Proteasomal protein degradation	2.44 ± 0.27	1
Pup3p	NP_011020	Proteasomal protein degradation	3.39 ± 0.43	1
Rpn5p	NP_010134	Proteasomal protein degradation	3.61 ± 0.18	1
Rpt6p	NP_011467	Proteasomal protein degradation	3.78 ± 0.10	1
Ufd1p	NP_011562	Proteasomal protein degradation	2.37 ± 0.32	1
Pep4p	NP_015171	Vacuolar protein degradation	2.66 ± 0.45	1

10.3 Appendix 3. List of individual protein components of digitonin-solubilized mitochondrial membrane protein supercomplexes separated by 1-D BN-PAGE, resolved by 2-D SDS-PAGE and stained by silver

Following silver staining, protein bands were excised from the gel, reduced, alkylated and in-gel digested with trypsin. The resulting peptides were separated by RP-HPLC/MS using an LTQ Orbitrap. The raw MS data file obtained by Xcalibur was analyzed using the Thermo Scientific Xcalibur Proteome Discoverer application (version 1.3), which was used to identify individual protein components of the isolated mitochondrial respiratory supercomplexes by comparing the raw data of mass spectra of digested fragments to the mass spectra of peptides within the Uniprot FASTA database. The analysis by the Thermo Scientific Xcalibur Proteome Discoverer coupled to the FASTA database was enabled by using the peak-finding search engine SEQUEST, which processes MS data using a peak-finding algorithm to search the raw data for generating a peak probability list with relative protein abundances.

Protein name	Protein description	NCBI accession number	Score	Sequence coverage (%)	Number of identified peptides	MW (kDa)	Calculated pI
Wild-type strain							
Protein supercomplex 1							
Aac2p	Major ADP/ATP carrier of the mitochondrial inner membrane	P18239	103.33	30.19%	10	34.4	9.79
Por1p	Mitochondrial porin (voltage-dependent anion channel)	P04840	251.47	43.46%	12	30.4	7.93
Ndi1p	NADH:ubiquinone oxidoreductase	P32340	177.99	35.67%	19	57.2	9.44
Nde1p	Mitochondrial external NADH dehydrogenase	P40215	56.52	34.64%	25	62.7	9.28
Pda1p	E1 alpha subunit of the pyruvate dehydrogenase complex	P16387	99.69	26.43%	15	46.3	8.1
Pdb1p	E1 beta subunit of the pyruvate dehydrogenase complex	P32473	84.43	34.43%	9	40	5.3
Lat1p	Dihydrolipoamide acetyltransferase component (E2) of	P12695	118.56	26.56%	11	51.8	7.8

	the pyruvate dehydrogenase complex						
Lpd1p	Dihydrolipoamide dehydrogenase component (E3) of the pyruvate dehydrogenase complex	P09624	253.54	51.70%	27	54	8.03
Sdh1p	Flavoprotein subunit of succinate dehydrogenase (respiratory complex II)	Q00711	112.55	38.59%	24	70.2	7.5
Sdh2p	Iron-sulfur subunit of succinate dehydrogenase (respiratory complex II)	P21801	212.02	31.20%	12	30.2	8.82
Sdh3p	Cytochrome b subunit of succinate dehydrogenase (respiratory complex II)	P33421	97.47	22.73%	6	22.1	10.23
Sdh4p	Membrane anchor subunit of succinate dehydrogenase (respiratory complex II)	P37298	129.27	24.31%	6	20.2	8.9
Cyt1p	Cytochrome b-c1 complex (respiratory complex III), cytochrome c1 component	P07143	49.94	27.83%	5	34	8.12
Qcr1p	Cytochrome b-c1 complex (respiratory complex III), subunit 1	P07256	154.4	32.82%	19	50.2	7.3
Qcr2p	Cytochrome b-c1 complex (respiratory complex III), subunit 2	P07257	188.18	54.62%	26	40.5	7.96
Qcr7p	Cytochrome b-c1 complex (respiratory complex III), subunit 7	P00128	106.36	22.83%	5	14.6	5.88
Qcr8p	Cytochrome b-c1 complex	P08525	92.45	24.47%	3	11	9.7

	(respiratory complex III), subunit 8						
Rip1p	Cytochrome b-c1 complex (respiratory complex III), ubiquinol-cytochrome-c reductase	P08067	68.73	18.60%	5	23.3	8.07
Atp1p	Mitochondrial F1F0 ATP synthase (respiratory complex V), alpha subunit	P07251	260.88	23.67%	15	58.6	9.04
Atp2p	Mitochondrial F1F0 ATP synthase (respiratory complex V), beta subunit	P00830	270.34	38.94%	20	54.8	5.71
Atp3p	Mitochondrial F1F0 ATP synthase (respiratory complex V), gamma subunit	P38077	207.02	47.91%	20	34.3	9.31
Atp4p	Mitochondrial F1F0 ATP synthase (respiratory complex V), b subunit	P05626	135.52	55.74%	18	26.9	9.13
Atp5p	Mitochondrial F1F0 ATP synthase (respiratory complex V), subunit 5	P09457	197.56	86.32%	21	22.8	9.57
Atp7p	Mitochondrial F1F0 ATP synthase (respiratory complex V), d subunit	P30902	256.15	66.67%	20	19.8	8.94
Atp17p	Mitochondrial F1F0 ATP synthase (respiratory complex V), f subunit	Q06405	91.74	41.58%	5	11.3	10.1
Protein supercomplex 2							
Aac2p	Major ADP/ATP carrier of the	P18239	92.94	38.99%	15	34.4	9.79

	mitochondrial inner membrane						
Por1p	Mitochondrial porin (voltage-dependent anion channel)	P04840	199.73	39.22%	10	30.4	7.93
Kgd1p	Component of the mitochondrial alpha-ketoglutarate dehydrogenase complex	P20967	409.94	56.21%	53	114.3	7.21
Cyt1p	Cytochrome b-c1 complex (respiratory complex III), cytochrome c1 component	P07143	35.71	27.83%	5	34	8.12
Qcr1p	Cytochrome b-c1 complex (respiratory complex III), subunit 1	P07256	636.69	36.32%	20	50.2	7.3
Qcr2p	Cytochrome b-c1 complex (respiratory complex III), subunit 2	P07257	248.78	67.12%	33	40.5	7.96
Qcr7p	Cytochrome b-c1 complex (respiratory complex III), subunit 7	P00128	122.57	22.83%	5	14.6	5.88
Qcr8p	Cytochrome b-c1 complex (respiratory complex III), subunit 8	P08525	26.43	24.47%	4	11	9.7
Rip1p	Cytochrome b-c1 complex (respiratory complex III), ubiquinol-cytochrome-c reductase	P08067	61.51	28.37%	6	23.3	8.07
Protein supercomplex 3							
Cyt1p	Cytochrome b-c1 complex (respiratory complex III), cytochrome c1 component	P07143	40.02	22.98%	6	34	8.12
Qcr1p	Cytochrome b-c1 complex (respiratory	P07256	124.86	34.14%	17	50.2	7.3

	complex III), subunit 1						
Qcr2p	Cytochrome b-c1 complex (respiratory complex III), subunit 2	P07257	156.88	57.61%	25	40.5	7.96
Qcr7p	Cytochrome b-c1 complex (respiratory complex III), subunit 7	P00128	142.84	51.97%	7	14.6	5.88
Qcr8p	Cytochrome b-c1 complex (respiratory complex III), subunit 8	P08525	40.05	24.47%	4	11	9.7
Rip1p	Cytochrome b-c1 complex (respiratory complex III), ubiquinol-cytochrome-c reductase	P08067	54.99	25.58%	6	23.3	8.07
Atp1p	Mitochondrial F1F0 ATP synthase (respiratory complex V), alpha subunit	P07251	174.59	28.26%	21	58.6	9.04
Atp2p	Mitochondrial F1F0 ATP synthase (respiratory complex V), beta subunit	P00830	129.72	55.77%	23	54.8	5.71
Atp3p	Mitochondrial F1F0 ATP synthase (respiratory complex V), gamma subunit	P38077	143.47	32.80%	12	34.3	9.31
Atp4p	Mitochondrial F1F0 ATP synthase (respiratory complex V), b subunit	P05626	254.25	50.82%	14	26.9	9.13
Atp5p	Mitochondrial F1F0 ATP synthase (respiratory complex V), subunit 5	P09457	91.52	55.19%	11	22.8	9.57
Atp7p	Mitochondrial	P30902	166.24	40.23%	11	19.8	8.94

	F1F0 ATP synthase (respiratory complex V), d subunit						
Atp17p	Mitochondrial F1F0 ATP synthase (respiratory complex V), f subunit	Q06405	83.21	32.67%	4	11.3	10.1
Protein supercomplex 4							
Aac2p	Major ADP/ATP carrier of the mitochondrial inner membrane	P18239	92.83	29.25%	10	34.4	9.79
Atp1p	Mitochondrial F1F0 ATP synthase (respiratory complex V), alpha subunit	P07251	255.88	28.07%	22	58.6	9.04
Atp2p	Mitochondrial F1F0 ATP synthase (respiratory complex V), beta subunit	P00830	292.07	31.70%	18	54.8	5.71
Atp3p	Mitochondrial F1F0 ATP synthase (respiratory complex V), gamma subunit	P38077	615.01	41.80%	16	34.3	9.31
Atp4p	Mitochondrial F1F0 ATP synthase (respiratory complex V), b subunit	P05626	90.24	40.57%	12	26.9	9.13
Atp5p	Mitochondrial F1F0 ATP synthase (respiratory complex V), subunit 5	P09457	225.76	66.51%	12	22.8	9.57
Atp7p	Mitochondrial F1F0 ATP synthase (respiratory complex V), d subunit	P30902	125.76	51.15%	14	19.8	8.94
Protein supercomplex 5							
Yme2p	Integral inner mitochondrial	P32843	194.31	35.65%	32	96.6	8.92

	membrane protein with a role in maintaining mitochondrial nucleoid structure and number						
Protein supercomplex 6							
Aac2p	Major ADP/ATP carrier of the mitochondrial inner membrane	P18239	184.97	51.26%	24	34.4	9.79
Atp1p	Mitochondrial F1F0 ATP synthase (respiratory complex V), alpha subunit	P07251	173.98	39.08%	28	58.6	9.04
Atp2p	Mitochondrial F1F0 ATP synthase (respiratory complex V), beta subunit	P00830	106.04	42.66%	21	54.8	5.71
Atp3p	Mitochondrial F1F0 ATP synthase (respiratory complex V), gamma subunit	P38077	162.87	26.05%	9	34.3	9.31
Atp4p	Mitochondrial F1F0 ATP synthase (respiratory complex V), b subunit	P05626	173.15	50.82%	15	26.9	9.13
Atp5p	Mitochondrial F1F0 ATP synthase (respiratory complex V), subunit 5	P09457	108.74	48.58%	11	22.8	9.57
Atp7p	Mitochondrial F1F0 ATP synthase (respiratory complex V), d subunit	P30902	101.36	58.05%	16	19.8	8.94
Protein supercomplex 7							
Cyt1p	Cytochrome b-c1 complex (respiratory complex III), cytochrome c1 component	P07143	36.2	22.65%	5	34	8.12
Qcr1p	Cytochrome b-c1	P07256	242.73	39.17%	20	50.2	7.3

	complex (respiratory complex III), subunit 1						
Qcr2p	Cytochrome b-c1 complex (respiratory complex III), subunit 2	P07257	178.59	74.46%	33	40.5	7.96
Qcr7p	Cytochrome b-c1 complex (respiratory complex III), subunit 7	P00128	131.52	22.83%	5	14.6	5.88
Qcr8p	Cytochrome b-c1 complex (respiratory complex III), subunit 8	P08525	26.82	24.47%	4	11	9.7
Rip1p	Cytochrome b-c1 complex (respiratory complex III), ubiquinol-cytochrome-c reductase	P08067	77.37	36.28%	10	23.3	8.07
Cox4p	Cytochrome c oxidase (respiratory complex IV), subunit 4	P04037	14.78	31.61%	3	17.1	6.9
Cox5Ap	Cytochrome c oxidase (respiratory complex IV), subunit 5A	P00424	160.43	47.71%	11	17.1	9.82
Cox5Bp	Cytochrome c oxidase (respiratory complex IV), subunit 5B	P00425	103.71	28.48%	5	17.2	9.8
Cox6p	Cytochrome c oxidase (respiratory complex IV), subunit 6	P00427	26.7	33.11%	8	17.3	6.05
Atp1p	Mitochondrial F1F0 ATP synthase (respiratory complex V), alpha subunit	P07251	180.84	48.44%	32	58.6	9.04
Atp2p	Mitochondrial F1F0 ATP synthase	P00830	158.5	40.51%	20	54.8	5.71

	(respiratory complex V), beta subunit						
Atp3p	Mitochondrial F1F0 ATP synthase (respiratory complex V), gamma subunit	P38077	387	30.55%	10	34.3	9.31
Atp4p	Mitochondrial F1F0 ATP synthase (respiratory complex V), b subunit	P05626	95.35	45.90%	18	26.9	9.13
Atp5p	Mitochondrial F1F0 ATP synthase (respiratory complex V), subunit 5	P09457	288.43	66.98%	14	22.8	9.57
Atp7p	Mitochondrial F1F0 ATP synthase (respiratory complex V), d subunit	P30902	196.03	44.25%	13	19.8	8.94
Protein supercomplex 8							
Ald4p	Mitochondrial aldehyde dehydrogenase	P46367	531.66	52.60%	24	56.7	6.74
Por1p	Mitochondrial porin (voltage-dependent anion channel)	P04840	114.07	42.05%	11	30.4	7.93
Cyt1p	Cytochrome b-c1 complex (respiratory complex III), cytochrome c1 component	P07143	32.23	29.77%	6	34	8.12
Qcr1p	Cytochrome b-c1 complex (respiratory complex III), subunit 1	P07256	206.37	30.85%	17	50.2	7.3
Qcr2p	Cytochrome b-c1 complex (respiratory complex III), subunit 2	P07257	152.45	48.10%	21	40.5	7.96
Qcr7p	Cytochrome b-c1 complex (respiratory complex III),	P00128	149.7	36.22%	6	14.6	5.88

	subunit 7						
Qcr8p	Cytochrome b-c1 complex (respiratory complex III), subunit 8	P08525	92.45	24.47%	3	11	9.7
Rip1p	Cytochrome b-c1 complex (respiratory complex III), ubiquinol-cytochrome-c reductase	P08067	36.14	33.95%	7	23.3	8.07
Atp1p	Mitochondrial F1F0 ATP synthase (respiratory complex V), alpha subunit	P07251	666.64	36.15%	27	58.6	9.04
Atp2p	Mitochondrial F1F0 ATP synthase (respiratory complex V), beta subunit	P00830	273.89	44.03%	20	54.8	5.71
Atp3p	Mitochondrial F1F0 ATP synthase (respiratory complex V), gamma subunit	P38077	432.23	40.19%	14	34.3	9.31
Atp4p	Mitochondrial F1F0 ATP synthase (respiratory complex V), b subunit	P05626	203.16	47.13%	15	26.9	9.13
Atp5p	Mitochondrial F1F0 ATP synthase (respiratory complex V), subunit 5	P09457	148.55	49.53%	11	22.8	9.57
Atp7p	Mitochondrial F1F0 ATP synthase (respiratory complex V), d subunit	P30902	112.24	40.80%	9	19.8	8.94
Idh1p	Subunit of mitochondrial NAD(+)-dependent isocitrate dehydrogenase	P28834	415.06	47.22%	19	39.3	9

Idh2p	Subunit of mitochondrial NAD(+)-dependent isocitrate dehydrogenase	P28241	238.75	39.84%	13	39.7	8.69
***atg32Δ* strain**							
Protein supercomplex 1							
Aac2p	Major ADP/ATP carrier of the mitochondrial inner membrane	P18239	142.9	31.45%	13	34.4	9.79
Por1p	Mitochondrial porin (voltage-dependent anion channel)	P04840	135.62	43.46%	12	30.4	7.93
Lat1p	Dihydrolipoamide acetyltransferase component (E2) of the pyruvate dehydrogenase complex	P12695	71.58	26.97%	14	51.8	7.8
Lpd1p	Dihydrolipoamide dehydrogenase component (E3) of the pyruvate dehydrogenase complex	P09624	171.86	37.07%	21	54	8.03
Cyt1p	Cytochrome b-c1 complex (respiratory complex III), cytochrome c1 component	P07143	68.38	31.07%	7	34	8.12
Qcr1p	Cytochrome b-c1 complex (respiratory complex III), subunit 1	P07256	216.4	34.79%	18	50.2	7.3
Qcr2p	Cytochrome b-c1 complex (respiratory complex III), subunit 2	P07257	134.35	56.25%	24	40.5	7.96
Qcr7p	Cytochrome b-c1 complex (respiratory complex III), subunit 7	P00128	160.32	36.22%	6	14.6	5.88
Qcr8p	Cytochrome b-c1 complex (respiratory complex III), subunit 8	P08525	26.43	24.47%	4	11	9.7
Rip1p	Cytochrome b-c1	P08067	56.97	29.77%	7	23.3	8.07

	complex (respiratory complex III), ubiquinol-cytochrome-c reductase						
Atp1p	Mitochondrial F1F0 ATP synthase (respiratory complex V), alpha subunit	P07251	293.31	28.26%	21	58.6	9.04
Atp2p	Mitochondrial F1F0 ATP synthase (respiratory complex V), beta subunit	P00830	329.47	43.84%	22	54.8	5.71
Atp3p	Mitochondrial F1F0 ATP synthase (respiratory complex V), gamma subunit	P38077	438.8	36.33%	13	34.3	9.31
Atp4p	Mitochondrial F1F0 ATP synthase (respiratory complex V), b subunit	P05626	298.9	62.30%	24	26.9	9.13
Atp5p	Mitochondrial F1F0 ATP synthase (respiratory complex V), subunit 5	P09457	573.45	75.47%	16	22.8	9.57
Atp7p	Mitochondrial F1F0 ATP synthase (respiratory complex V), d subunit	P30902	190.75	72.99%	15	19.8	8.94
Protein supercomplex 2							
Aac2p	Major ADP/ATP carrier of the mitochondrial inner membrane	P18239	167.8	34.91%	14	34.4	9.79
Por1p	Mitochondrial porin (voltage-dependent anion channel)	P04840	296.37	50.18%	14	30.4	7.93
Cyt1p	Cytochrome b-c1 complex (respiratory complex III),	P07143	61.72	27.83%	5	34	8.12

	cytochrome c1 component						
Qcr1p	Cytochrome b-c1 complex (respiratory complex III), subunit 1	P07256	110.93	39.17%	20	50.2	7.3
Qcr2p	Cytochrome b-c1 complex (respiratory complex III), subunit 2	P07257	152.7	54.08%	24	40.5	7.96
Qcr7p	Cytochrome b-c1 complex (respiratory complex III), subunit 7	P00128	101.24	36.22%	6	14.6	5.88
Qcr8p	Cytochrome b-c1 complex (respiratory complex III), subunit 8	P08525	13.41	21.28%	2	11	9.7
Rip1p	Cytochrome b-c1 complex (respiratory complex III), ubiquinol-cytochrome-c reductase	P08067	52.77	46.05%	11	23.3	8.07
Protein supercomplex 3							
Atp1p	Mitochondrial F1F0 ATP synthase (respiratory complex V), alpha subunit	P07251	109.69	35.78%	25	58.6	9.04
Atp2p	Mitochondrial F1F0 ATP synthase (respiratory complex V), beta subunit	P00830	512.23	38.16%	22	54.8	5.71
Atp3p	Mitochondrial F1F0 ATP synthase (respiratory complex V), gamma subunit	P38077	156.34	36.33%	12	34.3	9.31
Atp4p	Mitochondrial F1F0 ATP synthase (respiratory complex V), b subunit	P05626	242.42	58.20%	22	26.9	9.13
Atp5p	Mitochondrial	P09457	124.41	53.30%	11	22.8	9.57

	F1F0 ATP synthase (respiratory complex V), subunit 5						
Atp7p	Mitochondrial F1F0 ATP synthase (respiratory complex V), d subunit	P30902	348.32	79.89%	20	19.8	8.94
Protein supercomplex 4							
Aac2p	Major ADP/ATP carrier of the mitochondrial inner membrane	P18239	91.45	33.02%	11	34.4	9.79
Protein supercomplex 6							
Aac2p	Major ADP/ATP carrier of the mitochondrial inner membrane	P18239	176.99	45.60%	18	34.4	9.79
Protein supercomplex 7							
Atp1p	Mitochondrial F1F0 ATP synthase (respiratory complex V), alpha subunit	P07251	193.91	43.85%	27	58.6	9.04
Atp2p	Mitochondrial F1F0 ATP synthase (respiratory complex V), beta subunit	P00830	102.93	40.12%	17	54.8	5.71
Atp3p	Mitochondrial F1F0 ATP synthase (respiratory complex V), gamma subunit	P38077	138.31	36.33%	13	34.3	9.31
Atp4p	Mitochondrial F1F0 ATP synthase (respiratory complex V), b subunit	P05626	110.07	40.57%	14	26.9	9.13
Atp5p	Mitochondrial F1F0 ATP synthase (respiratory complex V), subunit 5	P09457	345.82	82.55%	19	22.8	9.57
Atp7p	Mitochondrial F1F0 ATP synthase	P30902	198.09	83.91%	24	19.8	8.94

	(respiratory complex V), d subunit						
Protein supercomplex 8							
Ald4p	Mitochondrial aldehyde dehydrogenase	P46367	211.93	51.25%	21	56.7	6.74
Por1p	Mitochondrial porin (voltage-dependent anion channel)	P04840	141.79	40.64%	10	30.4	7.93
Idh1p	Subunit of mitochondrial NAD(+)-dependent isocitrate dehydrogenase	P28834	367.21	43.06%	16	39.3	9
Idh2p	Subunit of mitochondrial NAD(+)-dependent isocitrate dehydrogenase	P28241	580.69	40.65%	14	39.7	8.69

10.4 Appendix 4. List of my publications and invited presentations

10.4.1 Manuscripts of papers submitted for publication

1. **Beach A**, Leonov A, Arlia-Ciommo A, Svistkova V, Lutchman V, Titorenko VI. Mechanisms by which different functional states of mitochondria define yeast longevity. Int J Mol Sci 2015 ; submission # ijms-77491.

2. **Beach A**, Richard VR, Bourque S, Boukh-Viner T, Kyryakov P, Gomez-Perez A, Arlia-Ciommo A, Feldman R, Leonov A, Piano A, Svistkova V, Titorenko VI. Lithocholic bile acid accumulated in yeast mitochondria orchestrates a development of an anti-aging cellular pattern by causing age-related changes in cellular proteome. Cell Cycle 2015; submission # 2014CC6373.

10.4.2 Published articles

1. Richard VR*, **Beach A***, Piano A*, Leonov A, Feldman R, Burstein MT, Kyryakov P, Gomez-Perez A, Arlia-Ciommo A, Baptista S, Campbell C, Goncharov D, Pannu S, Patrinos D, Sadri B, Svistkova V, Victor A, Titorenko VI. Mechanism of liponecrosis, a distinct mode of programmed cell death. Cell Cycle 2014; 13:3707-326.
    a. **Equally contributed first authors.**

2. Sheibani S, Richard VR, **Beach A**, Leonov A, Feldman R, Mattie S, Khelghatybana L, Piano A, Greenwood M, Vali H, Titorenko VI. Macromitophagy, neutral lipids synthesis, and peroxisomal fatty acid oxidation protect yeast from "liponecrosis", a previously unknown form of programmed cell death. Cell Cycle 2014; 13:138-147.

3. Goldberg AA, Titorenko VI, **Beach A**, Sanderson JT. Bile acids induce apoptosis selectively in androgen-dependent and -independent prostate cancer cells. PeerJ 2013; 1:e122.

4. **Beach A**, Richard VR, Leonov A, Burstein MT, Bourque SD, Koupaki O, Juneau M, Feldman R, Iouk T, Titorenko VI. Mitochondrial membrane lipidome defines yeast longevity. Aging 2013; 5:551-574.

2. **Beach A**, Titorenko VI. Essential roles of peroxisomally produced and metabolized biomolecules in regulating yeast longevity. Subcell Biochem 2013; 69:153-167.

5. Goldberg AA, Titorenko VI, **Beach A**, Abdelbaqi K, Safe S, Sanderson JT. Ring-substituted analogs of 3,3'-diindolylmethane (DIM) induce apoptosis and necrosis in androgen-dependent and -independent prostate cancer cells. Invest New Drugs 2014; 32:25-36.

6. **Beach A**, Burstein MT, Richard VR, Gomez-Perez A, Leonov A, Iouk T, Titorenko VI. A modular network regulates longevity of chronologically aging yeast. Cell Biol Res Ther 2013; 2:1000e110.

7. Richard VR*, Leonov A*, **Beach A***, Burstein MT, Koupaki O, Gomez-Perez A, Levy S, Pluska L, Mattie S, Rafesh R, Iouk T, Sheibani S, Greenwood M, Vali H, Titorenko VI. Macromitophagy is a longevity assurance process that in chronologically aging yeast limited in calorie supply sustains functional mitochondria and maintains cellular lipid homeostasis. Aging 2013; 5:234-269.
***Equally contributed first authors.**

8. **Beach A**, Burstein MT, Richard VR, Leonov A, Levy S, Titorenko VI. Integration of peroxisomes into an endomembrane system that governs cellular aging. Front Physiol 2012; 3:283.

9. Burstein MT, Kyryakov P, **Beach A**, Richard VR, Koupaki O, Gomez-Perez A, Leonov A, Levy S, Noohi F, Titorenko VI. Lithocholic acid extends longevity of chronologically aging yeast only if added at certain critical periods of their lifespan. Cell Cycle 2012; 11:3443-3462.

10. Kyryakov P, **Beach A**, Richard VR, Burstein MT, Leonov A, Levy S, Titorenko VI. Caloric restriction extends yeast chronological lifespan by altering a pattern of age-related changes in trehalose concentration. Front Physiol 2012; 3:256.

11. Burstein MT, **Beach A**, Richard VR, Koupaki O, Gomez-Perez A, Goldberg AA, Kyryakov P, Bourque SD, Glebov A, Titorenko VI. Interspecies Chemical Signals Released into the Environment May Create Xenohormetic, Hormetic and Cytostatic Selective Forces that Drive the Ecosystemic Evolution of Longevity Regulation Mechanisms. Dose Response 2012; 10:75-82.

12. Goldberg AA, **Beach A**, Davies GF, Harkness TA, Leblanc A, Titorenko VI. Lithocholic bile acid selectively kills neuroblastoma cells, while sparing normal neuronal cells. Oncotarget 2011; 2:761-782.

13. **Beach A**, Titorenko VI. In search of housekeeping pathways that regulate longevity. Cell Cycle 2011; 10:3042-3044.

14. Goldberg AA, Richard VR, Kyryakov P, Bourque SD, **Beach A**, Burstein MT, Glebov A, Koupaki O, Boukh-Viner T, Gregg C, Juneau M, English AM, Thomas DY, Titorenko VI. Chemical genetic screen identifies lithocholic acid as an anti-aging compound that extends yeast chronological life span in a TOR-independent manner, by modulating housekeeping longevity assurance processes. Aging 2010; 2:393-414.

15. Goldberg AA, Bourque SD, Kyryakov P, Boukh-Viner T, Gregg C, **Beach A**, Burstein MT, Machkalyan G, Richard V, Rampersad S, Titorenko VI. A novel function of lipid droplets in regulating longevity. Biochem Soc Trans 2009; 37:1050-1055.

16. Goldberg AA, Bourque SD, Kyryakov P, Gregg C, Boukh-Viner T, **Beach A**, Burstein MT, Machkalyan G, Richard V, Rampersad S, Cyr D, Milijevic S, Titorenko VI. Effect

of calorie restriction on the metabolic history of chronologically aging yeast. Exp Gerontol. 2009; 44:555-571.

10.4.3 Invited presentations

1. The 12th Euro Fed Lipid Congress in Montpellier (France), September 2014. Title of the talk: "Mechanism of “liponecrosis”, a novel form of programmed cell death".

2. The 10th Euro Fed Lipid Congress in Cracow (Poland), September 2012. Title of the talk: "Lithocholic acid delays aging and exhibits a potent anti-cancer effect by altering mitochondrial composition, structure, metabolism, dynamics and function".

3. The 2012 Yeast Genetics and Molecular Biology Meeting in Princeton University, August 2012. Title of the talk: "Chemical genetic screen identifies a compound that delays aging in yeast and exhibits a potent anti-tumor effect in human cells by altering mitochondrial composition, structure, metabolism, dynamics, and function".

4. The Journée Phare 2010 Meeting at Sherbrooke University, November 2010. Title of the talk: "A novel anti-aging compound extends longevity by altering the age-related dynamics of reactive oxygen species".

5. The 2010 Northeast Regional Yeast Meeting at the State University of New York – Buffalo, New York, USA, May 2010. Title of the talk: "A novel anti-aging compound extends longevity by altering the age-related dynamics of reactive oxygen species".

6. The Montreal Yeast Meeting, March 2010. Title of the talk: "A novel anti-aging compound extends longevity by altering the age-related dynamics of reactive oxygen species".